

UNIVERSITY OF NOVA GORICA
GRADUATE SCHOOL

**NUMERICAL ANALYSIS AND EXPERIMENTAL TESTS ON
DYNAMIC BEHAVIOUR OF GFRP PULTRUDED ELEMENTS
FOR CONSERVATION OF THE ARCHITECTURAL AND
ENVIRONMENTAL HERITAGE**

Giosuè Boscato

prof. Salvatore Russo

University Iuav of Venice, Venice, Italy

Venice, 2009

Scientific committee

Dr. J. T. Mottram, *University of Warwick, UK*
Prof. Maria Rosaria Pecce, *University of Sannio, Benevento, Italy*
Prof. Enzo Siviero, *University Iuav of Venice, Venice, Italy*

to my family

ACKNOWLEDGEMENTS

ABSTRACT

p.1

1. INTRODUCTION

p.3

General background

Static behaviour, preliminary researches

Aim and objectives

Limitations of study and possible research evolve

Organization

References

2. MATERIALS AND TECNOLOGIES

p.9

2.1. The materials

2.2. The mechanical characteristics of fibers, matrix and composite materials

2.3. Production technologies

2.3.1. Hand lay-up

2.3.2. Vacuum-Assisted Resin Transfer Molding

2.3.3. Vacuum Bag Molding

2.3.4. Autoclave Molding

2.3.5. Filament Winding

2.3.6. Pultrusion

2.4. Chapter overview

References

3. STATE OF THE ART

p.17

References

4. APPLICATIONS OF FRP STRUCTURAL ELEMENTS

p.25

4.1. FRP elements for new construction

4.2. GFRP pultruded elements for historical building conservation

4.2.1. Auxiliary floor

4.2.2. Reinforcement of wood deck

- 4.2.3. Reinforcement of old pedestrian bridge
 - 4.2.3.1. General description of pedestrian bridge structure
 - 4.2.3.2. Structural design approach with FRP beams
 - 4.2.3.3. Analytical design approach
 - 4.2.3.4. Structural performance
 - 4.2.3.4.1. Static behavior
 - 4.2.3.4.2. Dynamic behavior
 - 4.2.3.5. Comparison with traditional materials and analysis of results
 - 4.2.3.6. Assembling and installation phase
 - 4.2.3.7. Results of static experimental test
 - 4.2.3.8. In situ increment of stiffness and repair of FRP beams
 - 4.2.3.9. Final remarks
- 4.2.4. Further employment possibility

4.3. Chapter overview

References

5. DYNAMIC ANALYSIS OF GFRP ELEMENTS FOR APPLICATION IN CIVIL ENGINEERING

p.65

5.1. Introduction

5.2. Free vibrations

- 5.2.1. Mono-dimensional elements
 - 5.2.1.1. Experimental analysis
 - 5.2.1.1.1. Setup of experimental tests
 - 5.2.1.1.2. Damping
 - 5.2.1.1.3. Shape and torsional effects
 - 5.2.1.1.4. Parametric comparison and analysis of results
 - 5.2.1.2. Numerical analysis
 - 5.2.1.2.1. Mechanical characteristics
 - 5.2.1.2.2. Finite element analysis
 - 5.2.1.2.3. Comparison with traditional materials

- 5.2.1.3. Applications
 - 5.2.2. Two-dimensional frame
 - 5.2.2.1. Design and assembling phase
 - 5.2.2.1.1. Beam to column joint
 - 5.2.2.1.2. Rotational force
 - 5.2.2.2. Analysis of experimental results
 - 5.2.2.3. Numerical and finite element analysis
 - 5.2.2.4. Results comparison
 - 5.2.3. Three-dimensional structure
 - 5.2.3.1. Analysis of experimental results
 - 5.2.3.2. Finite element analysis
 - 5.2.3.3. Results comparison
- 5.3. Dynamic action behavior of GFRP structures**
- 5.4. An example in presence of a real dynamic load**
- 5.5. Chapter overview*

References

| | |
|---|-------|
| 6. FINAL CONSIDERATIONS | p.171 |
| APPENDIX A – Mono-dimensional elements, experimental results | p.175 |
| APPENDIX B – Two-dimensional frame, experimental results | p.189 |
| APPENDIX C – Three-dimensional structure, experimental results | p.197 |

ACKNOWLEDGEMENTS

First of all I would like to express gratitude to my thesis supervisor Prof. Salvatore Russo for his scientific and human support, encouragement and guidance.

I express my gratitude to the thesis defense committee, Dr. J. T. Mottram, Prof. Maria Rosaria Pecce and Prof. Enzo Siviero for the time and effort put into reading and evaluating this work.

The experimental program was possible thanks to the assistance of Structural Mechanics Laboratory (LabSCo) of the IUAV University of Venice through the collaboration of Ivano Aldreggetti, Giacomo Busetto, Mario Celebrin, Giorgio Costantini, Lorenzo Massaria, Vincenzo Scafuri and Italo Tofani.

Many thanks to Dr. Roberta Vencato for her unconditional support, Marco Tenderini and Valentina Vanzo for their friendship, help and cooperation.

I would like to acknowledge the support of Top Glass and Saimex for donating the material for the experimental program.

ABSTRACT

The definition of the application fields of composite materials in civil engineering, intended not as reinforcing applications of the existing structures but as perfectly independent structural elements passes through experimental and analytical identification of static and dynamic response. After an initial phase dedicated to the general setting to innovative technology, the present work draws attention to the structural response of the element GFRP (Glass Fibre Reinforced Polymer).

The identification of the dynamic parameters of the profiles and the GFRP structures was, however, analysed in detail as never before presented and generally not reported upon in any great detail in literature. This study looks at the response of the GFRP profiles and 2D and 3D structures in the free vibrations field so as to identify the spectral response, mode of vibration, damping and displacements to vary the geometric and typological configurations analysed. The experiment has allowed the definition of the most suitable analytical models and the simulation of the structural responses of the 2D and 3D systems with regards to dynamic actions varying the boundary conditions, the rotational stiffness of the internal joints and the global stiffness of the systems.

Upon completion, the structural response with regards to dynamic response of GFRP sheet pile subjected to dynamic action applied by traditional piling machine.

1. INTRODUCTION

General background

The aim of the research doctorate thesis is the evaluation of the structural performance of composite fibre-reinforced elements in the wider sector of the conservation of historical, architectonic and environmental heritage.

The study theme is inserted into a much wider line of research regarding the use of fibre-reinforced composite materials indicated by the acronym FRP (Fibre Reinforced Polymer) in the fields of civil engineering and architecture, both for reinforcing and for new construction.

At present, the use of FRP for reinforcing is widespread throughout the international field, whilst the application of structural profiles in FRP is uncommon even if it seems to be particularly promising.

The present research doctorate thesis is dedicated entirely to study of FRP structural elements and proposes several innovative discussion points.

Concerning the type of possible application, FRP structural profiles are characterised by their lightness, strength and durability. In this sense, among the typical applications in the new sector they distinguish footbridges, the bridge with contained span, also those suitable for vehicles, light removable structures and over elevation constructions.

With regards to use in reinforcing and for the conservation of historical, architectonic and environmental heritage, the mechanical characteristics and performance of the FRP material are highlighted as conciliating with the structural rehabilitation problems inasmuch it is a very light, resistant and reversible material. As an example, in the conservation of historical and architectonic heritage, it is possible to increase the flexural stiffness of deck with low increment of dead loads, its use as an lintel for the resolution of local problems, the increment of stiffness of historical masonry walls especially at higher levels. Furthermore, in the case of the structural rehabilitation of slender elements in historical masonry such as in towers and belfries, it is plausible to use the material as reinforcing ensuring a high level of strength in the face of reduced additional load. The FRP members guarantees moreover, in the long time, the maintaining of initial mechanical-structural performance.

Now the knowledgeable approach is sufficiently supported both from the point of view theoretical and relevant regulations (CNR, Eurocomp) and also by validation derived directly from experience attained in the research field and FRP applications realized up to the present.

Despite the relative youth of the material, certain applications in the national and international fields - some recent, some less so - have provided the incentive to verify behaviour and structural performance, Keller (2003) and Russo (2007).

All in all, the theme of application in the structural field of fibre-reinforced composite elements has been amply examined from the viewpoint of mechanical response to static actions, (Di Tommaso et al. 2002), while the information referring to dynamic characterisation results in being more contained, (Bastianini et al. 2007).

The issue is particularly interesting because the elastic-brittle constitutive law with orthotropic mechanical behaviour (in particular anisotropic transversally isotropic behaviour) together with the absence of ductile behaviour imposes some limitations. Nevertheless the low dead load of the material, 1600-1800 kg/m³ (variable according to the percentage of fibre present), compared with high values of strength and the possibility of being able to define in design phase the entity of stiffness, with a wide margin of variation, suggest the potential for the applications of GFRP elements in the seismic engineering field, (Russo 2007). This refers not only to the realisation of building entirely in composite but also to the possibility of using the profiles as local reinforcement in existing buildings to increase the bending stiffness of highest floor. Similar applicative interest also regards the possibility of achieving over elevation with a frame structure made entirely of fibre-reinforced composite.

In general terms, the absence of stiffness degradation upon increase of the applied loads seems to accurately circumscribe the variability of the damping ratio (Boscato and Russo 2007), inasmuch the experimental results illustrated below lend themselves to some interesting analysis.

Even the connection methods of the composite elements, guaranteed by bolting or bonding, or by using the two techniques in parallel, can be analysed with the same theoretical approach used in the presence of steel structure, with certain variations which take into account of the mechanics of the material. Equally, the high level of deformability should be considered when calibrating the dimensions of the elements in play, (Mottram and Zheng 1999, EUROCOMP 1996).

The current state of international literature underlines an effort to obtain encoding of the structural uses of this material, (ASCE 1984); in Italy was published a new CNR technical document dedicated to structural design with profiles in fibre-reinforced composite produced with pultrusion process, CNR-DT 205/2007.

Static behaviour, preliminary researches

A brief hint to the evaluations on researches carried out by author of present work, about the structural response of the GFRP element concerning the static behaviour, is shortly developed hereafter.

The mechanical performance of the profiles depends on the cross section typology, matrix and fibre, on the volume percentage of the components and on the direction of the fibres with regards to the applied load. In quantitative terms, if the load is applied parallel to the direction of the fibres, the composite profile maximises its structural response. If, however, the direction of the load is transversal to the fibres, the pultruded profile sees a reduction in performance of approximately 80-90%. Such decrement reaches 50% with slight rotations of 20° of the direction of the applied load with regards to the orientation of the fibre.

In the micro-mechanical analysis of the two composite layers, (mat and roving), the behaviour is evidently similar between the two parts. The global response highlights a good response of the matrix-fibre interface, justifying the use of laminate theory for numerical modelling and supporting the hypothesis of perfect bond in the mixing theory.

The time dependent behaviour of the GFRP pultruded profiles must be opportunely calibrated in function of the serviceability load level particularly with regards to the open cross-section profile. With contained applied loads, approximately 50-75% of collapse load, the response to cyclic action does not show relevant stiffness degradation.

The local repair of the GFRP profiles allows results to be reached which are generally similar to the structural response of the profile without cracks. For this purpose, the reinforcement, opportunely designed in function of the type of applied load, also guarantees a global increment in structural performance.

Research carried out on the structural interaction between composite elements and concrete offer interesting applicative suggestions. Regarding the flexural elements, the interface realized by

structural resin demonstrates a promising increment of flexural stiffness with an optimisation of cross section response with respect to external forces. The mixed cross-section (Concrete-GFRP) elements subjected to compression load suffers the effects of the low transversal strength of the pultruded profiles, in fact, for this application is desirable the use of elements produced via filament winding technology.

The high transversal deformability of the pultruded profiles induces phenomena of local buckling which influence the global structural response; indeed, during the design and dimensioning phase, it is necessary to use algorithms which take into account of shear deformability.

Aim and objectives

Considering the physical-mechanical properties of the composite material, the possibility of using the structural elements and FRP systems for the structural reinforcement of existing buildings or the achieving of completely independent structures was analysed so as to identify any referring guidelines.

This study was carried out via analytical and experimental approach, which allowed the characterisation of the composite materials and the defining of the structural behaviour of the GFRP elements with regards to dynamic actions.

Schematically the thesis develops the following topics:

- Numerical and experimental analysis of structural behaviour regarding dynamic actions.
- Determination of the most adequate analytical approach.
- FEM analysis so as to evaluate and to verify the experimental results.

Limitation of study and possible research evolve

For the analysis to be complete, it is necessary to consider a case study much wider of the GFRP structural typologies, thus identifying all the variables which define the structural factor.

With regards to dynamic actions, it is necessary to experimentally verify the structural response with respect to external harmonic actions.

Organization

Finally, in this overall perspective the thesis is developed in the following way: an initial part dedicated to FRP material and the technologies of fibre-reinforced element production; a second part which refers to the structural applications already built in the reinforcement and new

construction fields; a third part referring to a brief bibliographical excursus; a fourth part entirely dedicated to the innovative aspects distinguishing the doctorate thesis with specific reference to the dynamic response of GFRP profiles and structures; finally, the fifth part is dedicated to the conclusions.

References

Structural plastics design manual, Volume 1 and 2, ASCE manuals and reports on engineering practice, No. 63, ASCE NY, 1984.

Bastianini, F., Boscato, G., Russo, S., and Sciarretta, F., *Natural frequencies of pultruded profiles with different cross-sections*, in Proc. 3rd Inter. Conf. Advanced Composites in Construction - ACIC 2007, York Publishing Services, York, 2007.

Boscato G., Russo S., *Lo smorzamento nel comportamento dinamico degli elementi strutturali in composito fibrorinforzato*, Atti del Workshop Materiali ed Approcci Innovativi per il Progetto in Zona Sismica e la Mitigazione della Vulnerabilità delle Strutture, Università di Salerno, Salerno, Italy, 2007.

CNR-DT 205/2007 (2008). *Istruzioni per la Progettazione, l'Esecuzione ed il Controllo di Strutture realizzate con Profili Sottili Pultrusi di Materiale Composito Fibrorinforzato (FRP)*, Roma CNR. CNR-DT 205/2007.

Di Tommaso, A., Arduini, M., Focacci, F., Russo, S., *Le strutture in materiale composito*, E. Giangreco, *Ingegneria delle Strutture*, UTET, Volume 3, 2002.

Structural Design of Polymer Composites -EUROCOMP Design Code and Handbook, Edited by John L. Clarke, E. & F. N. Spon, London, 1996.

Keller, T., *Use of fibre reinforced polymers in bridge construction*, Structural Engineering Documents 7, Inter. Association for Bridges and Structural Engineering (IABSE-AIPC-IVBH), Zurich, 2003.

Mottram, J.T. and Zheng, Y., *Further tests on beam-to-column connections for pultruded frames: Web-cleated*, J. Composites for Construction, 3 1, 1999.

Mottram, J.T. and Zheng, Y., *Further tests on beam-to-column connections for pultruded frames: Flange-cleated*, J. Composites for Construction, 3 3, 1999.

Russo, S., *Strutture in composito – Sperimentazione, teoria e applicazioni*, Ulrico Hoepli Editore S.p.A., Milan, 2007. (In Italian) ISBN 978-88-203-3643-1.

2. MATERIALS AND TECNOLOGIES

The type of approach adopted to compare the themes of this chapter is deliberately synthetic given the fully detailed documentation already present in literature (Russo 2007) and draws attention instead to the analysis of the elements that concern only the composites produced via pultrusion technology. The presence of such an examination is, however, necessary to general definition of the material of composite structural element.

2.1. The materials

The term “Composite” is used to indicate the FRP material insomuch as it is composed of materials with different physical and mechanical characteristics. The association of the two base materials, fibre and matrix, does not guarantee the realisation of a final product characterised by the sum of the properties of the single associated materials and thus the achievement of a general improvement of the final product, see Figure 2.1.

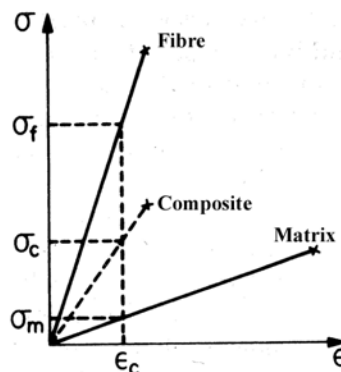


Figure 2.1, Tensile mean behavior of composite, fibre and matrix (Russo 2007)

Figure 2.1 illustrates, in fact, the reduction of the mechanical properties of the naked fibre caused by the presence of and interaction with the matrix.

The matrix results in being, however, necessary for the obtaining of the structural element as it creates continuity between the fibre filaments, transfers the applied forces to the fibres, guarantees the transmission of forces from fibre to fibre via its shear stiffness, protects the fibrous

reinforcing from local damage and chemical aggression and, finally, defines the form of the profile during the polymerisation process.

Generally speaking, the mechanical properties of the composite depend exclusively on the structural response of the fibrous reinforcing. The polymeric matrix fibre-reinforced composite shows a tension behaviour of a elastic-linear type up till its collapse which is generally characterised by a brittle failure with a reduced deformation capacity lacking yielding or plastic phases, or hardening and softening.

As regards compression strength, the fibre, and thus the composite, shows a behaviour of substantially low performance. Such a response is completely governed by the matrix component which, offering reduced transversal stiffness, is particularly vulnerable to buckling phenomenon. Furthermore, the orientation of the fibres and their structure are the determining factors for the mechanical and performance characterisation of the composite material.

In specific case the constitutive law of composite material for structural elements is elastic-brittle with orthotropic mechanical behaviour, in particular anisotropic and transversally behaviour that is also the weakest plane, dominated by matrix mechanical performance. The principal z axis, which corresponds to the direction of longitudinal roving fibres, sets the anisotropic condition, while the layer mat is defined by short fibres randomly linked on plane, (see Figure 2.2).

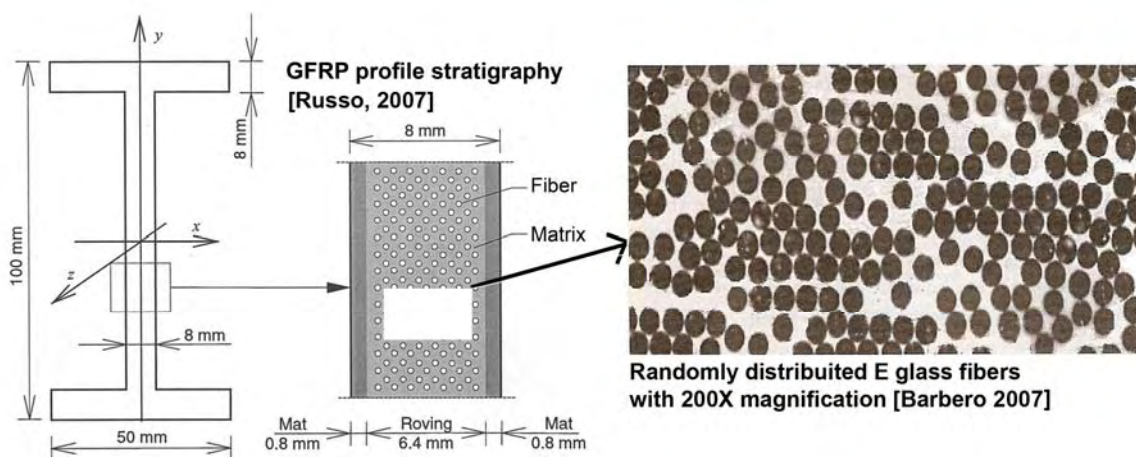


Figure 2.2, GFRP profile stratigraphy and detail

Except for the laminate elements, which, by their nature are produced in defined layers, the interface between the two constitutive materials is difficultly identified and modelled. The hypothesis of perfect adherence between the materials is of fundamental importance for the use of composite elements in a structural engineering field, and so is assumed as one of the base principals of calculation in the theory of mixing, (Russo 2007). The behaviour of the reinforcing-matrix interface is the first evaluation parameter on the mechanical homogeneity of the composite which conditions and defines the response of the FRP structural element with respect to longitudinal and transversal forces, durability respect to aggressive agents, and water impermeability.

The thermal and electrical properties of the composite material, they can be planned according to the type and quantity of elements of which they are composed, (Russo 2007).

2.2. The mechanical characteristics of fibers, matrix and composite materials

The characteristics of the fibre-reinforced composite material and the distinct production techniques, together with the slight differences in performance of the fibre and matrix components makes it, even today, difficult to define a series of mechanical values for the fibre-reinforced composite, also because of the percentage of elements (fibre and matrix) of which it is composed. For this reason, the study and the values reported below refer to standard materials and elements used in structural applications, with reinforcing in glass, of which the acronym GFRP (Glass Fibre Reinforced Polymer). The average percentages in volume among matrix and fibre are 60% and 40% respectively, the characteristics in terms of average values of the composite material components are illustrated in Table 2.1

Tabella 2.1, Mechanical characteristics of Glass fibre and vinyl-ether matrix (mean values)

| | | | | | |
|----------------------|------------------|---------|--------------------------------|------------------------------------|----------------|
| Fibre | σ_t (MPa) | E (MPa) | Diameter (μm) | Density (g/cm^3) | Elongation (%) |
| E-Glass | 4350 | 72400 | 10 | 2.54 | 4.8 |
| Matrix | σ_t (MPa) | E (MPa) | Flexural elastic modulus (MPa) | Flexural tensile strength (MPa) | Elongation (%) |
| Vinyl-ether (980-35) | 87 | 3309 | 3379 | 149 | 4.2 |

In Table 2.2, for an “I” shape profile produced via pultrusion technology, the average mechanical reference values are reported.

Tabella 2.2, Mechanical characteristics of FRP pultruded structural materials (range and mean values)

| | | |
|--|---------------------|-----------------------------|
| Longitudinal tensile strength (sample profile) | | 200~500 MPa |
| Tensile elastic modulus (sample profile) | | 20000~30000 MPa |
| Flexural elastic modulus (sample profile) | | 15000~20000 MPa |
| Longitudinal elastic modulus (profile) | E_Z | 23000 MPa |
| Transversal elastic modulus (profile) | $E_X=E_Y$ | 8500 MPa |
| Transversal shear modulus (profile) | G_{XY} | 3455 MPa |
| Shear modulus (profile) | $G_{ZX}=G_{ZY}$ | 3000 MPa |
| Longitudinal Poisson's ratio | ν_{XY} | 0.23 |
| Transversal Poisson's ratio | $\nu_{ZX}=\nu_{ZY}$ | 0.09 |
| Material Density | γ | 1600~1800 kg/m ³ |
| Fiber volume ratio | | 40% |

Note: The subscripts regard the cross section configuration depicted in Figure 2.2.

By comparing Tables 2.1 and 2.2, it is possible to verify the variations in performance in the passage from components to fibre-reinforced composite material and from this to the structural element. The strong influence of the production technology on the mechanical performance of the material puts a relevant difference between the parameters evaluated on the material proofing and on the specimen of structural element. Figure 2.3 is showing the strain in the mat and in the roving fibers during a tension test on a 500x15x8mm proofing illustrated in the picture. Moreover, UNI EN 13706 code emphasizes this double approach to the mechanical characterization of FRP materials. Finally, the complete reversibility of the strain until load values next to failure has to be remarked.

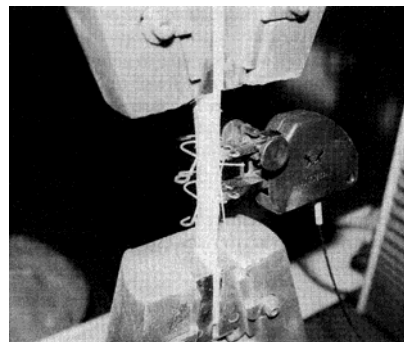
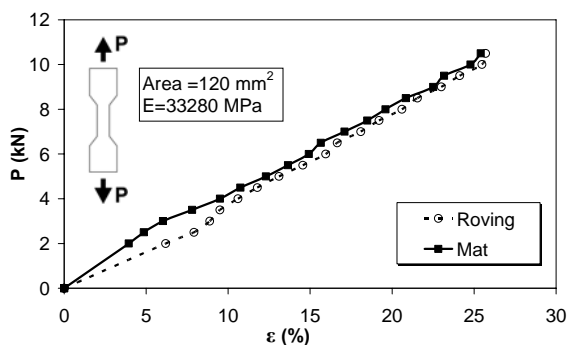


Figure 2.3, P- ϵ behaviour of mat and roving and detail of test (Russo 2007).

Experimental tests were carried out on a sample to determine the longitudinal elastic modulus under a tensile and compressive load, Figures 2.4.

It also should be noted that a GFRP composite has different values for the compressive and tensile moduli for the flange and the web, (Di Tommaso & Russo, 1998).

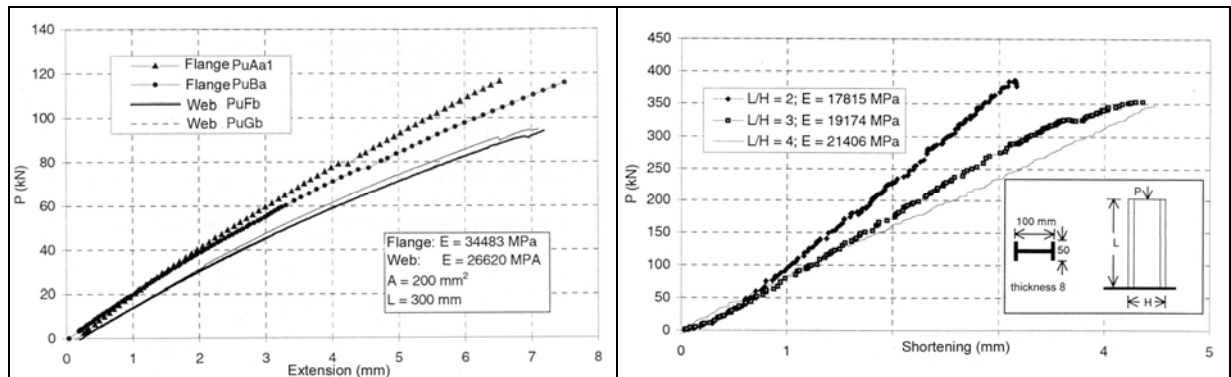


Figure 2.4, Modulus of elasticity in tension and compression for Flange and Web. GFRP sample.

2.3. Production technologies

Below are schematically described the main composite molding processes, for more details see <http://engineershandbook.com/MfgMethods/molding.htm>

2.3.1. Hand lay-up

Hand lay-up is the simplest and oldest open molding method of the composite fabrication processes. It is a low volume, labor intensive method suited especially for large components, such as boat hulls. Glass or other reinforcing mat or woven fabric or roving is positioned manually in the open mold, and resin is poured, brushed, or sprayed over and into the glass plies. Entrapped air is removed manually with squeegees or rollers to complete the laminates structure. Room temperature curing polyesters and epoxies are the most commonly used matrix resins. Curing is initiated by a catalyst in the resin system, which hardens the fiber reinforced resin composite without external heat. For a high quality part surface, a pigmented gel coat is first applied to the mold surface.

2.3.2. Vacuum-Assisted Resin Transfer Molding

During this process the reinforcing and fibre are combined in a uniformly heated mould (temperature varying from 90°C to 150°C); the resin is preheated in a separate container until it becomes plasticized so as to facilitate injection into the mould where the fibrous reinforcing is already at the pre-form state. Completion of the process occurs with polymerisation which allows the forming of the final product.

2.3.3. Vacuum Bag Molding

Vacuum bag molding, a refinement of hand lay-up, uses a vacuum to eliminate entrapped air and excess resin. After the lay-up is fabricated on either a male or female mold from precut plies of glass mat or fabric and resin, a nonadhering film of polyvinyl alcohol or nylon is placed over the lay-up and sealed at the mold flange. A vacuum is drawn on the bag formed by the film while the composite is cured at room or high temperatures. Compared to hand lay-up, the vacuum method provides higher reinforcement concentrations, better adhesion between layers, and more control over resin/glass ratios. Advanced composite parts utilize this method with preimpregnated fabrics rather than wet lay-up materials and require oven or autoclave cures.

2.3.4. Autoclave Molding

Autoclave molding is a modification of pressure-bag and vacuum-bag molding. This advanced composite process produces denser, void free moldings because higher heat and pressure are used for curing. It is widely used in the aerospace industry to fabricate high strength/weight ratio parts from preimpregnated high strength fibers for aircraft, spacecraft and missiles. Autoclaves are essentially heated pressure vessels usually equipped with vacuum systems into which the bagged lay-up on the mold is taken for the cure cycle. Curing pressures are generally in the range of 50 to 100 psi and cure cycles normally involve many hours. The method accommodates higher temperature matrix resins such as epoxies, having higher properties than conventional resins. Autoclave size limits part size.

2.3.5. Filament Winding

Filament winding consists of winding resin impregnated fibers or rovings of glass, aramid, or carbon on a rotating mandrel in predetermined patterns. The method provides the greatest control over fiber placement and uniformity of structure. In the wet method, the fiber picks up the low viscosity resin either by passing through a trough or from a metered application system. In the dry method, the reinforcement is in the preimpregnated form. After the layers are wound, the component is cured and removed from the mandrel. Traditionally used to produce pressure vessels, rocket motor cases, tanks, ducting, golf club shafts and fishing rods, filament winding technology has been expanded, and noncylindrical, nonspherical composite parts are now commonplace. Typical thermoset resins used in filament wound parts include polyesters, vinyl esters, epoxies, and phenolics.

2.3.6. Pultrusion

Pultrusion is a continuous method of manufacturing various reinforced plastic shapes of uniform cross sections. Glass reinforcements, such as unidirectional rovings or multi-directional glass fiber mat, are guided through a liquid resin bath to thoroughly wet every fiber. The reinforcements are then guided and formed, or shaped, into the profile to be produced before entering a die. As the material progresses through the heated die, which is shaped to match the design profile, the resin changes from a liquid to a gel, and finally, into a cured, rigid plastic. A pulling device grips the cured material and literally pulls the material through the die. Hence, the name pultrusion. It is the power source for the process. After the product passes through the puller, it is sawed into desired lengths. Although pultrusion is ideally suited for custom shapes, some standard products include rods, bars, angles, channels, and I-beams.

2.4. Chapter overview

The physical-mechanical characteristics of the composite structural elements produced via pultrusion technology define a specific and exclusive field of application.

Despite the fact that the standard production of the GFRP profiles follows the shapes of steel profiles, the composite material does not even enter into competition with this latter thanks to the

characteristics which set it apart and underline its excellence. The knowledge of the GFRP material permits the use of an adequate analytic approach which takes into account the peculiarity of the structural composite during the design phase. The possibility of achieving systems produced with different technologies constitutes a promising field of development which can compensate the negative and limiting aspects of the pultruded profiles.

References

Composite molding processes, <http://engineershandbook.com/MfgMethods/molding.htm>

Di Tommaso, A. and Russo, S., *Indagine sperimente sul comportamento a collasso di travi pultruse di luce variabile*, in Proc. 12th Congresso CTE, 1988. (in Italian)

Russo, S., *Strutture in composito – Sperimentazione, teoria e applicazioni*, Ulrico Hoepli Editore S.p.A., Milan, 2007. (In Italian) ISBN 978-88-203-3643-1

3. STATE OF THE ART

This chapter analyses the documentation present in literature in order to identify the most significant studies which put into the best possible context the level of knowledge obtained of the material, of the elements and of the composite structural systems. An important instrument used in this analysis is constituted by the complete and up-to-date database of Dr. J.T. Mottram (http://www2.warwick.ac.uk/fac/sci/eng/staff/jtm/pfrp_01_12_08.pdf).

With regards to the mechanical characterisation of the material, there are the supporting regulations UNI EN 13706 (2003) and the corresponding ASTM American regulations. In the detail ASTM D638 (2008), the reference to the compression test is the ASTM D695 regulation which results in being particularly effective in determining the behaviour of the fibre-matrix interface. For the flexural test, the relevant regulation is the ASTM D790 (three-point flexural test), while, for the resilience test, the relevant regulation is the ASTM D3846. The regulation which allows the determination of shear strength between fibre laminates and the matrix laminates is the ASTM D2344, further indications are to be found in the ASTM D3846 regulation. Important evaluations regarding the twisting response of the GRP pultruded elements is provided by the study carried out by Turvey (1998). With regards to the quality of the pultruded material, the non-destructive tests carried out by Agarwal and Broutman (1990) and Littles et al. (1998) give important information on homogeneity, imperfections, and on the principal mechanical parameters. Another parameter which qualifies the composite profile is the percentage of fibre present which can be determined via ISO 1172.

In Italy, an important instrument of support for the design, execution and control of executed structures with pultruded profiles in fibre-reinforced composite material is the technical document CNR DT 205/2007 (2007). In the international field, the technical documents and the handbooks are reference points which constitute a complete and reliable support for the knowledge and correct use of the pultruded structural element (ASCE 1984-1985, MMFG 1990, Fiberline 1999, Eurocomp 1996).

With regards to the general bibliography of studies conducted on the methodology and use of innovative technology, the themes of various principal reference points present in literature are

mentioned once again. Among the primary contributions are the works of Starr (1983), Liskey (1985, 1991) and Harvey (1993) who illustrate the first GFRP production, Aberfeldy footbridge. In the wake of these initial researches are the works of Holloway (1986, 1989), Ballinger (1990, 1991), Green et al. (1994), Mosallam (1993), Mottram (1995), Quinn (1995), Rizkalla and Abdelrahman (1995), Tarricone (1995), Seible and Karbhari (1996), GangaRao et al. (1996), Maji et al. (1997), Zureick (1998), Bakis et al. (2002) and Russo (2007). Ye et al. (2004) produce the first works on the state of FRP art in China. With reference to the general study, the works by Barbero (1999) introduces the composite material with in-depth detail on the beam, panel and shell elements. More specific attention to the field of civil engineering is reserved for the works of Holloway (1993) and more recently, that of Bank (2006). Librescu and Song (2006) produce interesting works on the narrow wall composite elements with specific and innovative study on the behaviour of FRP elements in the free vibration field.

From the first examples up to the present day, an important field of application of the composite structural elements regards the production of bridges, bridge framework and infrastructure in general, Zureick (1995), Harik (1996), Karbhari (1997), Thorning and Knudsen (1998), GangaRao and Craigo (1999), Lopez-Anido and Karbhari (2000), Keller (2003), Holloway and Hackman (2004), Knippers (2005), Bell (2007).

Among the most recent works, Kratmann (2008) analyses the state of production and the application of composite profiles.

Concerning the design approach, one of the relevant reference points is constituted by the works of Keller (2004). A recent study on the approach via analysis of finite elements of composite materials has been completed by Barbero (2007).

References

Agarwal, B.D., Broutman, L.J., *Analysis and performance of fiber Composites*, Second Edition, John Wiley & Sons, Inc., 1990.

Structural plastics design manual, Volume 1 and 2, ASCE manuals and reports on engineering practice, No. 63, ASCE NY, 1984.

Standard Test Method for Tensile Properties of Plastics, D638, ASTM West Conshohocken, Pa, 2008.

Standard test method for compressive properties of rigid plastics, D695, ASTM West Conshohocken, Pa, 2008

Standard Test Methods for Flexural Properties of Unreinforced and Reinforced Plastics and Electrical Insulating Materials, D790, ASTM West Conshohocken, Pa, 2007.

Standard Test Method for Short-Beam Strength of Polymer Matrix Composite Materials and Their Laminates, D2344, ASTM West Conshohocken, Pa, 2006.

Standard Test Method for In-Plane Shear Strength of Reinforced Plastics, D3846, ASTM West Conshohocken, Pa, 2008.

Bakis, C.E., Bank, L.C., Brown, V., Cosenza, E., Davalos, J., Lesko, J.J., Machida, A., Rizkalla, S. and Triantafillou, T., *FRP composites in construction state-of-the-art review*, 150th Anniversary Paper, J. Composites for Construction, 6 2, 2002.

Ballinger, C., *Structural FRP composites*, Civil Engrg., ASCE, 60 7,1990.

Ballinger, C.A., *Development of composites for civil engineers*, in Proc. Specialty Conf. Materials Engrg. -Advanced Composite Materials in Civil Engrg., Structures Division ASCE, ASCE NY, 1991.

Bank, L.C., *Composites for construction - Structural design with FRP materials*, John Wiley & Sons, New Jersey, 2006. ISBN 978-0471-68126-7

Barbero, E.J., *Introduction to composite materials design*, Taylor and Francis, Philadelphia, 1999. ISBN 1560327014

- Barbero, E. J., *Finite Element Analysis of Composite Materials*, Taylor & Francis Group, Boca Raton, FL, 2007.
- Bell, B., *The use of advanced composites in railway civil engineering in the UK*, in Proc. 3rd Inter. Conf. Advanced Composites in Construction - ACIC 2007, York Publishing Services, York, 2007.
- CNR-DT 205/2007 (2008). *Istruzioni per la Progettazione, l'Esecuzione ed il Controllo di Strutture realizzate con Profili Sottili Pultrusi di Materiale Composito Fibrorinforzato (FRP)*, Roma CNR, CNR-DT 205/2007.
- Structural Design of Polymer Composites -EUROCOMP Design Code and Handbook*, Edited by John L. Clarke, E. & F. N. Spon, London, 1996.
- Fiberline Design Manual for Structural Profiles in Composite Materials*, 1995.
- GangaRao, H.V.S., Lopez-Anido, R., Williams, D.L. and Winegardner, T., *Construction of a multi-cellular fiber reinforced plastic building*, in Proc. Composite Institute's 51st Annual Conf. and Exposition, SPI, 1996.
- GangaRao, H. and Craigo, C.A., *Fiber-reinforced composite bridge decks in the USA*, Structural Engineering Inter. (SEI), J. Inter. Association for Bridges and Structural Engineering (IABSE), 9 4, 1999.
- Green, A., Bisarnsin, T. and Love, E.A., *Pultruded reinforced-plastics for civil engineering structural applications*, J. Reinforced Plastics and Composites, 13 10, 1994.
- Harik, I.E., Szak, P.J., Robson, B.N., Hopwood, T.H., Witcher, D. and Brailsford, B., *Hybrid composite I-girder pedestrian bridge*, in Proc. 28th Inter. SAMPE Technical Conf. - Technology Transfer in a Global Community, SAMPE, 1996.
- Harvey, W.J., *A reinforced plastic footbridge, Aberfeldy, UK*, Structural Engineering Inter., 4, 1993.
- Hollaway, L., *Pultrusion*, Chapt. 1., in *Developments in Plastics Technology*, 3rd Ed., Whelan, A., and Craft, J.L. (Ed.), Elsevier Applied Science Publishers, London, 1986.
- Hollaway, L., *Pultrusion*, RAPRA Review Report, Pergamon Press, Oxford, 1989.
- Hollaway, L., *Polymer composites for civil and structural engineering*, Blackie Academic & Prof., London, 1993.

Hollaway, L.C. and Hackman, I., *Strengths and limitations of fiber reinforced polymers in the civil infrastructure, material advances and the influence on present and future developments*, in Proc. 2nd Inter. Conf. FRP Composites in Civil Engineering – CICE 2004, Taylor and Francis Group, London, 2004.

Karbhari, V., Seible, F., Hegemeir, G. and Zhao, L., *Fiber reinforced composite decks for infrastructure renewal – results and issues*, in Proc. Inter. Composite Expo 1997, SPI, 1997.

Textile-glass-reinforced plastics -- Prepregs, moulding compounds and laminates -- Determination of the textile-glass and mineral-filler content -- Calcination methods, ISO 1172:1996.

Keller, T., *Use of fibre reinforced polymers in bridge construction*, Structural Engineering Documents 7, Inter. Association for Bridges and Structural Engineering (IABSE-AIPC-IVBH), Zurich, 2003.

Keller, T., *Conceptual design of hybrid-FRP and all-FRP structures* Proc. 4th Inter. Conf. of Advanced Composite Materials in Bridges and Structures (ACMBS-IV), The Canadian Society for Civil Engineering, 2004.

Knippers, J., *Innovative design concepts for composite bridges in Germany – technology and aesthetics*, in Proc. COBRAE Conference 2005 – Bridge Engineering with Polymer Composites, COBRAE, Leusden, 2005.

Kratmann, K.K., Friis, H. H., Lilleheden, L. T. and Thorning, H., *Industrial production and application of composite profiles*, in Proc. 4th Inter. Conf. on FRP Composites in Civil Engineering (CICE2008), Empa, Duebendorf, 2008, ISBN 978-3-905594-50-8

Librescu, L., and Song, O., *Thin-Walled Composite Beams Theory and Application*, Published by Springer, Netherlands, 2006.

Liskey, K.A., *Pultruded fiberglass-reinforced plastics (FRP): A structural solution for corrosive environments*, Chemical Engrg., 92 23, 1985.

Liskey, K., *Structural applications of pultruded composite products*, in, Proc. ASCE Specialty Conf. - Advanced Composite Materials in Civil Engrg. Structures, Materials Engrg. Division, ASCE NY, 1991, 182-193.

Lopez-Anido, R. and Karbhari, V. M., Chapter 2 - *Fiber reinforced composites in civil infrastructure*, in Emerging Materials for Civil Infrastructure - State of the Art, Eds. Lopez-Anido and Naik, ASCE Press, Reston, VA, 2000.

Littles, J.W., Jacobs, L.J., Zureick, A.H., *Ultrasonic Techniques to Characterize Pultruded Composite Members*, Journal of Composites for Construction, August 1998.

Maji, A.K., Acree, R., Satathi, D. and Donnelly, K., *Evaluation of pultruded FRP composites for structural applications*, J. Materials Civil Engineering, 9 3, 1997.

MMFG, *Design Manual*, Morrison Molded Fiber Glass Company, Bristol, Virginia, 1990.

Mosallam, A.S., *Pultruded Composites: Materials for the 21st Century*, in Proc. Plastics Composites for 21st Century Infrastructure Session, 1993 Annual Convention & Exposition, ASCE, 1993 NY.

Mottram, J.T., *Pultruded profiles in construction: A review*, in Proc. 1st Israeli Workshop on Composite Materials for Civil Engineering Construction, NBRI, 1995.

Quinn, J.A., *The use of pultruded profiles in a structural application*, in Hollaway, L. (Ed.), 'BPF Handbook of Polymer Composites for Engineers,' Woodhead Publishing Ltd., 1994.

Rizkalla, S.H. and Abdelrahman, A.A., *FRP for the 21st century*, in Proc. Inter. Conf. on Fibre Reinforced Structural Plastics in Civil Engineering, Tata McGraw-Hill Publ. Co. Ltd., 1995.

Russo, S., *Strutture in composito – Sperimentazione, teoria e applicazioni*, Ulrico Hoepli Editore S.p.A., Milan, 2007. (In Italian) ISBN 978-88-203-3643-1

Seible, F. and Karbhari, V., *Advanced composites build on success*, Civil Engineering, ASCE, 66 8, 1996.

Starr, T.F. *Structural applications for pultruded profiles*, in Proc. Composite Structures 2, Inter. Conf. on Comp. Struct., Elsevier Applied Science Publishers, 1983.

Tarricone, P., *Composite sketch*, Civil Engineering, ASCE. 65 5, 1995.

Thorning, H. and Knudsen, E., *Design of the railway-crossing bridge at Kolding, Denmark*, in Proc. 4th EPTA World Pultrusion Conf., European Pultrusion Technology Association, The Netherlands, 1998.

Turvey, G.J., *Torsion tests on pultruded GRP sheets*, Composites Science and Technology, 58 8, 1998.

UNI EN 13706-3, *Compositi plastici rinforzati. Specifiche per profili pultrusi, requisiti specifici*, Marzo 2003.

Ye, L.P., Feng, P., Lu, X.Z., Qian, P., Huang, Y.L., Hu, W.H., Yue, Q.R., Yang, Y.X., Tan, Z, Yang, T., Zhang, N. and Li, R., *FRP in China: the state of FRP research, design guidelines and application in construction*, in Proc. 2nd Inter. Conf. FRP Composites in Civil Engineering – CICE 2004, Taylor and Francis Group, London, 2004.

Zureick, A.H., Shih, B. and Munley, E., *Fiber-reinforced polymeric bridge decks*, Structural Engineering Review, 7 3, 1995.

Zureick, A.H., *FRP pultruded structural shapes*, Progress in Structural Engineering and Materials, 1 2, 1998.

4. APPLICATIONS OF FRP STRUCTURAL ELEMENTS

The physical-mechanical characteristics of the composite material and thus GFRP structural elements define the specific fields of application both for the execution of structural systems all-FRP and for the use of single structural elements – mono-dimensional (beams) and bi-dimensional (panels) – in combination with other materials.

The structural typology that, at the present time, represents the main use of pultruded elements is the bridge, suitable for pedestrians or for vehicles, both for the new construction and for the reinforcement of existing constructions; the durability and the low dead load combined with a good structural performance of the composite material constitutes the excellence of this new technology and is the reason for its widespread use in the construction of bridges. Likewise, it provides functional and aesthetic solutions regarding multi-floor buildings, over elevation, roof and temporary structures.

4.1. FRP elements for new construction

The realizations illustrated below define the panorama of solutions built in FRP structural elements. This chapter not considers only the structure in GFRP pultruded elements but also the solutions built through others technologies which can be interesting for possible future researches.

In this classification of the principal characteristics of FRP applications in the structural engineering field, certain examples are fixed to define the evolutionary process and the important phases of changing of the different technologies of FRP materials. The first realization that introduced the composite material as a structural element in the civil engineering field dates back to around 25 years ago and refers to a cable-stayed footbridge, the Aberfeldy footbridge of 1992. The principal aspect of the all-Composite construction, with its favourable relationship between low dead load and strength, is evident in the Bonds Mill Lift bridge of 1995. A particularly interesting application from an ideational point of view and under the profile of scientific research regarding a two-span removable footbridge; the different solution adopted for the realisation of connection of the two parts, bonded and bolted, has allowed the analysis and

comparison of diverse structural behaviour both locally and globally, Pontresina footbridge of 1997. Such research is particularly interesting for the study of the long-term structural response, (Keller et al. 2007). The example of the use of GFRP profiles in the construction of buildings is represented by the Eyecatcher office building of 1999. The examples of applications which refer to structures in composite produced with technologies different from that of the pultrusion process are also illustrated (Tromp 2008, Toni 2005).

From the general analysis of the selected applications, the ease of assembly and installation of the structures, entirely in composite, is evident; the low dead load of FRP material allows the design of the support structures (bridge abutments, foundations, support frameworks) normally in traditional materials, with reduced dimensions and with a consequential saving on materials and manpower.

Illustrated below, in the form of analytic Tables, are the most significant All-Composite structures.



Aberfeldy Footbridge, Scotland, 1992

- cable-stayed footbridge;
- total length= 113 m (center span = 63 m)
- width = 2.12 m; h = 0.76 m;
- pylons height= 17.5 m
- dead load= deck 16000kg, pylons each 2500kg
- live load= pedestrian 10kN/m
- FRP cables= length from 13 to 31m
- deck and pylon have been produce by “ACCS-FRP system Maunsell”



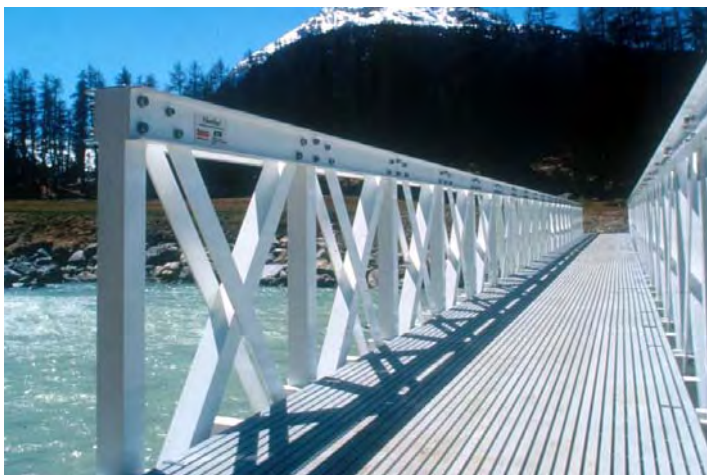
Bonds Mill Lift bridge, United Kingdom, 1995

- lift bridge
- span= 8 m;
- width= 4.5 m;
- dead load= 4500 Kg
- live load=trucks up to 40t, 10t wheel load
- first FRP driveway bridge;
- realized by “ACCS-FRP system Maunsell”.



Kolding Bridge, Denmark, 1997

- cable stayed bridge
- bolted GFRP pultruded profiles
- length= 40.3m
- span= 27 and 13m;
- width= 3.2m
- pylon height=18.5m
- girder depth= 1.5m
- total dead load=12000kg
- live load= pedestrians 5kN/m², vehicle 50kN



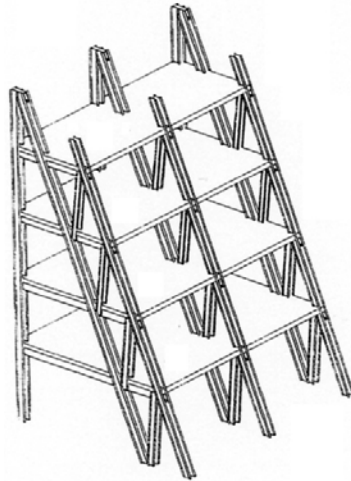
Pontresina Bridge, Switzerland, 1997

- two span truss footbridge
- one span realized by glued connections and one by bolted connections
- removable
- length= 25.5m
- span= 2x12.5m
- dead load= 2x1650kg
- live load= 5kN/m²



Expo Lisbon, Portugal, 1998

-realized by GFRP pultruded profiles with open cross section, the structural element are connected by steel bolts;



Eyecatcher, Basel, Switzerland, 1999

-5 floors building;
 -rectangular plan 10x12m;
 -total high is equal to 15m;
 -bearing structure has been realized by beams and columns GFRP profiles with respectively "I" and "C" cross section shapes;
 -wall plug is made by GFRP sandwich panels;
 -bolted or boned links.



Halgavor Bridge, Cornwall, United Kingdom, 2001

-it is constructed in three parts, 8.5x2m; the main span 32m long; the bridge is 4m wide;
 -bridge deck is of sandwich construction with girder section hand laminated along with the internal structure;
 -the span is suspended from steel masts and suspension cables attached to steel parapet posts bolted to the deck structure.



West Mill Bridge, Oxfordshire, United Kingdom, 2002

- span 10m, width 6.8m;
- total weight 37 t, the load-carrying and the bridge deck only weighs 12t;
- weight of bridge deck: 100kg/m²;
- Fiberline construction profiles in plastic composites were used for the load-carrying beams, the side panelling as well as the bridge deck itself; square profiles reinforced by carbon fibres used for load-carrying beams.



Bridge in Klipphausen, Dresden, German, 2002

- the bridge is built entirely of GRP profiles, and has the same load-carrying capacity as similar bridges in steel or concrete;
- the bridge was secured to the foundation by bolts.



The Staten Island September 11 Memorial, New York, USA, 2003

- dimensions of each panel: 8x4m;
- high-strength composite of fiberglass, foam core, and vinyl ester resin (FRP).
- the walls were prefabricated.



Pedestrian Cycle Footbridge, Pitigliano, Grosseto, Italy, 2004

- the bearing structure has been realized by two longitudinal box girder linked by transversal beams, braced, that support the deck.
- the assembling phase in construction site regards all structure with the exception of longitudinal box girder.
- self weight of one longitudinal beam: 610 kg;



Lleida Pedestrian Footbridge, Lleida, Spain, 2004

- dimensions: 38m span by 3m wide;
- bolts and brackets stainless steel;
- stainless steel cable diagonal elements;
- mortar of sand and resin embedded at the end of vertical elements to avoid the local buckling;



Chertanovo Pedestrian Bridge, 2004

- length= 41.4 m; width = 3m;
- total weight= 11.4t;
- the pultruded profiles are attached by using stainless steel brackets and bolts;
- the stair includes three types of pultruded profiles which are fastened by zinc-plated bolts;
- the upper surface of the deck is coated with a specially developed polymer-concrete coating;



Spacebox, Delft, The Netherlands, 2004

- the unit box = 6.5x3m;
- volume = 42m³;
- the unit is composed of 5 pre-molded components made of composite;
- hot-galvanised steel columns which are intended to carry the load of stacked units are integrated in the side walls;
- the units are constructed by sandwiching 88 mm wall and roof panels by way of a molding and vacuum-forming process;
- weight= 2500kg/box



Center Conference, Badajoz, Spain, 2005

- a cylindrical lattice of fiberglass-reinforced polyester-resin tubes encircles a drum clad in translucent Plexiglas tubes over clear glass panes;



Road Bridge, Cantabrico, Spain, 2005

- dimensions: 46m in length and 8.1m in width;
- the composite elements are three parallel spans of 0.8m deep hollow trapezoidal section (uni-directional, bi-axial carbon fibre, pre-impregnated with a special epoxy resin and with a polymer matrix);
- the low weight composite structure (100 kg/m supporting 2500kg/m of concrete road deck);



Pescara court, Pescara, Italy, 2006

-the roof has been realized by sandwich panels and profile with "I" shape; the panels are produced by two external FRP sheets with expanded polyurethane core;
The "I" shape members are GFRP pultruded profiles.



Mount Pleasant Bridge, 2006

-replacement of the old four span with a two span structure incorporated the innovative use of Fibre Reinforced Polymer (FRP), "plastic", deck units with steel beams and removed the requirement for verge piers;
-construction of new FRP and steel beam bridge deck;



Auxiliary floor, Verona, Italy, 2006

-double frame with four and two vertical "I" (200x100x10) GFRP profiles supports, through the steel cables, the auxiliary deck.
-the deck is realized by coupled "I" GFRP profiles that together to individual "I" profiles form a structural grid; for all joints have been used the steel bolts and flanges. The deck is realized by self bearing panels with a capacity equal to 250kg/m².
-the backstays are the steel cable of 6mm of diameter.



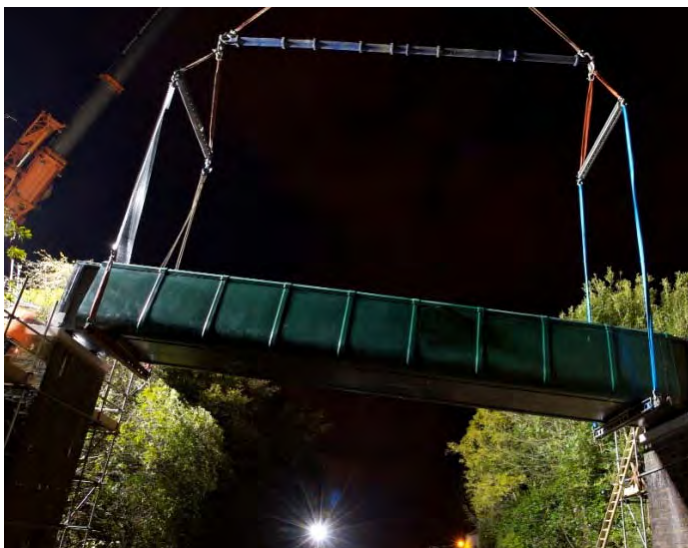
Stanislas Bridge, Delft, The Netherlands, 2007

- total length=44m;
- the biggest span of the bridge is 13.5m and the width is 1.5m;
- the load-bearing structure will consist of 2 segments of 22m of a glass fibre reinforced vinylester, U-shaped girder and a deck, both manufactured with vacuum infusion, the core competence of Lightweight Structures B.V. and bonded by an adhesive;



Dronten Bridge, Dronten, The Netherlands, 2007

- dimensions: 24.5x5m;
- weight bridge: 13.00kg;
- material: carbon fiber;



St. Austell railway Bridge, Cornwall, United Kingdom, 2007

- the bridge is made up of three sections – two six metre side span, each weighing two tones, and central 14m span weighing only five tones;
- the structure comprises pultruded FRP Advanced Composite Construction System in combination with moulded exterior panels and internal liner anti vandal plates;
- each bridge unit has a total of 27 ACCS toggle joints to make up each of the assemblies;



Metro Station, Copenhagen, Denmark, 2008

- the roof of the Lindevang Metro Station in Copenhagen is 60m long and 7.5m;
- the roof is a one-piece construction in plastic composites;
- the roof is constructed by means of Fiberline planks mounted on a steel frame. The roof hangs on wires between two pylons at each end. Fiberline supplied the roof in seven sections which were assembled and glued on site;



Friedberg bridge, Friedberg, Germany, 2008

- The 27 metre long bridge comprises two steel beams covered by an innovative multi-cellular GRP deck made of ASSET profiles from Fiberline Composites

4.2. GFRP pultruded elements for historical buildings conservation

The characteristics of the composite material - such as the versatility, due to the possibility of controlling and defining the structural performance during the design phase, the durability regarding the aggressive external agents together with the benefit of low dead load - suggest interesting possibilities of the FRP elements as the structural reinforcement, functional and the seismic adjustment.

The characteristics of FRP structural material allow an approach to the historical monuments reversible, durable, light and not intrusive; the design of an independent and recognizable structure will become an active collaboration action with the historical building, respecting the esthetic uniqueness and the primary structural conception considering always the historical building as *unicum*.

The two main topics of the structural reinforcement approach of monumental heritage are:

- The scientific knowledge of the historical building considered as *unicum* not repeatable;
- The design of structural rehabilitation must have a scientific approach to reduce the new structure and to find a structural, functional and esthetic collaboration with a historical building.

The approach of structural rehabilitation must develop the previous assertions through the following topics:

- Conservation and structural rehabilitation of architectural and environmental heritage to reduce the new structures;
- To respect the natural changes of the material characteristics;
- To respect the original structural configuration;
- To design the recognizable and reversible solution to collaborate with the historical building;
- Durability of the technologies and of the materials used for the conservation.

This goal defines the using field of GFRP structural elements.

Below are some examples achieved via the interaction between FRP elements, the structural systems and the traditional construction with a brief mention of further practical possibilities.

4.2.1. Auxiliary floor

The execution of the auxiliary floor in “Cogollo” house, better known as “Casa del Palladio”, was requested for functional motives in order to increase the useful surface area. During the design phase, given the historical-cultural context, two important conditions imposed by the purchaser and local council were respected: the low dead load of the new installation and its removability. The technology employed best responds to the requirements via a lightweight, reversible solution, thus non-invasive. The images in Figure 4.1 show the executive assembly phase and also images of the complete and installed auxiliary floor. The connection elements between GFRP profiles, the bolts and the braces are in steel; the auxiliary floor was constructed with 5cm thick multilayer wooden panels.

With the aim of dynamic identifying of the three-dimensional framework, tests were conducted in the free vibration field, described and analysed in detail in chapter 5.3.

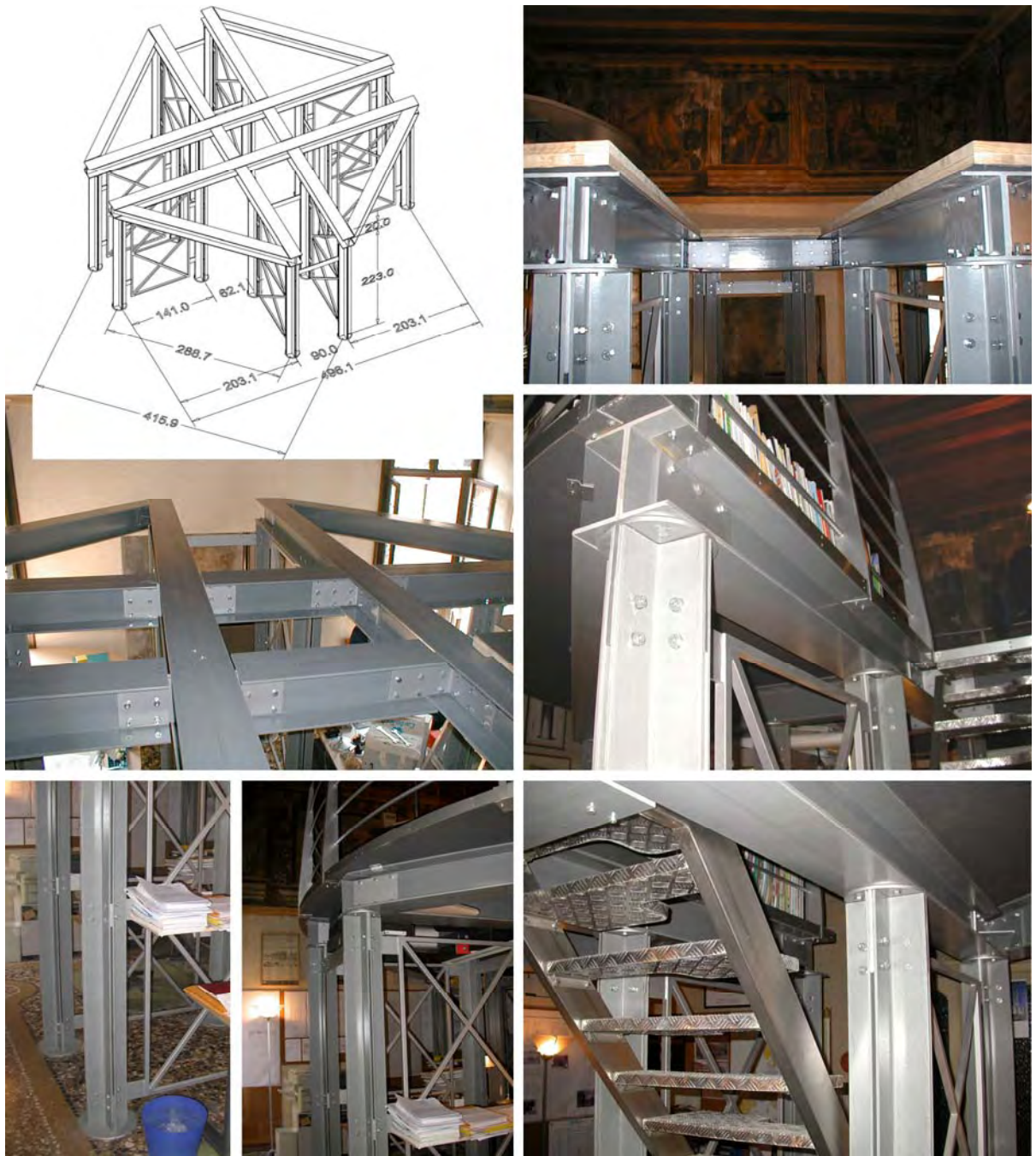


Figure 4.1, Assonometric view (cm dimension) and general views

4.2.2. Reinforcement of wood deck

The study by Borri and Corradi (2004), described synthetically in this chapter, concerns the so-called parallel reinforcement of a wooden deck; the proposed solution permits the increment of the lever in the internal actions of the mixed cross section of the wooden beam – GFRP profile, with consequent displacement of the neutral axis and reduction of compression and tension stress that, with this new configuration, concern respectively the pultruded profile and the wooden beam. The GFRP profile is therefore interested by compression actions with stress state still contained, Figure 4.2.

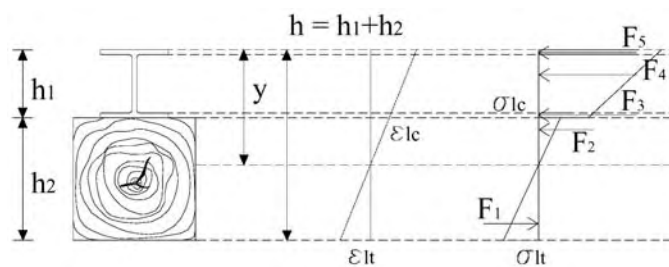


Figure 4.2, Cross-section analysis

The comparison between the experimental tests of the mono-dimensional Wood-GFRP mixed cross section elements, (Borri and Corradi 2004) is synthetically illustrated in Figure 4.3.

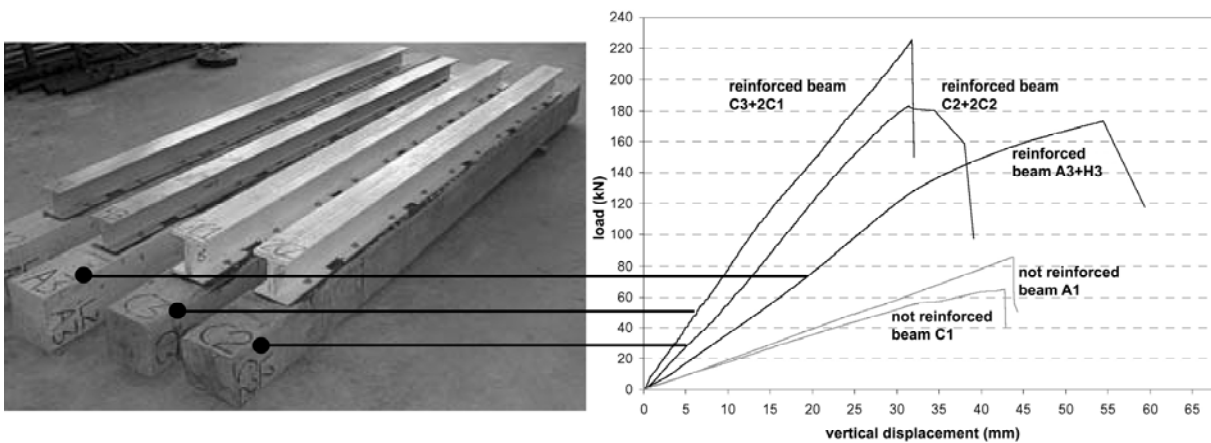


Figure 4.3, Comparison of structural behavior

In detail, the reinforced beams are constituted by wood beams and GFRP open cross section profiles with wide flanges for the configurations A3+H3 and composite coupled “C” shape for C3+2CI and C2+2C2.

The proposed solution has been applied to the wooden floor in the “Collicola” building in Spoleto in order to increase the global flexural stiffness. Figures 4.4 and 4.5 illustrate the execution phases – preparation of the structural resin and application and the insertion of fibreglass pegs to increase the adherence with the wooden beam – and the installation of the GFRP structural elements.



Figure 4.4, Executive and installation phases



Figure 4.5, detail of insertion of fiberglass pegs

Figure 4.6 shows the reduction of the vertical displacement – approx. 30% - of the adopted solution with respect to the initial configuration.

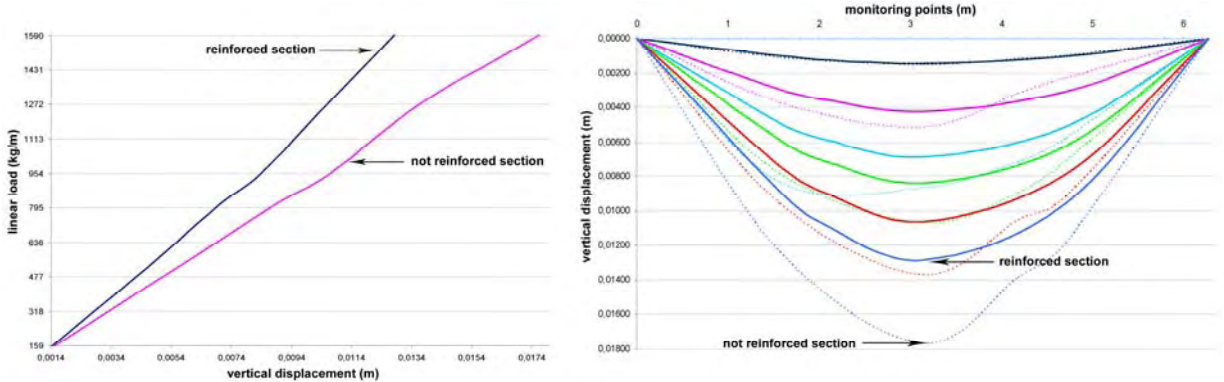


Figure 4.6, Structural behavior of deck

4.2.3. Reinforcement of old pedestrian bridge

The FRP material employment's in structural engineering field especially as reinforcement of existing structures made by R.C., steel, masonry or wood through bonding technology of carbon lamina or glass sheet glued with resin is by now really large and organized, besides with very good results in term of applications.

Starting from this point of view not less promising - especially for some solution in engineering field in both presence of static and seismic action, is the possibility to use FRP structural elements for news construction and local reinforcement. In the detail the global design approach with FRP beams is presented in function of possible application as flexural stiffness reinforcement of a deck in higher floor of a traditional framework-structure, as over-elevation on existing structures, or for new light structure as a pedestrian bridge.

In fact the analytical results starting by a recently application of pultruded FRP beams as reinforcement of existing pedestrian bridge are shown considering also all problems regarding the effective application of FRP reinforcement in presence of old materials.

In the detail the design by testing procedure realized through previously destructive testing carried out on three type of FRP beams were illustrated. In the first case has been considered a GFRP beams with open cross section – I shape – (Di Tommaso and Russo 1998), then the same beam with two different fibers reinforcement directly put inside, i.e. glass and carbon (Russo and Boscato 2003), and finally considering the GFRP beam damaged and reinforced through sheet carbon directly glued to the bottom, in this way increasing directly in situ the flexural stiffness (Russo 2007).

Therefore the comparison between the mechanical performance previously determined by destructive test on all type of FRP beams in function of the real application for reinforcement of the pedestrian bridge also with analytical evaluation of the global structural behavior is shown.

4.2.3.1. General description of pedestrian bridge structure

The pedestrian “Paludo” bridge is a typical historic (end of XIX century) building of Venice, with arc static scheme – 12.7 meters for the length and 3.25 meters for the width - built entirely

with iron and wood materials. As shown in Figures 4.7, 4.8 and 4.9 the bearing skill structure is constituted by two reticular longitudinal iron truss beams, located at the edge, and linked through iron transversal profiles; on the transversal iron profiles the traditional wood deck is placed.



Figure 4.7, Prospect view

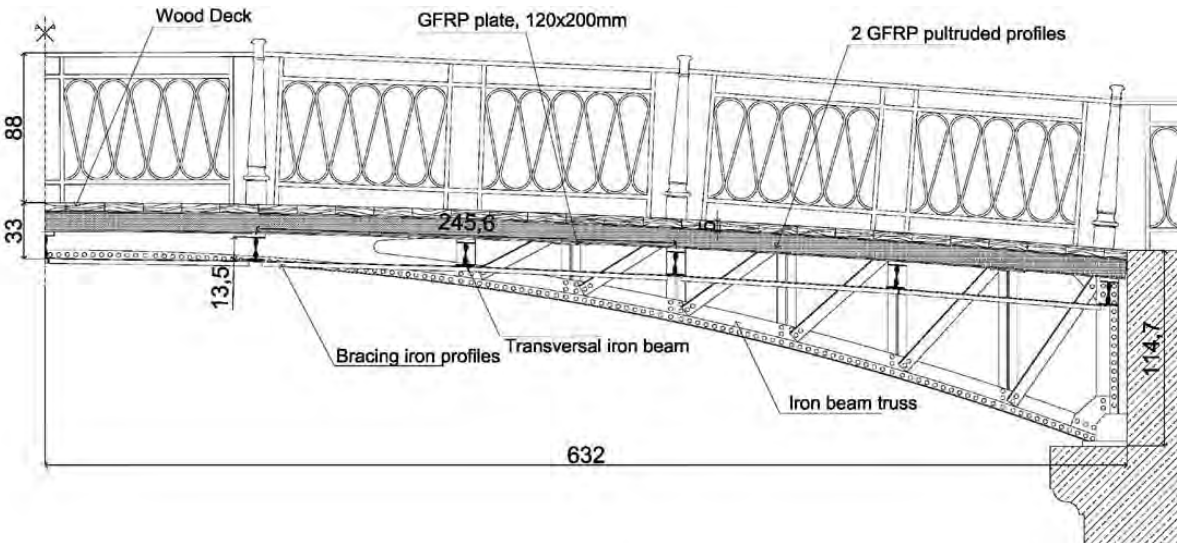


Figure 4.8, Longitudinal section

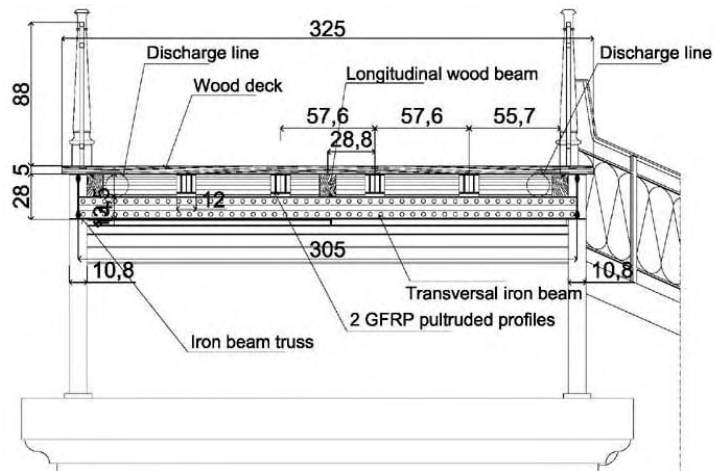


Figure 4.9, Transversal sections

Structural reinforcement and a global restoration was found necessary because of the serious deterioration; the aggressive environment conditions was the main cause of the local rust and reduction of mechanical characteristics in wood beams, Figures 4.10 and 4.11 (Boscato et al. 2006).



Figure 4.10, Global and local deterioration



Figure 4.11, Global and local deterioration

After the general restoration of the iron structure has been improve the flexural stiffness of the deck substituting the longitudinal wood beams with pultruded FRP profiles, see Figure 4.12.

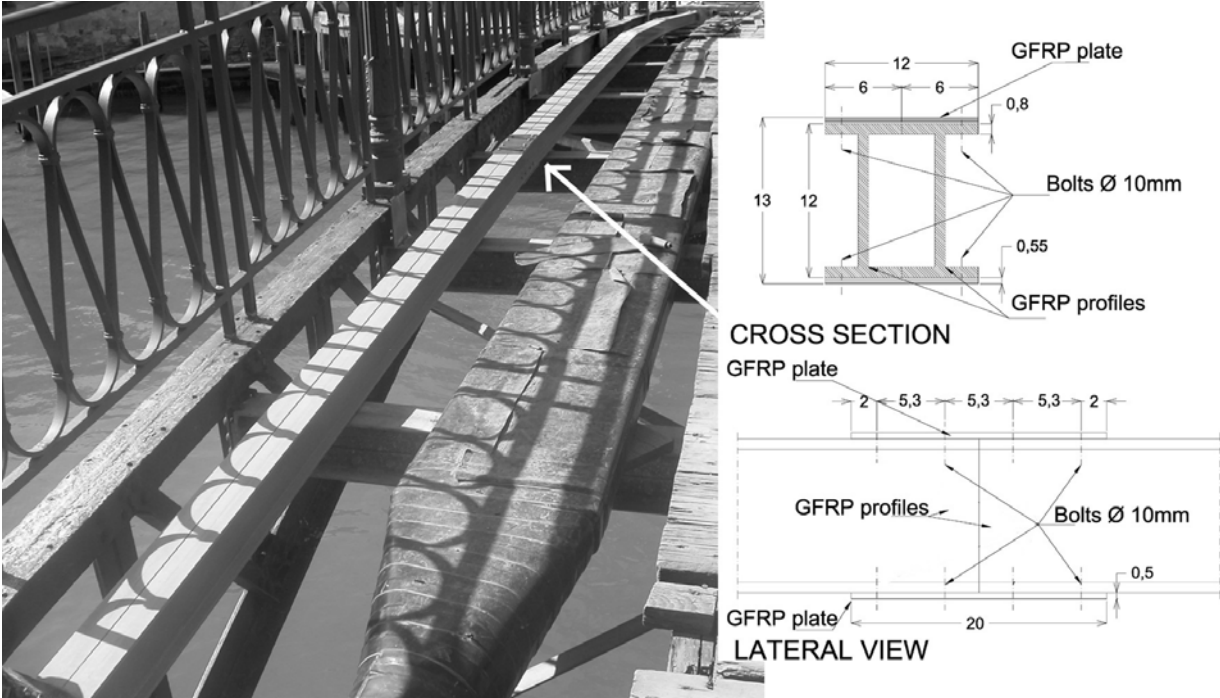


Figure 4.12, Installation of first GFRP profile and details of joint.

4.2.3.2. Structural design approach with FRP beams

To define the better solution for the footbridge structural re-habilitation a performance comparison on flexural behavior of two FRP profiles considered with same geometric slenderness, $\lambda = 10$ (length/height of profile) has been carry out.

In detail the FRP profiles reinforced with only glass fiber (GFRP) and hybrid profiles reinforced with glass and carbon fibers (GCFRP) has been analyzed.

For the pultruded GFRP profile the mechanical and physical characteristics are shown in Chapter 2. The hybrid profiles has been made with carbon and glass fibers embedded in vinilester matrix as whole pultruded structural elements considered for this application. In detail the carbon fiber is present only in both flanges, in compression and tensile zone, to increment the flexural stiffness.

The structural performance comparison between the analized profiles is shown in Figure 4.13.

In the same figure has been inserted the load-maximum deflection theoretical curve of linear elastic behavior of steel “I” profile (standard cross section 100x55x4.1x5.7mm); the steel profile have the same geometric slenderness of GFRP profile. This comparison highlights the stiffness difference between GFRP and steel profiles.

Altogether the chart of Figure 4.13 point out the good structural behavior of GFRP profile respect to hybrid profile GCFRP.

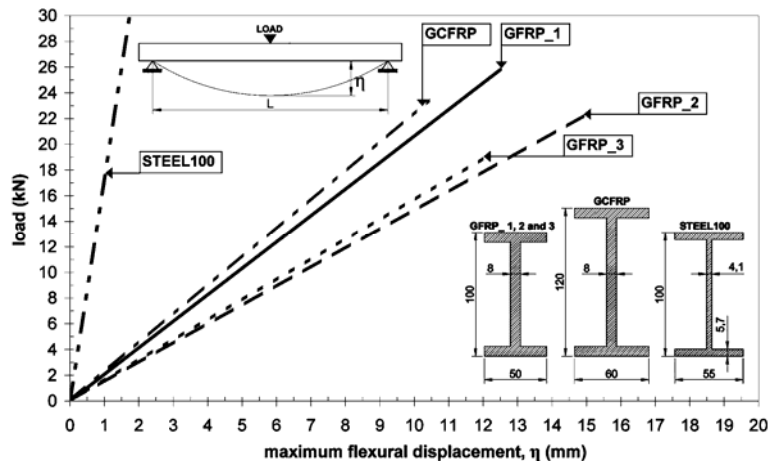


Figure 4.13, Maximum flexural displacement – load, $\lambda = 10$

The prevalence of longitudinal fibres constitutes a primary axis of mechanical stiffness, anyway the type of collapse highlights that the stratigraphy of profile is equal important in terms of contribute of strength.

As highlighted in the previous researches (Di Tommaso et al. 2002, Russo and Boscato 2003), in the short hybrid profiles the shear deformability is higher than GFRP structural elements.

For the beams with low parameter λ , in particular with $\lambda = 4$, the value of limit strength of GFRP profile is greater than 47% compared to hybrid profile with the same geometric slenderness ratio. The same trend, also with limited differences, is evident in the profile with $\lambda = 10$, Figure 4.13; the limit strength of GFRP_1 profile is, in fact, greater than 9% respect to hybrid profile.

Such difference is justified by the fact that for the short profiles the shear deformability effect is aggravate by the presence of different nature of the fibres – carbon and glass – and by the mechanical behaviour of interface between the carbon-glass fibres and fibre-matrix element that influences the mechanical characteristics of the material and the failure mode.

Considering the profiles with high value of slenderness parameter, the flexural strength of hybrid profiles is proportionally greater than GFRP profiles. As highlighted by Russo and Boscato (2003), for $\lambda = 21$ the hybrid profile shows a strength greater than 25% compared to GFRP profile. That is due to the presence of carbon fibre in the flanges, that with the high elastic modulus increase the flexural stiffness of hybrid profile.

4.2.3.3. Analytical design approach

The type of intervention adopted may be defined as “parallel” reinforcement, see Fig. 4.14 (Russo 2007).

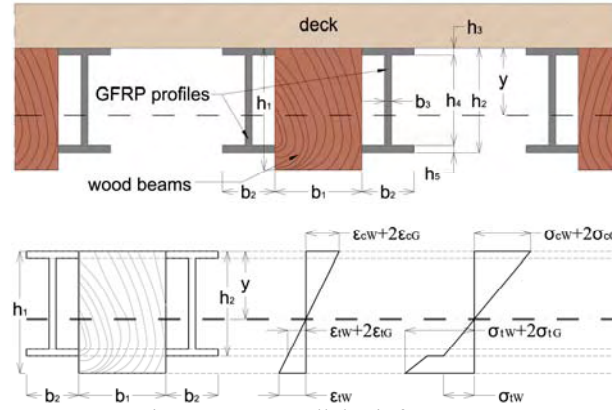


Figure 4.14, Parallel reinforcement

To optimize the analytical approach we have considered the linear-elastic behaviour for the GFRP pultruded elements and for the wood material the same assumptions but limited to the tensile behaviour. Following formulations, (4.1) and (4.2), show respectively the constitutive law for wood and GFRP

$$\begin{aligned}\sigma_{cW} &= E_W \cdot \varepsilon_{cW} \\ \sigma_{cW} &= \sigma_{c0} - m \cdot (\varepsilon_{cW} - \varepsilon_{cW0})\end{aligned}\quad (4.1)$$

$$\begin{aligned}\sigma_{cG-w} &= E_{G-w} \cdot \varepsilon_{cG-w} \\ \sigma_{cG-fl} &= E_{G-fl} \cdot \varepsilon_{cG-fl} \\ \sigma_{tG-w} &= E_{G-w} \cdot \varepsilon_{tG-w} \\ \sigma_{tG-fl} &= E_{G-fl} \cdot \varepsilon_{tG-fl}\end{aligned}\quad (4.2)$$

The following formulations – from (4.3) to (4.9) – show the analytical solutions given starting from the equilibrium between tensile and compression stresses applied to the diagrams in the hypothesis that the cross sections remain plan also during the deformation. So from equilibrium we will obtain the follow equation:

$$2F_{tG-w} + 2F_{tG-fl} + F_{tW} = 2F_{cG-w} + 2F_{cG-fl} + F_{cW} \quad (4.4)$$

And in compression zone:

$$F_{cG-w} = 2 \cdot \left(\frac{b_3 \cdot (y - h_3)}{2} \right) \cdot n \cdot \sigma_G \quad (4.5)$$

$$F_{cG-fl} = 2 \cdot \left(\frac{b_2 \cdot h_3}{2} \right) \cdot n \cdot \sigma_G \quad (4.6)$$

$$F_{cW} = \left(\frac{b_1 \cdot y}{2} \right) \cdot \sigma_{cW} \quad (4.7)$$

While in tensile zone:

$$F_{tG-w} = 2 \cdot \left(\frac{b_3 \cdot (h_3 + h_4 - y)}{2} \right) \cdot n \cdot \sigma_G \quad (4.8)$$

$$F_{tG-fl} = 2 \cdot \left(\frac{b_2 \cdot h_5}{2} \right) \cdot n \cdot \sigma_G \quad (4.9)$$

$$F_{tW} = \left(\frac{b_1 \cdot (h_1 - y)}{2} \right) \cdot \sigma_{tW} \quad (4.10)$$

Where y = neutral axis position; n_{WG} = homogenize ratio between materials elastics moduli, respectively GFRP profile with elastic modulus of Wood (4.11).

$$n_{WG} = \frac{E_{GFRP}}{E_{WOOD}} \quad (4.11)$$

Then, on the basis of this hypothesis we have calculated the neutral axis position starting from equation (4.4) and substituting from (4.5) to (4.10).

For the calculation of the moment of inertia J_x , we obtain:

$$J_x = \frac{b_1 \cdot (h_1)^3}{12} \quad (4.12)$$

$$J_x = J_W + n \cdot J_G + A_W \cdot \left(\frac{h_1}{2} - y\right)^2 + A_G \cdot n \cdot \left(y - \frac{h_2}{2}\right)^2 \quad (4.13)$$

For the calculation of the stress in compression and tensile zone we will have:

$$\sigma_{cW} = \frac{M \cdot (y)}{J_x} \quad (4.14)$$

for the scheme 1 and 2:

$$\sigma_{cG} = n \cdot \frac{M \cdot (y)}{J_x} \quad (4.15)$$

for the scheme 'type 0', the evaluation of tensile stresses gives:

$$\sigma_{tW} = \frac{M \cdot (h_1 - y)}{J_x} \quad (4.16)$$

for scheme 1 and 2:

$$\sigma_{cG} = n \cdot \frac{M \cdot (h_1 - y)}{J_x} \quad (4.17)$$

where M = maximum moment of beam with clamped-clamped static scheme with distributed load.

4.2.3.4. Structural performance

The global structural behavior of pedestrian bridge was investigated under the point of view of static action and dynamic response in the free vibrations field. In the first analysis, a uniform distributed static load equal to 400 kg/m^2 was considered; about the dynamic response, the frequencies of first modes of free vibrations were defined, during the changing of the acting load, to verify any resonance phenomenon.

The global structural analysis has been carry out in the linear elastic field by finite element method. This analysis has been developed considering the hypothesis of plan section conservation and the perfect bond between fiber and matrix.

4.2.3.4.1. Static behavior

The maximum deflection value equal to 6.2 mm was obtained by numerical modeling, considering that the admissible maximum deflections, $\eta_{\max} / L \leq 0.002$, is equal to 7.4mm. Such displacement is similar to the previous configuration before the structural reinforcement.

The detail of both analyzed schemes are illustrated in Figure 4.15.

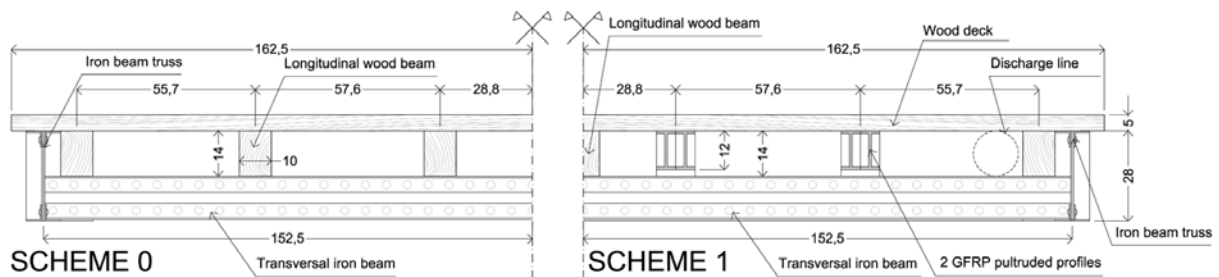


Figure 4.15, Detail of cross section deck, scheme 0 and 1

For the structural behavior of GFRP profile the Timoshenko beam model that evaluates the shear deformability in presence of uniform load has been considered, see formulation (4.18):

$$\eta = \frac{P \cdot l^2 \left(\frac{5 \cdot l^2}{48E \cdot J_{min}} + \frac{\chi}{G_{LT} \cdot A_{res}} \right)}{8} \quad (4.18)$$

where η =maximum deflection value, P =applied load, l =length of profile, E =elastic modulus, J_{min} =minimum moment of inertia, A =Area of cross section, G_{LT} = shear modulus in transversal direction and χ is shear coefficient.

The global structural response obtained by finite element analysis is shown in Figure 4.16.

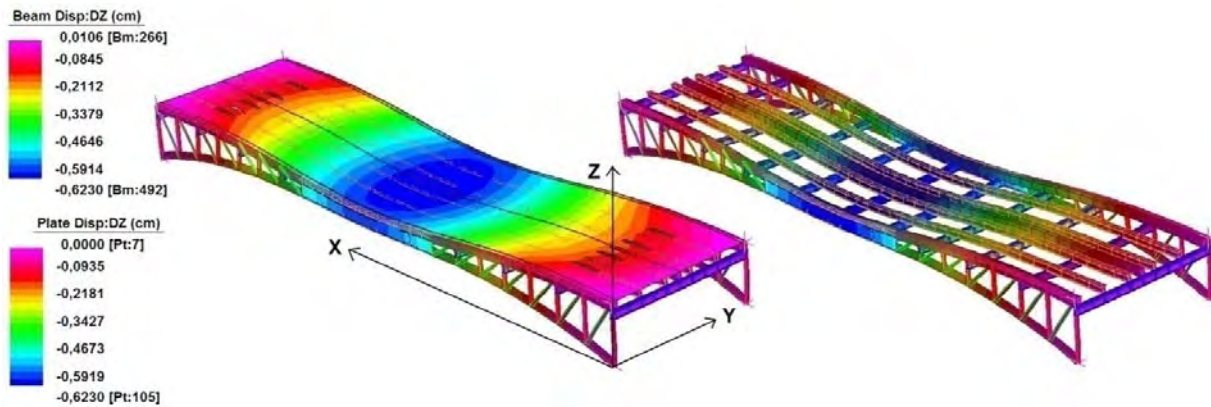


Figure 4.16, Maximum vertical displacements of bridge

In detail the structural response results and the maximum stress values of GFRP profiles and wood beams of the new configuration (Wood-GFRP, scheme 1) are shown in Table 4.1. The initial configuration values (scheme 0) with the only wood longitudinal beams are shown to be compared in the same table. The values of GFRP beams (scheme 1) refer to one pultruded profile and not to the section with coupled profiles.

Table 4.1, Structural performance of cross sections and stress values

| Scheme | η_{max} (cm) | Y_W (cm) | Y_G (cm) | σ_{cW} (Mpa) | σ_{cG} (Mpa) | σ_{tW} (Mpa) | σ_{tG} (Mpa) |
|--------|-------------------|------------|------------|---------------------|---------------------|---------------------|---------------------|
| 0 | 0.63 | 10 | - | -1.164 | - | 0.462 | - |
| 1 | 0.62 | 11.2 | 9.7 | -0.830 | -3.178 | 0.208 | 0.773 |

Where η_{max} is maximum deflection, Y_W and Y_G are the distance of neutral axis respectively of wood and GFRP elements, σ_c and σ_t are the stress values in compression and tensile zone of wood (w) and GFRP (G). Analysing the two configurations with equal applied load, the decrease

of the maximum stresses in the tensile and compression zone of the wood beams is clearly visible - respectively equal to 55% and 28% from scheme 0 to scheme 1.

4.2.3.4.2. Dynamic behavior

The structural response to vertical and horizontal dynamic loads induced by human body motions was verified too. The analysis was developed considering the natural frequencies of the vibration modes with different accidental load to verify the resonance phenomena with external harmonic load. Table 4.2 shows the changing of the fundamental frequency with the increase in vertical load; in detail the comparison between the calculated frequency values of the dynamic responses of scheme 0 and scheme 1 are shown.

Table 4.2, Natural frequencies of fundamental flexural vibration for different live load

| Scheme | Live Load | | | | | |
|--------|------------------------|--------------------------|--------------------------|--------------------------|--------------------------|--------------------------|
| | 0 (kg/m ²) | 100 (kg/m ²) | 200 (kg/m ²) | 300 (kg/m ²) | 400 (kg/m ²) | 500 (kg/m ²) |
| 0 | 17.49Hz | 11.72 Hz | 9.4 Hz | 8.08 Hz | 7.19 Hz | 6.54 Hz |
| 1 | 17.08 Hz | 11.64 Hz | 9.39 Hz | 8.09 Hz | 7.21 Hz | 6.57 Hz |

We can see a similar dynamic behavior in both configurations; in the specific case, it has to be highlighted that with the increment of load from 300 kg/m², scheme 1 (Wood+GFRP) has higher in frequency values than scheme 0 (Wood). The frequencies of lateral vibration are shown in Table 4.3 for both analysed schemes.

Table 4.3, Natural frequencies of transversal lateral vibration for different live load

| Scheme | Live Load | | | | | |
|--------|------------------------|--------------------------|--------------------------|--------------------------|--------------------------|--------------------------|
| | 0 (kg/m ²) | 100 (kg/m ²) | 200 (kg/m ²) | 300 (kg/m ²) | 400 (kg/m ²) | 500 (kg/m ²) |
| 0 | 23.61 | 17.57 | 14.58 | 12.74 | 11.45 | 10.48 |
| 1 | 23.39 | 17.43 | 14.47 | 12.64 | 11.37 | 10.41 |

There are no resonance effects for either vertical and horizontal dynamic action induced by human body motions, as shown in the following Table 4.4.

Table 4.4, Vertical and horizontal forcing frequencies (Bachmann et al. 1995)

| Vertical vibrations (Hz) | | | Horizontal vibrations (Hz) |
|--------------------------|---------|---------|----------------------------|
| Walking | Running | Jumping | |
| 1.6-2.4 | 2.0-3.5 | 1.8-3.4 | 0.6-1.7 |

4.2.3.5. Comparison with traditional materials and analysis of results

To understand the real advantages of the use of FRP composite profiles, a comparison with steel (scheme 1S) and aluminium (scheme 1AL) profiles was made. These structural elements have the same length and an optimized section to assure an equivalent performance based on the maximum deflection value during linear elastic regime.

Table 4.5 shows the geometrical and physical characteristics of the traditional materials profiles, highlighting the percentage ratio between dead load and volume for GFRP, steel and aluminum.

Table 4.5, Geometrical and physical characteristics of steel and aluminum profiles and relations with GFRP material

| Traditional Materials | Cross Section dimension (cm) | J_{xx} (cm ⁴) | A_{TM} (cm ²) | A_{TM}/A_{GFRP} % | DL_{TM} (kg/cm) | DL_{TM}/DL_{GFRP} % |
|-----------------------|------------------------------|-----------------------------|-----------------------------|---------------------|-------------------|-----------------------|
| Aluminum | 9.1x4.55x0.6 | 125.26 | 10.34 | 57 | 0.028 | 84 |
| Steel | 6.9x3.45x0.46 | 41.24 | 5.93 | 33 | 0.046 | 140 |

Where J_{xx} is the moment of inertia, A and DL are respectively the section area and Dead Load of traditional material ($_{TM}$) and of GFRP profiles ($_{GFRP}$).

The static behavior shown in Table 4.6 emphasizes the optimum relationship between the static scheme first reinforced with traditional material (scheme 1S and 1AL) and then with FRP profiles (see Table 4.1, scheme 1).

Table 4.6, Structural performance of cross sections and stress values of steel and aluminum profiles

| Scheme | η_{max} (cm) | Y_w (cm) | Y_{MT} (cm) | σ_{cW} (Mpa) | σ_{cMT} (Mpa) | σ_{iW} (Mpa) | σ_{iMT} (Mpa) |
|--------|-------------------|------------|---------------|---------------------|----------------------|---------------------|----------------------|
| 1S | 0.62 | 10.8 | 6.31 | -0.79 | -16.36 | 0.24 | 1.52 |
| 1AL | 0.62 | 11 | 7.75 | -0.82 | -6.8 | 0.22 | 1.19 |

Where $_{MT}$ is the subscript that indicates traditional materials (steel and aluminum).

The dynamic response results of scheme 1 is similar to the one of the section reinforced with steel and aluminum profiles; in detail, the variations are equal to 1-2% for vertical and horizontal lateral vibrations.

Generally speaking, the static and dynamic behavior is similar to the cases of reinforcement with traditional materials; thus the advantages in the use of GFRP must be evaluated in terms of durability and ease of assembling.

4.2.3.6. Assembling and installation phase

This footbridge is an important link between a school and people residences; to substitute all the longitudinal wood beams, the bridge had to be out of service for only one day. This was possible because of the low self-weight of the FRP composite material - which made the executive phase easier (transport, assemblage and the installation). The photo sequence in Figure 4.17 shows the assemblage between the two “I” FRP profiles and the beam-beam joint of FRP pultruded plates and stainless bolts; this figure shows also the management, the positioning and finally the mechanical connection to the bridge abutments through the galvanic steel gussets. The workers’ ease in making the cut, the holes and the final assemblage is evident. Such operations were necessarily carried out in yard during the positioning phase because some problems were to be solved directly in situ. In fact the bridge has a complex geometry, for the plan and elevation present two different radius of curvature.

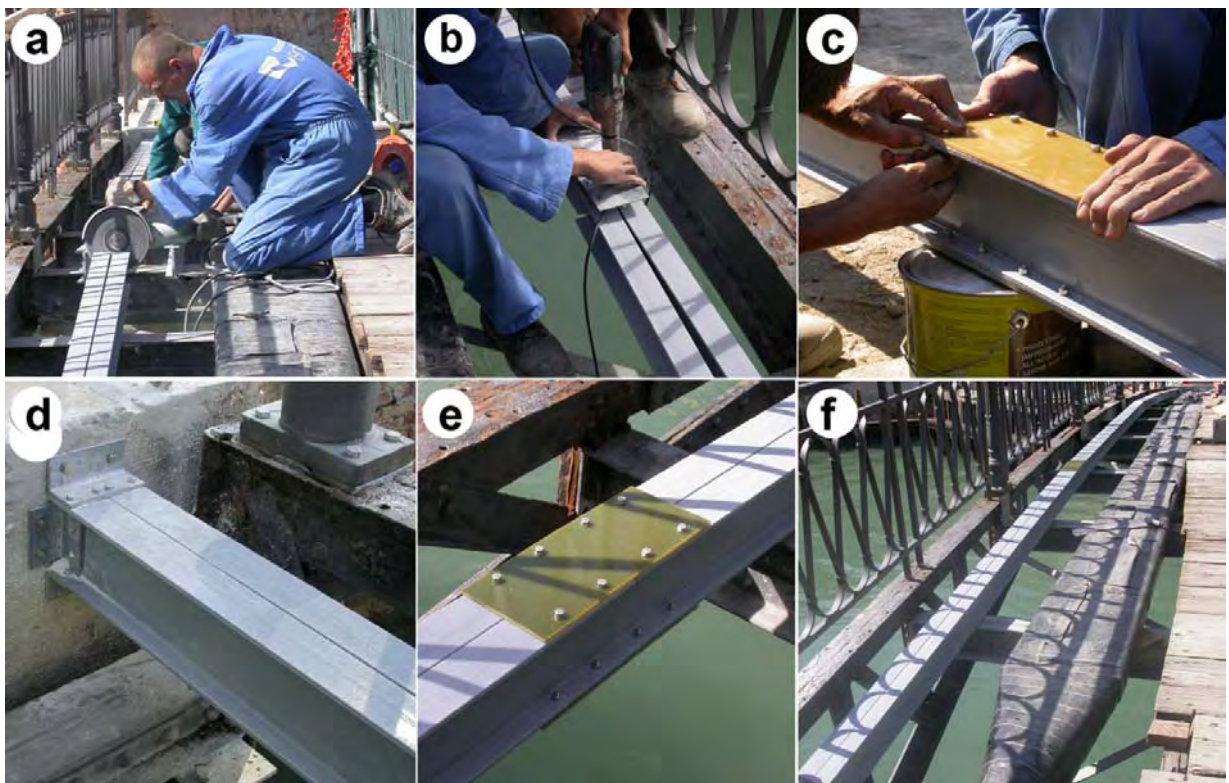


Figure 4.17, Executive phases of GFRP profile assemblage

Furthermore very important advantages are related to the very easy transport and installation, Figure 4.18 and final result of intrados view, Figures 4.19 and 4.20.



Figure 4.18, Transport and installation phase

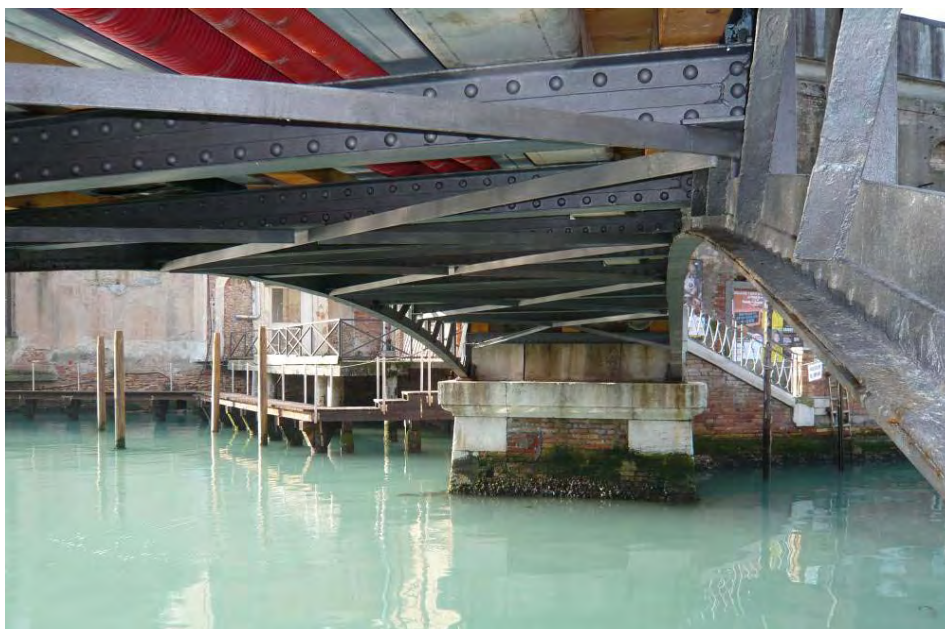


Figure 4.19, Intrados



Figure 4.20, Intrados detail

4.2.3.7. Results of static experimental test

The static test was carried out according to the technical regulation relevant to the testing of bridges and footbridges. The global structural response was analysed pointing out a variation in transversal displacement upon an increase in load. The test load – equal to 400 kg/m^2 – was applied to the extrados of the bridge deck.

For the measuring points and the consequential measurement, the supports and the centre line were considered (Figures 4.21 and 4.22), taking one of the two iron truss beams (North side points 1,2,3) situated at the perimeter of the bridge structure as reference points. During the unloading phase, the truss beam situated on the South side (points 4,5,6) was also considered. In order to take down any vertical displacement increase, the load value reached was maintained for 1 hour and 30 minutes before proceeding with the unloading phase; overall, no relevant vertical displacement increase was recorded. Tables 4.7 and 4.8 list the values recorded corresponding to each point monitored; Figure 4.23 instead illustrates the bridge during loading phase.

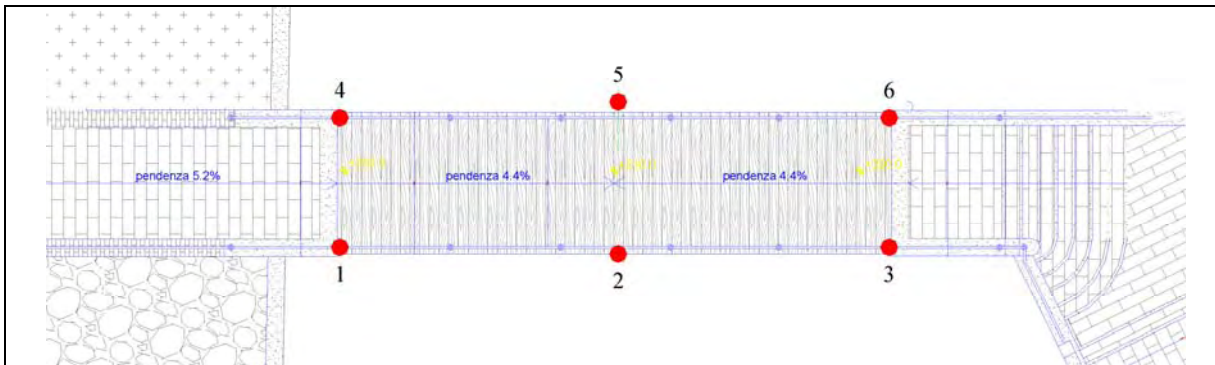


Figure 4.21, Monitoring points, plan

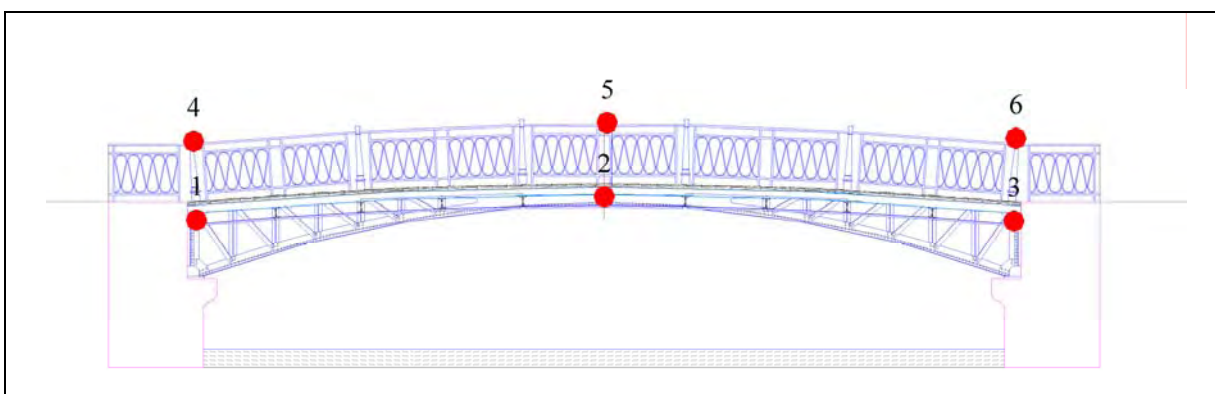


Figure 4.22, Monitoring points, frontal prospect

Table 4.7, Values of monitoring points, north side

| Monitoring points | | 1 | | 2 | | 3 | |
|-------------------|------------------------|------------|------------|------------|------------|------------|------------|
| Water high | Load kN/m ² | value (mm) | difference | value (mm) | difference | value (mm) | difference |
| Ref. value | 0 | 9.241 | 0 | 9.329 | 0 | 9.425 | 0 |
| 0.14m | 1.4 | 9.240 | 0.001 | 9.328 | 0.001 | 9.425 | 0.001 |
| 0.23m | 2.3 | 9.239 | 0.002 | 9.327 | 0.002 | 9.424 | 0.001 |
| 0.32m | 3.2 | 9.239 | 0.002 | 9.326 | 0.003 | 9.424 | 0.001 |
| 0.405m | 4.05 | 9.239 | 0.002 | 9.325 | 0.004 | 9.424 | 0.001 |
| 0.2m | 2 | 9.239 | 0.002 | 9.326 | 0.003 | 9.424 | 0.001 |
| download | 0 | 9.240 | 0.001 | 9.329 | 0 | 9.424 | 0.001 |

Table 4.8, Values of monitoring points, south side

| Monitoring points | | 4 | | 5 | | 6 | |
|-------------------|------------------------|------------|------------|------------|------------|------------|------------|
| Water high | Load kN/m ² | value (mm) | difference | value (mm) | difference | value (mm) | difference |
| Ref. value | 4.05 | 10.111 | 0 | 10.427 | 0 | 10.309 | 0 |
| 0.405m | 4.05 | 10.111 | 0 | 10.428 | -0.001 | 10.309 | 0 |
| 0.2m | 2 | 10.111 | 0 | 10.429 | -0.002 | 10.309 | 0 |
| download | 0 | 10.112 | -0.001 | 10.431 | -0.004 | 10.309 | 0 |



Figure 4.23, Load phase

4.2.3.8. In situ increment of stiffness and repair of FRP beams

In the perspective of a need in term of increment flexural strength also the possibility to realize a stiffer beam or to repair an existing FRP beams, applying sheet carbon on the bottom of profile, has been considered.

The sheet carbon and resin characteristics are shown in Table 4.9; the reinforcement has been applied on a GFRP beam with the same properties already illustrated in Table 2.2.

Table 4.9. Mechanical characteristics of Carbon sheet and epossidic resin

| Fibers | Weight | Tensile Elastic Modulus | Tensile strength | Elongation strength | |
|-----------|-----------------------|-------------------------|---------------------------|----------------------|-------------------|
| Carbon | 320 g/cm ² | 235GPa | 3530 MPa | 1.5% | |
| Resin | Density | Tensile strength | Flexural tensile strength | Compression strength | Elastic modulus E |
| Epossidic | 1.1 g/cm ³ | 30 MPa | 50 MPa | 95 MPa | 2200 MPa |

The comparison in term of load-displacement curves between the plain GFRP beam and the same profile with two different type of reinforcement, GFRPsC_1 and GFRPsC_2 (Glass Fibre Reinforced Polymer sheet Carbon), glued trough resin to the bottom are shown in Figure 4.24. Particularly in presence of GFRP beams reinforced with carbon after local damage the maximum level of load reached is higher than plain GFRP beam, GFRP_1,2,3, but also with higher deformability at the collapse.

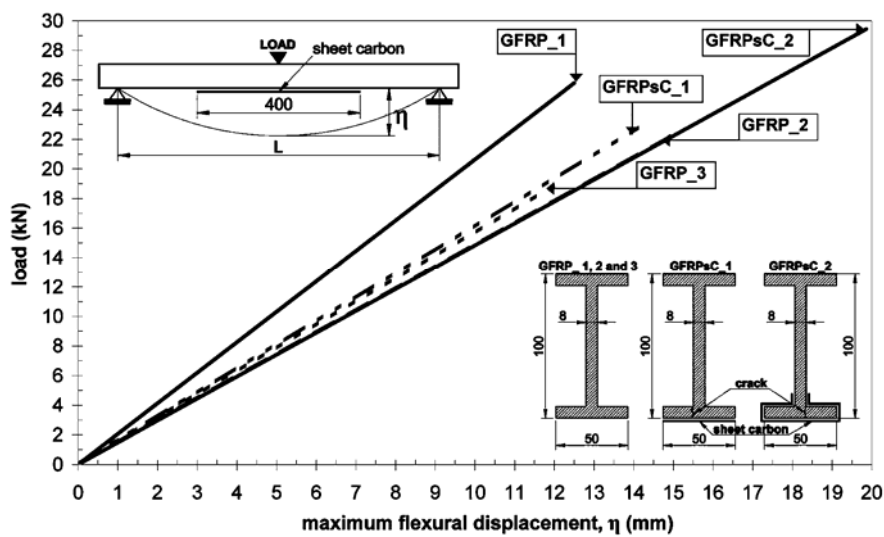


Figure 4.24. Comparison between plain GFRP and repaired GFRP profiles, $\lambda = 10$

The repair of GFRPsC_2 allows an increment of value of collapse load greater than 22% compared to the configuration adopted for the repair of GFRPsC_1 beam.

To exclusion of the undamaged GFRP_1 beam, the repaired beams have a structural response similar or better than the undamaged beams, GFRP_2 and 3, for the stiffness and for the reached collapse load level.

4.2.3.9. Final remarks

This research highlights that the use of FRP structural elements for the structural reinforcement assures important achievements in the static and dynamic behavior and suggests the following evaluations:

- through FEM analysis the comparison with steel points out the optimum relation between structural strength and dead load of composite material. With the optimized section the use of steel material causes an increment of dead load 1.4 times higher than the reinforcement with GFRP profiles. The participant mass to total load (dead load + accidental load) of the configuration with composite material is equal to 1.75%, while for steel is equal to 2.45% (see Table 4.10). In the whole total load the FRP material, with its low self weight, allows a greater accidental load.

Table 4.10. Load comparison between steel and GFRP configuration

| LOAD | Configuration with steel beam | Configuration with GFRP beam |
|---|-------------------------------|------------------------------|
| Dead load | 3800 kg | 3664 kg |
| Dead load of beams | 469 kg | 333 kg |
| Accidental load (400 kg/m ²) | 15349 kg | 15349 kg |
| Total load (accidental load + dead load) | 19149 kg | 19013 kg |

- Altogether, the maximum displacement values of analysed schemes, through FE analysis, are similar; with the applied load of 400kg/m², the maximum deflection is about 6mm for each verified scheme. Such a comparison must be evaluated considering the high resistance to the aggressive environment conditions of the composite material compared to traditional materials, the facility in moving and placing during the installation phase.

- The stress level in wood beams (in the wood-GFRP cross section) is 30% less than the stress level in only wood cross section.

- A relevant reduction of the compression stress level in wood beams – that prevents the material from entering the plastic phase – was assured by the use of GFRP beams.

- Regarding the general structural approach, the adopted reinforcement represents a good solution without increase of the deck's thickness and allows to reach low values of compression stress in GFRP profile.

- The advantages of structural reinforcement regard a good load distribution on bearing structure and consequently the reduction of local stress.

-The global bridge stiffness, with the structural reinforcement, assures a good response to dynamic actions induced by vertical and horizontal harmonic loads.

- The easy way in term of repairing of GFRP beams with sheet carbon fiber bonded on the bottom represents a not negligible way to have added solutions during the yard in presence of more requirements in term of strength.
- In reinforcing of existing light structure the use FRP beams instead of steel beams seems to offer more advantages; obviously a very different structural approach we have to take in to account in presence of higher requirements.
- Not negligible benefit are shown through finite element analysis using very light and strength structural material as FRP. In detail in presence of not very high bearing capacity requested by pedestrian bridge is enough using fiber reinforced polymer structural profiles.
- Overall, the static test highlighted an high flexural stiffness of the bridge. Despite the fact that the radius is notably large, the “arch” behaviour results in being relevant with regards to the “beam” behaviour. At the moment of unloading, no significant vertical displacement values were noted, highlighting overall uniform global behaviour of the two principal beams.
- The comparison between the results of the static test and the numerical modelling highlights a percentage difference equal to 32.5%. To applied load equal to 400kg/m² the vertical displacement is 6.23 mm for FE analysis and 9.23 for static experimental test; the difference is due to joints between the elements that build the bearing truss beams, with the rotational stiffness of FE model greater than the real configuration.

4.2.4. Further employment possibility

Considering the impossibility of classifying all the cases which concern historical structures and without having the pretense, therefore, to deal with the themes regarding structural collaboration - among systems constituted by heterogeneous materials, innovative or not - in a simplistic way or by way of handbook, certain applicative examples of structural reinforcing achieved via new technologies are reported. Such solutions, despite the diversity of the composite material, can be used as reference points for the approach to possible uses of FRP structural elements.

For the reinforcement of slender elements in historic masonry, the example which best illustrates the possibility of interaction between the structural system entirely in composite with the existing structures is represented by the design synthetically described in the images of Figure 4.25, (S.

Dalmazio Tower, Pavia, Italy). In particular, the structural rehabilitation of the tower building was made possible due to a steel structural frame, partly in carbon zinc steel and partly in stainless steel, installed internally, recognizable and completely removable.

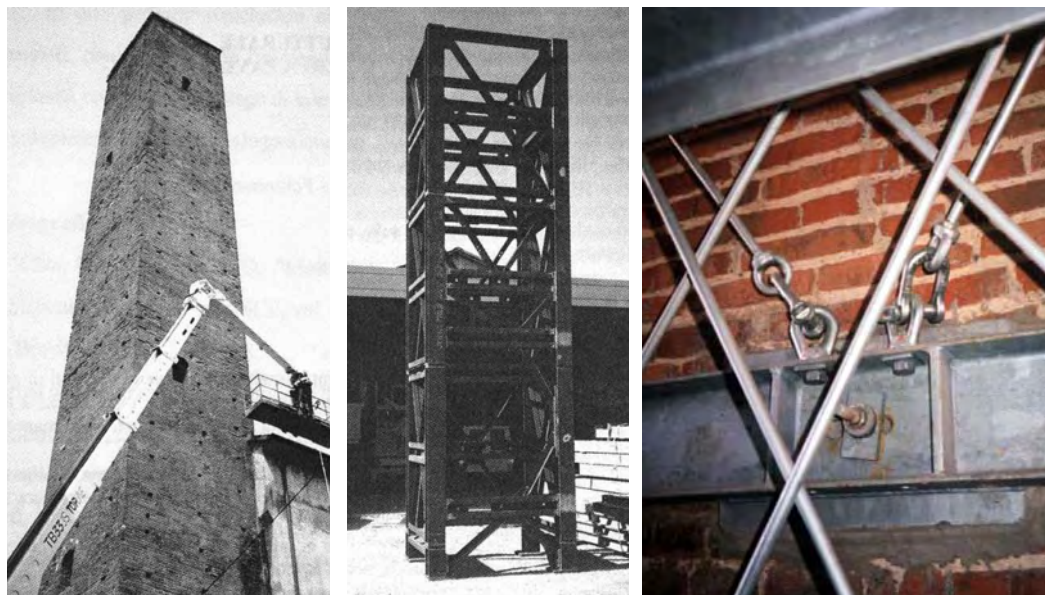


Figure 4.25, stiffness increment of S. Dalmazio Tower, Pavia, Italy (Jurina 1995)

In line with the executions which take advantage of the high tensile strength of the composite materials was analysed an other applications that may be with FRP structural elements.

The approach of design of Jurina (2003) is well adapted to being used in the possible applications of GFRP pultruded elements, Figure 4.26.

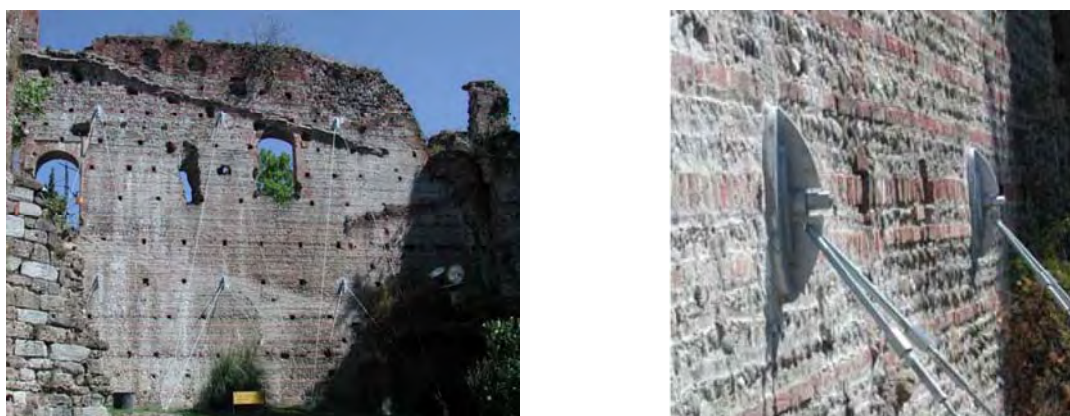


Figure 4.26, reinforcement of wall by cable-stayed
Castello di Trezzo d'Adda, Milan, Italy (Jurina 2003)

4.3. Chapter overview

All in all, it is possible to speak of constructions with FRP structural elements as of indispensable applications, of emergency which constitute the best solutions among the possible alternatives. Such approach defines the specificity of the applications, both in the reinforcement and new construction field. In the latter case, aside from certain demonstrative examples, the physical-mechanical properties of the material satisfy the restrictions of the boundary conditions, such as the particularly aggressive environmental situation, the necessity to guarantee electro-magnetic transparency, the needs of easily removable, and thus lightweight.

For the reinforcement of existing structures, the favourable ratio between strength and dead load associated with durability constitute the optimal conditions for structural use of FRP elements.

Having surpassed, in part, the limit of the absence of supporting calculation codes, the principal limit of this innovative technology is still linked to high, and so non-competitive, costs.

References

Borri, M. Corradi, *Rinforzo di travi lignee con elementi pultrusi in FRP*, *Meccanica delle Strutture in Muratura Rinforzate con FRP – materials*, Venice, Italy, 6-8 dicembre 2004.

Boscato, G., Russo, S. & Siviero, E., *The FRP Beams as Reinforcement of Pedestrian Bridge*, 2nd International fib Congress, Naples, Italy, 2006.

Di Tommaso, A., Russo, S., Siviero, E., & Boscato, G., *I profili strutturali ibridi in composito*, 14° Congresso C.T.E., Mantova, 7-8-9 Novembre 2002, pp. 729-738.

Jurina, L., *Il consolidamento strutturale della Torre San Dalmazio a Pavia*, Giornate Italiane della Costruzione in Acciaio, Riva del Garda, Italy, 15-18 October 1995.

Jurina, L., *La possibilità dell'approccio reversibile negli interventi di consolidamento strutturale*, Convegno Internazionale di Scienza e Beni Culturali, "La reversibilità nel Restauro", Bressanone, Italy, 2003.

Keller, T., Bai, Y. and Vallee, T., *Long-term performance of a glass fiber-reinforced polymer truss bridge*, J. of Composites for Construction, 11 1, 2007.

Russo, S. & Boscato, G., *Carbonio + Vetro. Elementi strutturali in FRP e doppia fibra di rinforzo*, L'Edilizia "Speciale FRP". N°127 March April May 2003.

Russo, S., *Strutture in composito – Sperimentazione, teoria e applicazioni*, Ulrico Hoepli Editore S.p.A., Milan, 2007. ISBN 978-88-203-3643-1

Toni, M., *FRP Architettura. Costruire con materie plastiche rinforzate con fibre*, Casa Editrice Alinea, 2005.

Tromp, L., *Can Resin Infusion Technology complement Pultrusion in Bridge – and Civil Engineering*, EPTA 9th World Pultrusion Conference, Rome, Italy, 26-28 March 2008.

5. DYNAMIC ANALYSIS OF GFRP ELEMENTS FOR APPLICATION IN CIVIL ENGINEERING

5.1. Introduction

The study examines the topic of dynamic characterisation of the elements and FRP structural systems starting from the definition and quantification of the fundamental parameters of dynamic engineering, natural frequencies, modes of vibration and damping.

The research illustrates the results of an extended campaign of experimental tests on mono-dimensional elements, panels and framework systems, subject to free vibration. The boundary conditions for the structural elements are of simply supported and fully clamped, for the two-dimensional 2D frame and three-dimensional 3D structure, they are clamped and supported respectively.

The tests concern profiles with open cross-sections with one or two axis of symmetry, tubular sections and panel.

The dynamic response of FRP structural elements, subject to free vibration, depends principally on the macro-mechanical properties and constitutive law as well as the composition of the material. Some authors have examined these properties via micromechanical analysis with particular regard for the constituent materials, such as the matrix, the fibrous reinforcing and the fiber-matrix interface, (Hashin and Rosen 1965, Sun and Lu 1995, Lesieutre 1994). The fibers have a linear elastic behaviour, with brittle failure and are characterised by independent elastic moduli of varying frequencies. The polymeric matrix have a linear elastic behaviour upon stretching and viscoelastic in a transversal direction; the shear deformability of the matrix results in slightly dependence on frequency (Gibson and Plunkett 1976).

Gibson and Plunkett (1976) studied the dependence of the mechanical characteristics on the variation of the vibration frequency on a unidirectional composite laminate, with frequencies included in the interval from 0 to 500Hz. The influence of the percentage and of the fiber type on the dynamic behaviour of the pultruded composite materials was previously developed by Nori et al. (1996); the research showed that the stretching properties of the composite samples are

independent from the distribution of the fibers which instead influence the properties of the flexural behaviour of the pultrusion.

For each configuration and typology analysed, the experimental study is supported by the results determined via a numeric approach and a finite element method.

The FE analysis was conducted at a macro-mechanical level in order to obtain results which allowed the definition of the dynamic response of the FRP structural elements; the researches show as of today on similar topics the works of Qiao and Zou (2002), Turvey and Mulcahy (2004) and Turvey et al. (2000).

The dynamic mechanical response of the material and the FRP structure was examined via modal analysis, as well Schultz and Tsai (1968) and Gibson (2000).

The experimental results of the dynamic behaviour of the GFRP structural elements were compared with the data of traditional materials, steel and aluminium, determined via analytical approach; all in all the results highlight a good agreement. For the profiles with cross sections most suitable for use in civil engineering, simulation of a possible application for the realization of a load-bearing deck structure was conducted. Such study was developed in order to evaluate the variation of applied load and span, considering fundamental frequency respect to vibration induced by human action. Again with reference to the analysis of the dynamic behaviour of structural elements, the currently available numerical formulations were compared to verify the most reliable approach. As regards models for natural frequency analysis of pultruded FRP elements, the currently available literature gives prominence to Timoshenko's shear-deformable beam theory (Timoshenko 1921) for isotropic beams, rather than to Euler-Bernoulli's beam theory, since the latter neglects the effects of transverse shear deformations and torsional stiffness. Starting from Timoshenko's beam model, further research was developed by Huang (1961) and Nowinski (1969).

The works of Bank and Kao (1990) and Librescu (2006) took into consideration the effects of rotational inertia and shear deformability on the frequencies of free vibration concerning specific composite beams. Starting from the defined notions of analysis of single elements, the dynamic response of GFRP structural systems was subsequently evaluated.

The passage from the element to the structure and so the theme of framework in composite materials is, even now, the object of interesting researches. The approach is the same adopted by metalworkers who assign structural-static value to every constituent element of joint beam-column. Considering the constitutive law of composite materials, it is necessary to take into account certain basic advice during the design phase such as the use of cross sections with higher stiffness, rigid nodes, limited dimensions and the positioning of elements that assure the increment of global stiffness, Russo (2007). The effects of shear deformability on the material influence the global behaviour of the structure, condition the vertical displacement of the beams, facilitate the flexural-twisting phenomenon and consequently compromise the stability of elements subjected to compression load. The first study on the structural behaviour of GFRP framework was conducted by Mosallam and Bank in 1992; the authors studied the collapse of the beam-column connection and the local buckling of the beam flange, defining a numerical model to analyse the non-linear behaviour of the framework. Important evaluation on the effects of shear deformability on the global behaviour of a GFRP framework are present in the researches proposed by Abbaker and Mottram (2004) and Mottram (2007, 2008).

In line with the present work, the research by Dicuonzo et al. (2008) into the design and production of a GFRP temporary structure module is mentioned.

In the present research of PhD thesis, particular attention has been given to the production of the beam-column node which, considering the transversal deformation of the material, becomes a key part of a composite system (Holloway 1990, Eurocomp 1996, Zheng and Mottram 1996, 1999a,b, Smith et al. 1999, Mosallam 1997, Turvey and Cooper 2004, Oppe et al. 2007) calculating the effect of rotational stiffness (Faella et al. 2000) and evaluating the efficiency of the rotational force applied to the bolt. Such research, in fact, is part of a wider research currently in course aimed at analysing the static and dynamic response of a GFRP system at variation of the configuration of the restrains.

Via the experimental results, it has been possible to model the frameworks 2D and structure 3D by finite element method, in order to evaluate, via modal analysis and seismic analysis with a spectrum of response, the structural behaviour upon variation of the typology, stiffness of the system braced and unbraced, and restraint conditions. Considering the application of FRP

structural elements for the conservation of environmental heritage, in the same chapter, the structural behaviour of the GFRP sheet piles subject to dynamic action during the fixing phase, were analysed.

5.2. Free vibrations

5.2.1. Mono-dimensional elements

5.2.1.1. Experimental analysis

This research is showing the results coming from a testing programme aimed to find out the parameters of dynamic behaviour – i.e. response spectrum, natural vibration modes, damping and displacements – of structural FRP (Fiber Reinforced Polymers) elements subjected to natural vibrations. The present tests and analysis were performed on a number of thin-walled profiles, of glass fiber and vinilester matrix, mainly employed in civil engineering for new all-GFRP buildings as well as for structural reinforcement.

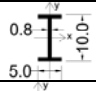
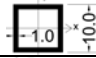
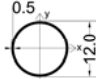
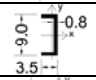
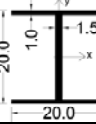
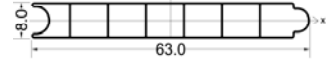
Hereafter is depicted the test setup and is developed the analysis of experimental results on dynamic parameters of mono-dimensional elements, whereas the most significant data of each profile are collected in the figures of Appendix A.

5.2.1.1.1. Setup of experimental tests

The physical and geometric characteristics of pultruded elements in free vibration field are illustrated in Table 5.1. The sections analysed are those that are frequently used in the structural engineering field. One- and two-dimensional elements with beam, column and slab deck functions, respectively, are investigated.

The restrain conditions of clamped-clamped refer to open cross-section profiles (“I” profile and “C” profile) and closed section profiles of square and circular shapes, whilst the supported conditions refer to all structural elements. In order to highlight longitudinal and twisting flexural vibrations have been analysed the greater L/h ratio between length and the height of cross section of the elements. The setting of the tests, with reference to excitation points and to the position of the accelerometers, was defined on the basis of the geometry of each profile analysed, (Figure 5.2).

Table 5.1. Characteristics of GFRP structural elements

| Structural elements (cm) | | J (cm ⁴) | Length (cm) | Area (cm ²) | Weight (kg) |
|---|-----------------------|----------------------|----------------|----------------------------|----------------|
|  | “I”, J _{max} | 209.22 | 300 | 14.72 | 8.65 |
| | “I”, J _{min} | 17.02 | | | |
|  | “Q” | 492 | 240 | 36 | 14.87 |
|  | “O” | 299.20 | 240 | 18.06 | 7.85 |
|  | “C”, J _{max} | 121.45 | 200 | 11.52 | 4.2 |
| | “C”, J _{min} | 11.27 | | | |
|  | “H”, J _{max} | 4342.3 | 500 | 67 | 62 |
| | “H”, J _{min} | 1338.4 | | | |
|  | “P” | 808.66 | 420 | 74.57 | 57.3 |

Modal analysis was conducted by applying excitation pulses through a Dytran 5850A instrumented hammer and recording the structural response through multiple BBN 507LF accelerometer.

Both hammer and sensors include piezoelectric sensing elements in shear stress configuration with integral charge preamplifier and are connected to the digitizer unit by means of high stability coaxial cables.

The digitizer unit is based on commercial 12-bit data acquisition boards, each being capable of managing 16 multiplexed channels, completed by a custom front-end conditioning electronics that, for each single channel, provides constant-current power to the sensor preamplifier, a further amplification with selectable gain, low-pass filtering and simultaneous sample-and-hold.

Each signal conditioning channel has independent constant current supply capable of sourcing 4mA up to +24V with respect to the channel signal ground. The AC signal is capacitively coupled into an amplifier with a -3dB bandwidth spanning from 0.1Hz to 250kHz @ ×10 voltage gain.

A 2500Hz low-pass filter follows, for anti-aliasing purposes. The filter is designed for a 8th order Butterworth amplitude response and is tailored for a minimum -74dB signal/noise ratio required

by the 12bit digitizer running at 15000 S/s per channel, providing a nominal 80.8dB stopband attenuation. Butterworth transfer function was chosen in order to keep the phase delay within tolerable limits of $\pm 10^\circ$ and is obtained through 4 stages wired in Sallen-Key topology.

Each anti-aliasing filter is then followed by a track-and-hold circuitry that is synchronized with the scan timing circuitry so that all channels are simultaneously sampled and each value is held during all the scan sweep of the multiplexer/digitizer. Each track-and-hold is designed with a multi-stage topology in order to provide a maximum 5% drift error with a minimum aperture time of 12.5 μ s and a maximum hold time of 25ms.

All settings are digitally controlled and automatically applied in order to minimize the incidence of erroneous test equipment configuration.

All acceleration sensors are installed on the element under test by means of high-stiffness bi-adhesive tape, providing a mechanical coupling with substantial 10% gain flatness up to 3000Hz (5% to 2200Hz) and shock self-limiting feature through plastic flow at around 150g acceleration considering the mass of the sensor used.

In order to equalize the amplitude gain of the different channels, each channel has been individually matched with a specific accelerometer sensor and all of them have been trimmed against the same reference standard by using a Brüel & Kjaer 4294 accelerometer calibrator.

The start of the digitizer recording window has been synchronized with the trigger pulse coming from the instrumented hammer, allowing a 5% pre-trigger buffer in order to ensure the complete caption of the start of the vibration.

The vibration data digitized at 15kS/s in the time domain for 16384 (or 32768) samples were then analyzed using a fast Fourier transform algorithm, thus providing a spectral representation with theoretical frequency resolution of ≈ 0.45 Hz (or 0.22Hz).

Being the record length (between 1.09 and 2.18s) much longer than most of the observed vibration decays, no appreciable finesse improvement was in general obtained by applying either Hamming or Von Hann window to the data stream prior to the Fourier transform.

The restrain condition of simply supported was achieved by positioning the beam on cylindrical supports; for every support have been recorded the transversal displacements of cross section, along x and y axis, through the wire transducers positioned as shown by T1 and T2 references

(Figure 5.1, scheme a). Such check highlighted that for every profile the excitation not generate the displacements to the ends of profiles showing that the only dead load of structural element guarantees the stability of profile respect to applied excitation. The clamped configuration was achieved by applying an axial load, whose entity was varied according to the stiffness offered by each structural element; the clamp of the ends has been guaranteed by external joint built with steel elements (Figure 5.1, scheme b)

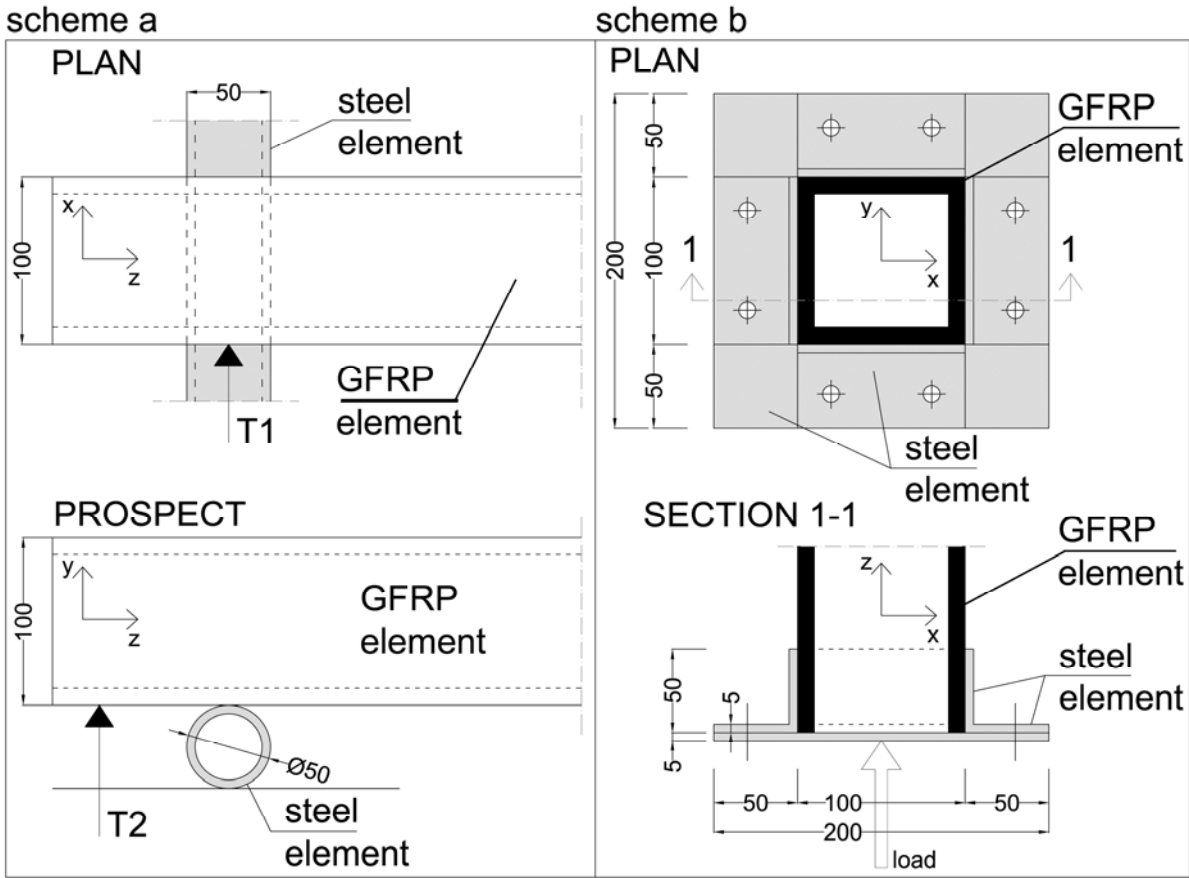


Figure 5.1. Schemes of constraints conditions for simply supported (scheme a) and clamped (scheme b) configuration

The accelerometers were opportunely positioned in order to recorder the most significant acceleration according to each single cross section examined (see Figure 5.2).

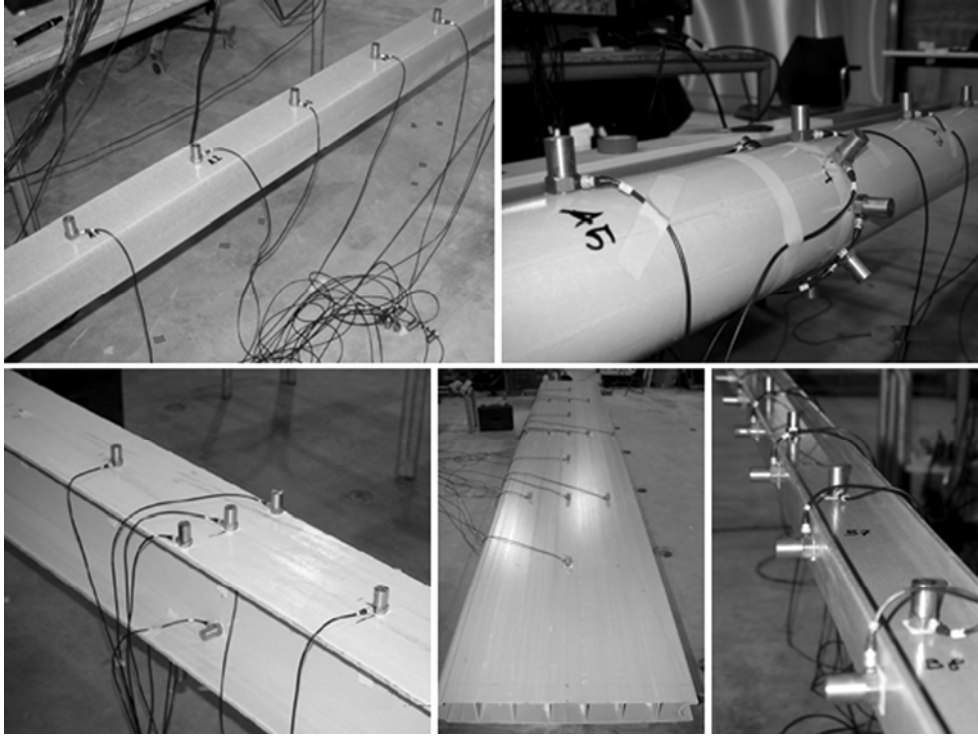


Figure 5.2. Experimental tests

5.2.1.1.2. Damping

Considering the mechanical characteristics of the fiber-reinforced composite materials (Gibson 1992), and the presence of natural vibrations of a small size, an approach is proposed which takes into account the expected damping ζ of a linear viscoelastic type.

To evaluate the reduction of amplitude values that sinusoidal oscillatory behaviour undergoes in time domain - in relation to which the damping percentage value is subsequently determined – a method of logarithmic decrement obtained from the relationship between two consecutive maximum amplitude is used in the time range of a damped time period of one or more cycles, according to (5.1) and (5.2).

$$\delta = \ln \frac{x_0}{x_n} \quad (5.1)$$

$$\delta = \frac{1}{n} \cdot \ln \frac{x_0}{x_n} \quad (5.2)$$

Having defined with δ = logarithmic decrement; x_0 = initial amplitude; x_n = final amplitude; n = number of cycles. The coefficient of damping ξ is determined via (5.3).

$$\xi = \left(1 + \frac{4 \cdot \pi^2}{\delta^2}\right)^{-0.5} \quad (5.3)$$

which can then be simplified with small values of ξ , that is when $(1 - \xi^2)^{0.5}$ is approximately equal to 1, becoming $\xi \cong \frac{\delta}{2 \cdot \pi}$

In Tables 5.2 and 5.3, the obtained values of damping are listed, for every boundary conditions, highlighting the variation of the coefficient for consecutive cycles and the final value in percentage.

Table 5.2. Damping ξ , (supported configuration)

| Structural element | Stiffness axis | Damping ratio ξ | | | |
|--------------------|----------------|---------------------|-----------|-----------|------------------|
| | | 7 cycles | 14 cycles | 21 cycles | final (%) |
| “I” | J_{\min} | 0.0085 | 0.0090 | / | 0.96 (20 cycles) |
| | J_{\max} | 0.0217 | 0.0218 | 0.0240 | 2.59 (28 cycles) |
| “Q” | J | 0.0405 | 0.0309 | 0.0306 | 2.72 (28 cycles) |
| “O” | J | 0.0503 | 0.0276 | / | 2.26 (16 cycles) |
| “C” | J_{\min} | 0.0145 | / | / | 1.45 (7 cycles) |
| | J_{\max} | 0.0383 | 0.0211 | / | 2.71 (20 cycles) |
| “H” | J_{\min} | 0.0185 | 0.0145 | 0.0132 | 1.18 (30 cycles) |
| | J_{\max} | 0.0333 | 0.0265 | 0.0240 | 3.4 (27 cycles) |
| “P” | J | 0.0167 | 0.0123 | 0.0116 | 0.97 (35 cycles) |

Table 5.3. Damping ξ , (clamped configuration).

| Structural element | Stiffness axis | Damping ratio ξ | | | |
|--------------------|----------------|---------------------|-----------|-----------|------------------|
| | | 7 cycles | 14 cycles | 21 cycles | final (%) |
| “I” | J_{\min} | 0.0223 | 0.0426 | / | 4.23 (15 cycles) |
| | J_{\max} | 0.0406 | 0.0282 | 0.0241 | 2.56 (37 cycles) |
| “Q” | J | 0.0173 | 0.0141 | / | 1.66 (15 cycles) |
| “O” | J | 0.0126 | 0.0129 | 0.0122 | 2.08 (41 cycles) |
| “C” | J_{\min} | 0.0278 | 0.0281 | / | 4.11 (17 cycles) |
| | J_{\max} | 0.0306 | 0.0321 | 0.0264 | 3.5 (27 cycles) |

Considering the simply supported configuration the comparison between damping values highlights as for the slender structural elements (“I”, “C”, “H” profiles with J_{\min} and panel) the range of damping ratio is between ζ 0.9-1.5%. The damping values for the profiles with low slenderness (“I”, “C”, “H” profiles with J_{\max} and tubular profiles) are included in the interval between 2.25-3.5%. For the clamped-clamped configuration the “I” and “C” profiles show the higher value of damping, circa 4%.

Figures 5.3 and 5.4 compare the different capacity to dissipate energy in function of time. To give an immediate comparison of the curves of each element, the initial part relative to vibration induced by excitation has been eliminated.

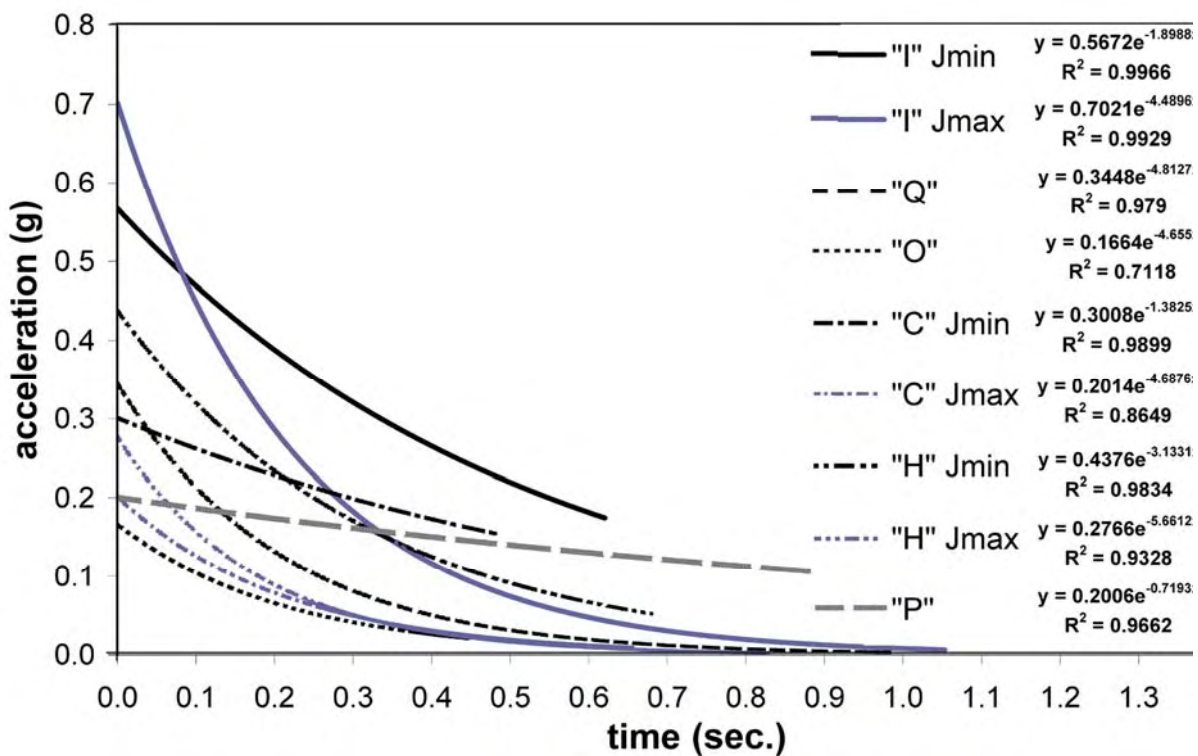


Figure 5.3. Comparison between all structural elements, supported configuration.

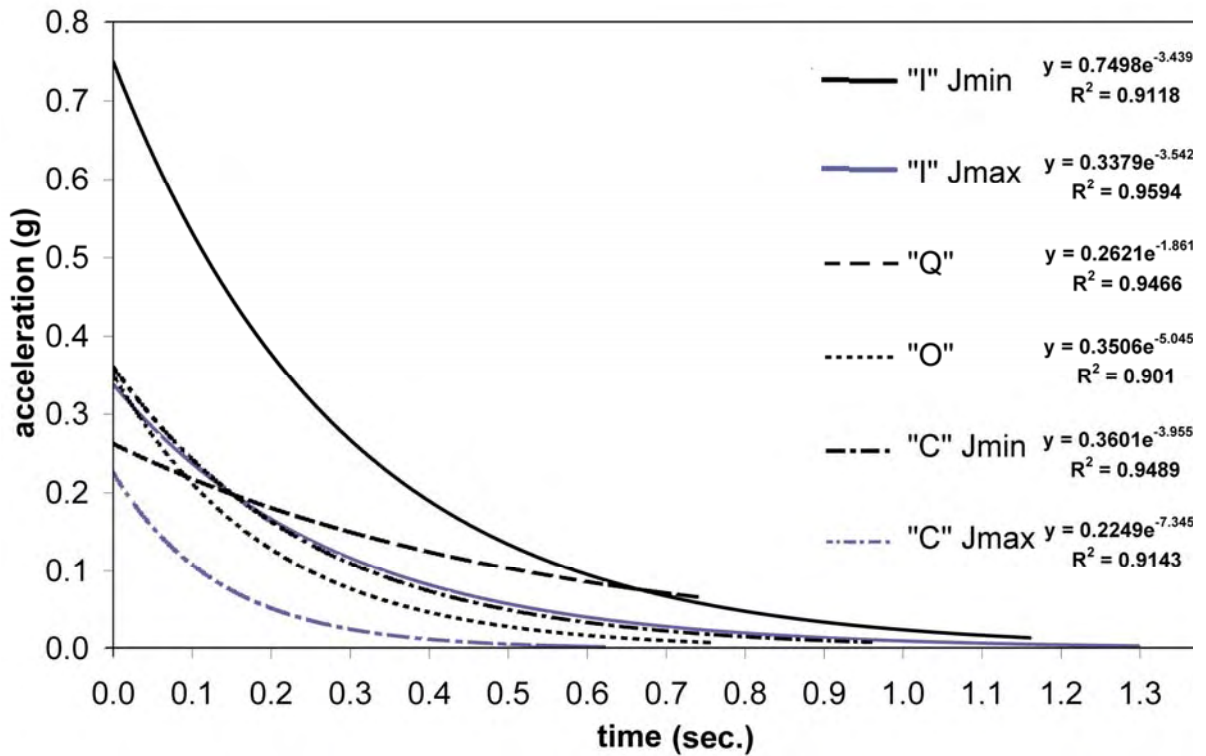


Figure 5.4. Comparison between all structural elements, clamped configuration.

Concerning the acceleration dissipation capacity of GFRP structural elements, for the simply supported configuration the decrease of the cumulative acceleration is 10 times greater in comparison to the one detected at the starting instant; the panel element reduces the initial acceleration of 1.4 times. For the clamped configuration the decrease of the initial acceleration is 6 times less than for the “I” profile. About the reduction of acceleration of closed cross section profiles, the “O” profiles is characterized by a great decrease, while the “Q” profile, in the same time interval is characterized by a decrease equal to 2.5 times respect to the cumulative acceleration at the beginning.

Figures 5.5 and 5.6 illustrate instead the accelerograms of each structural element.

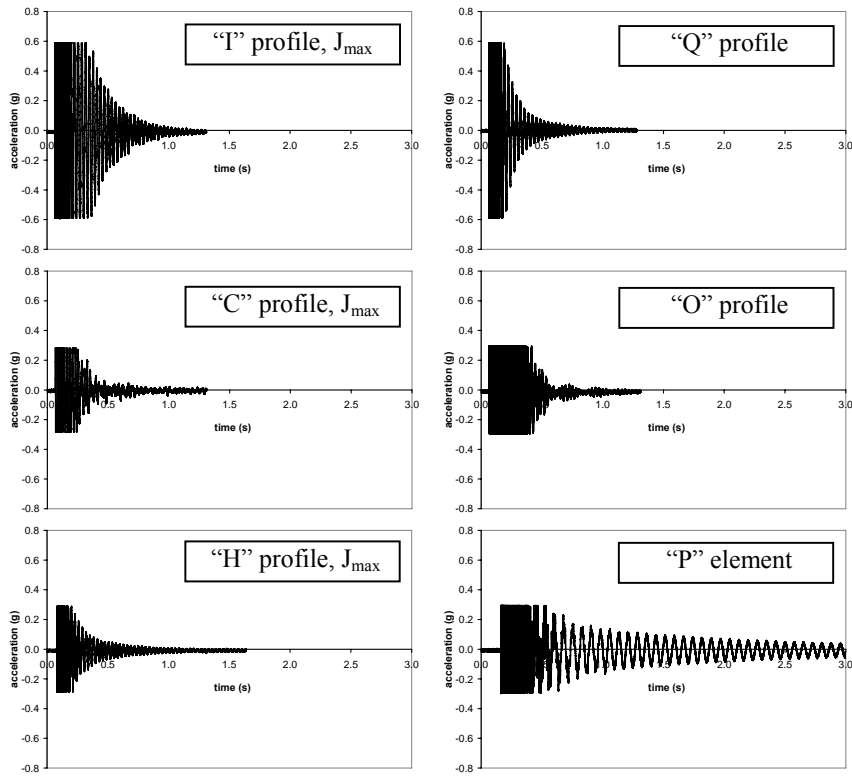


Figure 5.5. Free vibration response in time domain, supported configuration

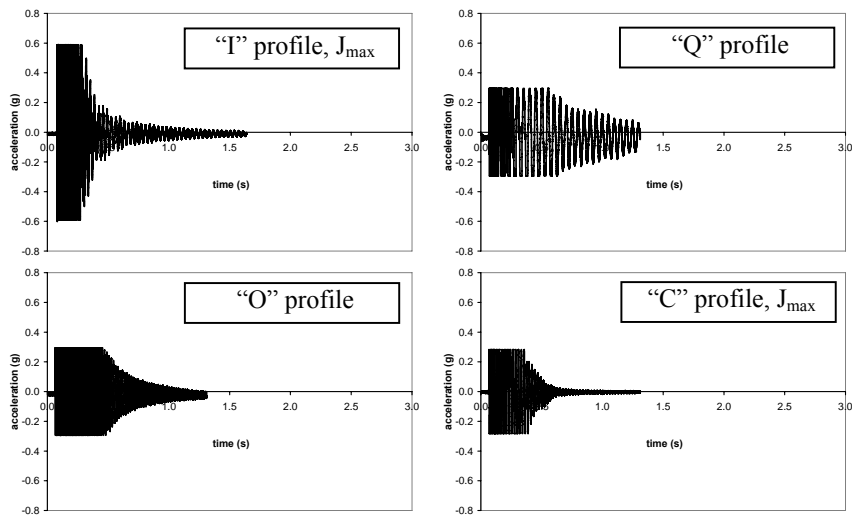


Figure 5.6. Free vibration response in time domain, clamped configuration

Overall, the diagrams highlight good agreement between the experimental data in relation to the peaks of the acceleration-time spectra and the interpolation line determined by the equation (5.4):

$$y = A \cdot e^{-\xi \omega x} \quad (5.4)$$

with ω = pulsation and A = acceleration

In the condition of clamped-clamped restrain (Figure 5.4), the structural elements result in accumulating an high quantity of acceleration, in particular in the initial phase of oscillation and in the presence of open cross-sections, whilst such tendency is less evident for the profiles with simply supported configuration.

Table 5.4 compares, for both boundary conditions, the values of acceleration of each profile in the free vibration at the t_0 and t_1 (0.5 seconds). The table shows as at 0.5 seconds, for the profiles simply supported, the classification between profiles with different slenderness values is evident; while for clamped configuration, considering the same interval of time, the variation between the accelerations is similar.

Tabella 5.4. Acceleration variation (g), interval t_0 - t_1

| Structural element | Stiffness axis | Supported configuration | | | Clamped configuration | | |
|--------------------|----------------|-------------------------|--------------------|--------------------|-----------------------|--------------------|--------------------|
| | | (g_0) to t_0 | (g_1) to t_1 | Var. g_1/g_0 (%) | (g_0) to t_0 | (g_1) to t_1 | Var. g_1/g_0 (%) |
| “I” | J_{\min} | 0.5672 | 0.2200 | 61.22 | 0.7498 | 0.1350 | 81.99 |
| | J_{\max} | 0.7021 | 0.0760 | 89.17 | 0.3379 | 0.0580 | 82.83 |
| “Q” | J | 0.3448 | 0.0310 | 91.00 | 0.2621 | 0.1040 | 60.32 |
| “O” | J | 0.1664 | 0.0165 | 90.08 | 0.3506 | 0.0290 | 91.73 |
| “C” | J_{\min} | 0.3008 | 0.1535 | 48.96 | 0.3601 | 0.0510 | 85.83 |
| | J_{\max} | 0.2014 | 0.0200 | 90.07 | 0.2249 | 0.0070 | 96.88 |
| “H” | J_{\min} | 0.4376 | 0.0930 | 78.74 | / | / | / |
| | J_{\max} | 0.2766 | 0.0200 | 92.77 | / | / | / |
| “P” | J | 0.2006 | 0.1420 | 29.21 | / | / | / |

5.2.1.1.3. Shape and torsional effects

The dynamic response of the A-A cross section of “H” profile is analysed in detail, Figure 5.7. The “H” structural element was excited along the longitudinal axis (excitation points B0 near the support, B2 to L/4 and B4 to L/2, briefly indicated in schemes a, b and c of Figure 5.7) and along the transversal axis at the points B5 and B6, as shown in scheme d of Figure 5.7. The maximum

displacement values concerning the fundamental frequency are reported for each scheme referred to the analysed cross section.

The maximum displacements highlighted in scheme d of Figure 5.7 are particularly interesting, especially if compared with those of schemes a, b, c and d in the same figure, and with the global structural response of beam illustrated in Figure A.8 of appendix A, considering the only excitation point B7. In particular, the asymmetric excitation B6 (scheme d of Figure 5.7) causes important differences between the half flanges, being the maximum displacement of 0.059mm and 0.058mm and the minimum displacements of 0.021mm and 0.025mm respectively.

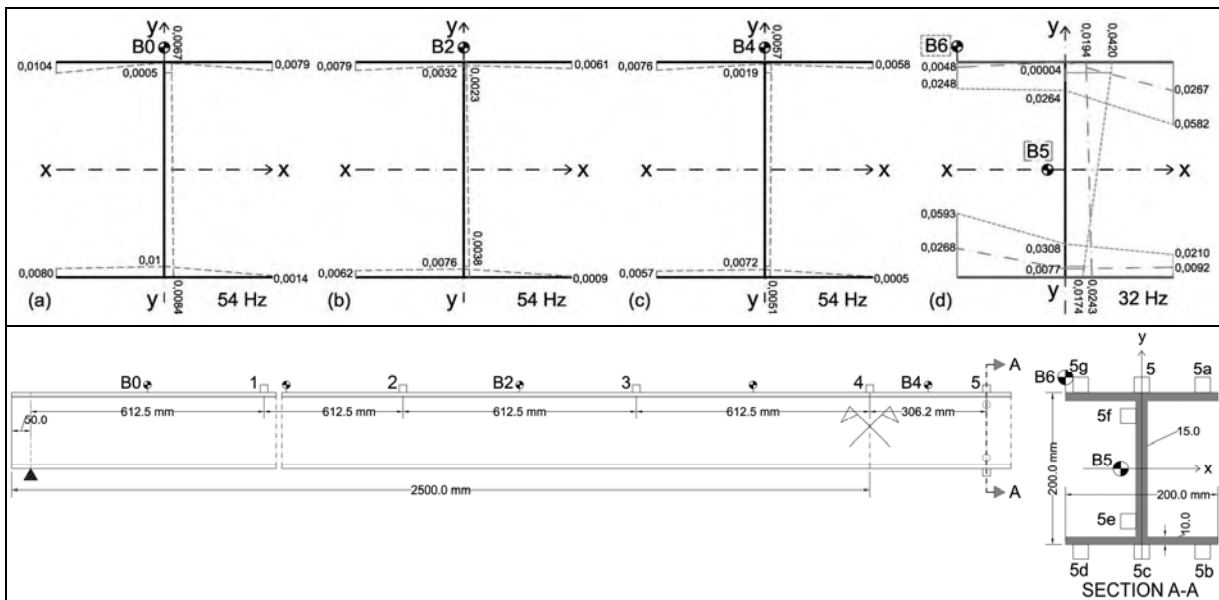


Figure 5.7. Displacements (mm) of section A-A for every excitation; (a) excitation B0 near the support; (b) excitation B2 to $L/4$; (c) excitation B4 to $L/2$; (d) excitation B5 horizontal to $L/2$ and excitation B6 vertical asymmetrical to $L/2$.

The shape modes of the hollow profile “O” instrumented through eight accelerometers set to $L/2$, with a spacing of 45° , were analysed. The section was excited through instant excitations at first at 0° and then, with excitation points at 90° , 120° and 180° as indicated in the test scheme, Figure 5.8. This figure shows one of the most remarkable spectra concerning the excitation point at 0° and the related modes of vibration (modes 2 and 4) both via the development of the circumference of the circular profile and via the polygonal approximation of the circular section. To investigate the structural response to free vibration of the cross section of the circular section

element, singular displacement was derived from the two frequencies of the principal modes, 30.51 Hz and 440.97 Hz respectively, for each type of excitation (Figure 5.8).

The polygonal oversimplification of the section, for each principal mode and for each single excitation has been proposed in Figure 5.8.

For the frequency 30.51Hz of second mode of vibration the sectional response of the “O” shaped member (Figure 5.9) highlights a maximum transversal displacements (0.017mm) greater than the global maximum flexural displacements (0.011mm), as depicted in Figure A.5 of appendix A, for the same excitation point.

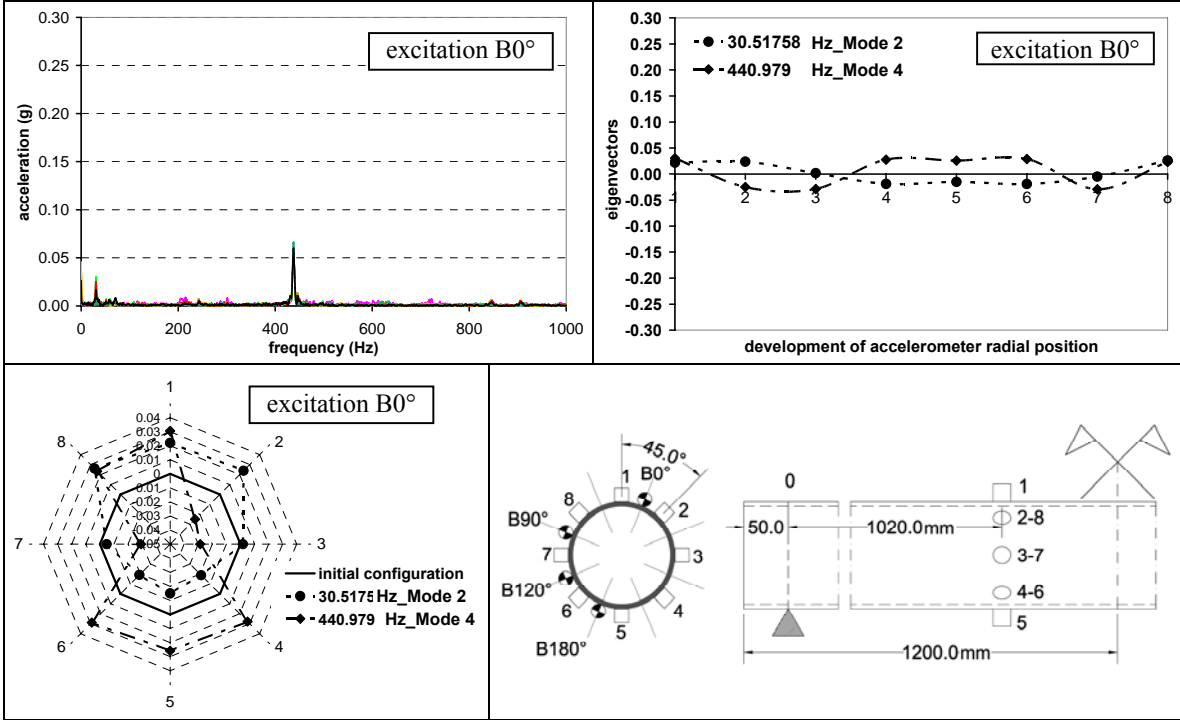


Figure 5.8. Spectrum in frequency domain for every excitation and modal shapes, “O” profile.

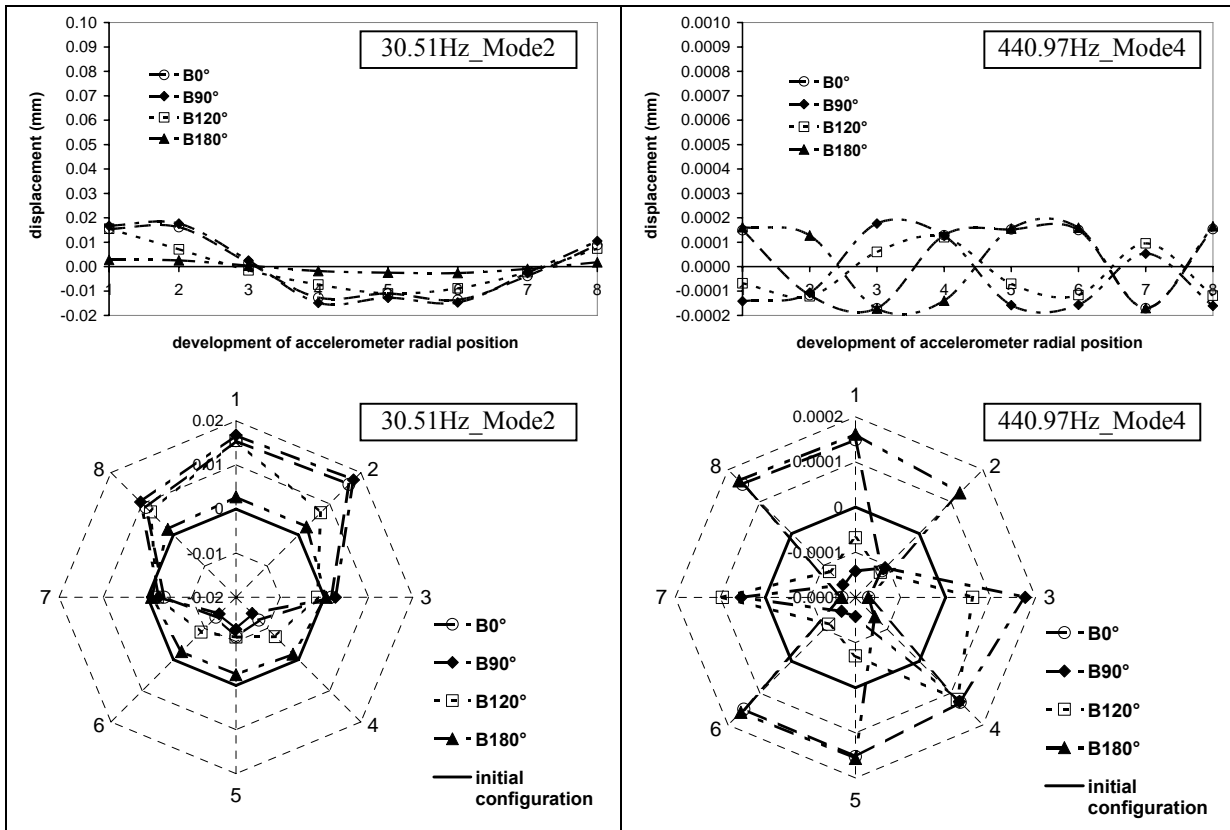


Figure 5.9. Displacements of transversal section, "O" profile

5.2.1.1.4. Parametric comparison and analysis of results

A comparison of the experimental results is proposed through the analysis on the variations of the dynamic parameters for the diverse physical-mechanical characteristics of the profiles. Of the comparison of spectra in the frequency domain (Figures 5.10 and 5.11), considering the interval which includes the fundamental frequency of each profile, the influence of the relationship between length (L) and the maximum height of the cross section of the profile (h) is evident. For the structural elements with L/h ratio included between 20 and 30, the fundamental frequencies are in the interval 25-40 Hz for the supported configuration and 28-55 Hz for the fully clamped elements; in the presence of L/h ratio included in the interval 50-60, the structural elements present a range of fundamental frequencies between 8-16 Hz and 12-17 Hz, for simply supported and fully clamped configuration, respectively.

The same subdivision is maintained, with a tendency to accentuate, also for the second and third mode of vibration as represented in the Figures 5.12 and 5.13.

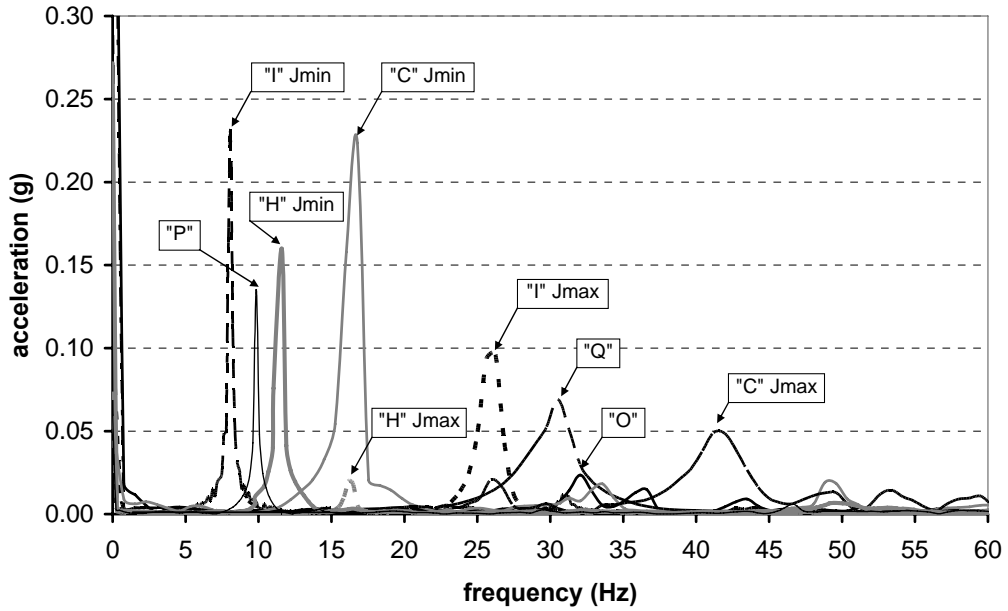


Figure 5.10. Free vibration response in frequency domain, first mode. Supported configuration

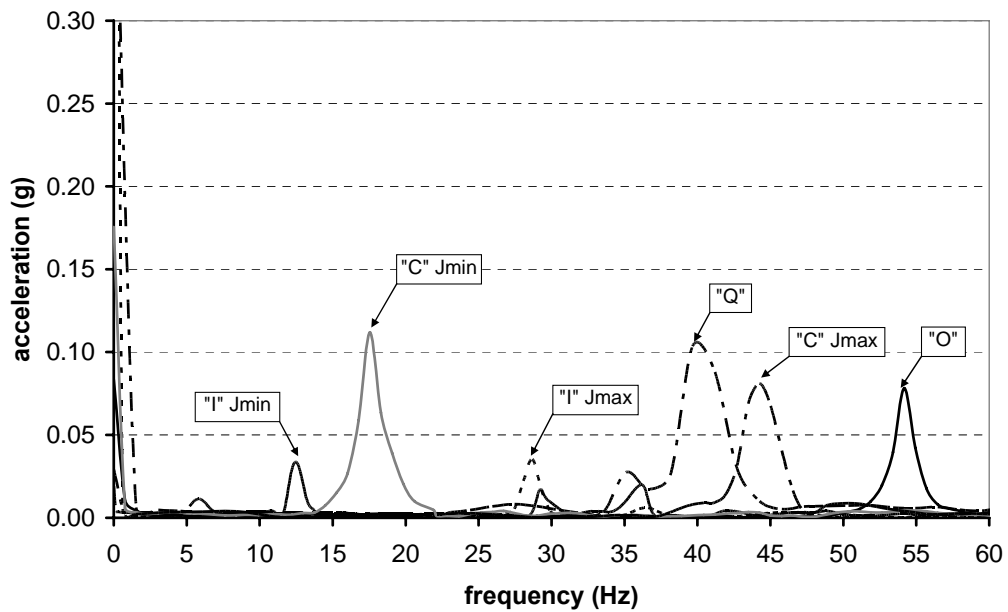


Figure 5.11. Free vibration response in frequency domain, first mode. Clamped configuration

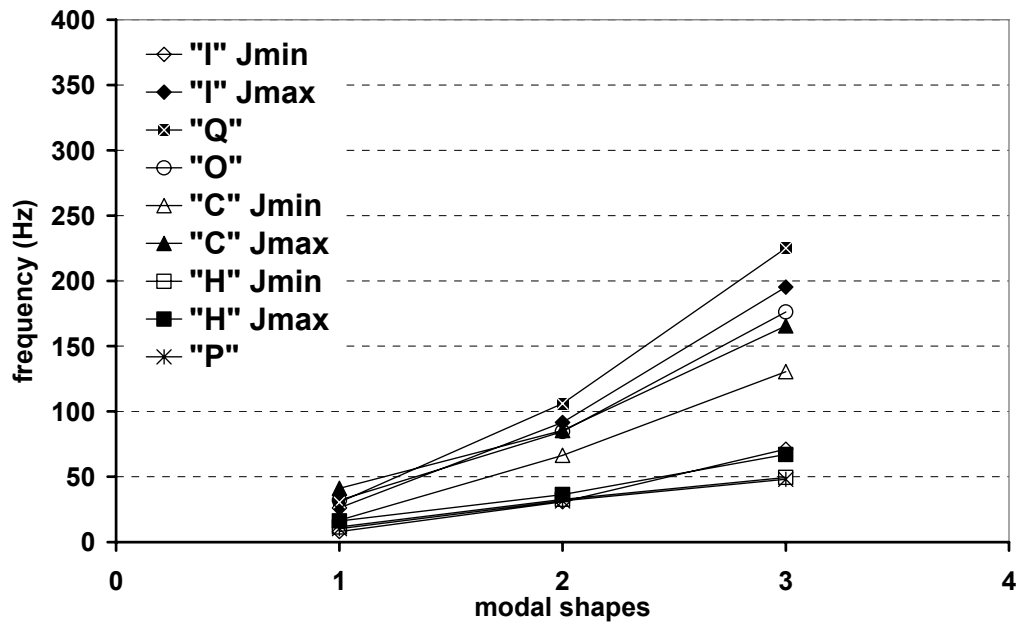


Figure. 5.12. Mode of vibration, supported configuration

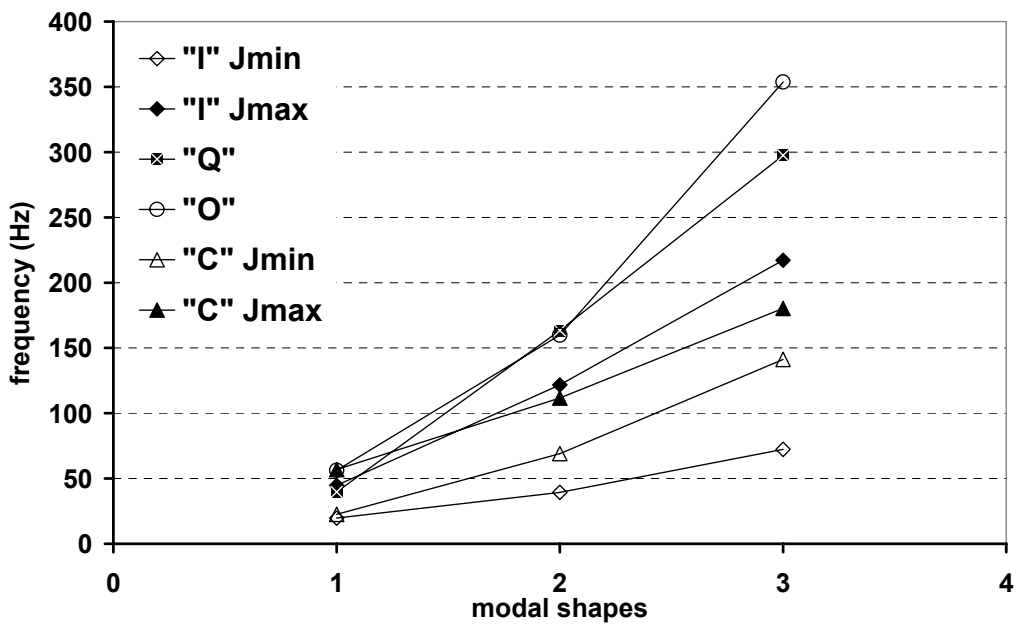


Figure. 5.13. Mode of vibration, clamped configuration

Figures 5.14 and 5.15 illustrate the trend of the damping ratio upon dead load variation, P_p , of the single structural elements for the two restrain conditions analysed.

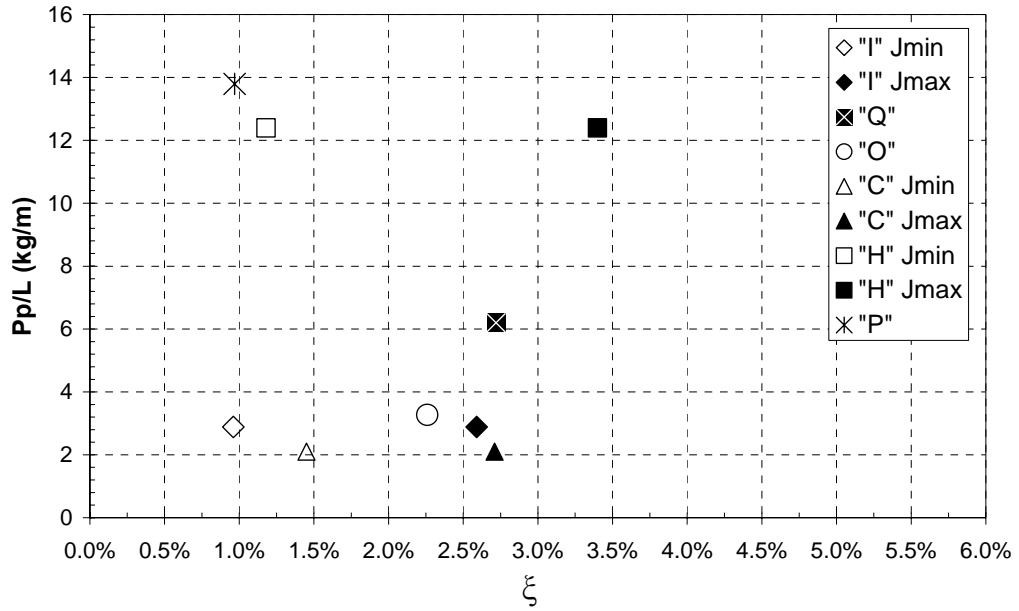


Figure 5.14. P_p/L - ξ , supported configuration

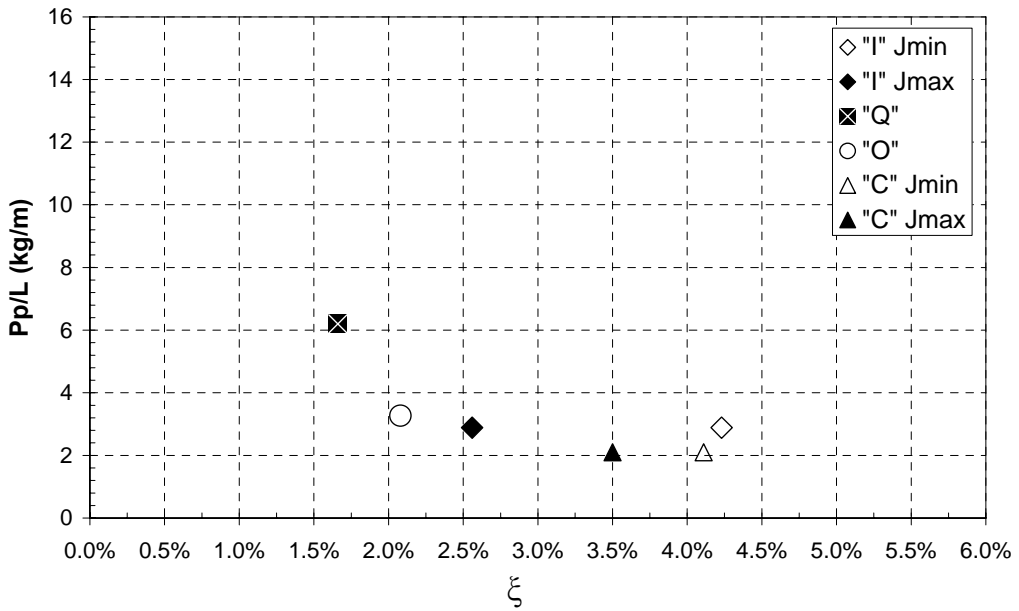


Figure 5.15. P_p/L - ξ , clamped configuration

Figures 5.16 and 5.17 allow the verification of the relationship between the derived damping percentage and the a-dimensional value of transversal displacement.

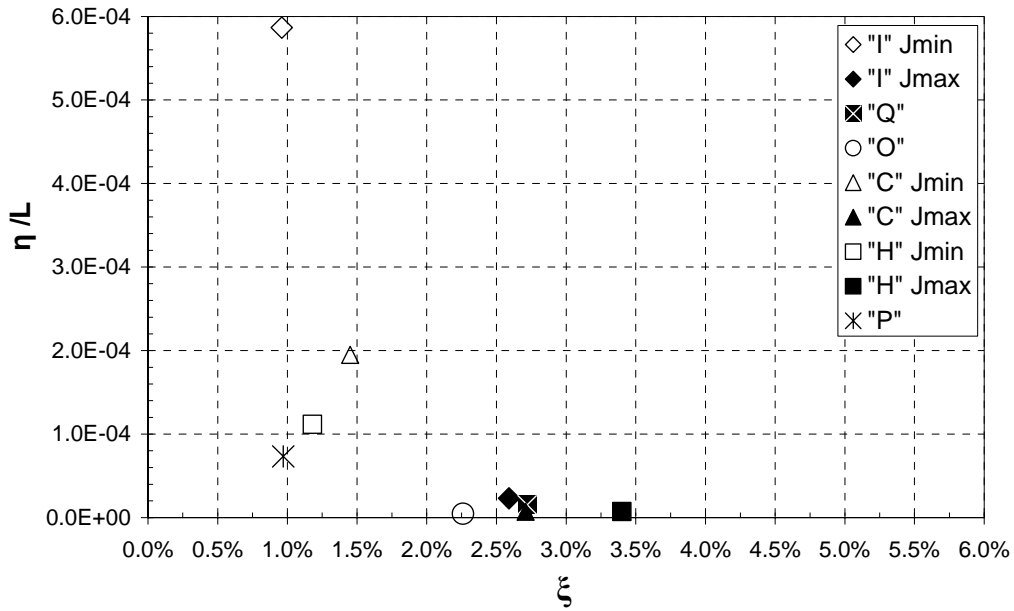


Figure 5.16. η/L - ξ , supported configuration

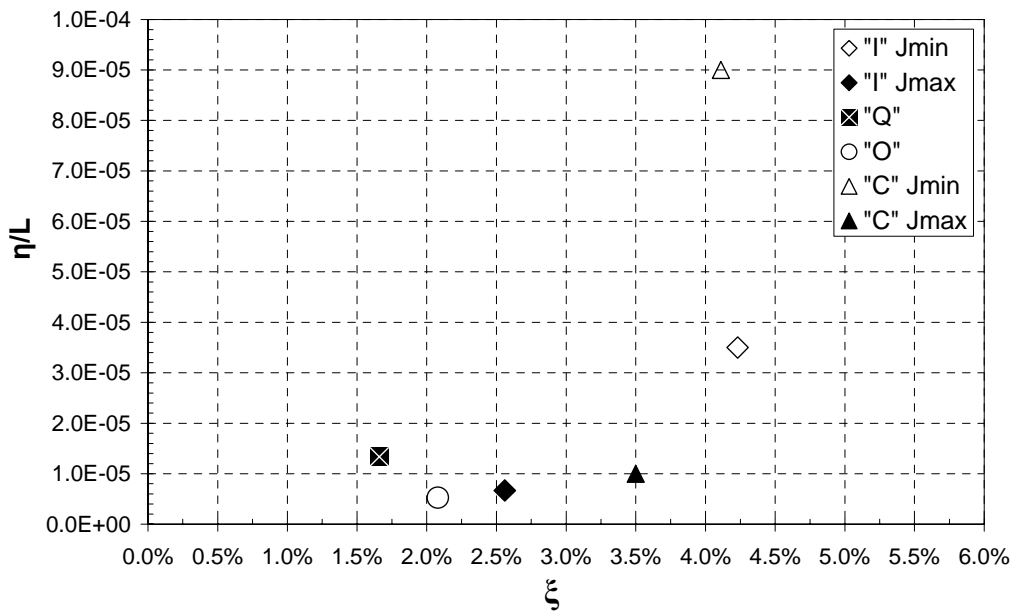


Figure 5.17. η/L - ξ , clamped configuration

For both boundary conditions the geometric effect connected to the cross sections analysed with regards to the trend of the experimental results appears to be important both in terms of dead load, of displacement and of damping.

5.2.1.2. Numerical analysis

The purpose of the present part of the research is to examine and verify by analytical ways the experimental results presented. The comparison between experimental and numerical values and the FEM results is showing a basically good agreement. The experimental dynamic behaviour of fiber-reinforced composite structural elements is here described and analysed through a comparison with profiles of traditional materials considered analogous for employment and performance (i.e. steel and aluminium); to make the comparison accurate, the cross sections were previously optimized.

The usual formulation relative to flexural vibration were used in the numerical approach for both boundary conditions considering the different geometrical properties. For the determination of natural frequencies with simply supported condition, f_{n-s} , the following equation was used:

$$f_{n-s} = n^2 \cdot \frac{\pi}{2} \cdot \frac{1}{L^2} \cdot \sqrt{\frac{E_Z \cdot J \cdot ag}{A \cdot \gamma}} \quad (5.5)$$

While in presence of subjected to axial load the natural frequencies, f_{n-c} , are determined through:

$$f_{n-c} = \frac{(kl)^2}{L^2} \cdot \sqrt{\frac{E_Z \cdot J \cdot ag}{A \cdot \gamma}} \quad (5.6)$$

The kl is the eigenvalue, where $kl = 4.730$ for the fundamental mode, $kl = 7.853$, 10.996 for the second and third modes of vibration respectively (Timoshenko 1954).

For a more complete analytical approach, it is necessary to use algorithms which take into account shear deformation and twisting stiffness. From the complete equation (5.7) relating to the natural frequency of a prismatic bar with supported ends, the reduced version (5.9), as described by Timoshenko (1921) was used.

$$\left(\sqrt{\frac{E_Z \cdot J \cdot ag}{A \cdot \gamma}} \right)^2 \cdot \frac{\pi^4 \cdot n^4}{L^4} - (\omega)^2 - \frac{n^2 \cdot \pi^2 \cdot \rho^2}{L^2} \cdot \left(1 + \frac{E_Z}{k \cdot G_{ZX,ZY}} \right) \cdot (\omega)^2 + \left(\frac{\rho^2 \cdot \gamma}{k \cdot ag \cdot G_{ZX,ZY}} \right) \cdot (\omega)^4 = 0 \quad (5.7)$$

Where the coefficient k , depending on the form of the cross section, is equal to:

$$k = \frac{J \cdot b_0}{S_0 \cdot A} \quad (5.8)$$

Limiting the evaluation of the shear effect for the elements simply supported, we thus have:

$$f_{n-s}^{-1} = \frac{\pi}{2} \cdot \sqrt{\frac{E_Z \cdot J \cdot ag}{A \cdot \gamma}} \cdot \frac{n^2}{L^2} \cdot \left[1 - \left(\frac{1}{2} \cdot \pi^2 \cdot \rho^2 \cdot \frac{n^2}{L^2} \right) \cdot \left(1 + \frac{E_Z}{k \cdot G_{ZX,ZY}} \right) \right] \quad (5.9)$$

In the case of experimental tests with members subjected to axial load, the vertical structural elements were subjected not only to their dead load but also to a constant axial load equal to 10kN. To consider the axial load the analytical approach gives the following equations:

$$f_{n-c(\text{exp})} = f_{n-c}^{-1} \cdot \sqrt{1 - \frac{P}{P_{cr}}} \quad (5.10)$$

where P_{cr} is:

$$P_{cr} = \frac{n^2 \cdot \pi^2 \cdot E_Z \cdot J_{\min}}{L_0^2} \quad (5.11)$$

The value $f_{n-c(\text{exp})}$ agree with the experimental data, while f_{n-c}^{-1} without axial load (shown in Table 5.5) has been extracted from the equation (5.10) obtaining:

$$f_{n-c}^{-1} = f_{n-c(\text{exp})} \cdot \sqrt{\frac{P_{cr}}{P_{cr} - P}} \quad (5.12)$$

The letter P indicates the sum of the applied load and the dead load, P_{cr} = critical value (induced by compression load P) corresponding to deformation with n semi-wave.

Table 5.5 lists the experimental results of the frequencies of profiles with clamped-clamped configuration, with axial force and dead load, f_{n-c} , and without the applied load, f_{n-c}^{-1} .

Tabella 5.5. Frequency values with and without axial load, clamped configuration

| Mode of vibration | "I" | | | | "Q" | | "O" | | "C" | | | |
|-------------------|--------------------------|--|--------------------------|--|--------------------------|--|--------------------------|--|--------------------------|--|--------------------------|--|
| | J _{min} | | J _{max} | | f _{n-c} (Hz) | f _{n-c} ⁻¹ (Hz) | f _{n-c} (Hz) | f _{n-c} ⁻¹ (Hz) | J _{min} | | J _{max} | |
| | f _{n-c} (Hz) | f _{n-c} ⁻¹ (Hz) | f _{n-c} (Hz) | f _{n-c} ⁻¹ (Hz) | | | | | f _{n-c} (Hz) | f _{n-c} ⁻¹ (Hz) | f _{n-c} (Hz) | f _{n-c} ⁻¹ (Hz) |
| 1 | 9.530 | 19.72 | 28.68 | 44.69 | 39.67 | 39.93 | 55.70 | 56.30 | 17.54 | 22.51 | 44.25 | 56.79 |
| 2 | 37.80 | 39.31 | 112.3 | 121.6 | 167.8 | 168.1 | 159.4 | 159.9 | 65.61 | 69.09 | 106.0 | 111.7 |
| 3 | 77.62 | 72.33 | 209.9 | 217.2 | 292.9 | 293.0 | 535.2 | 353.6 | 138.1 | 141.2 | 176.2 | 180.2 |

For fundamental frequency the influence of applied load is greater for “I” profile with 51% and 36% for J_{\min} and J_{\max} respectively; while for “C” profile the frequency value of first mode of configuration subjected to axial load decreases of 22% respect to configuration without the axial load. For “Q” and “O” profile the first frequency value with and without load is similar.

5.2.1.2.1. Mechanical characteristics

The longitudinal dynamic elastic modulus E_Z^* was determined from equation (5.9) on the basis of the experimental frequencies of first mode of vibration indicated in Table 5.7. Formula (5.9) was solved for E_Z by the usual solution method for third-grade equations.

Table 5.6 shows the variation of dynamic elastic modulus according to the frequency of the structural element considered. For the analyzed configuration, the variation of E_Z^* against the mean value of static elastic modulus E_Z (see chapter 2.2) is relevant for open cross section profiles. Altogether the elastic modulus values are very close to the static modulus highlighting the validity of the experimental technique.

Tabella 5.6. Dynamic elastic modulus E_Z^* of first mode of vibration

| Structural element | E_Z^* (MPa) |
|--------------------|---------------|
| “I”, J_{\max} | 26390 |
| “Q” | 23520 |
| “O” | 22610 |
| “H”, J_{\max} | 20250 |
| “P” | 23300 |

The dynamic shear modulus G_{XY}^* has been defined in structural profile type “O” through the equation of the torsional natural vibration replacing f_n with experimental data, as shown in Equation (5.13):

$$f_n = \frac{n}{2 \cdot L} \cdot \sqrt{\frac{G_{XY}}{\gamma}} \quad (5.13)$$

obtaining therefore:

$$G_{XY}^* = f_n^2 \cdot \left(\frac{2 \cdot L}{n}\right)^2 \cdot \gamma \quad (5.14)$$

The G_{XY}^* value determined from (5.14) is equal to 9112 MPa for the first of the frequencies (30.51 Hz) of the recorded torsional vibrations.

5.2.1.2.2. Finite element analysis

The finite element modelling was carried out to determine natural frequency and modal shapes and, as for the numerical approach, considering the behaviour of the FRP elements for the two restrain conditions (Figure 5.18).

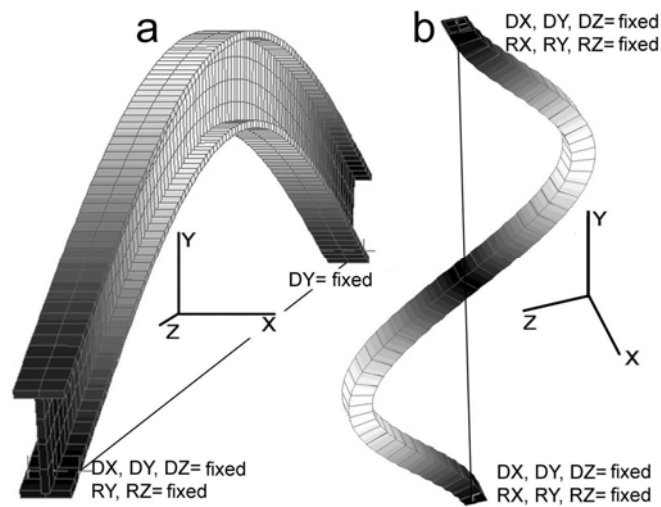


Figure 5.18. (a) First mode of vibration (“I” profile, supported configuration);
(b) second mode of vibration (“Q” profile, clamped configuration)

Finite element analysis was carried out in the linear elastic field considering the beams constituted by homogenous materials and with orthotropic elastic properties. A commercial Finite-Element software was used to perform the natural frequencies analysis, four-node isoparametric shell elements were employed in the modeling. The mechanical characteristics used during analysis are illustrated in Table 5.6.

Tabella 5.6. Average values of mechanical characteristics

| | | |
|-----------------|------------------------|-------------------------|
| Density | γ | 1800 daN/m ³ |
| Elastic modulus | E_L (Longitudinal) | 23000 MPa |
| | E_T (Transversal) | 8500 MPa |
| Shear modulus | G | 3000 MPa |
| Poisson's ratio | ν_L (Longitudinal) | 0.23 |
| | ν_T (Trasnversal) | 0.09 |

Table 5.7 compares the values of natural frequency obtained from the numerical approach (Th), from a finite element analysis (FEM) and from experimental data (Exp).

In detail for the supported configuration the numerical values were obtained by equation 5.5 and 5.9, for isotropic and orthotropic material that considers the shear deformation and twisting stiffness.

The experimental results shown in Table 5.7 are the values included in the intervals defined by a variation of data which, altogether, refer to the frequency of the mode evaluated. In the specific case, the experimental data of Table 5.7 correspond to intervals of fundamental frequencies that are the closest to the analytical results, which highlights the good agreement between experimental and numerical results.

As for hollow and open “H” profiles with low slenderness, it is evident that formula (5.9) minimizes the difference between experimental and analytical data.

For the configuration subjected to axial load the experimental results (Exp) are obtained by equation (5.12) that allows to extract the frequency values without the influence of axial force. Always for clamped boundary condition the numerical values (Th) were determined by the approach that considers the isotropic material through the equation 5.6.

Table 5.7. Natural frequencies of mode of vibration

| Structural elements | Mode | Supported configuration | | | | Subjected to axial load | | |
|-------------------------|------|-------------------------|---------------------|---------------------|----------|-------------------------|---------------------|-----------------------|
| | | FEM (Hz) | Th (Hz) by eq.(5.5) | Th (Hz) by eq.(5.9) | Exp (Hz) | FEM (Hz) | Th (Hz) by eq.(5.6) | Exp (Hz) by eq.(5.12) |
| “I” J _{min} | 1 | 7.07 | 7.01 | 6.54 | 7.02 | 13.69 | 14.85 | 19.72 |
| | 2 | 28.23 | 28.05 | 26.06 | 30.82 | 37.64 | 40.95 | 39.31 |
| | 3 | 63.24 | 63.12 | 58.26 | 71.10 | 73.48 | 80.29 | 72.33 |
| “I” J _{max} | 1 | 24.38 | 24.59 | 22.81 | 24.41 | 51.94 | 52.01 | 44.69 |
| | 2 | 92.78 | 98.36 | 89.39 | 91.55 | 136.47 | 143.58 | 121.59 |
| | 3 | 191.68 | 221.32 | 194.1 | 195.31 | 252.80 | 281.52 | 217.17 |
| “Q” | 1 | 37.66 | 38.34 | 34.71 | 35.09 | 74.50 | 79.275 | 39.67 |
| | 2 | 140.04 | 153.34 | 133.1 | 106.04 | 189.42 | 153.08 | 163.27 |
| | 3 | 275.07 | 345.03 | 277.8 | 225.06 | 339.93 | 345.48 | 297.54 |
| “O” | 1 | 41.48 | 42.21 | 38.46 | 38.14 | 81.91 | 87.83 | 56.30 |
| | 2 | 154.39 | 168.83 | 150.4 | 84.68 | 207.11 | 242.21 | 159.88 |
| | 3 | 297.79 | 379.87 | 325.6 | 176.24 | 369.79 | 474.90 | 353.66 |
| “C” J _{min} | 1 | 15.14 | 14.37 | 13.52 | 14.49 | 30.75 | 29.41 | 22.51 |
| | 2 | 60.16 | 57.50 | 53.62 | 66.37 | 83.82 | 81.07 | 69.09 |
| | 3 | 133.84 | 129.39 | 118.9 | 130.46 | 161.96 | 158.95 | 141.21 |
| “C” J _{max} | 1 | 48.36 | 43.42 | 57.47 | 41.19 | 94.24 | 88.83 | 56.79 |
| | 2 | 178.88 | 173.68 | 218.5 | 85.45 | 239.61 | 244.85 | 111.68 |
| | 3 | 342.89 | 390.78 | 448.9 | 165.55 | 429.98 | 480.07 | 180.22 |
| “H” J _{min} | 1 | 9.97 | 10.21 | 9.75 | 10.5 | \ | \ | \ |
| | 2 | 38.55 | 40.84 | 38.35 | 32.65 | \ | \ | \ |
| | 3 | 80.73 | 91.90 | 83.89 | 49.44 | \ | \ | \ |
| “H” J _{max} | 1 | 18.80 | 18.39 | 17.54 | 16.47 | \ | \ | \ |
| | 2 | 67.95 | 73.57 | 68.83 | 36.31 | \ | \ | \ |
| | 3 | 160.83 | 165.54 | 149.8 | 67.14 | \ | \ | \ |
| “P” | 1 | 11.93 | 10.74 | 10.22 | 11.9 | \ | \ | \ |
| | 2 | 46.26 | 42.98 | 40.72 | 31.58 | \ | \ | \ |
| | 3 | 98.92 | 96.72 | 90.97 | 48.06 | \ | \ | \ |

The experimental values of the “C” profile, in the asymmetrical configuration, highlight a greater dispersion compared to the results obtained analytically.

5.2.1.2.3. Comparison with traditional materials

The study compares the dynamic response of the experimental and numerical results of frequency values of GFRP profiles with the numerical data, obtained through equation 5.5, of steel and aluminum structural elements. The comparison was carried out considering the same static scheme and the same length of the GFRP element. The cross sections of steel and aluminum

profiles were properly optimized according to an equivalent structural performance which takes into account the maximum elastic transverse displacement achieved in the elastic field of a simple supported bending element subjected to dead load only. This comparison was carried out for the open cross-section profiles, “I”, and “H”, for the hollow profiles “Q” and “O” and for the panel element. In Table 5.8 are reported the mechanical characteristics of the traditional materials used for numerical modelling.

Table 5.8. Mechanical characteristics of profiles

| Materials | E_L (MPa) | G (MPa) | ν_L | γ (daN/m ³) |
|-----------|-------------|---------|---------|--------------------------------|
| Steel | 210000 | 80000 | 0.25 | 7850 |
| Aluminium | 69000 | 25862 | 0.334 | 2700 |

The detail of the equivalent cross sections of the profiles in steel and aluminium and the relationships with GFRP structural elements is recorded in Tables 5.9 and 5.10.

Table 5.9. Dimensions of steel profiles and comparison with GFRP profile

| Structural elements | Cross section dimensions (cm) | L (cm) | J_{max} (cm ⁴) | J_{min} (cm ⁴) | A_A (cm ²) | A_A / A_{GFRP} (%) | Pp_A (kg/m) | Pp_A / Pp_{GFRP} (%) |
|---------------------|-------------------------------|--------|------------------------------|------------------------------|--------------------------|----------------------|---------------|------------------------|
| “I” | 5.75x2.9x0.46 | 300 | 22.89 | 1.86 | 4.87 | 33.08 | 3.82 | 132.49 |
| “H” | 11.5x11.5x0.86x0.58 | 500 | 475.5 | 146.6 | 22.17 | 33.09 | 17.4 | 140.35 |
| “Q” | 5.75x5.75x0.575 | 240 | 53.88 | | 11.91 | 33.08 | 9.35 | 150.91 |
| “O” | Ø6.92, thick0.29 | 240 | 32.77 | | 6.00 | 33.19 | 4.72 | 144.46 |
| “P” | 36.2x4.6x0.23 | 420 | 88.56 | | 24.59 | 32.98 | 19.3 | 139.78 |

Table 5.10. Dimensions of aluminum profiles and comparison with GFRP profile

| Structural elements | Cross section dimensions (cm) | L (cm) | J_{max} (cm ⁴) | J_{min} (cm ⁴) | A_{AL} (cm ²) | A_{AL} / A_{GFRP} (%) | Pp_{AL} (kg/m) | Pp_{AL} / Pp_{GFRP} (%) |
|---------------------|-------------------------------|--------|------------------------------|------------------------------|-----------------------------|-------------------------|------------------|---------------------------|
| “I” | 7.6x3.8x0.6 | 300 | 69.69 | 5.671 | 8.49 | 57.68 | 2.29 | 79.42 |
| “H” | 15.2x15.2x1.1x0.76 | 500 | 1447.2 | 446.22 | 38.68 | 57.73 | 10.44 | 84.23 |
| “Q” | 7.6x7.6x0.76 | 240 | 163.99 | | 20.78 | 57.72 | 5.61 | 90.52 |
| “O” | Ø9.13, thick0.38 | 240 | 99.74 | | 10.46 | 57.85 | 2.82 | 86.37 |
| “P” | 48x6x0.3 | 420 | 269.54 | | 43.05 | 57.73 | 11.62 | 84.16 |

It is interesting to note that the equivalent cross section of steel A_A and aluminium A_{AL} profiles are equal to 33% and 57%, respectively, in comparison with the area of GFRP profile (A_{GFRP}). As regards the incidence of the material dead load, the GFRP profiles (Pp_{GFRP}) show, compared to steel (Pp_A), a reduction of dead load which varies between 34% and 25%. The values of

frequency and modes of vibration, shown in Figures from 5.19 to 5.25, show the comparison between the experimental results “Exp”, the values derived from numerical analysis “Th” and the modelling of finite element analysis “FEM”.

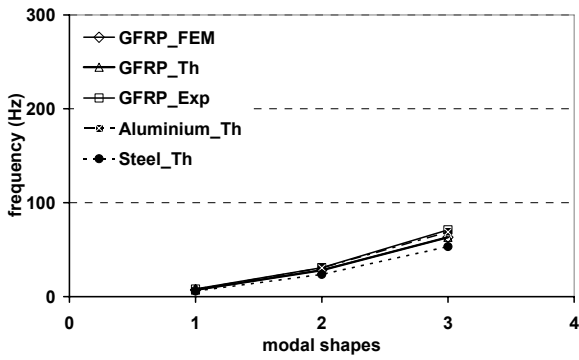


Figure 5.19. “I” profile, J_{min} , supported configuration

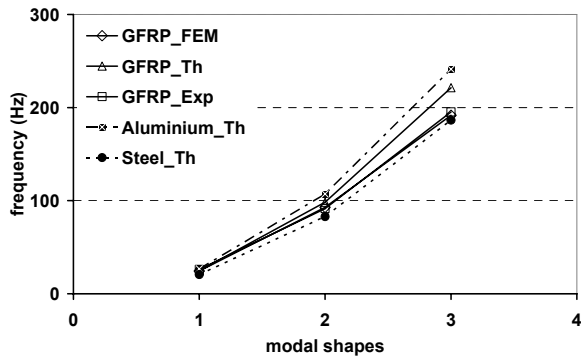


Figure 5.20. “I” profile, J_{max} , supported configuration

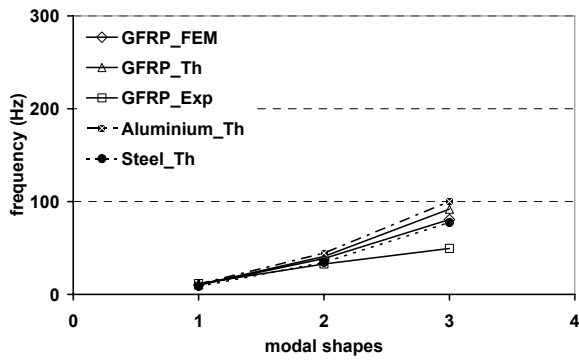


Figure 5.21. “H” profile, J_{min} , supported configuration

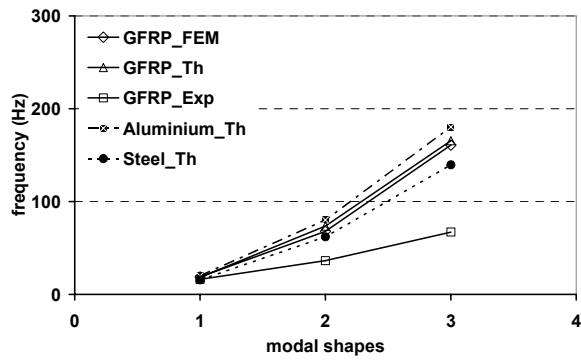


Figure 5.22. “H” profile, J_{max} , supported configuration

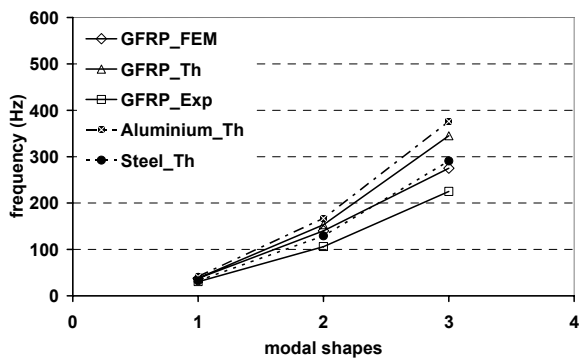


Figure 5.23. “Q” profile, supported configuration

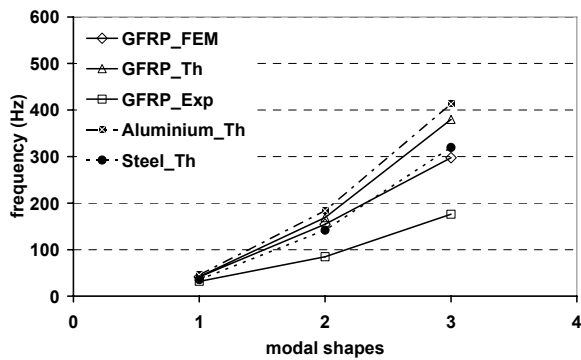


Figure 5.24. “O” profile, supported configuration

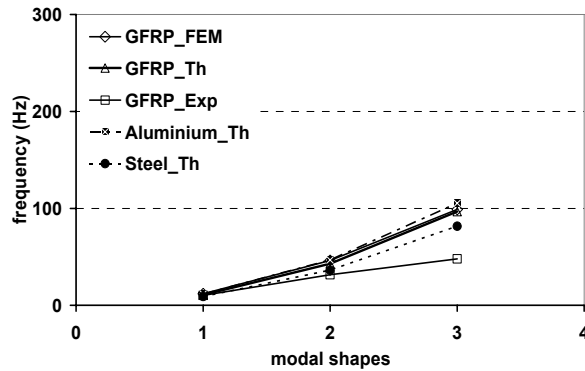


Figure 5.25. “P” structural element, supported configuration

The trend of ratios between the theoretical values of the analysed traditional materials concerning the frequency of the modes of vibration and referential experimental data of GFRP structural elements ($H_{ZA}/H_{Z_{GFRP}}$ and $H_{Z_{AL}}/H_{Z_{GFRP}}$), reported in Table 5.11, allow a better comparison of structural performance.

Table 5.11. Natural frequencies comparison, simply supported configuration

| Materials | Mode 1 | Mode 2 | Mode 3 |
|------------------------|--------|---------|---------|
| “I” profile, J_{min} | | | |
| Aluminium | 5.41% | 0.80% | 3.25% |
| Steel | 26.81% | 23.25% | 25.14% |
| “I” profile, J_{max} | | | |
| Aluminium | 2.11% | 17.07% | 23.47% |
| Steel | 21.04% | 9.48% | 4.53% |
| “H” profile, J_{min} | | | |
| Aluminium | 4.09% | 36.31% | 102.53% |
| Steel | 25.80% | 5.45% | 56.69% |
| “H” profile, J_{max} | | | |
| Aluminium | 23.92% | 120.73% | 168.59% |
| Steel | 4.13% | 70.77% | 107.80% |
| “Q” profile | | | |
| Aluminium | 36.90% | 57.55% | 67.02% |
| Steel | 5.90% | 21.89% | 29.22% |
| “O” profile | | | |
| Aluminium | 43.29% | 116.86% | 134.45% |
| Steel | 10.81% | 67.72% | 81.31% |
| “P” structural element | | | |
| Aluminium | 13.70% | 48.29% | 119.23% |
| Steel | 11.83% | 14.91% | 69.91% |

The comparison between the results determined via analytical approach and experimental data, shows a good dynamic behaviour of GFRP profile compared with the response of elements in

steel and aluminium. The “I” profile, for both the principal axis of inertia, with conditions of supported restraint, shows a negligible difference in the passage from composite material to aluminium. The fundamental frequencies of the composite profile, with J_{max} , are equal to 24.41 Hz (experimental) and 24.59 Hz (theoretical), while, for the profiles in aluminium, the value determined via analytical approach is equal to 26.79 Hz. The same tendency is maintained also in the presence of minor inertia for the first three modes of vibration. For the simply supported closed section profile, the frequencies of the first fundamental mode are, for GFRP structural elements, equal to 35.09 Hz (“Q”) and 38.14 Hz (“O”) while for steel they are 32.31 Hz and 35.5 Hz respectively. A good correspondence between the results was also found for the open-cross section profile – wide flanges – which presents values of the first vibration frequency very similar to steel for J_{max} , and to aluminium for J_{min} . GFRP panel has a frequency of the first vibration mode similar to traditional materials with values equal to 10.29 Hz for FRP element, 11.7 Hz for aluminium and 9.07 Hz for steel.

5.2.1.3. Applications

Through the analysis of the experimental dynamic response of GFRP structural elements, some of the likely applications in the structural engineering field are analysed, with particular reference to the structural static function of the deck.

The fundamental frequency is analysed considering both the increment of live load and the variation of the beam length, comparing it with the frequency induced by human action, Table 5.12, in order to verify the presence of resonance phenomena. In detail, the table lists the data obtained from one referential code (BS5400 1978; ISO10137 2005; CEB209 1991) and from previous studies on vibrations induced by human action (Bachmann et al. 1995; Dallard et al. 2001). For the analysis, the supported configuration was considered; the live load applied was defined by considering an area in proximity to the single beam determined by its length and transversally by the one metre inter-axis.

Table 5.12. Regulations in term of vibrations

| Standard and reference | Vertical vibrations (Hz) | | |
|------------------------|--------------------------|---------|---------|
| | Walking | Running | Jumping |
| BS 5400 (1978) | <5 | / | / |
| ISO 10137 (2005) | 1.7-2.3 | / | / |
| CEB 209 (1991) | 2.0-2.4 | 2.0-3.0 | 2.0-3.0 |
| Bachmann et al.(1995) | 1.6-2.4 | 2.0-3.5 | 1.8-3.4 |
| Dallard et al.(2001) | 1.2-2.2 | / | / |

Figures 5.26 and 5.27 illustrate, for three load conditions - dead load (DL) in combination with a different live load (LL) - the variation of the fundamental frequency according to the beam length. The frequency values were derived from the FEM analysis carried out with the same procedure described in previously chapter 5.2.1.2.2, simulating the dynamic response of elements with different lengths. The experimental results highlight, overall, a good approximation of the curves of tendency obtained from theoretical data. Figures 5.26 and 5.27 illustrate the interval of frequency regarding the vibration induced by human action, with reference to the value limits proposed by Bachmann et al. (1995).

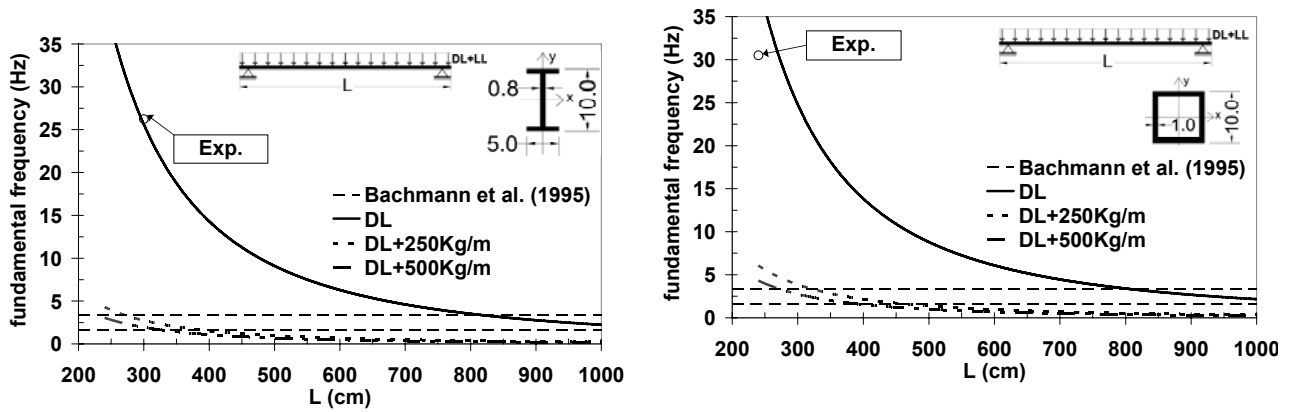


Figure 5.26. Natural frequencies of “I” and “Q”, FEM analysis and experimental results

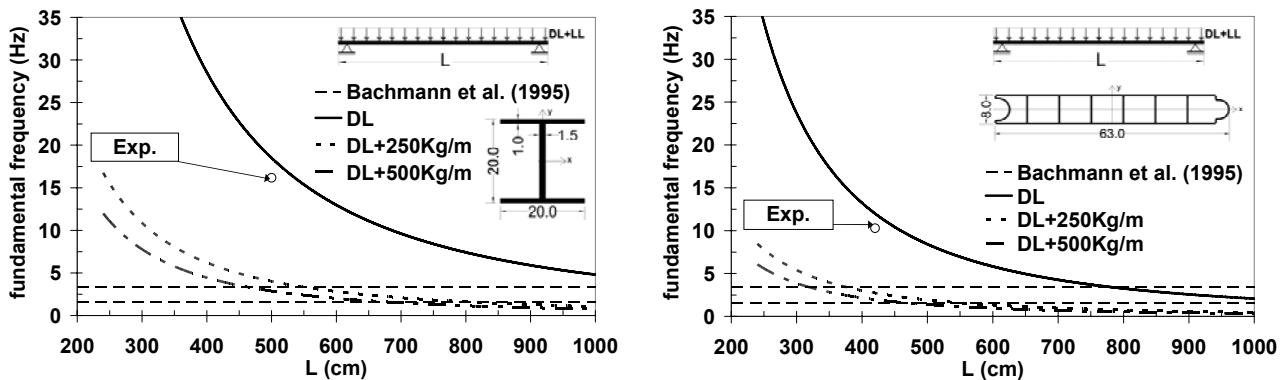


Figure 5.27. Natural frequencies of “H” and “P”, FEM analysis and experimental results

For all figures the curves that concern only the case of dead load obtained from theoretical analysis reveal a good agreement with experimental data highlighted with Exp.

For every profiles analysed and for the three load conditions is highlighted a dynamic response in good agreement with the variation of length beam; in particular the fundamental frequency decreases with increment of length. The trend of the frequency-length relationship of the element is substantially similar for each load condition. For the profiles “I” and “Q”, a reduction of the fundamental frequencies, 89% and 84% respectively, is evident, passing from the dead load only to the live load equal to 250kg/m^2 . As regards the “H” profile and the “P” element, for the same increment of live load, the fundamental frequency decreases by about 29%. From the dead load only to the applied load of 500 kg/m^2 the reduction in the fundamental frequency is equal to about 90% for “I” and “Q” profiles and approximately 84% for “H” and “P” elements. These behaviour confirm that the main decrease occurs with initial overloading.

It is important to highlight, that for the profiles analysed, the fundamental frequency regards the interval of vertical vibration frequency induced by human action (Bachmann et al. 1995) also in the case of limited applied loads and reduced element length.

Considering the increment of applied load and variation of length the “H” profile shows greater values of fundamental frequency. From a comparison with the steel profile, with the cross section properly optimised (see chapter 5.2.1.2.3.), the resulting of dynamic response is similar; with a live load of 100 kg/m^2 , the profile with length equal to 250cm has a frequency equal to

26.81 Hz for the GFRP and 27.12 Hz for steel. For double length (500cm) the frequencies for GFRP and for steel structural element are 5.9 Hz and 5.97 Hz respectively, while at 1000cm they are equal to 1.44 Hz and 1.46 Hz. Such agreement must be considered as a direct effect of the favourable relationship between the dead load (DL) and total load (TL) of the GFRP profile than steel profile; GFRP profile has a mass equal to 11% of the total load, while, for the steel element, the percentage is equal to 15%.

5.2.2. Two-dimensional frame

5.2.2.1. Design and assembling phase

The design of the GFRP framework was carried out by defining certain base hypotheses, such as; the linear elastic behaviour with the conservation of the plan cross section during deformation phase, the effect of shear deformability of the GFRP structural elements, the external constraints considered as infinitely rigid and beam to column joint with a defined rotational stiffness, K_ϕ , (chapter 5.2.2.1.1.).

The framework was designed with a bearing capacity equal to 250 kg/m². For such dimensioning, only the bending moment of the plan were assigned to the beam, ignoring the shear stress and the twisting effects generated by the deck. The mechanical and geometric characteristics of the material and profiles used are described in the Design Manual Fiberline Composites, Table 5.13 and Figure 5.28.

Table 5.13. Mechanical characteristics of GFRP profiles used for 2D framework

| Ultimate strengths | | MPa | Standard |
|----------------------|-----------|-----|--------------------------|
| Flexural Strength | $f_{b,1}$ | 240 | Full scale |
| Flexural Strength | $f_{b,2}$ | 100 | EN 63 - 78 |
| Tensile Strength | $f_{t,1}$ | 240 | EN 61 – 78 |
| Tensile Strength | $f_{t,2}$ | 50 | EN 61 – 77 |
| Compression Strength | $f_{c,1}$ | 240 | Full scale |
| Compression Strength | $f_{c,2}$ | 70 | DIN 53 454 - 71 |
| Shear Strength | f_s | 25 | ASTM D 2344–89/D 3846-85 |

| Stiffness, Transverse Contraction | | [MPa] | [-] | Standard |
|-----------------------------------|------------|-------|-------|-----------------|
| Modulus of Elasticity | E_1 | 23000 | | Full scale |
| Modulus of Elasticity | E_2 | 8500 | | DIN 53 457 - 87 |
| Modulus in Shear | G | 3000 | | |
| Poisson's ratio | ν_{12} | | 0.23 | EN 61 - 78 |
| Poisson's ratio | ν_{21} | | 0.09 | EN 61 – 78 |

| Serviceability Limit State | | Short-term [MPa] | Long-term [MPa] |
|----------------------------|----------------|------------------|-----------------|
| Flexural Stress | $\sigma_{b,1}$ | 135 | 70 |
| Flexural Stress | $\sigma_{b,2}$ | 50 | 25 |
| Tensile Stress | $\sigma_{t,1}$ | 135 | 70 |
| Tensile Stress | $\sigma_{t,2}$ | 25 | 20 |
| Compressive Stress | $\sigma_{c,1}$ | 135 | 70 |
| Compressive Stress | $\sigma_{c,2}$ | 50 | 25 |
| Shear Stress | τ | 17 | 8 |

The subscript 1 shows the longitudinal direction parallel to fibers, while 2 the perpendicular directions to fibers.

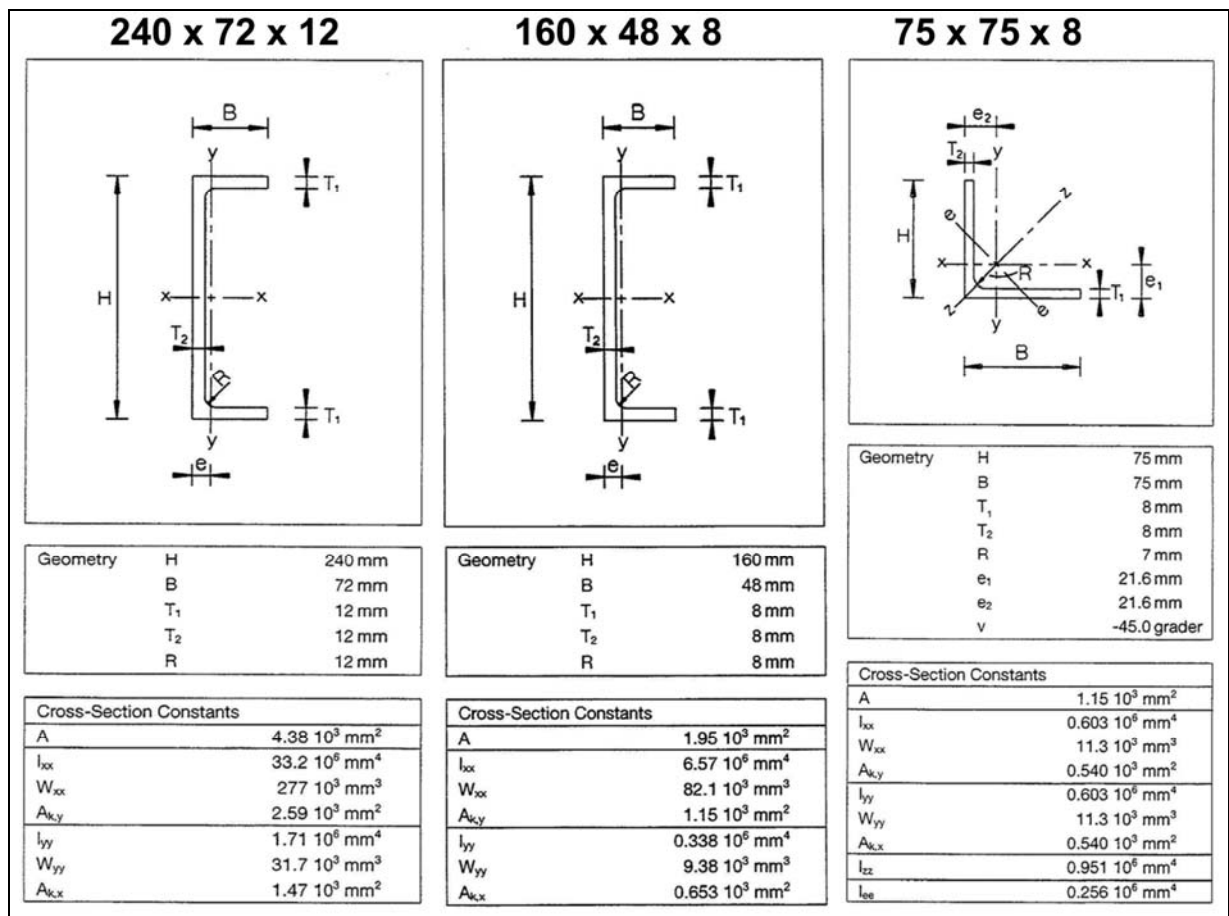


Figure 5.28. Profiles of GFRP frame.

The geometric characteristics of each structural element, beam and column, produced via the coupling of two profiles, are reported in Table 5.14.

Table 5.14. Characteristics of beams and columns.

| Structural Elements | A (cm ²) | J _{xx} (cm ⁴) | J _{yy} (cm ⁴) |
|---------------------|----------------------|------------------------------------|------------------------------------|
| Beam | 38.4 | 1286.144 | 165.888 |
| Column | 86.4 | 6511.104 | 760.32 |

Considering the static scheme previously described and depicted in Figure 5.29 the stress analysis are illustrated in Figure 5.30; the maximum displacement at the midpoint of the beams, equal to 14.86mm, is lower than the adopted reference parameter equal to 1/300 of span (Russo 2007).

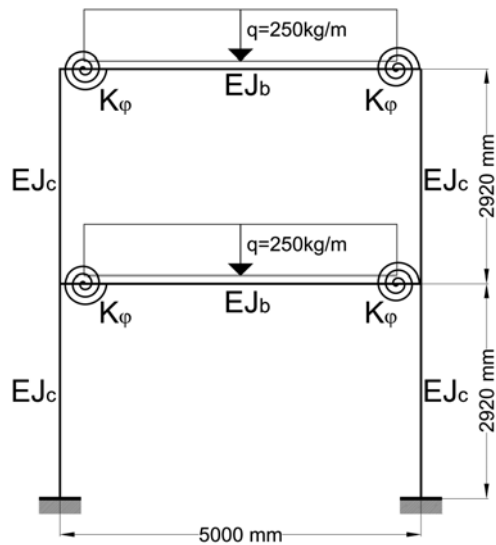


Figure 5.29, Static scheme

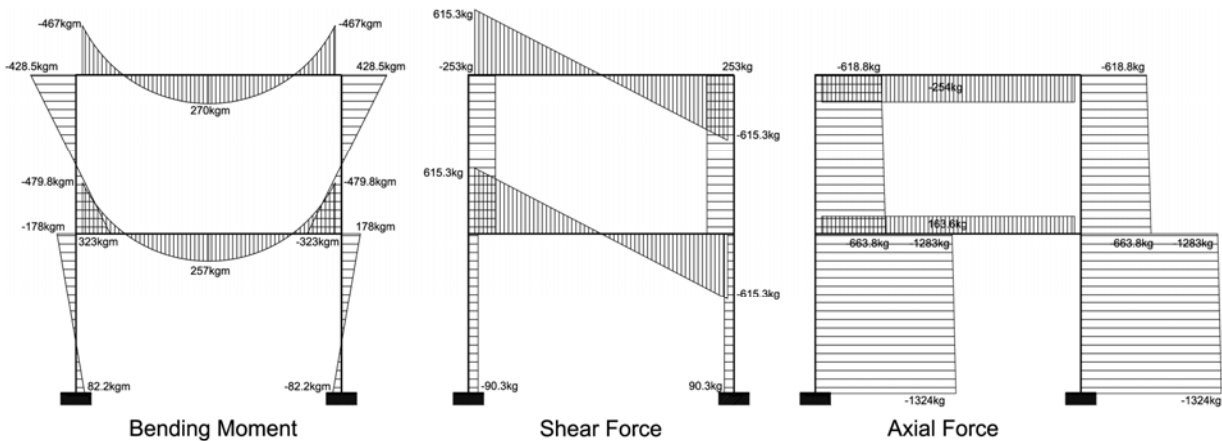


Figure 5.30, Diagrams

Starting from stress analysis were designed all the external and internal joint of GFRP framework through the DT CNR 205/2007 code and the EUROCOMP manual.

Figure 5.31 illustrates the framework while the Figure 5.32 shows the particulars of the internal beam to column joint and external joint. The elements of internal joints are in GFRP material, the steel bolts used are M8 type, class 8.8. The external joint was produced by steel plate, opportunely fixed to the floor by a threaded rod and a contrast plate blocked with a bolt. To this

steel plate were welded the perforated flanges for the assembling of the GFRP column. The bolts used for the external joint of the column are in steel material (8.8 class), M12 and M14 type, for the flanges and web of the GFRP profiles respectively.

For each GFRP element, the symbol that indicates the direction of the fiber is depicted in each drawing.

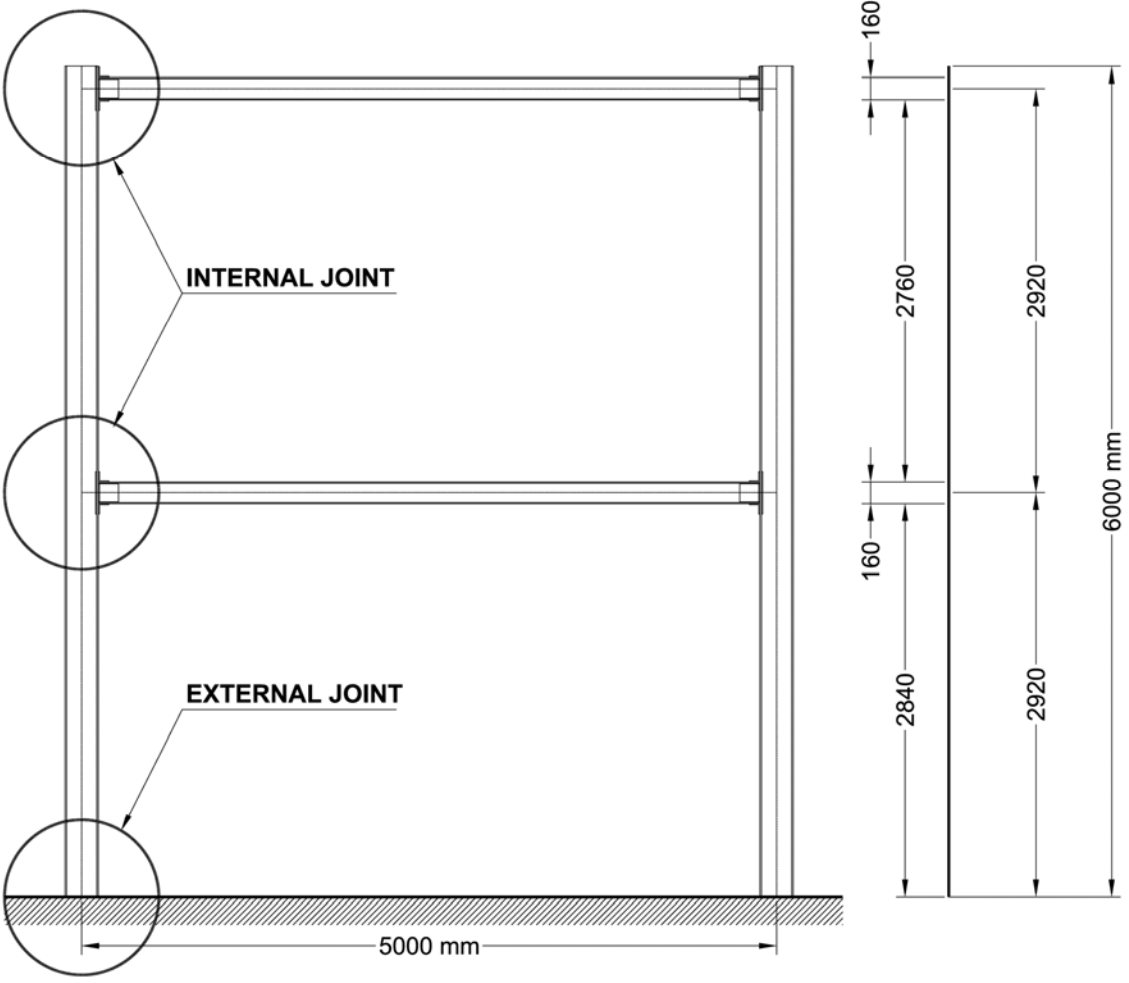


Figure 5.31. Global view

The sequence of images in Figures 5.33 and 5.34 illustrate the building phase of the GFRP framework. The figures highlight the executive ease of the only one person to cut, to execute the holes for the bolts, to assemble the structural elements and, finally, to position and to install the GFRP framework.



Figure 5.33. Assembling phase



Figure 5.34. Assembling phase

5.2.2.1.1. Beam to column joint

The analytical approaches analysed in appendix J of EC3 (Eurocode 3, 1997) and developed by Faella et al. (2000) were adopted for a global analysis of the GFRP framework and a correct modelling and classification of the internal joint which characterises the framework. Generally the conventional schematization of the restraints between the elements of a structure must be opportunely calibrated in function of the real restraint conditions obtained during the building phase. For the bolted joint, of the rigid or complete replace conditions, clamped and hinge respectively, the configuration that is in a good agreement with the reality is the intermediate condition of semi-rigid configuration, Figure 5.35. For unbraced framework with semi-rigid joint, it has been established that the external joint is infinitely rigid and the section profiles used belong to the 4th class (for which it is stated that the determination of the resistant moment and compression strength are considered the effects of local buckling).

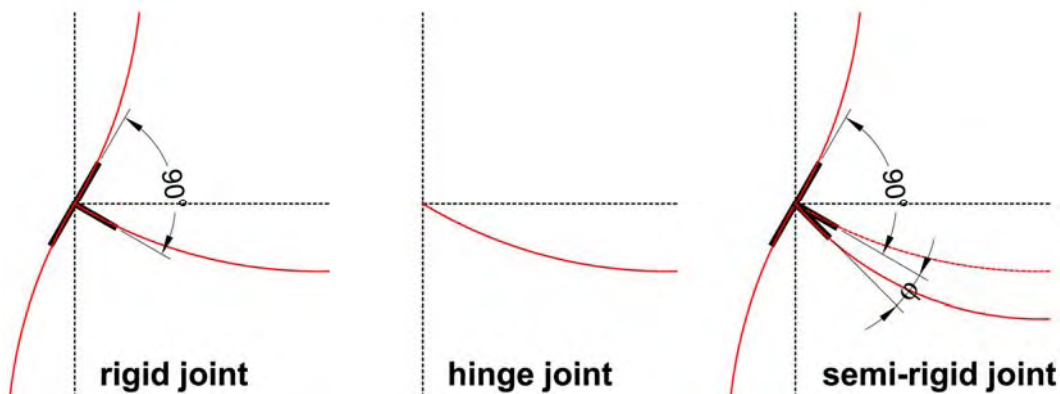


Figure 5.35 joint beam to column schemes

In modelling, the diverse deformation of joint may be represented by the rotational spring with different stiffness. The constitutive law of the joint defines the transmitted moment and the relative rotation of the connected elements identifies the global structural response of the system via stress, displacement and stiffness to the translation of the framework.

The configuration of the assembled joint which characterises the beam-column joint of the framework is one way and belongs to the bolted joint with angulars typology. The final classification of the node defined by EC3 in relation to stiffness, strength and type of analytical approach is synthetically illustrated in Table 5.15.

Table 5.15. Joint model

| Model | Analysis | | |
|---------------|------------|------------------|--|
| | Elastic | Rigid-plastic | Elastic-plastic |
| Continue | Rigid | Complete replace | Rigid to complete replace |
| Semi-continue | Semi-rigid | Partial replace | Rigid to complete replace Semi-rigid to complete replace Semi-rigid to partial replace |
| Simple | Hinge | Hinge | Hinge |

The behaviour of the bolted joint is exclusively of non-linear type. The mechanical phenomena which characterise the behaviour of the joint can be identified in an approximate way via experimental tests or numerical analysis which allow the definition, respectively, of the mathematical model of connection or the response of the joint considering the constituent components. Waiting the experimental tests of the structural response of the joint, the behaviour of the semi-rigid joint was analysed by the method of the base components, (Eurocode 3 2000). The joint components are identified in the compression and shear zones, which involve the beam-column connection, see Figure 5.36.

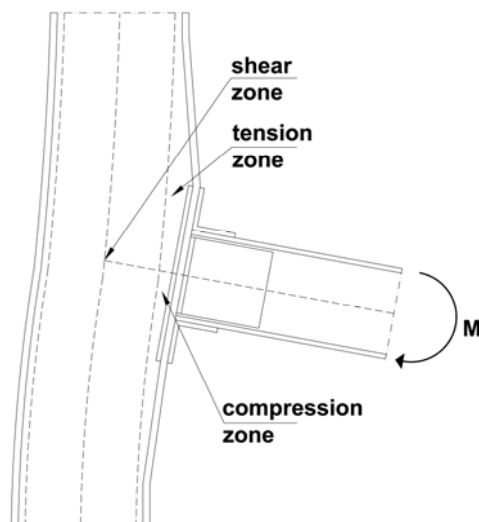


Figure 5.36. Joint scheme of structural behaviour

For the analysis of the strength and rotational properties of the joint, the areas of the base components relative to the respective bolt rows were identified in detail.

The contribution of the internal connection between “C” profiles, both for the columns and the beams, obtained by GFRP plate which constitutes the final joint beam-column is purposely ignored.

Considering that the proposed methodology concerns steel material, for each reference to mechanical response at yielding is opportunely considered the minimum value of the ultimate strength of GFRP material.

Through the numerical analysis of Eurocode 3 (2000) and Faella et al. (2000) the rotational stiffness K_φ of beam-column joint of GFRP framework is determined by the following relation

$$K_\varphi = \frac{h_t^2}{\frac{1}{K_{cwc}} + \frac{1}{K_t}} = 6.103 \cdot 10^8 \frac{Nmm}{rad} = 610.3 \frac{kNm}{rad} \quad (5.15)$$

Through the Equation 5.16, the lever h_t is defined between the resultant of tension force and the centre of compression identified at half of thickness of the angular flange of the compression zone close to beam.

$$h_t = \frac{\sum_{i=1}^{n_b} K_i \cdot h_i^2}{\sum_{i=1}^{n_b} K_i \cdot h_i} \quad (5.16)$$

With h_i = distance between the i -esima bolt row and the centre of compression and n_b = the number of bolt rows.

Therefore, the contribution of all the bolt rows is represented by a spring with a K_t stiffness (5.17) which acts in correspondence with the centre of tension.

$$K_t = \frac{\sum_{i=1}^{n_b} K_i \cdot h_i}{h_t} \quad (5.17)$$

Then with the column web in compression that is equal to:

$$K_{cwc} = E \cdot \frac{0.5 \cdot b'_{eff.cwc} \cdot t_{wc}}{d_{wc}} = 174800 \frac{N}{mm} \quad (5.18)$$

Where

$$b'_{eff.cwc} = 2 \cdot t_{sa} + 0.6r_{sa} + 2 \cdot (t_{fc} + s) = 60.8mm \quad (5.19)$$

With t_{sa} =seat angle thickness, r_{sa} =fillet radius of the seat angle, $s = r_{sa}$

The flexural strength of the connected element – the beam, $M_{b,Rd}$ – is equal to the maximum M_e elastic moment in the instant in which tension in the extreme fibers reaches the collapse value of the material:

$$M_e = W_{xx} \cdot f_{b,2} \Rightarrow M_{b,Rd} = 160/6800 \text{ Nmm} = 16.0/kNm \quad (5.20)$$

With $f_{t,2}$ = tension of flexural collapse and W_{xx} =strength modulus.

In function of the relationship between the flexural strength of the joint and that of the beam, the internal beam-column joint is classified, according to the Table 5.16, as a hinge joint, (Eurocode 3).

Table 5.16. Frame braced, joint classification

| | |
|---------------------------|---|
| Joint to complete replace | $M_{i,Rd} \geq M_{b,Rd}$ |
| Hinge joint | $M_{i,Rd} \leq 0.25 M_{b,Rd}$ |
| Joint to partial replace | $0.25 M_{b,Rd} \geq M_{i,Rd} \geq M_{b,Rd}$ |

Based on the relationship between the rotational stiffness of the joint and the flexural stiffness of the connected beam, EC3 allows the identification of the type of beam-column joint according to the classification reported in Table 5.17 and Figure 5.37.

Table 5.17. Frame unbraced, joint classification

| | | |
|------------------|---------------------------------------|--------|
| Rigid joint | $K\varphi \geq 25 EJ/L$ | zone 1 |
| Hinge joint | $K\varphi \leq 0.5 EJ/L$ | zone 3 |
| Semi-rigid joint | $0.5 EJ/L \geq K\varphi \geq 25 EJ/L$ | zone 2 |

Where $EJ/L = 62145613\text{Nmm} = 62.14\text{kNm}$

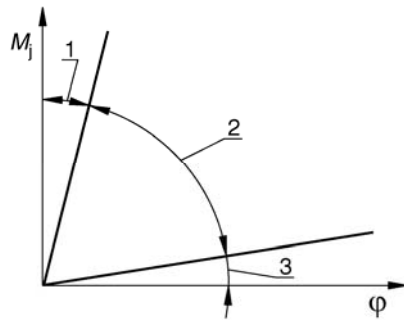


Figure 5.37. Unbraced frame

In order to verify the actual rotation of the GFRP framework induced by excitation, which will be applied on the framework itself to identify the dynamic response in the free vibration field, the external fixed joints and the two internal joints – via inclinometers – was monitored, (Figures from 5.38 to 5.41).

The inclinometers used, of a micro-capacitive type, have the sensitivity of 25 mV/°, with resolution of the data acquisition system at 0.35°.

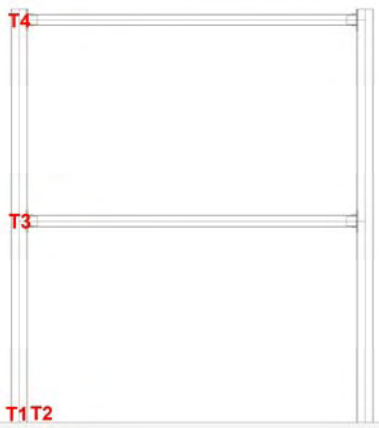


Figure 5.38. Scheme of inclinometers position

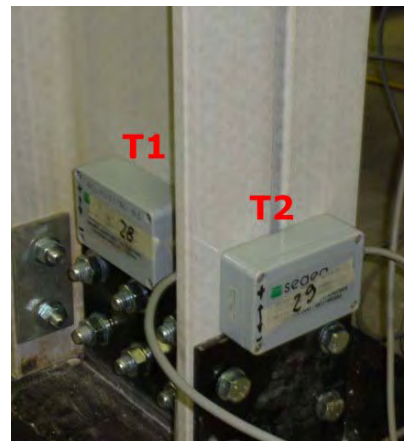


Figure 5.39. Inclinometers, T1 e T2

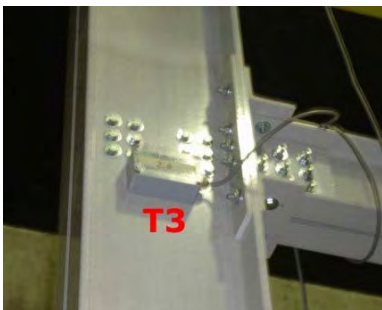


Figure 5.40. Inclinometer T3



Figure 5.41. Inclinometer T4

The excitations via a automatic instrumented hammer was carried out on the framework according to the layout of Figure 5.42, both on the plan of maximum moment of inertia and on the plan of minimum moment of inertia. The rotation type, positive in a clockwise sense, is indicated in Figure 5.42.

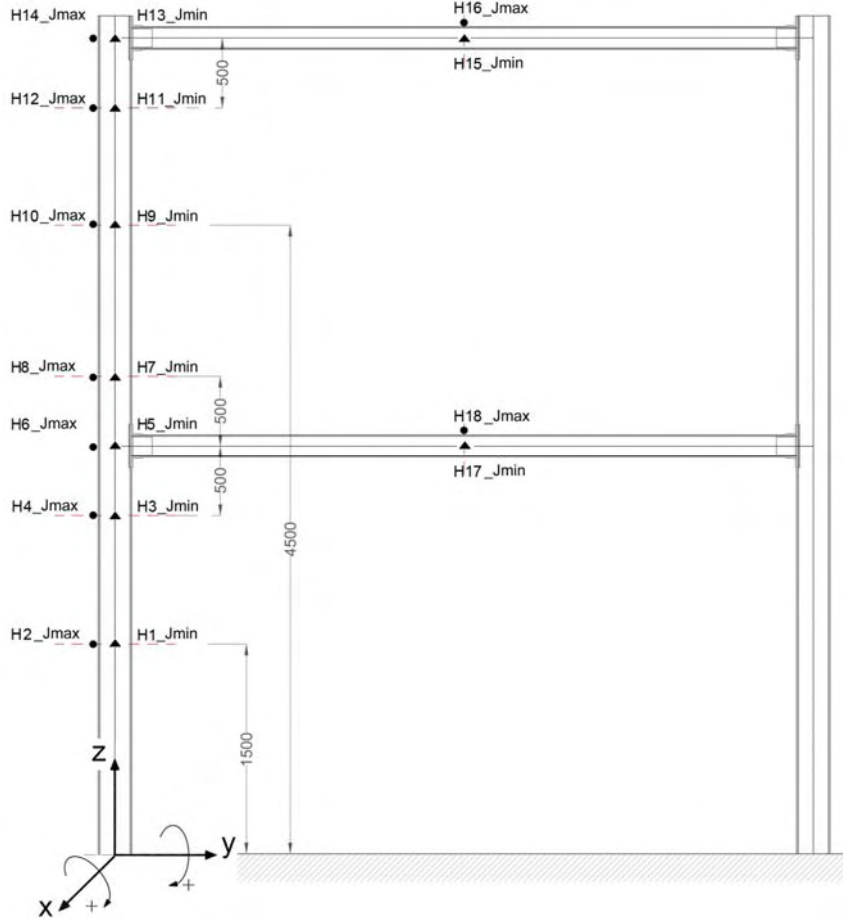


Figure 5.42. Excitation positions

Figures from 5.43 to 5.46 illustrate the recorded data of each inclinometer relative to the degrees of rotation in relation to the energy of the excitation, H_{it} , expressed in Nm.

The maximum rotations were registered by the T4 inclinometer with values which reached approximately 0.3° . The T3 inclinometer, however, registered a maximum rotation of 0.12° . The inclinometers positioned at the external joint, T1 and T2, did not register any relevant rotation.

These results highlight the efficiency of the external joint compared to the excitations which, overall, can be identified in the interval $2.0E^{-18} \text{ Nm} - 5.0E^{-18} \text{ Nm}$.

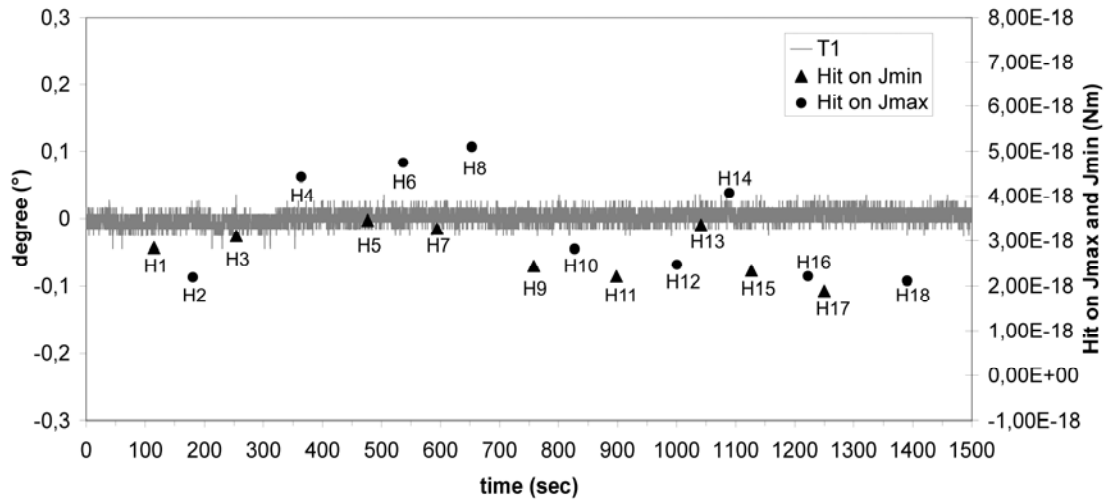


Figure 5.43. Results of inclinometer T1

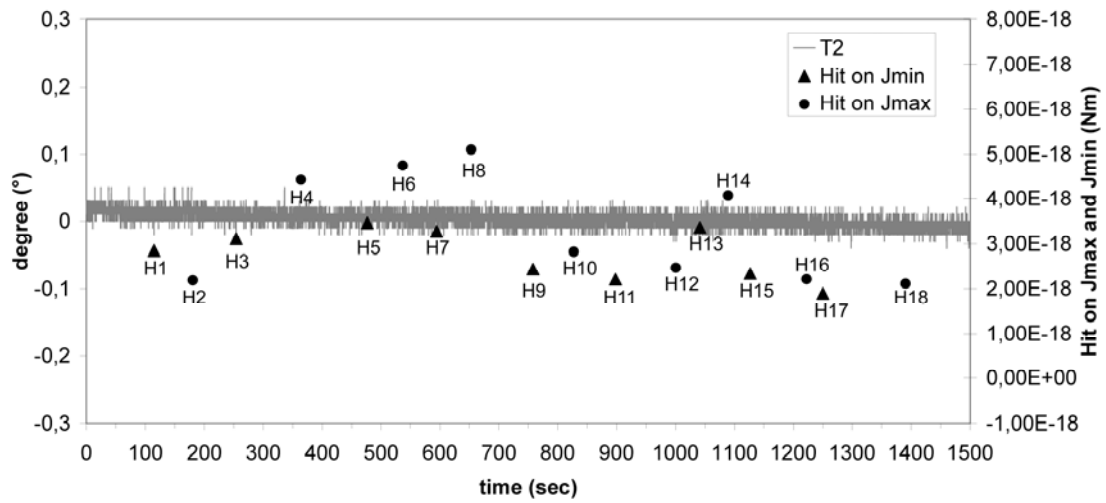


Figure 5.44. Results of inclinometer T2

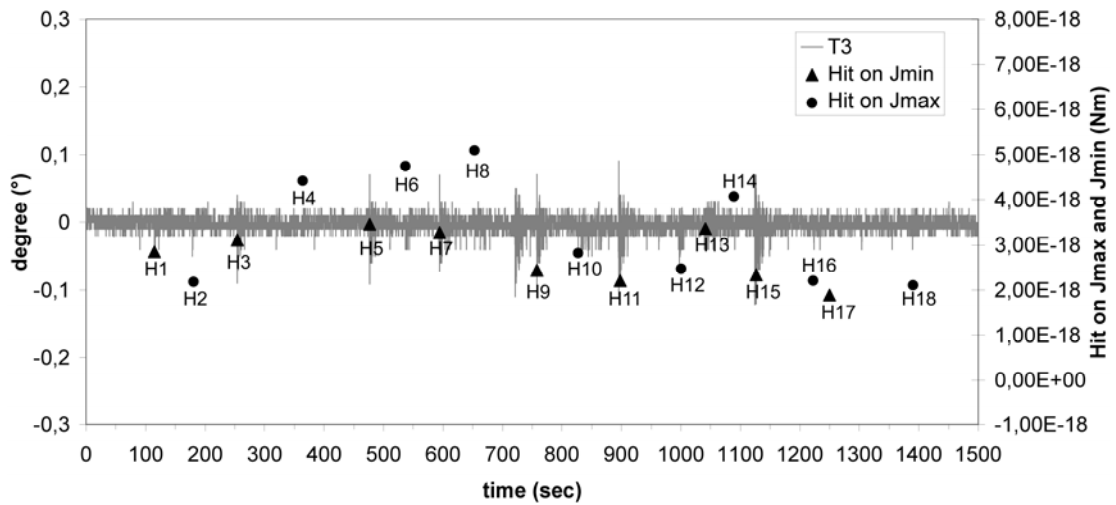


Figure 5.45. Results of inclinometer T3

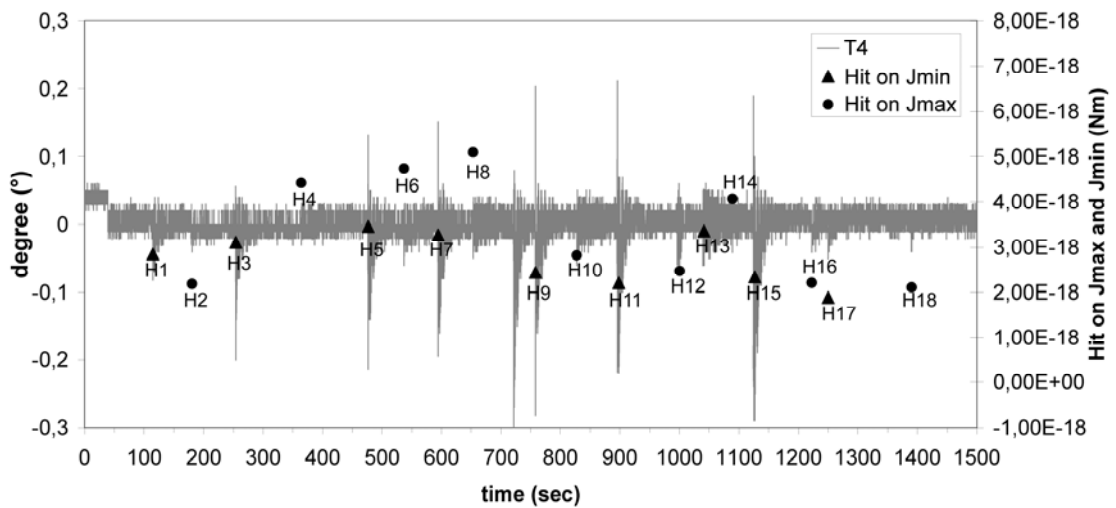


Figure 5.46. Results of inclinometer T4

5.2.2.1.2. Rotational force

The research analyses the structural response in the static and dynamic fields upon variation of the rotational force applied to the bolts of the external and internal joint (beam-column).

The rotational force applied to the bolt involves a turning of the nut and a consequential lengthening of the shank. The rotational force is therefore absorbed by the friction between the GFRP elements of the joint, the head of the screw, the nut and the shank.

With the completed action of rotational force, the union is subjected to one state of auto-stress which is performed thus:

- pre-tension of the bolt balanced by pre-compression of the GFRP elements;
- twisting of the bolt balanced by friction between the element and the bolt;

Rotational force is efficacious because increases the performance of the union respect to the limit of serviceability state, such as;

- the sliding of the plates with consequent recovering of the hole-bolt for unions in which the bolts work to shear
- the detachment of the plates in which the bolts are subjected to tension forces.

The rotational force must not exceed beyond a certain limit so as to not compromise the final capacity of the union. The current regulation DIN 267 defines a table in which the maximum rotational force of the screws is described based on relative diameters. Table 5.18 shows the data relevant to the bolts used in the connection of the GFRP.

Table 5.18. Part of regulation DIN 267

| Bolts | | Head bolts (mm) | Nm | |
|-------|------------------|-----------------|----------------|-----------------|
| class | Fine thread (mm) | | Friction = 0.1 | Friction = 0.14 |
| M8 | 1.0 | 13 | 22 | 27 |
| M12 | 1.5 | 19 | 72 | 89 |
| M14 | 1.5 | 22 | 118 | 148 |

The rotational forces reported in Table 5.18 correspond to 80% of yield limit; furthermore, for each bolt class are reported the values refer to two friction coefficients, 0.10 and 0.14. By dealing with elements in composite materials, experimental tests were carried out on the joints in order to identify the response of the parts in play upon variation of the rotational force action.

The rotational force applied was defined via calibrated torque wrench so as to apply a pre-fixed torque.

The nodes analysed were constituted of 2, 3 and 5 GFRP elements, with thickness equal to 8mm, in order to simulate the different configurations of the joint built. The elements of joint were fixed by M8 bolts, strength class 8.8 and with respective shank of 3, 5 and 7 cm (Figure 5.48). From the moment M , it is possible to detect the axial N force present on the shank (Figure 5.47) via Equation 5.21, see (Ballio et al. 1987).

$$N = \frac{M}{0.20 \cdot d} \quad (5.21)$$

Where 0.20 is an average coefficient, taken up by steel, which depends on the material and on the conditions of the surface; whilst d is equal to the diameter of the bolt.

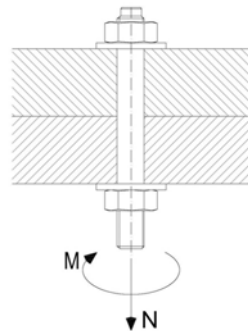


Figure 5.47. Bolted joint scheme

The test began by applying to the node a rotational force equal to 15 Nm and continuing with increments of 5Nm up to 60Nm, the limit at which the collapse of the bolt was verified. Figures from 5.49 to 5.56 illustrate the response of the node to a torque action of 25 Nm, purposely ignoring the precedents rotational forces where no damage or deformation of the GFRP elements was identified.

Therefore, the test allowed the analysis of the level of local damage to the FRP profile upon variation of the rotational force.

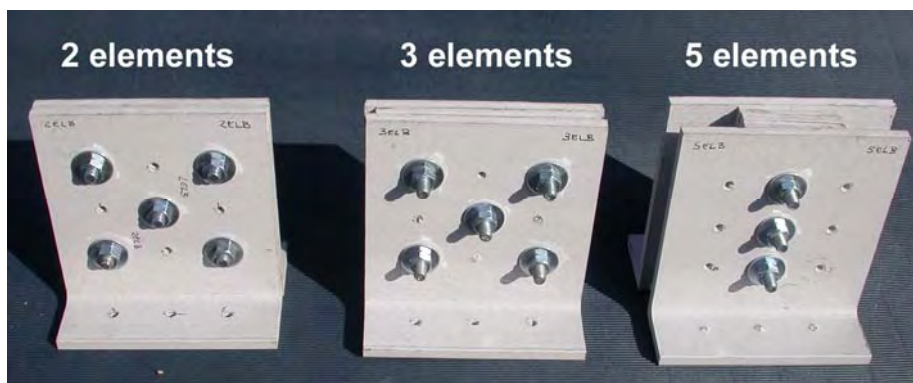


Figure 5.48. Different joint configurations

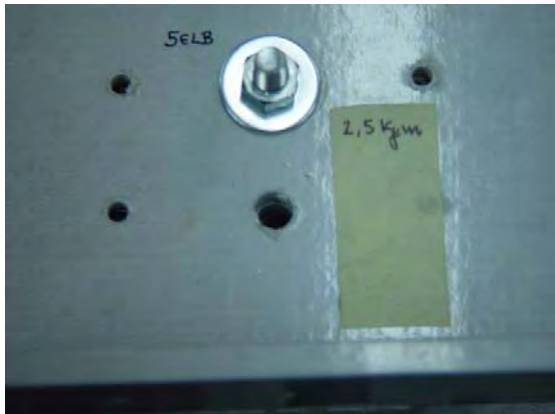


Figure 5.49. View after application of 25 Nm (equal to 15625 N) on bolt

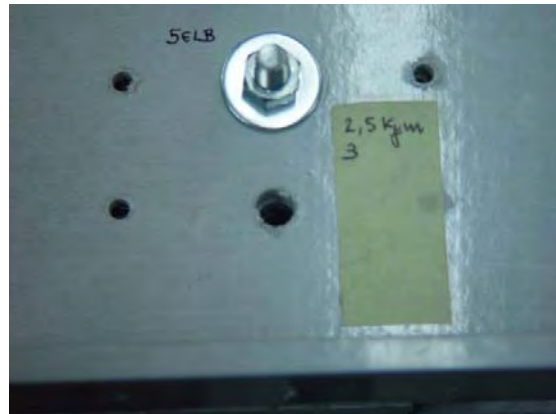


Figure 5.50. View after application of 30 Nm (equal to 18750 N) on bolt



Figure 5.51. View after application of 35 Nm (equal to 21875 N) on bolt



Figure 5.52. View after application of 40 Nm (equal to 25000 N) on bolt



Figure 5.53. View after application of 45 Nm (equal to 28125 N) on bolt



Figure 5.54. View after application of 50 Nm (equal to 31250 N) on bolt



Figure 5.55. View after application of 55 Nm (equal to 34375 N) on bolt



Figure 5.56. View after application of 60 Nm (equal to 37500 N) on bolt

In this phase, considering the response of the GFRP elements to the variation of the rotational force, the rotational force equal to 25Nm was applied to the bolts of the beam-column joints of framework. For the external fixed joint the rotational force is in function of the bolts used, M12 and M14, with values of 80Nm and 135Nm respectively.

The local deformation of the GFRP profiles upon variation of the moment of rotational force is illustrated by the load-deformation curve, Figure 5.57.

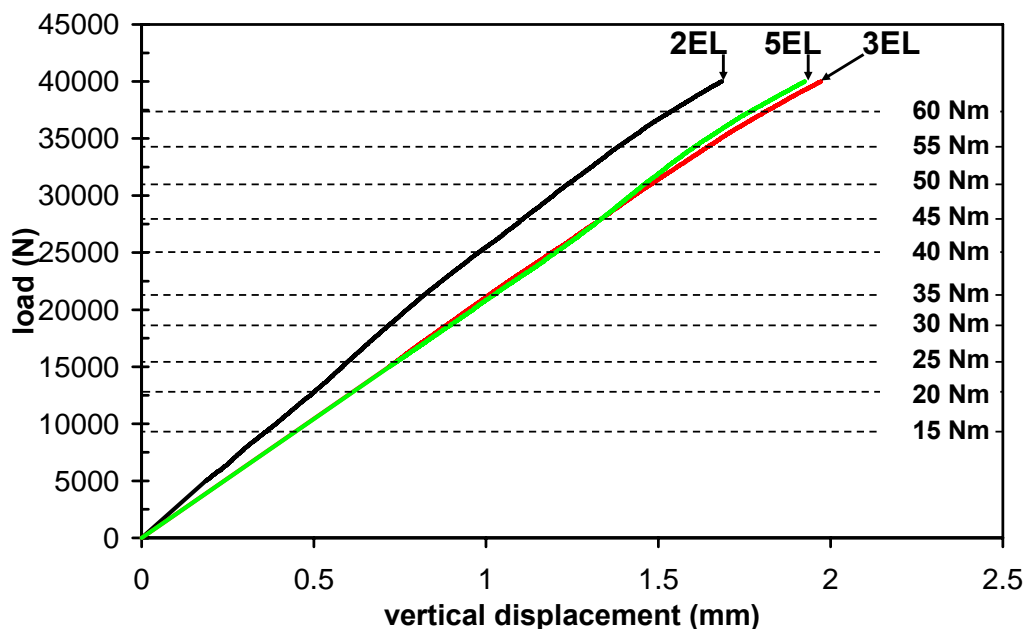


Figure 5.57. Load-vertical displacement of three configurations

The trend of the curves highlights the different incidence of the deformation of the connection composed of 2 elements (2EL) compared to the configurations constituted by 3 and 5 elements (3L and 5L respectively). For the rotational force equal to 15Nm is highlighted an increment of local deformation equal to 22% passing from 2 to 3-5 elements; with the rotational force equal to 25Nm the increment is equal to 20%, while for the torque value of the collapse of the bolt (60Nm), the increment in deformation is 15%. Only for GFRP element, directly subject to compression load applied to the bolt-head (Figure 5.58), the local deformation of circa 0.3mm was detected. Considering the linear load-deformation behaviour it is possible to define that with the rotational force of 15Nm and 25Nm the local deformation is equal to 0.11 and 0.07mm, respectively.

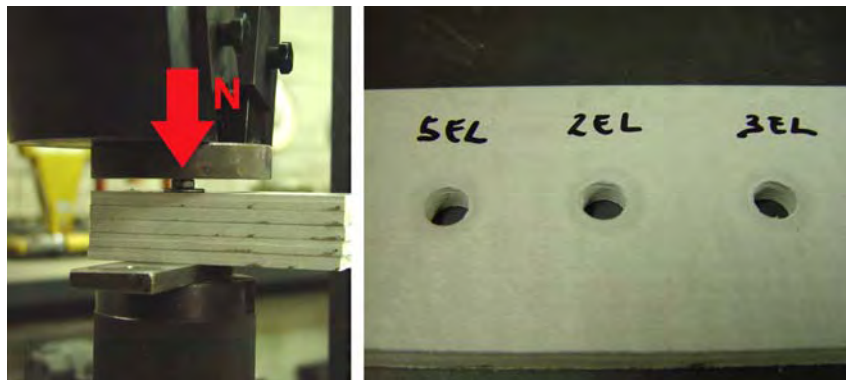


Figure 5.58. Experimental setup

Through the analysis of experimental results, the rotational force of 25Nm causes only a local damage, in correspondence to the hole, during the phase prior to the bolt collapse due to the high temperature reached caused by energy accumulated during pre-tension of the bolt. To resolve such problem, it is possible to use steel collar jackets which ensure an increment of strength of the area subject to the action of the bolt, (Oppe et al. 2007).

5.2.2.2. Analysis of experimental results

The variations in dynamic response due to the passage from the element to the GFRP structure have been analysed in the framework. Considering the effects induced by the joints and by the

geometric typology of the pultruded profiles, which constitute the beam and the column, the methodology and the setup of the experimental tests is the same adopted for mono-dimensional elements. The study was conducted by monitoring and carrying out the excitations for maximum moments of inertia.

Figure 5.59 shows the test phases; the layout of the test configuration, the position of the accelerometers and excitation points, are described in detail in Figure 5.60.

The most significant experimental data are collected in the figures of Appendix B.



Figure 5.59. Setup details

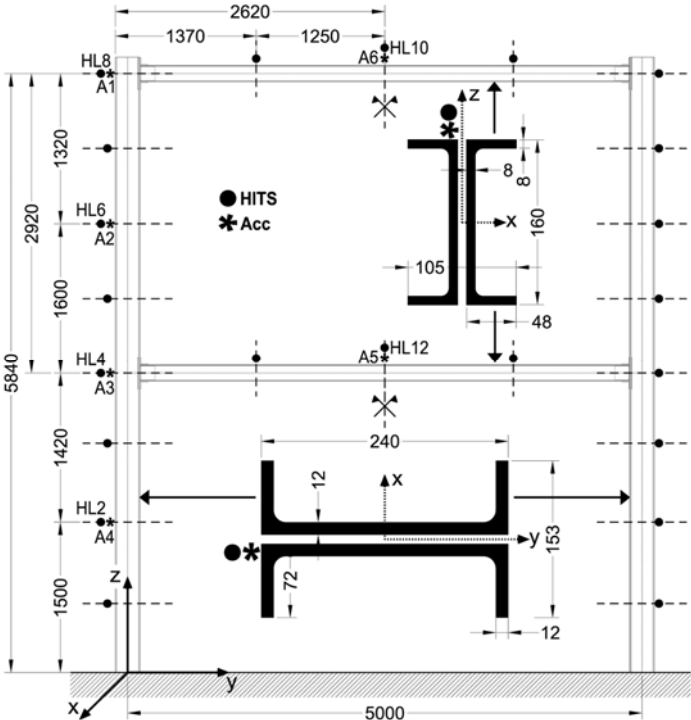


Figure 5.60. General scheme of accelerometer and excitation points (mm dimensions)

The Figures from 5.61 to 5.66 compare the different capacity to dissipate energy in function of time through the curves obtained by the interpolation lines of the peaks of the acceleration-time spectra (see Appendix B); as the mono-dimensional element also for these cases the diagrams highlight the good agreement between the experimental data and the function determined by Equation (5.4). For each excitation point it is reported the response of all accelerometers; the initial part of curves, relative to vibration induced by excitation, has been deliberately eliminated to give the dynamic behaviour in free vibrations field.

The Figures form 5.61 to 5.64 regard the excitations applied at the column, while the Figures 5.65 and 5.66 concern the beams.

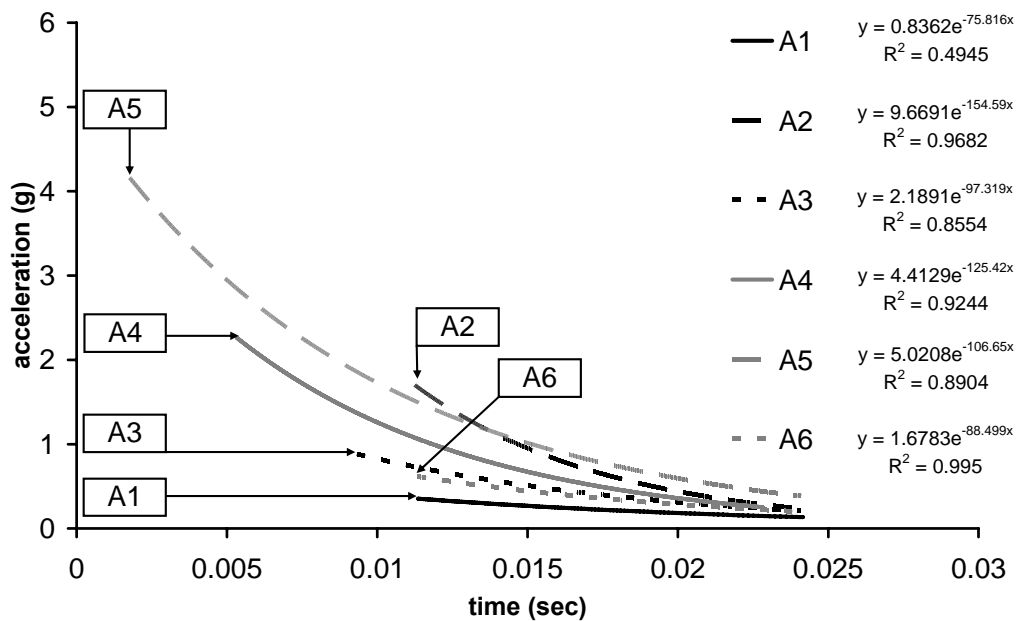


Figure 5.61. Comparison between all free vibration response in time domain. Excitation HL2

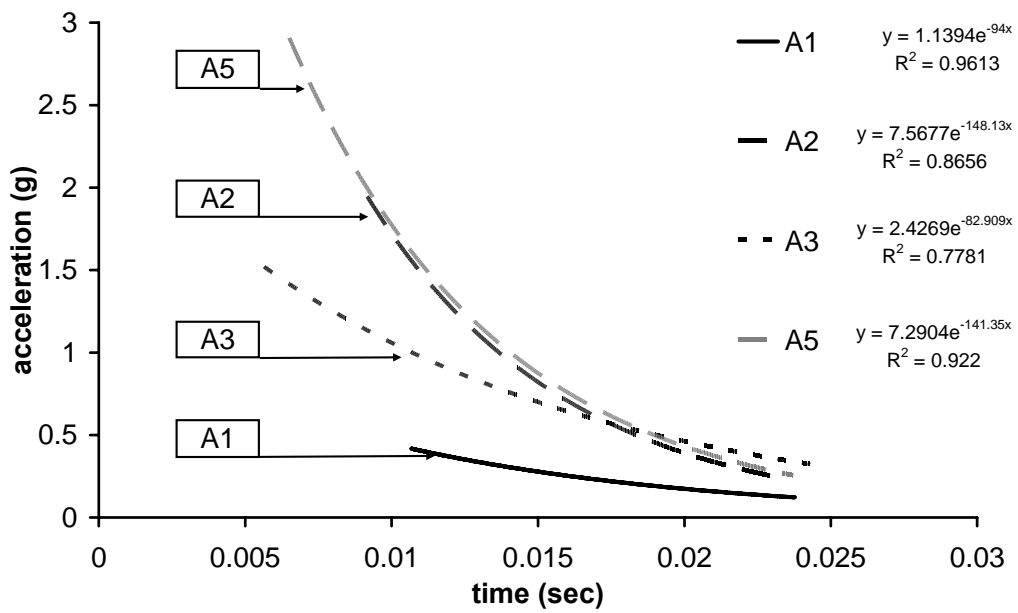


Figure 5.62. Comparison between all free vibration response in time domain. Excitation HL4

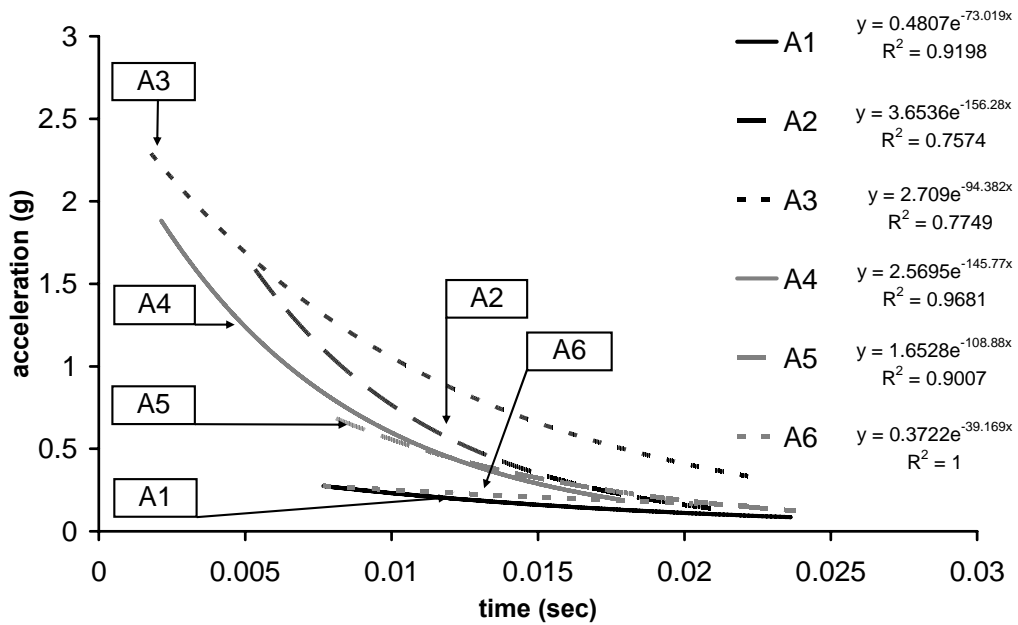


Figure 5.63. Comparison between all free vibration response in time domain. Excitation HL6

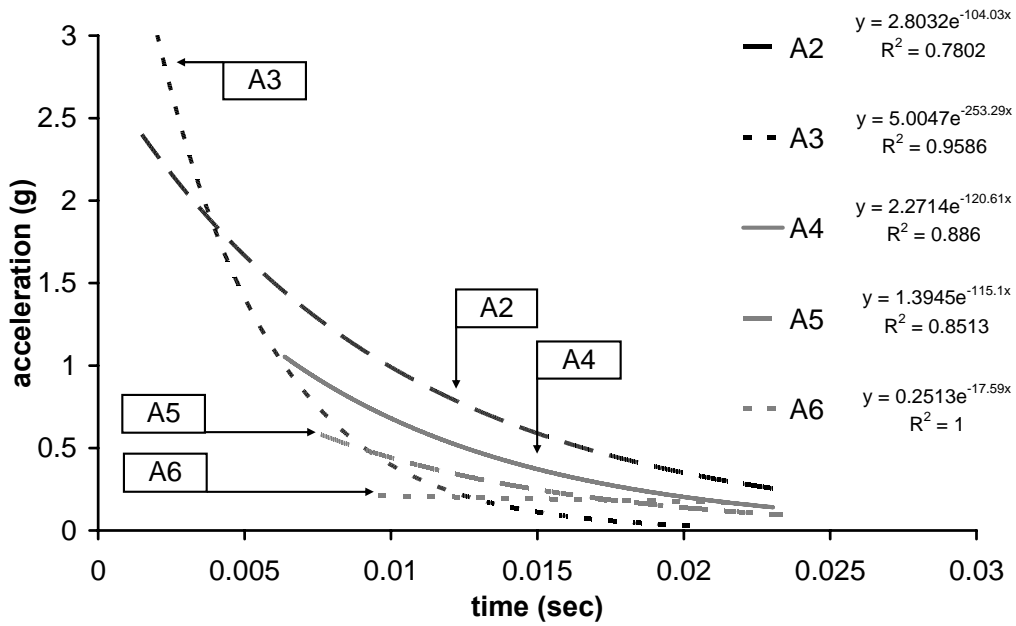


Figure 5.64. Comparison between all free vibration response in time domain. Excitation HL8

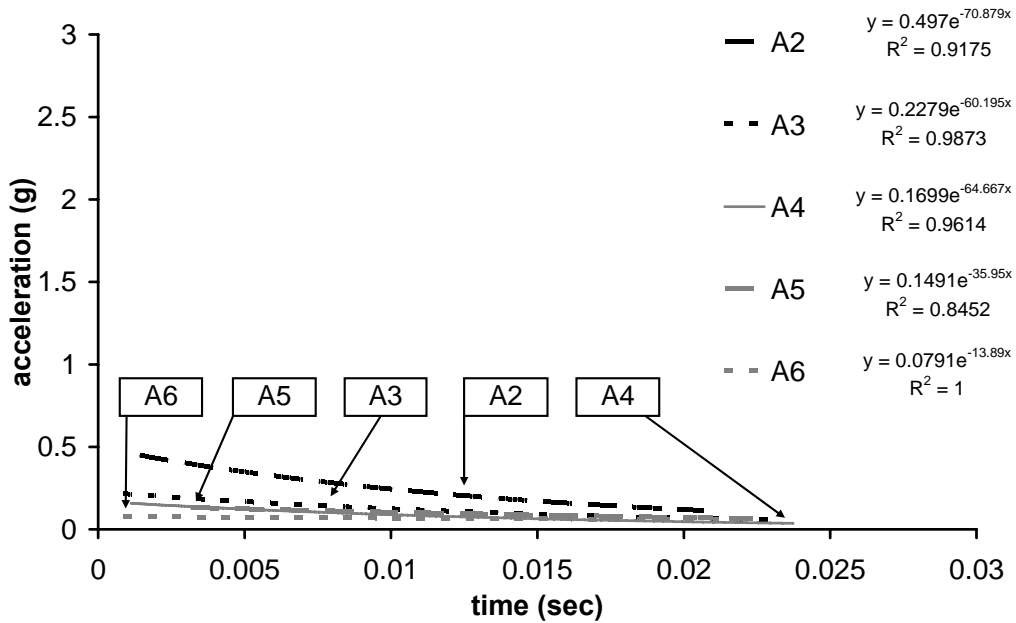


Figure 5.65. Comparison between all free vibration response in time domain. Excitation HL10

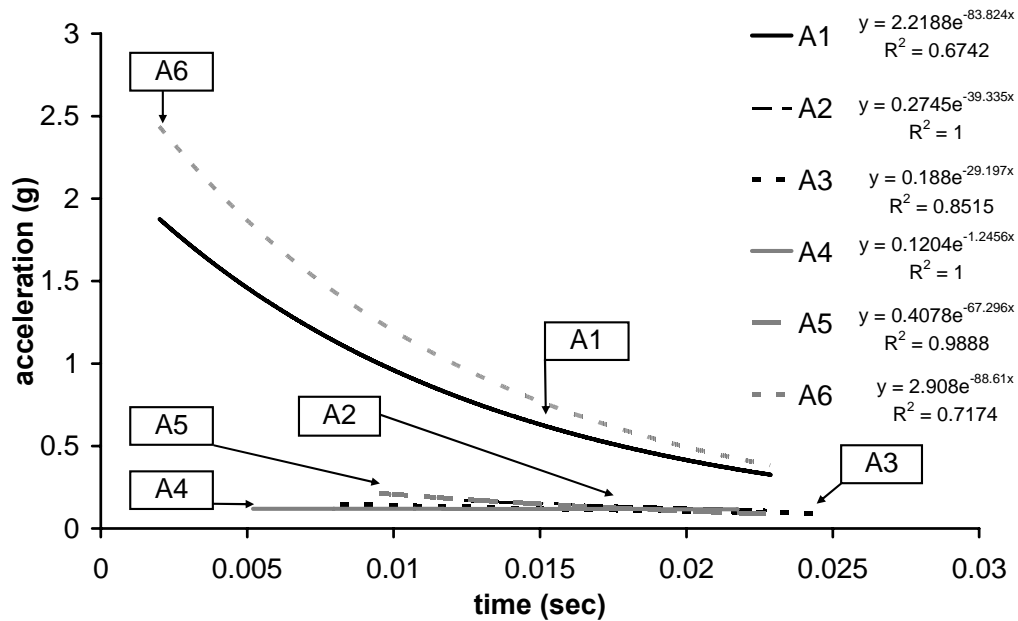


Figure 5.66. Comparison between all free vibration response in time domain. Excitation HL12

The damping ratio determined according to the logarithmic decrement method (see chapter 5.2.1.1.3.) is reported in Table 5.19.

Table 5.19, Damping ζ of 2D frame

| Excitation point | Column | | | | Beam | |
|------------------|--------|-------|-------|-------|-------|-------|
| | Acc 1 | Acc 2 | Acc 3 | Acc 4 | Acc 5 | Acc 6 |
| HL2 | 1.14% | 1.9% | 1.5% | 1.6% | 1.24% | 1% |
| HL4 | 1.8% | 1.9% | 1.4% | / | 2.8% | / |
| HL6 | 1% | 1.8% | 1.8% | 1.74% | 1.6% | 0.6% |
| HL8 | / | 1.96% | 1.92% | 2% | 1.6% | / |
| HL10 | / | 1.8% | 1% | 1.1% | 0.7% | / |
| HL12 | 3.1% | 1.6% | 1.25% | / | 1.2% | 2.4% |

Altogether it is possible to identify an interval of average values of damping ratio, 1.3%-2%, which allows the identifying of the dissipative capacity of the GFRP framework.

5.2.2.3. Numerical and finite element analysis

The theoretical approach adopted to determine the free frequencies of GFRP framework refers the semi-rigid joint configuration. The approach includes a schematization of the frame to vertical elements opportunely restrained to the beams by elastic constants which take into account of the rotational stiffness defined in chapter 5.2.2.1.1.

The horizontal displacements of every level identify the motion and then the out of shape of structure, shear-type. For every level the free coordinates are the horizontal displacements u_1 and u_2 , respectively for first and second level, and the related mass values m_1 and m_2 , (Figure 5.67).

The deformation work is obtained by relation between external forces and associated displacements. Such forces, applied on free points, keep the equilibrium state of out of shape system as defined by displacements u_1 and u_2 , respectively to first column joint of scheme (c) and to second column joint of scheme (d), as depicted in Figure 5.67. Via superposition principle each external action can be considered as sum of k_{ij} – determined so that the only one of free coordinate is equal to 1 and the others nulls – multiplied for the corresponding value of free coordinate u_j , scheme (c) with $u_1=1$ and $u_2=0$, scheme (d) with $u_1=0$ and $u_2=1$. The out of shapes of scheme (c) and (d) have been obtained via the restrains force, that avoid the displacement detected by free coordinates and impose on each restrain a unitary displacement, (Figure 5.67). The restrain reactions determine the coefficient k_{ij} of stiffness matrix.

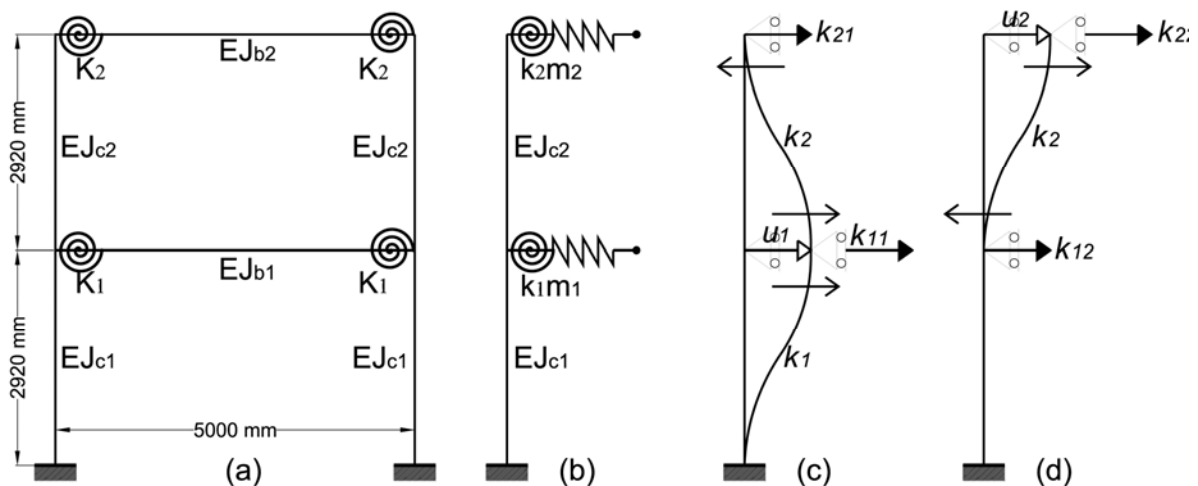


Figure 5.67, General static scheme (a) and detail of calculation scheme for first and second column (b, c and d)

Every reaction, obtained by sum of acting forces on the each beam end that converge in the restrained point, is equal to:

$$\begin{aligned} k_{11} &= k_1 + k_2 & k_{12} &= -k_2 \\ k_{21} &= -k_2 & k_{22} &= k_2 \end{aligned} \quad (5.22)$$

considering that,

$$k_1 = k_2 = 2 \cdot \frac{12 \cdot E_t \cdot J_c}{L^2} = 2 \cdot \frac{12 \cdot 85000 \cdot 6511}{292^2} = 155800 \text{ kg / cm}$$

$$J_{c1} = J_{c2} = 6511 \text{ cm}^4 \quad (5.23)$$

$$m_1 = m_2 = L \cdot A \cdot \gamma = 500 \cdot 38.4 \cdot 0.00185 = 35.5 \text{ kg}$$

Where J_{c1} is equal to maximum moment of inertia of column, E_t correspond to transversal elastic modulus, A area of cross section, L length of beam and γ is equal to density of material.

The transversal elastic modulus E_t ($E_t = 8500 \text{ MPa}$), to consider the influence of shear deformability, has been utilized.

The free vibrations of undamped system are considered by following relation (5.24):

$$m\ddot{u} + mu = 0 \quad (5.24)$$

so that:

$$\begin{bmatrix} m & 0 \\ 0 & m \end{bmatrix} \begin{bmatrix} \ddot{u}_1 \\ \ddot{u}_2 \end{bmatrix} + \begin{bmatrix} 2k & -k \\ -k & k \end{bmatrix} \begin{bmatrix} u_1 \\ u_2 \end{bmatrix} = \begin{bmatrix} 0 \\ 0 \end{bmatrix} \quad (5.25)$$

The system eigenvalues are the square roots of the following characteristic Equation (5.26)

$$k_1 [k - \omega^2 \cdot m] = 0 \quad (5.26)$$

or

$$k_1 \begin{bmatrix} 2k - \omega m & -k \\ -k & k - \omega m \end{bmatrix} = 0 \quad (5.27)$$

assuming

$$\alpha = \frac{m_1}{k_1} \cdot \omega^2 \quad (5.28)$$

The matrix determinant produces a second-grade polynomial in the unknown quantity α , from respective square roots are determined the two first free pulsations ω .

from square root 1

$$\omega_1^2 = \alpha_1 \cdot \frac{k_1}{m_1} \Rightarrow \omega_1 = \sqrt{0.385 \cdot \frac{155800}{35.5}} = 41.1 \frac{rad}{sec} \quad (5.29)$$

from square root 2

$$\omega_2^2 = \alpha_2 \cdot \frac{k_1}{m_1} \Rightarrow \omega_2 = \sqrt{2.615 \cdot \frac{155800}{35.5}} = 107.13 \frac{rad}{sec} \quad (5.30)$$

5.1. Finally the results of numerical elaboration on dynamic behaviour of framework in free vibration field are shown in Table 5.20.

Table 5.20. Mode 1 and 2 – numerical analysis

| Modes of vibration | ω (rad/sec) | T (sec) | f_n (Hz) |
|--------------------|--------------------|---------|------------|
| 1 | 41.1 | 0.153 | 6.67 |
| 2 | 107.13 | 0.059 | 16.9 |

The finite element analysis has been carried out with the same approach adopted in chapter 5.2.1.2.2.

The beam-column joint has been modeled assuming the rotational stiffness determined in chapter 5.2.2.1.1.

The external joint has been characterized by fully clamped configuration.

The analysis results relative to dynamic response of framework in free vibration field are illustrated in Table 5.21.

Table 5.21. Mode 1 and 2 – FEM analysis

| Modes of vibration | ω (rad/sec) | T (sec) | f_n (Hz) |
|--------------------|--------------------|---------|------------|
| 1 | 44.85 | 0.14 | 7.055 |
| 2 | 209.3 | 0.03 | 26.46 |

The out of shapes of two first modes of vibration are illustrated in Figure 5.68.

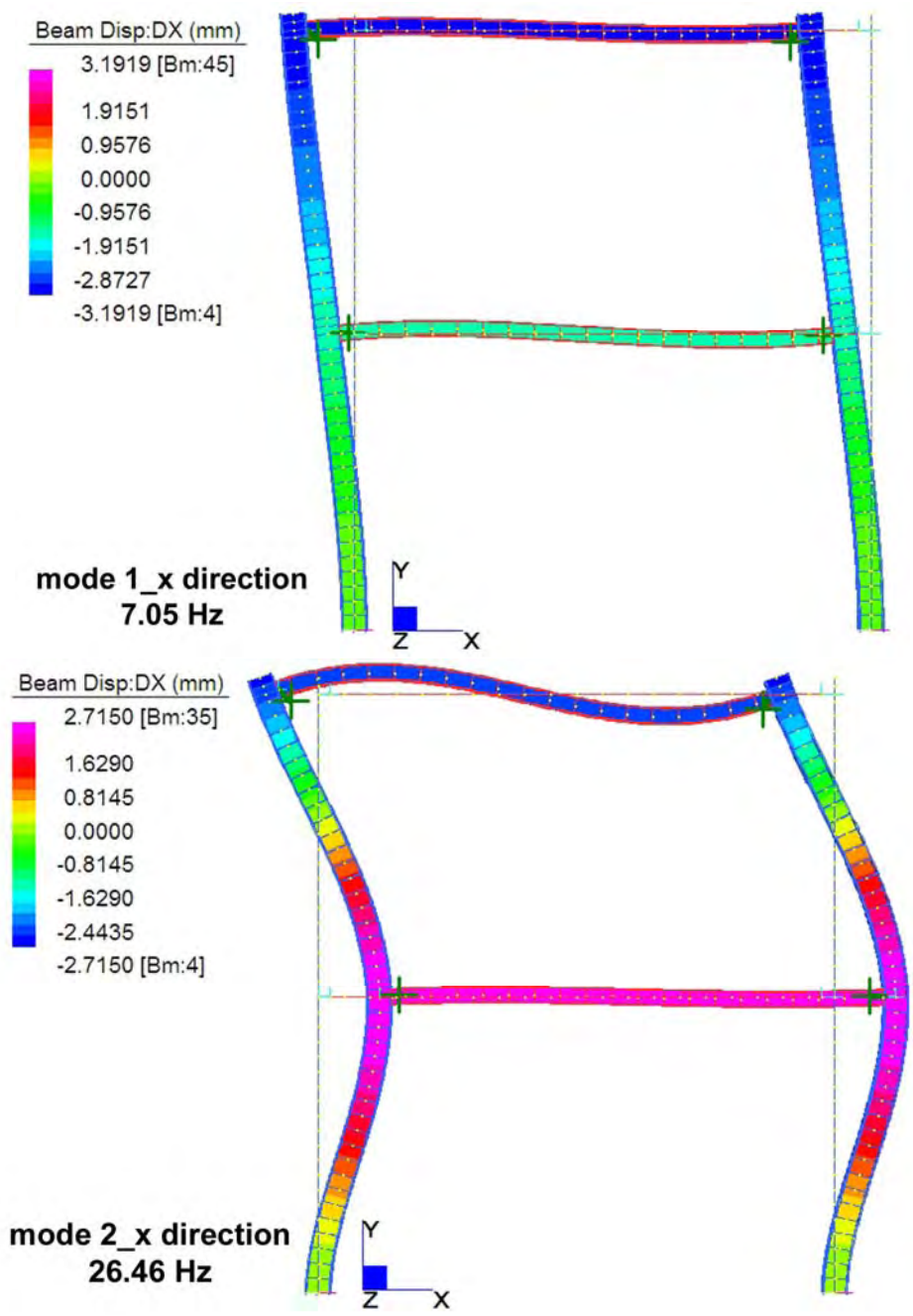


Figure 5.68. First and second modes of vibration

5.2.2.4. Results comparison

Considering the mean values of fundamental frequency experimentally determined for each accelerometer and for every excitation points – shown in Appendix B – the good agreement with numerical and FEM results of chapter 5.2.2.3. is highlights.

Table 5.22 compares such results considering the time of vibration T and the pulsation value ω of the first mode of vibration.

Table 5.22. Results comparison of first mode of vibration, 2D frame

| Analysis | ω (rad/sec) | T (sec) | f_n (Hz) |
|--------------|--------------------|---------|------------|
| Experimental | 44.86 | 0.14 | 7.12 |
| Numerical | 41.1 | 0.153 | 6.67 |
| FEM | 44.85 | 0.14 | 7.055 |

The difference between the results of three adopted approaches is equal to 6% between numerical analysis and the others two. For the values determined by experimental analysis and FE method the difference is equal to 1%. This last relation highlights the quality both of adopted model for FEM analysis and of rotational stiffness values for the column-beam joint.

5.2.3. Three-dimensional frame

The dynamic response of GFRP structure was analysed in the auxiliary floor built in the “Casa Cogollo” known as “Casa del Palladio”, Vicenza, Italy. In order to consider all the parameters which condition the vibration behaviour of the structure it is necessary to specify, in addition to what has been stated in chapter 4.2.1, that the all composite structure is simply supported on the existing floor. The geometric properties of the every structural elements are the beam (“H” shape 200x200x15x10mm) and the composed cross-section column (four angle 10x10x8mm) with the geometric properties depicted in Table 5.23. Figure 5.69 shows the general view of 3D structure and the detail of analysed part; Figure 5.70 highlights the internal and external joints with the details of the steel element used for the connections between GFRP profiles. The joints were built by steel bolts M10 type class 8.8.

Table 5.23. Characteristics of beams and columns.

| Structural Elements | A (cm ²) | J _{xx} (cm ⁴) | J _{yy} (cm ⁴) |
|---------------------|----------------------|------------------------------------|------------------------------------|
| Beam | 67 | 4342.33 | 1338.39 |
| Column | 61.44 | 1260.08 | |

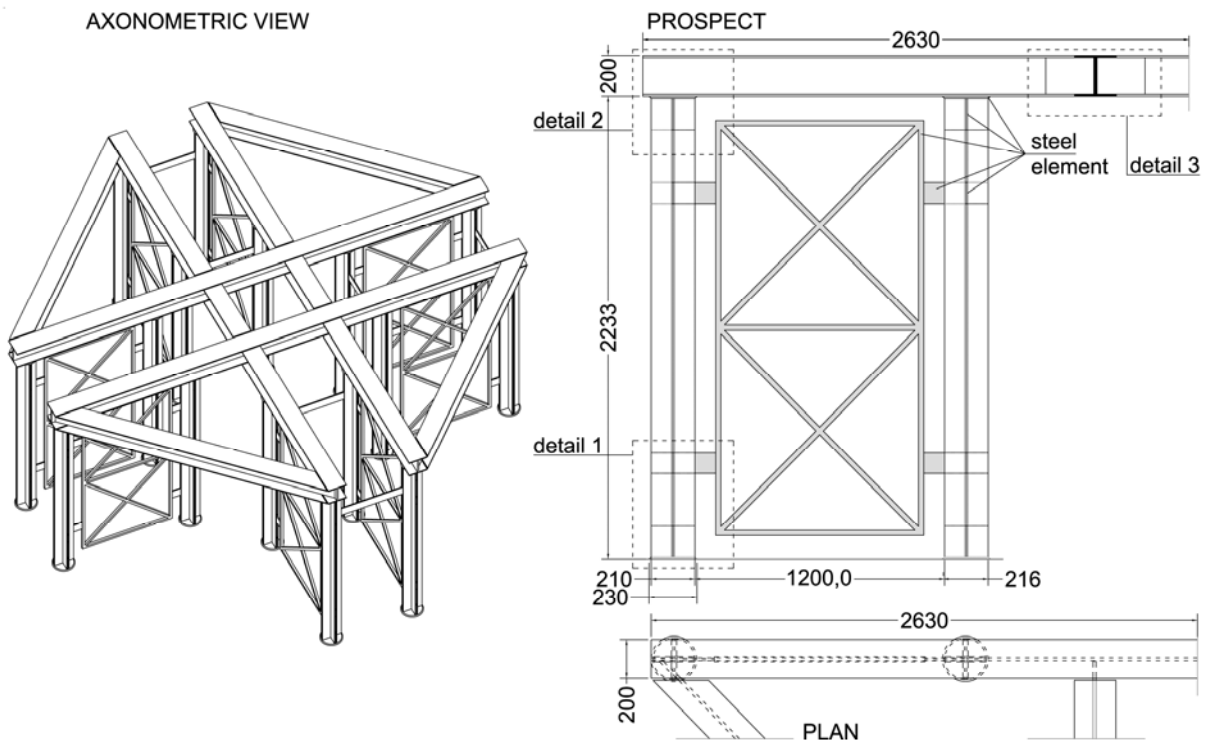


Figure 5.69. General view, mm dimensions

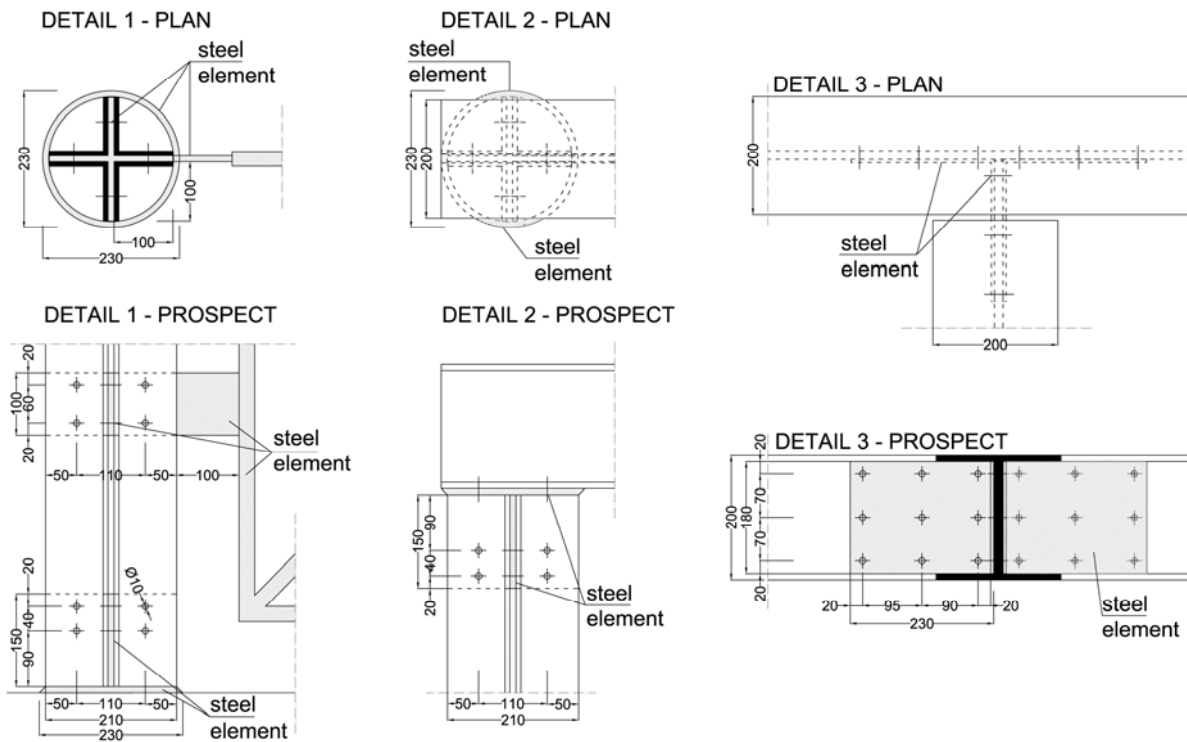


Figure 5.70. Joint detail, mm dimensions

5.2.3.1. Analysis of experimental results

Dynamic identification in the free vibration field was carried out by using the same methodology and equipment described in detail in chapter 5.2.1.1.1.

The images in Figure 5.71 illustrate the details of the positioning of the accelerometers on the beam and on the columns.



Figure 5.71. Setup details

Besides the identification of the dynamic parameters of the material and of the structural elements, the dynamic response with regards to vertical excitation induced by human action was also analysed.

Considering that a structure has two axis of symmetry, (Figures 5.72 and 5.73), only some parts were analysed. In particular were analysed the two beams, parallel to x and y axis respectively (Figure 5.72), and two of the four columns (internal and external) which build one of four two-dimensional frames, see highlighted parts in Figure 5.73.

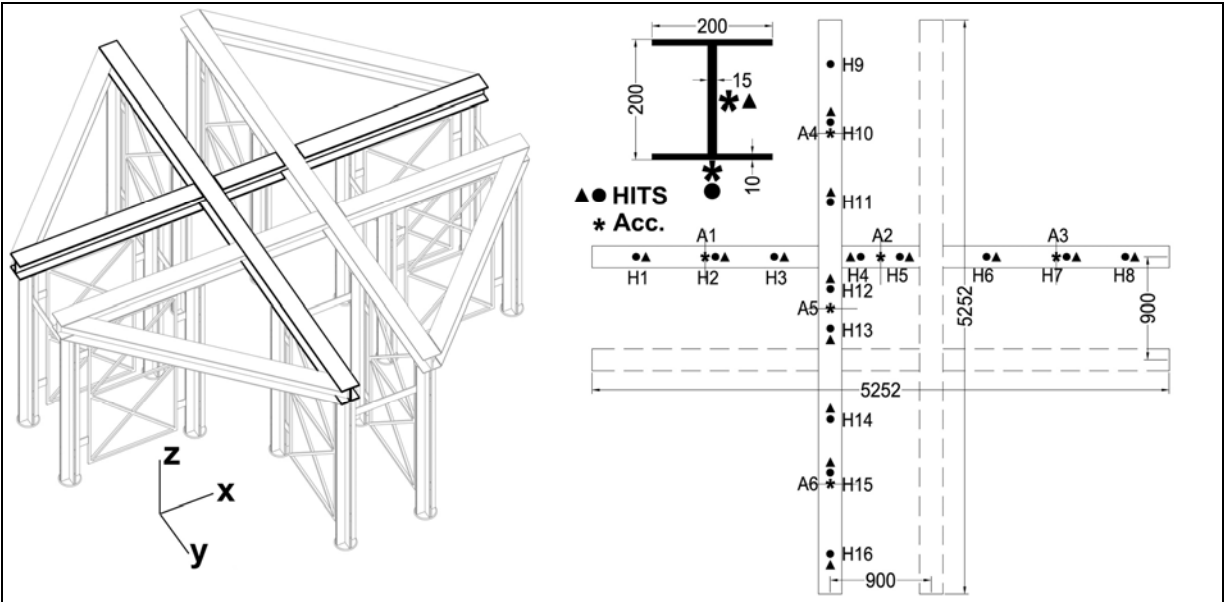


Figure 5.72. Axonometric view and detail of beams

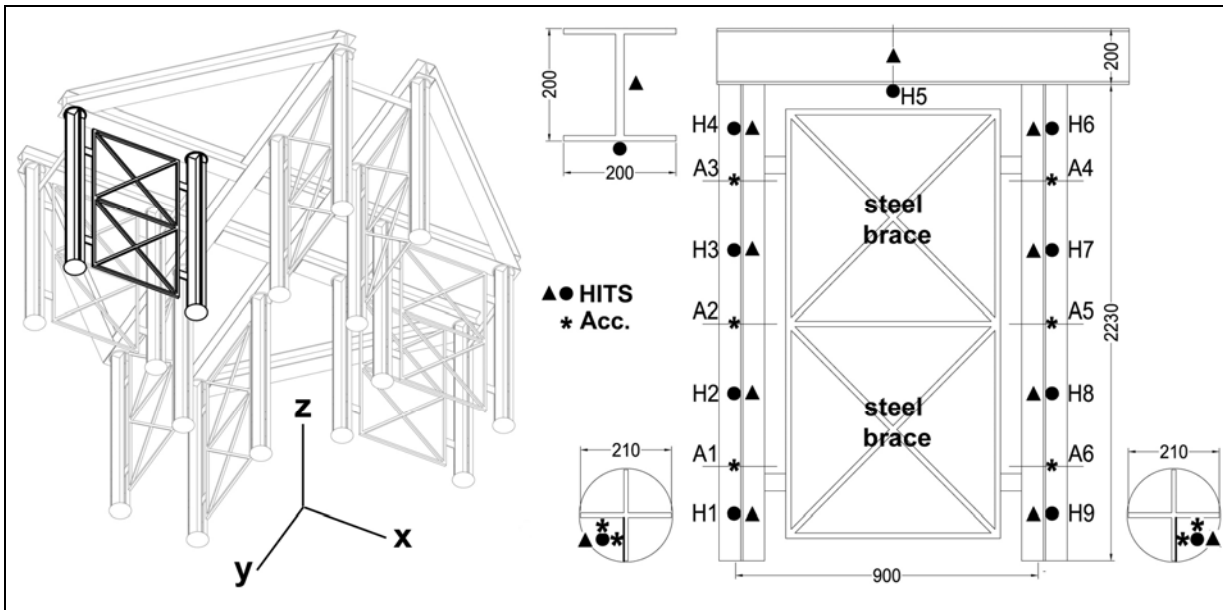


Figure 5.73. Axonometric view and detail of columns

The structure configuration guarantees a homogenous distribution of the mass in play and ensures a uniform transversal behaviour with a closed circuit behaviour of the twisting flow.

The most significant experimental data are collected in the figures of Appendix C.

The comparison between the different capacities to dissipate the accumulated energy during the excitation phase is illustrated in the Figures from 5.74 to 5.77. The equation of the exponential curve which interpolates the points relative to global behaviour in the free vibration field is shown in each figure. As for the mono-dimensional elements also for the structure the diagrams highlight the good agreement between the experimental data and the function determined by Equation (5.4).

The flexural dynamic behaviour of each beam regards both the maximum and minimum moment of inertia of the cross section for the excitation points H4 and H12.

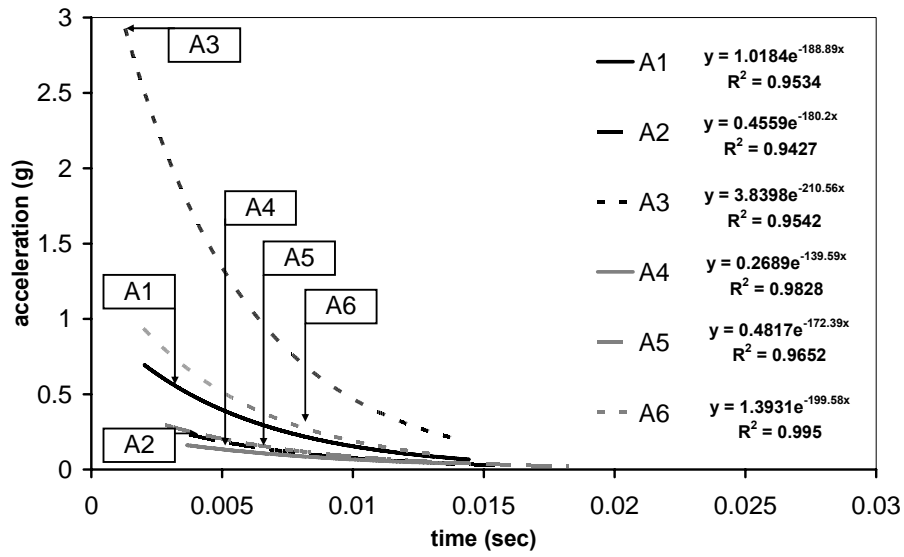


Figure 5.74. Excitation H4, J_{max}

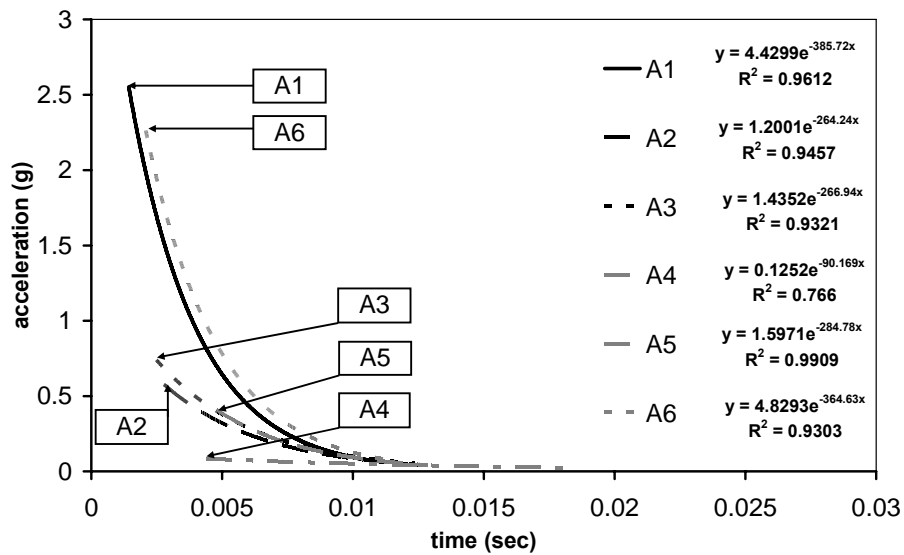


Figure 5.75. Excitation H12, J_{max}

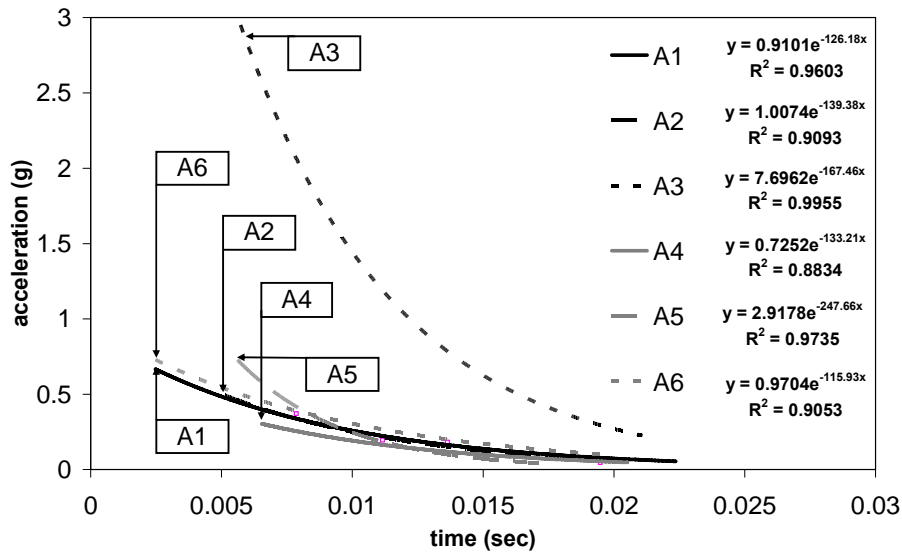


Figure 5.76. Excitation H4, J_{min}

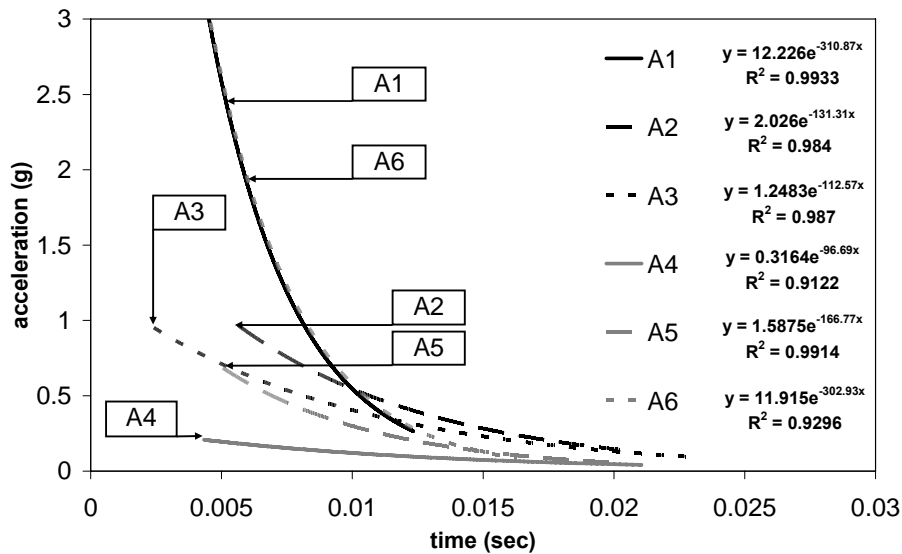


Figure 5.77. Excitation H12, J_{min}

The same methodology was adopted for the columns; Figures 5.78 and 5.79 show the comparison between the diverse capacities of dissipating the energy accumulated by the vertical structural elements – specifically, internal and external – with respect to the two excitations, H2 (external) and H8 (internal).

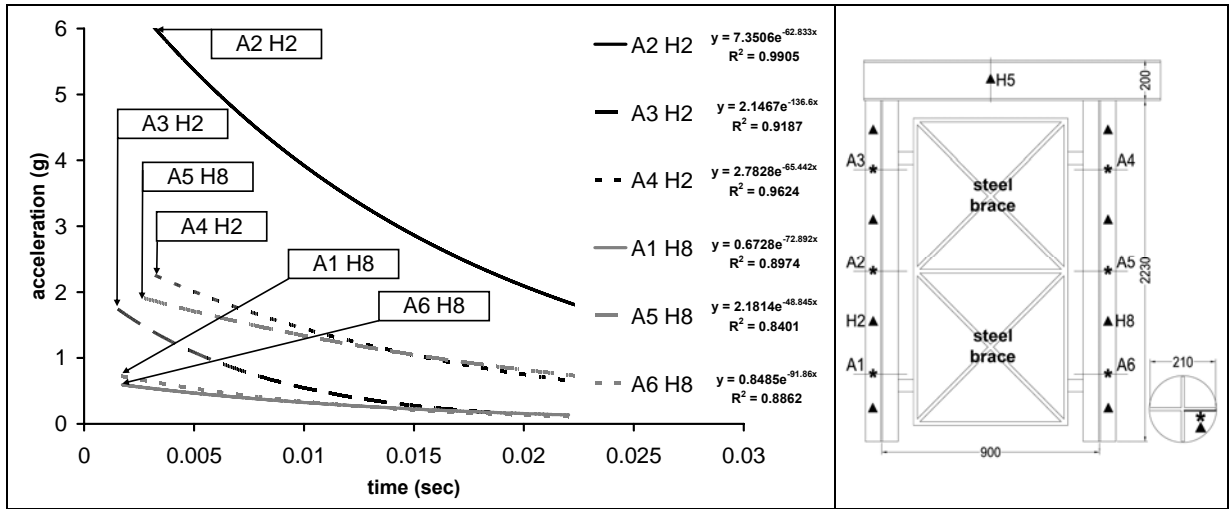


Figure 5.78. Excitation H2 and H8, accelerometers and excitation points parallel to y axis

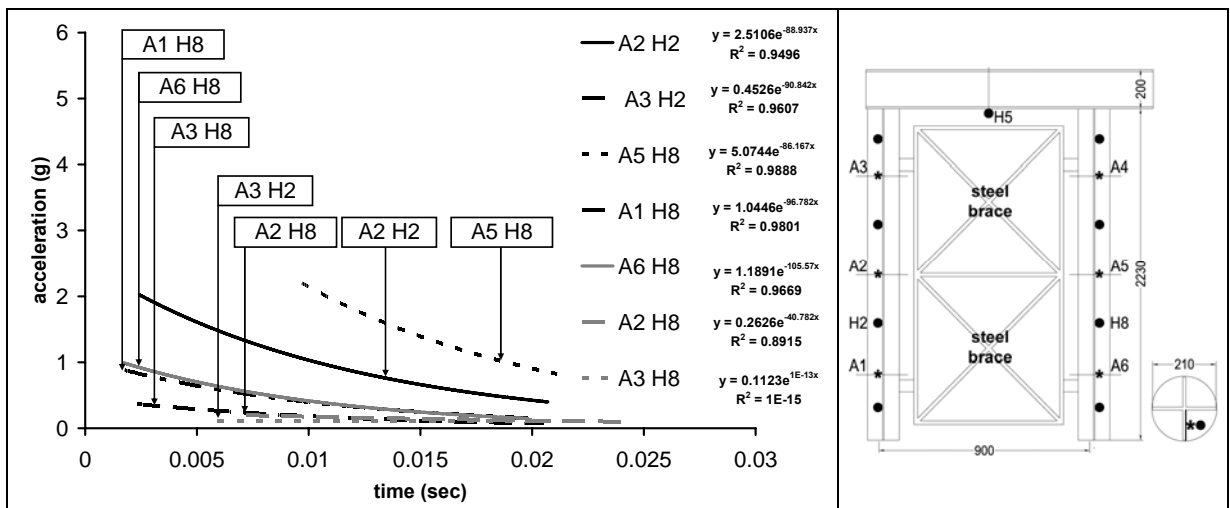


Figure 5.79. Excitation H2 and H8, accelerometers and excitation points parallel to x axis

The dynamic response of the configuration illustrated in Figure 5.79 results in being beyond half of the configuration adopted in Figure 5.78, this is due to presence of twisting phenomena.

In the test configuration of Figure 5.79, the elements of column investigated has a greater stiffness due both to the presence of steel braces and to direction, of exciting action, along the plan of the two-dimensional frame analysed as part of structure. Despite this, in the test configuration of Figure 5.78, the flange of column – parallel to x axis (Figure 5.73) - results in

being more stiff for the presence of steel connecting plates between the column and the steel braces.

In conclusion in the GFRP angular which constitute the column, the flange monitored – parallel to y axis (Figure 5.73) - results in being more deformable and so less dissipative.

Tables 5.24 and 5.25 report the damping ratio, for the beam and for the column respectively, determined by means of the logarithmic decrement method, see chapter 5.2.1.1.3.

Table 5.24, Damping ζ of beam

| Excitation point | | Beam parallel to x axis | | | Beam parallel to y axis | | |
|------------------|-----------|-------------------------|-------|-------|-------------------------|-------|-------|
| | | Acc 1 | Acc 2 | Acc 3 | Acc 4 | Acc 5 | Acc 6 |
| H4 | J_{max} | 2.6% | 1.5% | 1.6% | 1.1% | 2.2% | 1.8% |
| | J_{min} | 1.7% | 1.8% | 1.8% | 1.7% | 2.6% | 1.7% |
| H12 | J_{max} | 3.4% | 3% | 3.2% | 1.1% | 3.7% | 3% |
| | J_{min} | 2.8% | 1.5% | 1% | 3% | 1.9% | 2.6% |

Table 5.25, Damping ζ of column

| Excitation point H2 and H8 | Acc 1 | Acc 2 | Acc 3 | Acc 4 | Acc 5 | Acc 6 |
|--|-------|-------|-------|-------|-------|-------|
| H2-Acc. and excitation points parallel to x axis | \ | 1.6% | 3% | 1.3% | \ | \ |
| H8-Acc. and excitation points parallel to x axis | 1.7% | \ | \ | \ | 1.9% | 2% |
| H2-Acc. and excitation points parallel to y axis | \ | 2.1% | 1.76% | \ | \ | \ |
| H8-Acc. and excitation points parallel to y axis | 2.06% | 0.65% | \ | \ | 1.65% | 2.31% |

It is evident the optimum response of the continuous beam – parallel to axis y – with excitation and the position of the accelerometers along the axis of maximum inertia of the beam section. The mean dynamic parameter of damping of the beam in a GFRP structural system can be identified in the interval 1.7%-3.2% for the dynamic behaviour along the axis of maximum inertia and 1.7%-2% for the dynamic response along the axis of minimum inertia.

With regards to the columns, the mean values of damping are included in the interval 1.5%-2% taking into consideration both the different test configurations and the position of the columns.

With the same test configuration used for the analysis of the beams, the dynamic response of the GFRP structure regarding the excitation induced by human action was verified. Specifically, this action was conducted on the extrados of the deck floor, Figure 5.80.

From the accelerograms, it was possible to record the variation of signal intensity and so quantify and compare the attenuation of the signal itself induced by the presence of the beam-beam joint (beam parallel to the x axis) with respect to the continuous element (parallel to the y axis), Figures 5.81 and 5.82. The curves relative to accelerometers A1 and A4 were eliminated insomuch as, in relation to the excitation point, they do not allow direct comparison of the two consecutive accelerometers.

In order to increase the case study, two tests were carried out via two different excitation which were applied in the same position (point indicated with HITS) by a man weighing 80kg jumping, as illustrated Figure 5.80.

The data recorded demonstrate a good agreement between the results. For both experimental tests, it is evident that the sensors A3 and A6, far from the excitation point, recorded the signal more quickly ($x_{a6} < x_{a5}$ e $x_{a3} < x_{a2}$) and with a higher intensity compared to the accelerometers, A2 and A5, positioned close to the excitation point. The signal recorded by A3 and A6 regards the P longitudinal wave of compression and rarefaction, while the oscillations recorded by the accelerometers A2 and A5 are part of the transversal S wave.

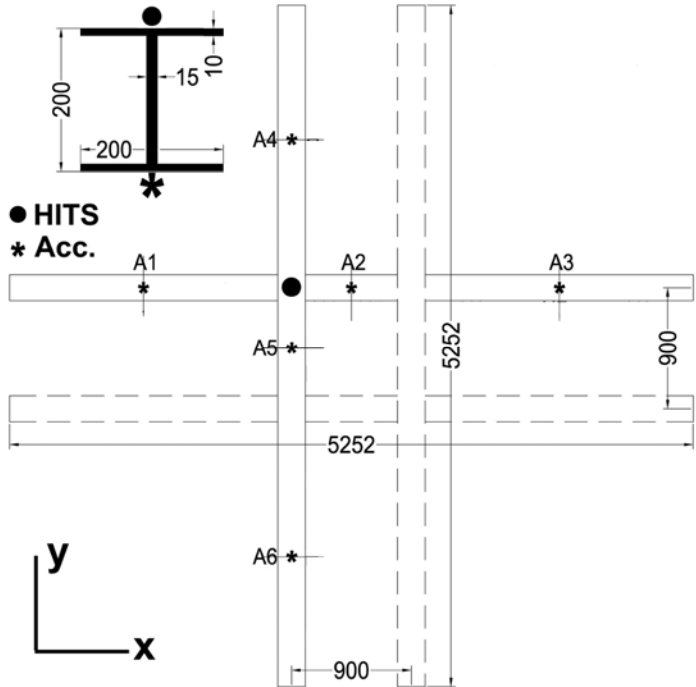


Figure 5.80. Excitation human action_ Jmax

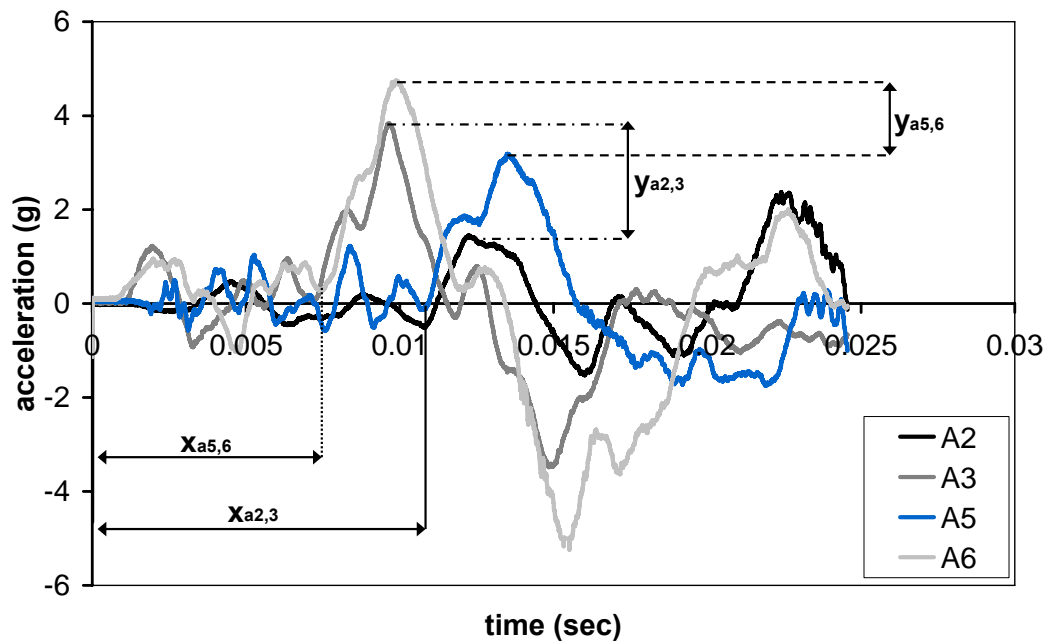


Figure 5.81. Human action_excitation 1

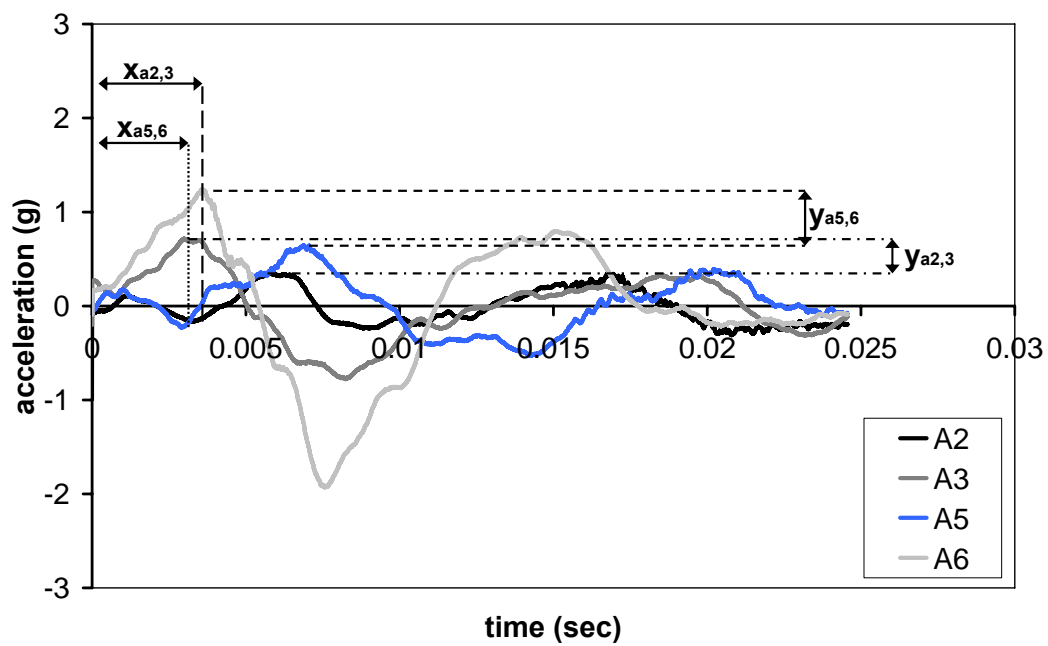


Figure 5.82. Human action_excitation 2

From the global analysis which considers the effect of the floor deck on the distribution of elastic vibration, a reduction in intensity of the signal induced by the presence of discontinuity due to the beam-beam joint is evident. The signal of discontinuous beam ($y_{a2,3}$) suffers a decrement of approximately 63%, of the value recorded by accelerometer A3 compared to what was revealed by accelerometer A2. This signal attenuation is almost double the attenuation of the signal (approx. 33%) of the continuous beam ($y_{a5,6}$) obtained from the accelerations recorded by accelerometers A5 and A6.

With regards to the spectra in frequency domain, the Figure 5.83 represents the dynamic behaviour of the GFRP structure regarding both excitations.

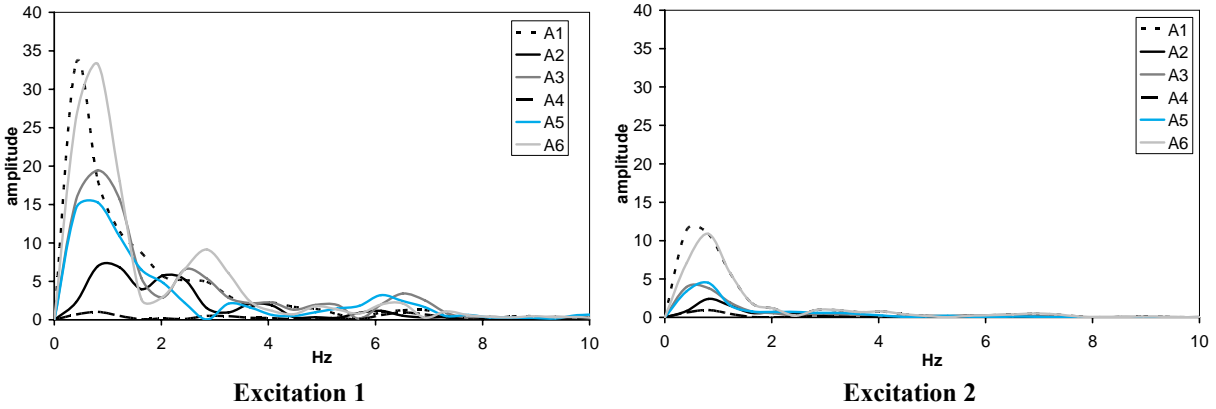


Figure 5.83. Spectra in frequency domain

The fundamental frequency of the structure regarding human action is equal to 0.81 Hz, the fundamental frequency detected is not included in the interval of frequencies induced by human action, see Table 5.12. As regards the determination of the capacity to dissipate the accumulated energy from the excitation of 80kg, the Half Power Bandwidth (HPB) method was employed.

The HPB was used for this type of excitation in that a reduced capacity of energy dissipation was detected, (Naghipour M. et al. 2005). The band width corresponds to the interval of included frequency, of the free oscillation of the considered frequency, within an N quantity (with $N > 1$) of the respective peak size (see Figure 5.84), indirectly quantifying the response velocity at the onset and at the disappearance of the vibration. The following figure, Figure 5.84, shows the bandwidth BW within the band frequencies f_i and f_{i+1} .

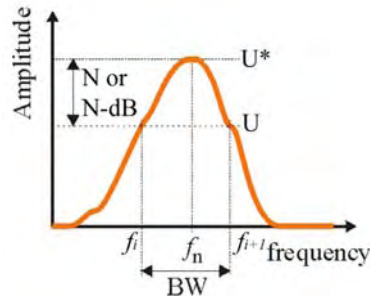


Figura 5.84. Band width

The duration of the free oscillation, which is directly linked to the band width, is measured considering the initial and final points of the oscillogram in the interval N (with $N=U/U^*$ with N always >1) which was placed equal to the logarithmic type measure $\pm 3\text{dB}$ (for $20 \cdot \log_{10} U/U^* = \pm 3\text{dB}$). In free mechanical oscillation, the damping is analytically quantified by the relationship between free frequency of vibration and the band width as expressed in the Equation (5.31).

$$BW = f_n \cdot \sqrt{1 - 2\xi^2 + 2\xi \sqrt{(N^2 - 1) \cdot (1 - \xi^2)}} - \sqrt{1 - 2\xi^2 - 2\xi \sqrt{(N^2 - 1) \cdot (1 - \xi^2)}} \quad (5.31)$$

where f_n = natural frequency; $BW = f_{i+1} - f_i$ (band width) and $N=U/U^*$.

The linear relationship between ξ and BW/f_n is valid only for low values of ξ (Jones D. I. G. 2001); with low values of ξ and with $N=2^{1/2}$ the Equation (5.31) is simplified obtaining the following formulation, Equation (5.32):

$$\xi_{BW} = \frac{BW}{2 \cdot f_n} \quad (5.32)$$

where ξ_{BW} = the coefficient of damping determined via the band width method.

The damping ratios obtained from the spectra in frequency domain of each signal have been reported in Table 5.26.

Table 5.26, Damping ξ of beam

| Excitation type | | Beam parallel to x axis | | | Beam parallel to y axis | | |
|-----------------|------------|-------------------------|-------|-------|-------------------------|-------|-------|
| | | Acc 1 | Acc 2 | Acc 3 | Acc 4 | Acc 5 | Acc 6 |
| 1 | J_{\max} | 0.5% | 0.37% | 0.61% | 0.5% | 0.74% | 0.5% |
| 2 | J_{\max} | 0.83% | 0.3% | 0.67% | 0.46% | 0.41% | 0.4% |

The mean value of damping, obtained for both excitations, is approximately 0.5%. Such value should be opportunely calibrated in function of the response registered with the excitations applied directly to the bearing structure as previously analysed.

5.2.3.2. Finite element analysis

As for the two-dimensional framework the FE analysis of three-dimensional system has been carried out with the same approach adopted in chapter 5.2.1.2.2. The mechanical properties employed to modeler the structure are the same of chapter 2.2. The modeling of GFRP components using the “beam” element that considers the shear deformability of each profile has been realized. For the external boundary conditions the joint has been modeled in order to guarantee the rotation and to restrain each displacement.

For the configuration of internal restrain, beam to column joint, semi-rigid joint with a rotational stiffness equal to 755 (kNm/rad) have been assumed.

Such value has been defined as mean value of corresponding interval determined by Eurocode 3, as foreseen for braced framework. Via the pulsation value ω , of period of vibration T and of corresponding fundamental frequency f_n the results of dynamic response of GFRP structure in the free vibration field, respect to main directions x and y (see Figures from 5.85 to 5.87), are shown in Table 5.27.

Table 5.27. Mode 1 – FEM analysis

| Direction | ω (rad/sec) | T (sec) | f_n (Hz) |
|-----------|--------------------|---------|------------|
| x | 157 | 0.04 | 21.71 |
| y | 52.3 | 0.12 | 8.29 |

In Figures 5.85, 5.86 and 5.87 the first modes of vibration are illustrated. The displacements of modal shapes are highlighted in the figures, respect to y direction (8.29 Hz), torsional behaviour (8.38 Hz) and respect to x direction (21.71 Hz).

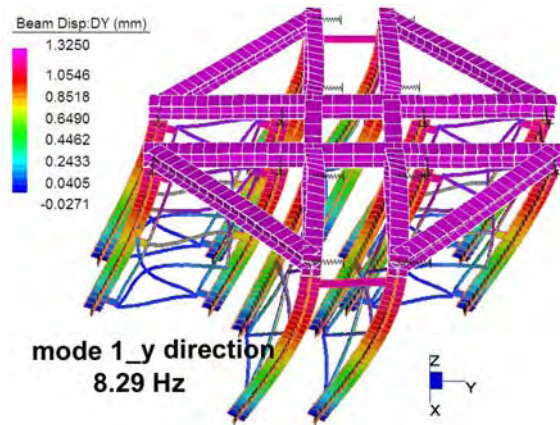


Figura 5.85. First mode of vibration_y direction

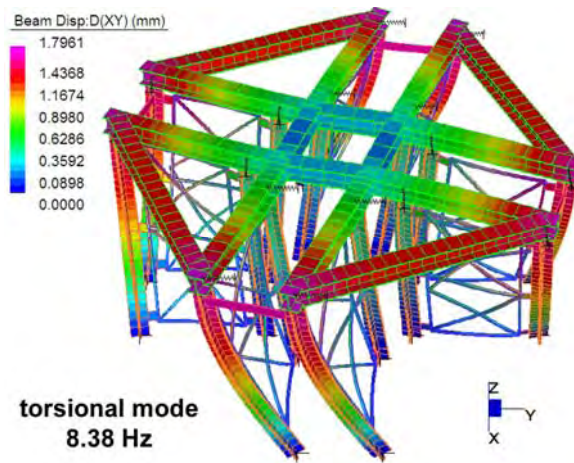


Figura 5.86. First torsional mode of vibration

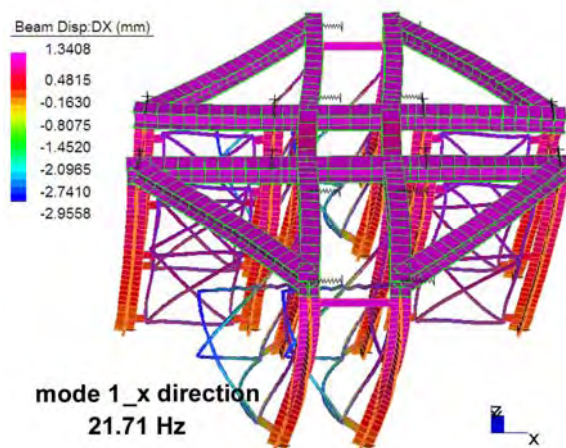


Figura 5.87. First mode of vibration_x direction

5.2.3.3. Results comparison

The analysis of experimental results highlights two spreads of fundamental frequency values, one for the columns and another for the beams.

From the modal analysis, the spread of values that regards the fundamental frequency of deck is wide. Such results dispersion is caused to high sensibility of horizontal elements respect to vibrations, even if of low entity, of existing structure that in this case contains the GFRP structure and above all of the low flexural stiffness of the historical wood deck. Moreover the hyperstatic typology effect of realization empathize this dynamic response.

This behaviour is amplified by the presence of wood deck that constitutes an element of vibrations transfer, and then of disturb, that not allow to recorder the flexural vibrations only of bearing structure.

Concerning the columns, nevertheless are constituted by assembled GFRP profiles, the boundary conditions allow to obtain the results with a good agreement.

In order to identify the fundamental frequency of structure the experimental values are detected, as shown in Table 5.28.

Table 5.28. Main value of frequencies, first mode of vibration for every structural elements

| Structural element | Excitation direction and accelerometer position | Main values f_n (Hz) |
|------------------------------|---|------------------------|
| Internal column | x | 6.51 |
| | y | 7.73 |
| External column | x | 6.51 |
| | y | 8.92 |
| Beam parallel to x direction | x | 20.34 |
| Beam parallel to y direction | y | 9.36 |

The comparison between the experimental results and FEM values, that highlights a good agreement between the data, is shown in Table 5.29.

Table 5.29. Comparison between experimental and FEM results of mode 1

| Analysis | Direction | ω (rad/sec) | T (sec) | f_n (Hz) |
|--------------|-----------|--------------------|---------|------------|
| FEM | x | 157 | 0.04 | 21.71 |
| | y | 52.3 | 0.12 | 8.29 |
| Experimental | x | 125.6 | 0.05 | 20.34 |
| | y | 62.8 | 0.1 | 9.36 |

5.3 Dynamic action behavior of GFRP structures

With respect to dynamic action, it is particularly difficult to classify a material as being more or less suitable than another; all the factors in play must be considered, such as the finality of the building, the structural typology, the technology and the material to be used.

The lightness of the FRP material and therefore the all-FRP structure guarantees a good structural behaviour with respect to dynamic actions thanks to the reduced incidence of mass participation in the inertial forces of the elements and the relevant structural system. Despite the lightness and transversal deformability of the GFRP pultruded elements, they must be controlled so as to avoid excessively flexible structures incapable of facing buckling phenomena due to P- Δ (load-deformation) effects. As regards, owing to the mechanical properties of the material, it is opportune to evaluate the stiffening effects of the braced systems.

The geometry, global dimensions and typology influence the dynamic response of GFRP structure if compared to the behaviour of structural elements in the free vibrations field. Furthermore, the typology of mechanical joint – bolted or bonded – owing to the constitutive law and the orthotropic behaviour of the material, greatly influences the response of the FRP structure in presence of dynamic action. The bonded joint offers a stiff and then a brittle structural response of beam-column joint; whereas the bolted joint assure, however, a ductile behaviour of joint. This refers in particular to the impossibility, as already highlighted, of being able to use the plastic deformation of the GFRP material to dissipate dynamic actions. Considering the results of the modal analysis carried out in this work, it is plausible the use of FRP elements as reinforcement in the 4 seismic zones, (OPCM 3274).

With regards to new buildings, the investigation conducted on two-dimensional frame (2D) and structure (3D) has allowed the dynamic characterisation of the GFRP structure with steel bolts and the definition of the influence of the OPCM parameters on the differing efficiency of the structural systems at dynamic action.

Since this is a material with brittle-elastic behaviour, the relationship between the final displacement and the displacement at the limit of the elastic behaviour, which defines the coefficient of static ductility, is equal to 1. As regards the first classification of OPCM on the conceptual aspects of the design of wood buildings – the wood is a material taken as an example

for the similar mechanical behaviour to GFRP material, which anisotropic and transversally isotropic with brittle-elastic failure to the collapse – through the technological solutions adopted, the two FRP frameworks analysed show a reduced dissipative capacity (behaviour b, OPCM 3274). With regard to the study of joint solutions for GFRP elements that guarantee a strength beyond their elastic limit is a topic of certain interest for future research (behaviour a, OPCM 3274).

In terms of what has been expressed by OPCM, referring to ordinary constructions of the III category, the factor of importance γ_i of GFRP systems is equal to 1.

Via the modal analysis and dynamic analysis with spectral response approach – using the dynamic parameters defined experimentally - it has been possible to identify, via simulation by FEM analysis, the effects of the variation of structural and technology design in order to constitute an initial evaluation and a relevant initial classification of GFRP structure subjected to dynamic action. Going into the detail of the approach adopted, modal analysis has permitted the definition of the mechanical characteristics of the structures analysed and the respective response capacities with respect to the principal directions; analysis with a spectrum of response has facilitated the identification of levels of displacement compared to the directions of horizontal dynamic action.

During the design phase and definition of the finite element models of GFRP structural elements, the definition and modelling of the internal and external joint is important.

As regards, according to what is defined by Eurocode 3, three typologies of internal joint were adopted: rigid, semi-rigid and pinned.

As regards the 2D framework the semi-rigid joint has a rotational stiffness K_ϕ equal to 610.3 kNm/rad, as defined in chapter 5.2.2.1.1. The value of the rotational stiffness of the semi-rigid joint 3D structure was determined as the average value in the corresponding interval of Eurocode 3, entirely considering the length of the beam equal to 4961mm, (braced $100.66 \leq K_\phi \leq 1610$ and unbraced $100.66 \leq K_\phi \leq 5033$).

For both the frameworks – 2D and 3D – the analysis were conducted by considering, or otherwise, the effect of the braces. The structural elements composed of the union of more profiles, such as beam and column, were modelled as perfectly collaborative.

The profiles were modelled considering the material as homogenous and taking into account, in any case, of the shear deformability of the pultruded material.

In the specific case of 2D framework, only the dynamic response regarding the acceleration applied in the direction of maximum moment of inertia, axis X, was evaluated.

In reference to what has been determined in the chapter 5.2.1.1.2. the Table 5.30 demonstrates the period of vibration of the first mode of vibration and the mass participation of the mono-dimensional elements.

Following the same procedure, the application of the GFRP profiles as reinforcement of the footbridge (see chapter 4.2.3.) was investigated.

Table 5.30. Mono-dimensional GFRP structural elements, first flexural mode, FEM analysis

| Boundary conditions | Profile typology | Hz | Time (s) | Mass participation (%) |
|-------------------------|----------------------|-------|----------|------------------------|
| Supported configuration | “I” J _{max} | 24.38 | 0.041 | 31.64 |
| | “Q” | 37.66 | 0.026 | 31.47 |
| | “H” J _{max} | 18.8 | 0.053 | 78.76 |
| | “P” J _{max} | 11.93 | 0.084 | 0.103 |

The global dynamic response of the “Paludo” bridge (chapter 4.2.3.) is investigated in detail in the Table 5.31 below.

Table 5.31. Footbridge, first flexural mode

| Typology | Hz | Time (s) | Mass participation (%) |
|---|-------|----------|------------------------|
| Increment of flexural stiffness by GFRP profile | 17.08 | 0.06 | 19.12 |

The modal analysis of the 2D framework was conducted on the three boundary conditions, clamped, pinned and clamped-pinned considering the three configurations of internal restrain – rigid, semi-rigid and pinned – to evaluate the mode of vibration upon variation of the stiffness, with or without braces (Figure 5.88 and Table 5.32).

Specifically, the brace was produced with GFRP pultruded rods with a diameter of 20 mm with the same mechanical characteristics of profile, Figure 5.88.

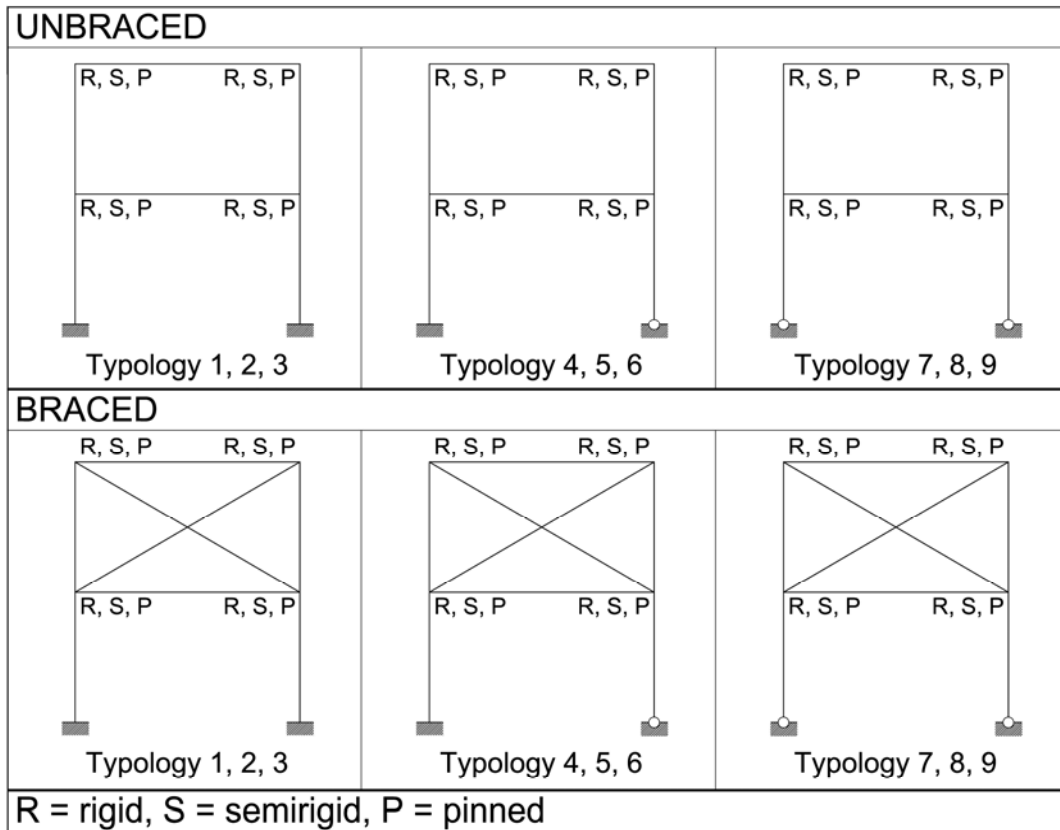


Figure 5.88 Schemes of 2D framework, braced and unbraced configuration with different constraint conditions

Table 5.32. 2D frame braced and unbraced, first mode in x direction

| External joint | Typology | Internal joint K_{ϕ} (kNm/rad) | | | unbraced | | | braced | | |
|----------------|----------|---|---|----------|----------|----------|------------------------|--------|----------|------------------------|
| | | | | | Hz | Time (s) | Mass participation (%) | Hz | Time (s) | Mass participation (%) |
| Clamped | (1) | rigid | R | ∞ | 12.02 | 0.08 | 83.16 | 12.62 | 0.08 | 87.11 |
| | (2) | semirigid | S | 610.3 | 7.05 | 0.14 | 72.95 | 9.76 | 0.1 | 84.02 |
| | (3) | pinned | P | 0 | 5.71 | 0.17 | 69.78 | 9.28 | 0.1 | 83.54 |
| Pinned-Clamped | (4) | rigid | R | ∞ | 9.89 | 0.1 | 87.89 | 10.12 | 0.1 | 89.97 |
| | (5) | semirigid | S | 610.3 | 5.98 | 0.17 | 78.83 | 7.84 | 0.13 | 87.39 |
| | (6) | pinned | P | 0 | 4.82 | 0.2 | 75.55 | 7.43 | 0.13 | 86.94 |
| Pinned | (7) | rigid | R | ∞ | 6.7 | 0.15 | 91.9 | 6.69 | 0.15 | 92.62 |
| | (8) | semirigid | S | 610.3 | 3.93 | 0.25 | 85.84 | 5.03 | 0.2 | 90.73 |
| | (9) | pinned | P | 0 | 2.91 | 0.34 | 83.19 | 4.68 | 0.21 | 90.36 |

For the external constraint of 3D structure was adopted the same approach of 2D framework. Tables 5.33 and 5.34 concern the behaviour of 3D structure in directions x and y for the braced

and unbraced configuration. Figure 5.89 shows the different schemes of 3D structure with the details on constraints for the braced and unbraced configuration.

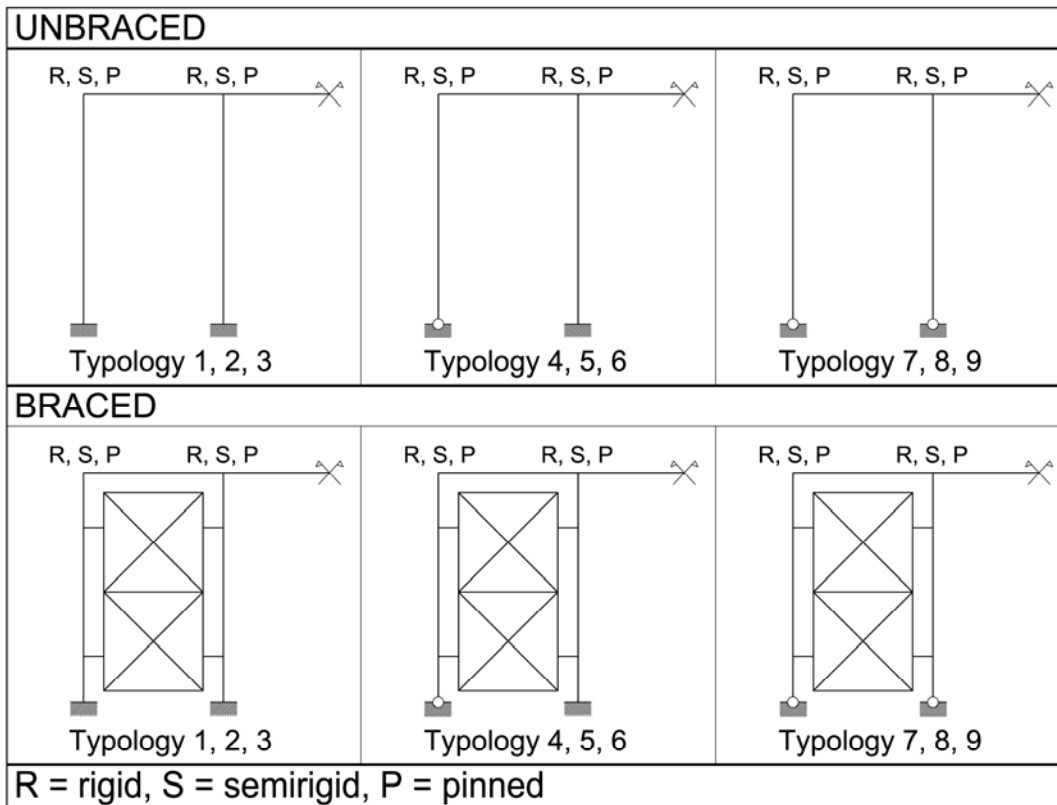


Figure 5.89 Schemes of 3D structure, braced and unbraced configuration with different constraint conditions

Table 5.33. 3D frame braced, first mode

| External joint | Typology | Internal joint K_{ϕ} (kNm/rad) | | | X direction | | | Y direction | | |
|----------------|----------|---|---|----------|-------------|----------|------------------------|-------------|----------|------------------------|
| | | | | | Hz | Time (s) | Mass participation (%) | Hz | Time (s) | Mass participation (%) |
| Clamped | (1) | rigid | R | ∞ | 23.82 | 0.042 | 67.76 | 13.80 | 0.072 | 79.28 |
| | (2) | semirigid | S | 755 | 23.69 | 0.042 | 67.43 | 13.46 | 0.074 | 78.92 |
| | (3) | pinned | P | 0 | 23.68 | 0.042 | 67.38 | 13.41 | 0.075 | 78.87 |
| Pinned-Clamped | (4) | rigid | R | ∞ | 22.39 | 0.044 | 65.89 | 11.17 | 0.089 | 81.62 |
| | (5) | semirigid | S | 755 | 22.29 | 0.045 | 65.52 | 10.84 | 0.092 | 81.29 |
| | (6) | pinned | P | 0 | 22.27 | 0.045 | 65.46 | 10.79 | 0.092 | 81.24 |
| Pinned | (7) | rigid | R | ∞ | 21.8 | 0.046 | 65.92 | 8.65 | 0.11 | 84.54 |
| | (8) | semirigid | S | 755 | 21.71 | 0.046 | 65.46 | 8.29 | 0.12 | 84.24 |
| | (9) | pinned | P | 0 | 21.69 | 0.049 | 65.37 | 8.23 | 0.12 | 84.2 |

Table 5.34. 3D frame unbraced, first mode

| External joint | Typology | Internal joint K_{φ} (kNm/rad) | | | X direction | | | Y direction | | |
|----------------|----------|--|---|----------|-------------|----------|------------------------|-------------|----------|------------------------|
| | | | | | Hz | Time (s) | Mass participation (%) | Hz | Time (s) | Mass participation (%) |
| Clamped | (1) | rigid | R | ∞ | 13.31 | 0.075 | 81.56 | 13.31 | 0.075 | 81.56 |
| | (2) | semirigid | S | 2466 | 13.01 | 0.076 | 81.26 | 13.01 | 0.076 | 81.26 |
| | (3) | pinned | P | 0 | 12.96 | 0.077 | 81.22 | 12.96 | 0.077 | 81.22 |
| Pinned-Clamped | (4) | rigid | R | ∞ | 9.07 | 0.11 | 82.694 | 9.68 | 0.10 | 83.637 |
| | (5) | semirigid | S | 2466 | 9.624 | 0.10 | 84.517 | 9.624 | 0.10 | 84.516 |
| | (6) | pinned | P | 0 | 9.59 | 0.10 | 84.486 | 9.59 | 0.10 | 84.485 |
| Pinned | (7) | rigid | R | ∞ | 6.62 | 0.151 | 88.22 | 6.62 | 0.151 | 88.22 |
| | (8) | semirigid | S | 2466 | 6.43 | 0.155 | 88.04 | 6.43 | 0.155 | 88.04 |
| | (9) | pinned | P | 0 | 6.4 | 0.156 | 88 | 6.4 | 0.156 | 88 |

From the analysis of the results, the interval of the values which defines the fundamental periods of all configurations is particularly low, 0.026-0.34 seconds. Considering that the GFRP structures can also collaborate with existing buildings, it is necessary to clarify that the analysis carried out considers the GFRP structure as independent and, then, not influenced by the dynamic behaviour of structure built with different material and typology. It is also necessary to add that, in the case of the all-FRP structure being part of a more complex configuration, the application point of the acceleration must be evaluated in terms of the actual position with respect to the principal structure.

For each typology analysed of the braced 3D structure and for the directions considered, the mass participation in play in direction x – in reference to the fundamental mode – are low, less than 70%. The significant value of the total mass participation is reached with a considerable number of modal contributions. Nevertheless, evaluating the low values of the mass participation in relation to the modal out shape (for example, that it is symmetrical and follows the symmetry of the structure), and considering the mass participation in different directions of that mode of vibration, the higher stiffness of the structure for both configurations analysed is evident.

With regards to the braced and unbraced 2D framework, analysed only in direction x, the mass participation immediately reaches extremely high values with the first mode of vibration. In relation to the period for each of the three boundary conditions (clamped, pinned-clamped, pinned), the variation of rotational stiffness of the internal restrains from the braced configuration

to the unbraced configuration indicates an increment in deformation of approximately 35-40% for the pinned restraint and 20-30% for the semi-rigid restraint. The variation of the internal restraint condition is particularly evident in the unbraced framework with an average increment of deformation of approximately 41% from the pinned joint to the semi-rigid joint and of approximately 20% from the semi-rigid joint to the rigid joint.

The different design approach of the 3D structure demonstrates much briefer periods, which do not vary for the two internal restraint conditions analysed - pinned and clamped - but which register a difference compared to the external constraint configurations.

As regards the analysis of the GFRP structure response to the dynamic action it has been considered only an earthquake excitation which ignores the parameters, what non-linear behaviour, ductility and failure mode, which would allow a complete evaluation on the seismic performances of GFRP building.

The different structural typologies reported in Table 5.35 were analysed via spectral response approach for zone 2 (average seismicity with $a_g=0.25g$) and category of soil B according to what is defined by Eurocode 8 (2003) and by OPCM 3274.

Table 5.35. Rotational stiffness and boundary conditions

| External joint | Typology | Internal joint | | 2D Frame | 3D Frame braced | 3D Frame unbraced |
|----------------|----------|----------------|---|--------------------------|-----------------|-------------------|
| | | | | K _φ (kNm/rad) | | |
| Clamped | (1) | rigid | R | ∞ | ∞ | ∞ |
| | (2) | semirigid | S | 610.3 | 755 | 2466 |
| | (3) | pinned | P | 0 | 0 | 0 |
| Pinned-Clamped | (4) | rigid | R | ∞ | ∞ | ∞ |
| | (5) | semirigid | S | 610.3 | 755 | 2466 |
| | (6) | pinned | P | 0 | 0 | 0 |
| Pinned | (7) | rigid | R | ∞ | ∞ | ∞ |
| | (8) | semirigid | S | 610.3 | 755 | 2466 |
| | (9) | pinned | P | 0 | 0 | 0 |

In order to evaluate the influence both of the internal and external constraint grade and of the stiffness offered and of the geometry on dynamic response of structure GFRP, the qualifying parameters of the project - such as displacement and strength of the system and elements - were analysed.

The structural behaviour of the 2D framework upon variation of the restrain conditions is illustrated in Figure 5.90 via the most significant displacement of the braced and unbraced configurations.

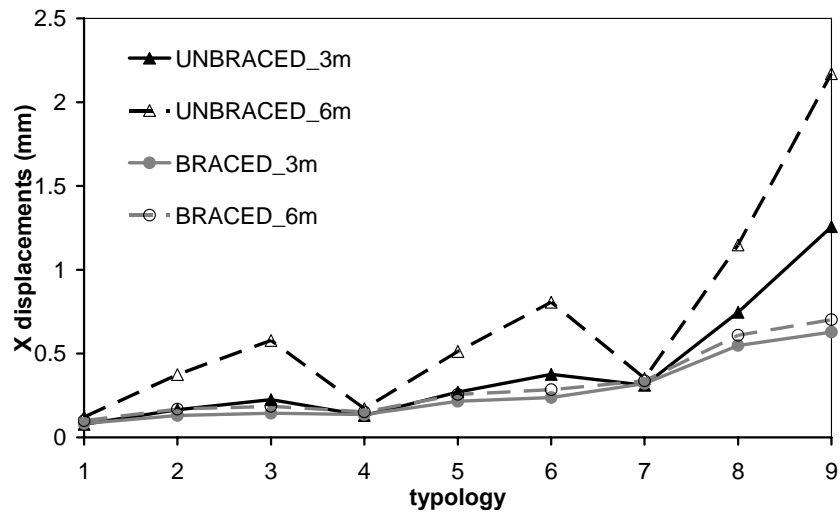


Figure 5.90, 2D frame, displacements of column to 3m and 6m

Figure 5.90 highlights that for the unbraced configuration the increment of displacements to 6m is continuous and almost of 10-15% compared to the displacements obtained to 3m. All in all, again for the unbraced typology, the displacements caused by variation of external and internal joints are equally important. From Clamped condition to Pinned-Clamped configuration the displacements increase by about 30% while from Pinned-Clamped to Pinned configuration the increment is equal to about 55%. For each external constraint the variation of internal restrain causes an increment of displacement values equal to circa 70% from rigid to semirigid configuration and equal to 35% from semirigid to pinned joint. For the braced configuration the displacements to 3m and 6m are similar. For this braced typology is important the increment of displacements caused by variation of external joints respect to the variation of rotational stiffness of internal joints. From Clamped to Pinned-Clamped configuration the increment is equal to 35% while from Pinned-Clamped to Pinned condition is equal to 55%. As regards the internal restraints evaluated for each external constraints, the change from rigid to semirigid joint causes an increment of displacement equal to 40% while from semirigid to pinned configuration the

increment is equal to 10%. All in all the contribution given by braced compared to unbraced configuration is highlighted by the decrement percentage of displacement values according to the relationship between the displacement values of Braced and Unbraced configurations, Table 5.36.

Table 5.36. Displacement values comparison between Braced and Unbraced configuration

| External joint | Typology | Internal joint | | Braced/Unbraced (%) |
|----------------|----------|----------------|---|---------------------|
| Clamped | (1) | rigid | R | 18 |
| | (2) | semirigid | S | 55 |
| | (3) | pinned | P | 68 |
| Pinned-Clamped | (4) | rigid | R | 11.5 |
| | (5) | semirigid | S | 50 |
| | (6) | pinned | P | 65 |
| Pinned | (7) | rigid | R | 4 |
| | (8) | semirigid | S | 47 |
| | (9) | pinned | P | 68 |

The trend of stresses is illustrated in the Figure 5.91, the curves refer to the maximum axial stresses at compression of the mono-dimensional elements, beam and column.

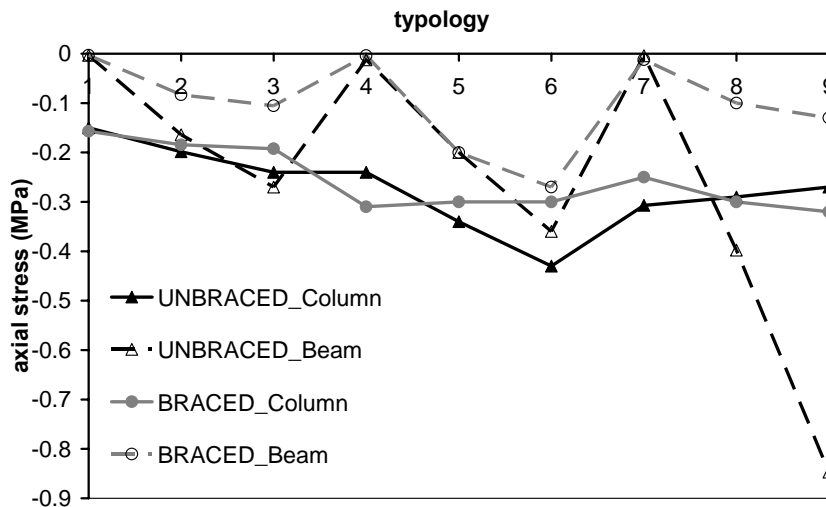


Figure 5.91. 2D frame, stress behaviour

The presence or absence of the braces has not important effects on the stress level of the columns thanks to the higher inertial stiffness offered by the columns themselves; the beams, however, because of the their slenderness are influenced by the action of the braces. Again in reference to the beams, for both configurations – braced and unbraced - the slenderness exalts the difference

of the structural response to the variation of constraint conditions, internal and external, of the framework.

In particular the internal rigid joint for each typology of external joint and for each configuration – braced and unbraced – has a negligible stress level that varies from -0.003MPa to -0.0121MPa. For the braced configuration the typologies characterized by Clamped and Pinned external joints have the mean stress value equal to -0.09MPa and -0.012MPa, respectively. The Pinned-Clamped typology highlights an increment of the stress level of two times both for the semirigid joint and for the pinned joint compared to the configurations with Clamped and Pinned external joints. As regards to the unbraced configuration the level of stress value increases from Clamped, to Pinned-Clamped and to the final Pinned configuration both for the internal semirigid joint and for the pinned joint, with increment percentage of 40%, 45% and 53%, respectively.

The structural response of the 3D structure is illustrated in Figures 5.92; the overall behaviour regarding the two principal directions of dynamic action that was analysed.

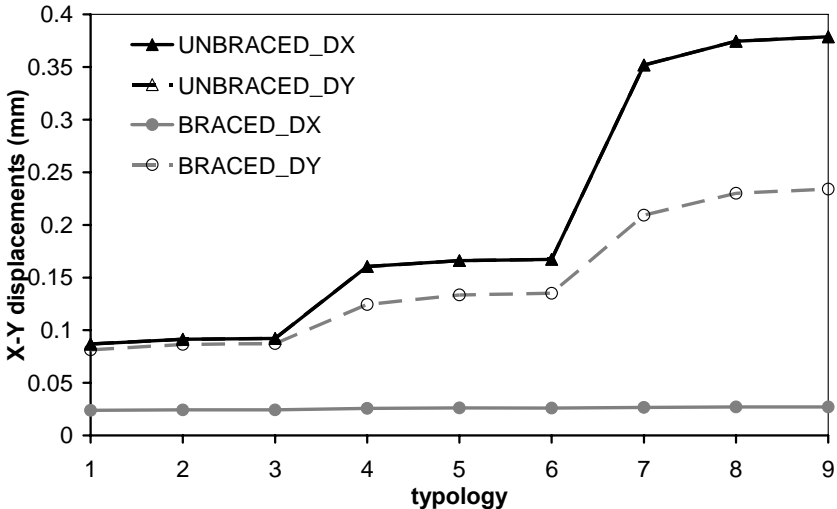


Figure 5.92. 3D frame, displacements

In the case of displacements detected, the influence of the external constraint is particularly evident compared to the variation of the rotational stiffness of the internal joint.

In particular, for the unbraced configuration with the dynamic action along y direction, the increment of displacements is equal to about 45% from Clamped to Pinned-Clamped

configuration and equal to about 55% from Pinned-Clamped to Pinned configuration. As regards the braced configuration – for the same direction - the increment of displacements is 35% from Clamped to Pinned-Clamped and equal to about 42% from Pinned-Clamped to Pinned configuration. The relationship between the braced and unbraced configurations shows a similar behaviour for the Clamped external joint and the increment of displacement values - of the unbraced configuration compared to the braced configuration – equal to 20% and 40%, respectively.

The structural response of the framework with unbraced configuration with respect to the dynamic action applied in directions x and y is coincident. The braced typology registers different behaviour between the two directions analysed; an almost constant structural behaviour for the dynamic action applied along x and growing along y are highlighted by Figure 5.92.

Figure 5.93 illustrates in detail the maximum level of stress reached by the elements with regards to compression axial stress.

Also in this case, the higher stiffness of the system does not seem to be affected by the presence, or otherwise, of the braces. The same variation of internal restrain conditions influences in negligible way the global dynamic response.

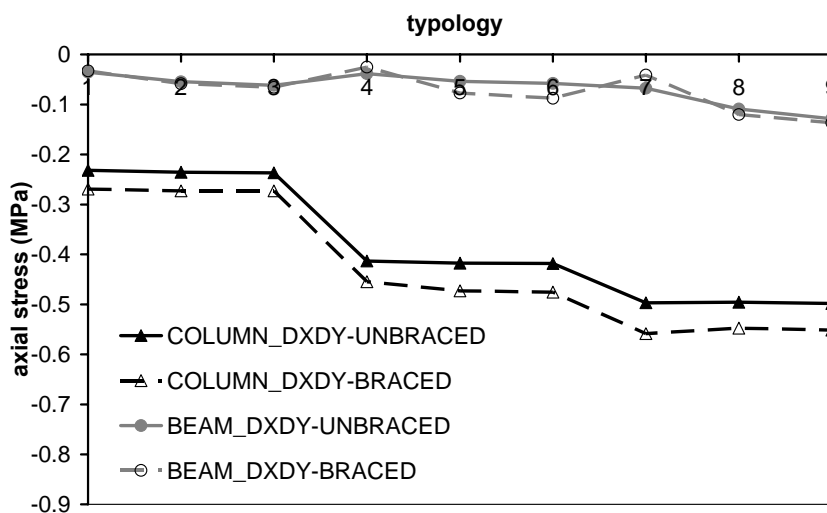


Figure 5.93. 3D frame, stress behaviour

The variation of external constraint conditions influences the stress level of the columns; from Clamped to Pinned-Clamped configuration the stress value increases of about 43%, while for the next step – from Pinned-Clamped to Pinned configuration – the increment is equal to 16%.

5.4 An example in presence of a real dynamic load

In this section the author shall present the first experiments and FEA results for the vibration response of a pultruded GFRP sheet pile while it is being forced into the ground using a traditional (steel) piling machine. Such a machine applies the dynamic action through a 10 kN fixture at the top of the pile. The application of pultruded components for waterfront sheet piling is relatively new. In general the first studies on the water absorption of laminated FRPs were developed by Pritchard and Speake (1987) and Davies (1996). As regards the FRP profiles for waterfront retaining wall applications was shown by Lampo et al. (1998). The work of Giroux and Shao (2003) analyses the structural behaviour of composite sheet pile while Shao and Kouadio (2002) carried out a study on durability in water. Shao (2006) determined the mechanical characteristics, the maximum percent water absorption and the corresponding mechanical property change of a pultruded FRP sheet pile, the resistance to freeze-thaw cycling to analyse the long-term structural performance of sheet pile walls.

The mechanical and geometrical properties of the pultruded pile shape in this study are given in Table 5.37, with the x-, y- and z- directions defined with the cross-section shape in Figure 5.94. Each pile component is 610 mm wide and has a depth of 255 mm. As Figure 5.94 shows the wall thickness is 7.6 mm in the inclined webs and 9 mm in the flanges.

Table 5.37. Mechanical and geometrical characteristics of sheet pile

| E_{xx} (MPa) | E_{yy} (MPa) | E_{zz} (MPa) | ν_{xz} | ν_{zy} | ν_{yz} | G (MPa) | Density (kg/cm ³) | A (cm ²) | J_{xx} (cm ⁴) | J_{yy} (cm ⁴) |
|-------------------|-------------------|-------------------|------------|------------|------------|------------|----------------------------------|----------------------|-----------------------------|-----------------------------|
| 8500 | 8500 | 23000 | 0.09 | 0.23 | 0.09 | 3000 | 0.00185 | 85.67 | 8271.5 | 28378.2 |

Where E is the elastic modulus, ν is the poisson's ratio, G is the shear modulus, A is the area of cross section and J is the moment of inertia.

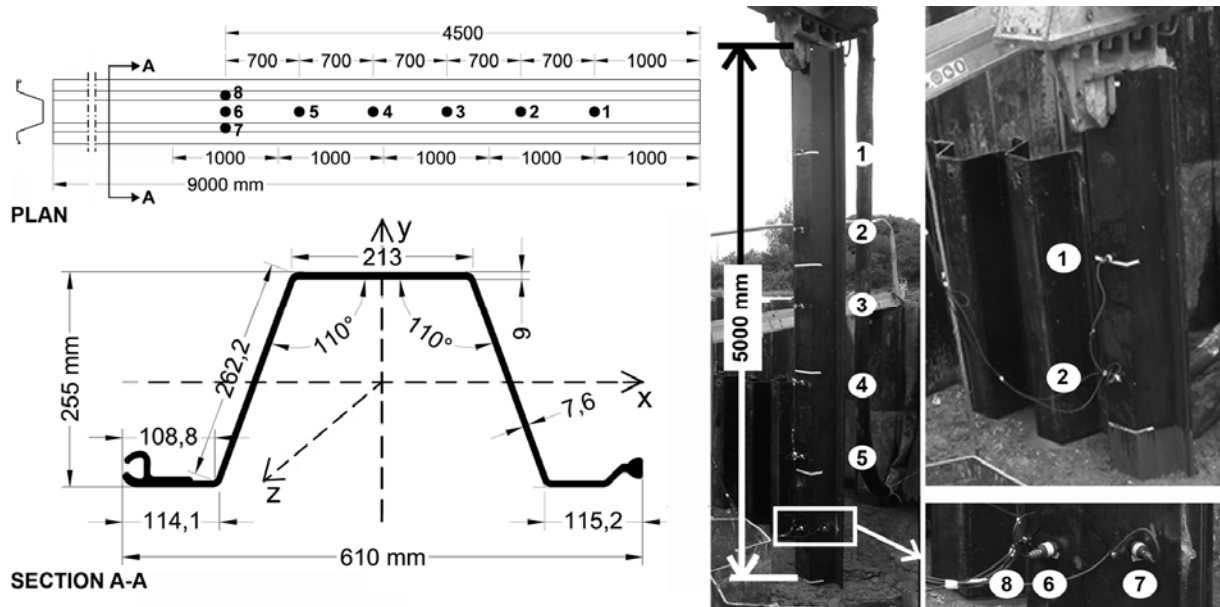


Figure 5.94. Sheet pile shape and accelerometer location

To connect piles together there is a male and female detail along the longer sides that combine to form a mechanical interlock when two shape slide together. Further development of the connection between two piles can be achieved by the introduction of adhesive bonding. It is observed that the shape of the pile unit in Figure 5.94 is similar to that of the Larsen sheet pile, which is generally of steel. The E-glass fiber loading is 48% by volume fraction and the matrix using a vinylester polymer. Table 5.37 shows that the elastic constants of the pultruded material are similar to those for the standard structural shapes that are studied in chapter 2.2.

In this study the author measures the first vibration mode, the acceleration and distribution of lateral displacement along the length of a pile unit. Dynamic testing was carried out using two impact actions that can be associated with 380 and 760Hz excitations, both for the penetration of a single pile and for a restrained sheet piles that has the mechanical interlock connection fully adhesively bonded. The photographs in Figure 5.94 show the single pile specimen and restrained pile under testing.

Using the FE modeling methodology for pultruded members given in Section 5.2.1.2.2. the pile problem has been analysed so that a comparison can be made between computational analysis and what is measured on-site. In FEA modeling the dynamic load, 10 kN, is applied at the top of the pile that, to avoid the transversal displacement, is restrained for all directions except for displacements along to Z global axis.

For this comparison Figure 5.94 shows the locations of the eight accelerometers along the length of the pile. These sensors are piezoelectric elements featuring a cylindrical shear stress configuration. The profile geometry and the boundary conditions were considered in defining test setup with reference to kind and accelerometer positions. They have a sensitivity of 1000 mV/g, a variation field assumed to be $\pm 10g$ and a resolution of 1×10^{-5} g in a frequency range of 0.25 to 800Hz. Each accelerometer is equipped with an integral charge preamplifier and is connected to the digitizer unit by means of high stability coaxial cables. The digitizer unit is based on commercial 13-bit data acquisition boards (from Data Shuttle Express). The signal has been acquired with a low-pass filter with a cut-off frequency of 2 kHz; the signal's scan is 1000 Hz.

Figure 5.95 shows a measured acceleration trace for the time period 14.5 to 16.5 s that is from the dynamic events for the free sheet pile driven two metres into the ground. The acceleration characteristic was from sensor number 6, located on the thicker flange. The sensor 6 obtains, during the working of piling machine, in the interval of 0.53 s 20 oscillations, so corresponds a dominant frequency $f=20/0.53=37.7$ Hz. The same signal, analysed at the end of working of piling machine, considering the interval of 0.90 s with 30 oscillations gives a frequency $f=30/0.90=33.3$ Hz.

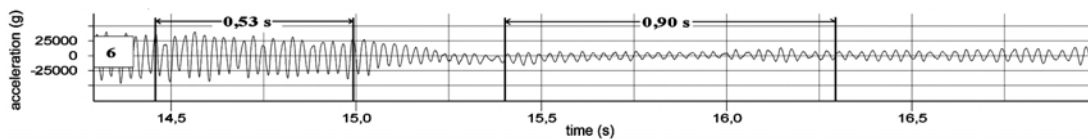
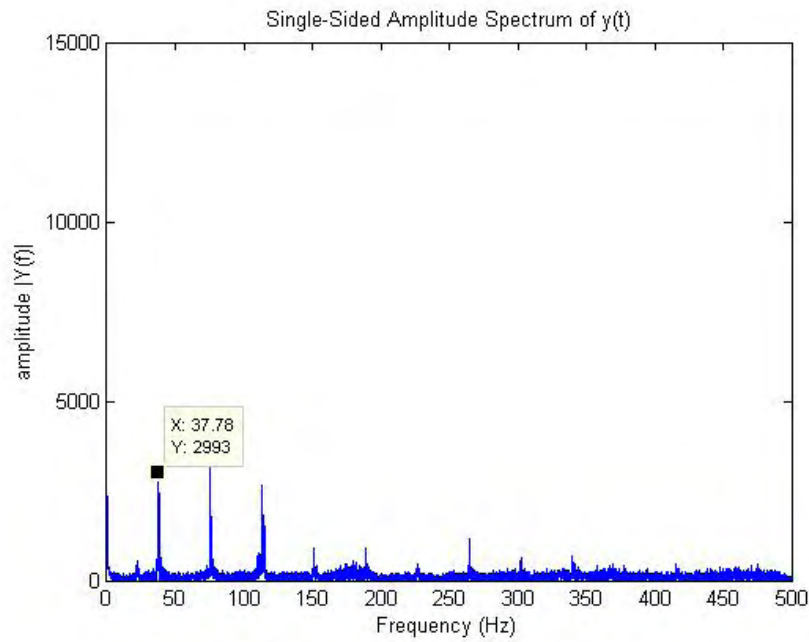


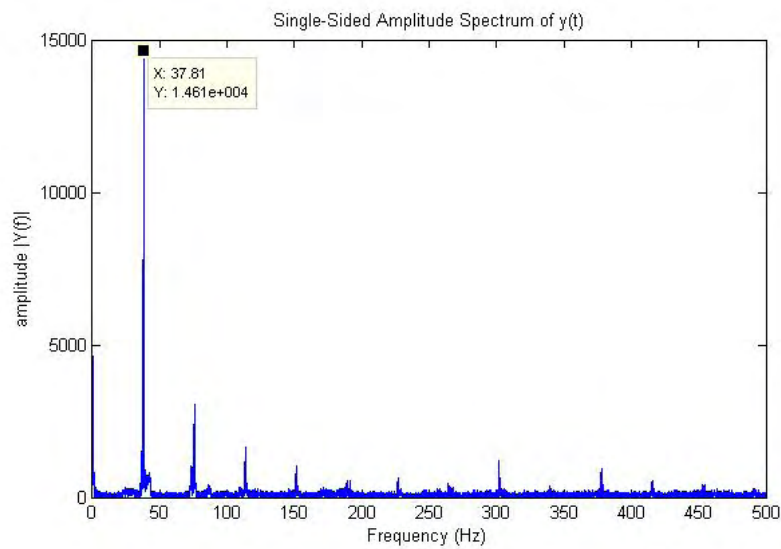
Figure 5.95. Experimental evaluation of vibration response in time domain

Similar traces from sensors 7 and 8, which are at the same height as sensor 6 but on the two thinner webs, show differences that can be linked to the different panel stiffnesses. For each depth in Figures 5.96 and 5.97 the dominant frequencies are plotted having calculated the Fast

Fourier Transform using all the accelerometer with 760 Hz excitation. The first frequency is 37.7Hz.

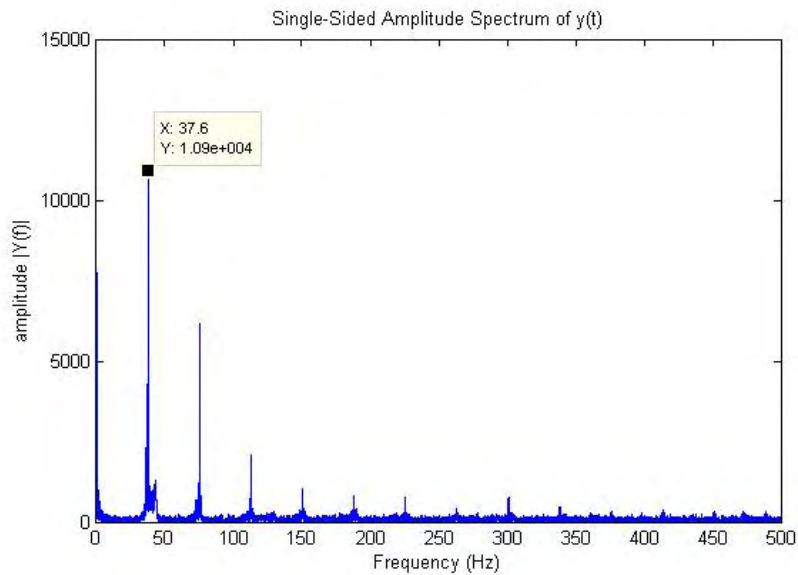


1 meter into the ground

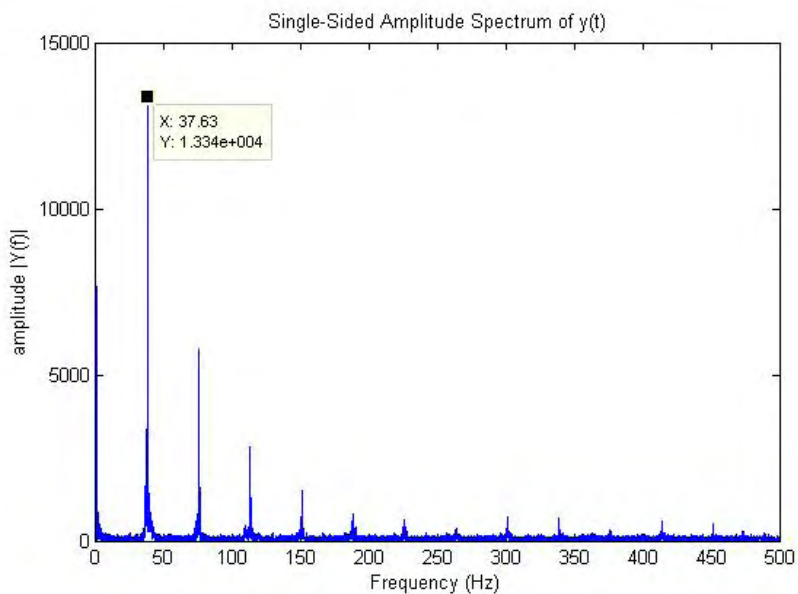


2 meters into the ground

Figure 5.96. Experimental evaluation of vibration response in frequency domain, 1 and 2 meters into the ground



3 meters into the ground



4 meters into the ground

Figure 5.97. Experimental evaluation of vibration response in frequency domain, 3 and 4 meters into the ground

To verify the quality of the experimental results the piling problem is analysed by finite element analysis. The mesh for the vertical pile using the Straus 7 software release 2.2.3 requires 37800 four-node isoparametric shell elements.

Finite element analysis has been employed in the linear elastic field. Structural elements made of homogeneous material with orthotropic elastic properties are considered and the damping ratio is assumed to be 2.5% from Boscato and Russo (2007).

Each modeling element is proportionate to the total size of the respective cross-section, every node has five degrees of freedom, i.e. translation along local x, y and z axes and rotation around local x and y, with z always normal to the shell element.

To model the two excitation cases required two approaches. For the 380Hz case the pile length is 9m (Figure 6.94) and the ends are assumed to be simply supported, scheme 1. The length is 7m and the ground end has a clamped boundary condition for the 760Hz situation, scheme 2.

The analysis has been carried out evaluating the steps of each meter of depth without considering the friction effect produced by the penetrating phase.

FE results for the 380Hz situation are presented in Figure 5.98, and for the higher frequency case they are given in Figure 5.99. Figures 5.98(A) and 5.99(A) show the lateral displacement shape along the length of the piles for their fundamental frequency without pile loading, and it is determined that their frequencies are 8.45Hz and 11.17Hz, respectively. Parts (B) and (C) in these figures are for the natural frequency closest to the applied frequency and the response at the piling machine’s forcing excitation. It is seen from these parts that the closest frequencies are within 3Hz of the excitation value. Equivalent plots for the axial direct stress down the length of the piles are given in Figures 5.100 and 5.101.

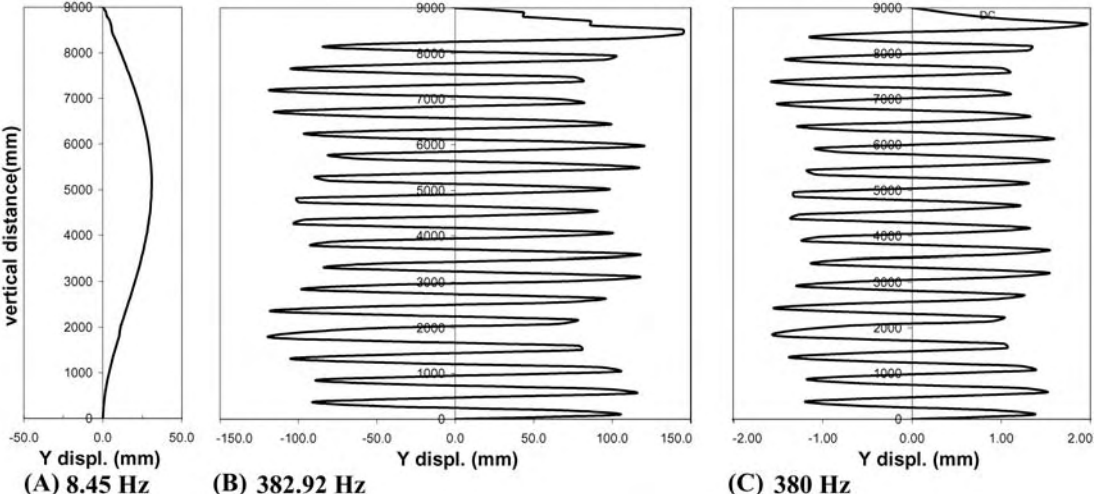


Figure 5.98. Lateral displacement, scheme 1

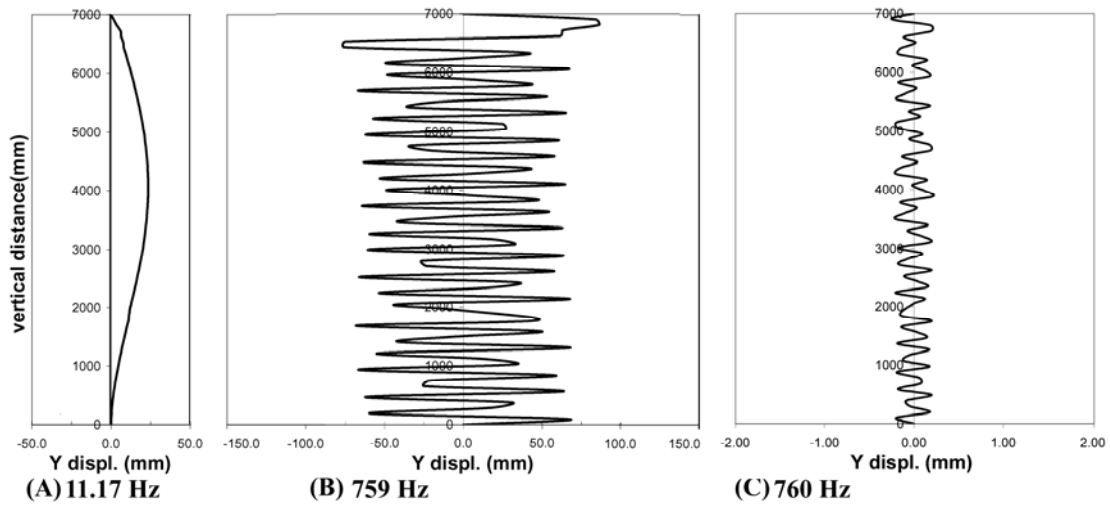


Figure 5.99. Lateral displacement, scheme 2

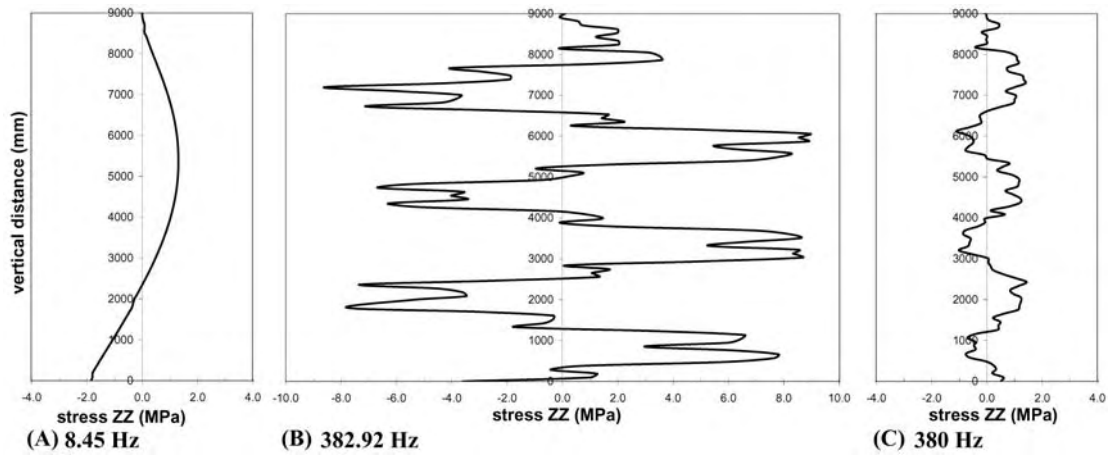


Figure 5.100. Vertical stress, scheme 1

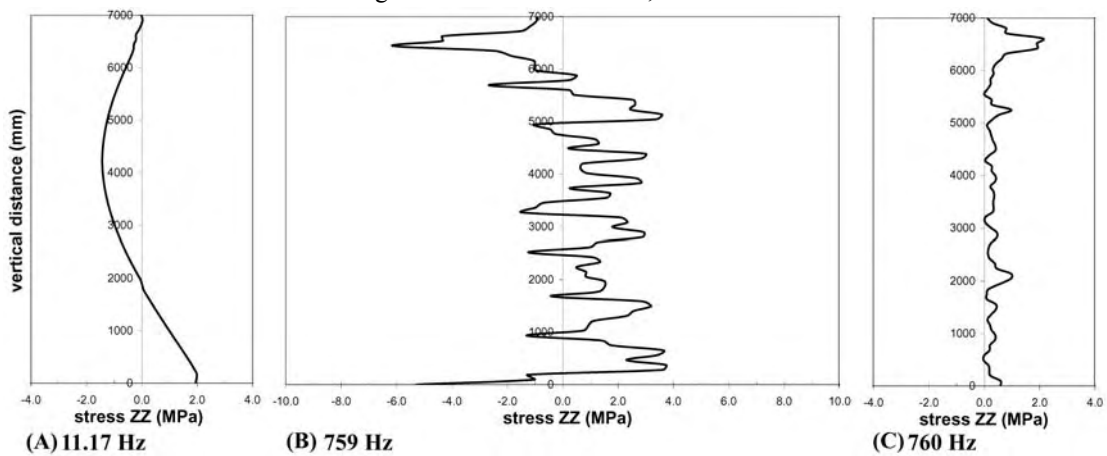


Figure 5.101. Vertical stress, scheme 2

Presented in Figure 5.102 is a comparison of lateral displacements of the 9m long pile for each step of experimental test – with sheet pile inserted into the ground at 1, 2, 3 and 4 meters of depth - with dynamic action equal to 380Hz for the first dynamic mode frequency of 37.7 Hz; in fact the dynamic response of this pile has been recorded at each 1 m depth of penetration (i.e. label D1m is for Depth 1 meter relative to 1 meter into the ground, considering the value 0 of length as the point where has been applied the dynamic action). With the experimental values (exp) are the FE predictions (FEM) for the global behaviour in which, to simulate the real situation, the ground surrounding the pile is assumed to behaviour as Winkler soil with spring elastic-plastic equal to 0.4kg/cm^3 (clayey medium dense sand $K=4000/5000\text{ kN/m}^3$ ($0.4/0.5\text{ kg/cm}^3$)). At the top of the pile where the impact loading is applied this FE model of piling has a sliding pin restraint.

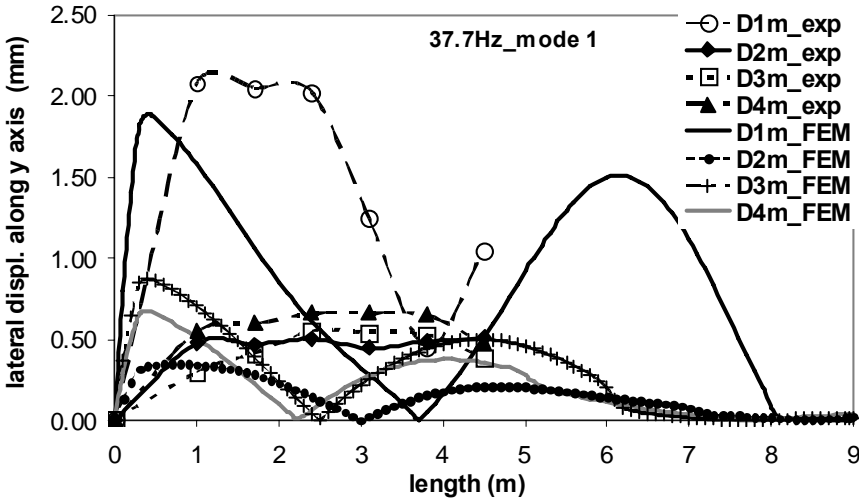


Figure 5.102. Comparison between experimental and FEM results

Given the degree of uncertainty and the complexity of the dynamic problem the computational displacements from the Straus 7 simulation in Figure 5.102 are seen to show a good agreement with the experimental measurements, not for global behaviour, but for the maximum values of displacement only. It is believed that differences between paired curves (e.g. D1m_exp and D1m_FEM) are principally due to the variables of difficult definition which must be assumed for the FEM model, as the soil's properties in depth and the angle of pile when it is driven into the ground.

Concerning to dynamic response of GFRP sheet piles by experimental results and finite element analysis it is possible to draw the first conclusions as follows:

- the experimental results highlight the asymmetrical behavior of FRP sheet pile, mainly due to the different stiffness of the two flanges.
- The response of 9 meters long sheet pile is controlled by global structural behavior; in the initial phase of the insertion, displacements involve exclusively the web - that is vulnerable mostly for applied external dynamic load. The greater stiffness of 7 meters is achieved by boundary conditions, in this case the displacements are really lower along the sheet pile; in the FE analysis negligible local instability is observable too.
- The longitudinal stress values obtained by finite element analysis are negligible.
- The higher deformability of pultruded elements is highlighted by finite element analysis in the free vibrations field; however this deformability decreases with the increment of vibration dynamic load.
- Generally speaking, the whole insertion process of GFRP sheet piles can be done with the same operations usually employed for the steel sheet piles.

5.5 Chapter overview

In reference to the experimental and analytical results relative to the response of fiber-reinforced composite elements and structures subjected to free vibration, the following conclusive considerations are proposed both on dynamic parameters of mono-dimensional element and on dynamic response of structures and, in particular, on the transformation from profile to structural system.

Nevertheless the different geometric parameters, the spectrum of response and the modes of vibration demonstrate a good mechanical homogeneity which results in not being substantially influenced by the formation of the base material via the fiber and matrix components; vice versa the eventual presence of defects in the form of voids and a lack of homogeneity would be highlighted by the experimental tests.

The incidence of twisting phenomenon is evident in slender pultruded profile as shown by dynamic response of the cross section “H” profile asymmetrically excited. Corresponding to the cross section of the midpoint, a difference in terms of displacement was detected between the half flanges with a maximum displacements of 64.5% greater than the minimum displacements.

As regards the numerical approach the analysis of the modes of vibration of the GFRP open-cross section pultruded elements and with an higher slenderness can be developed with existing theories and computational methods relative to isotropic materials.

The formulations which take into account the influence of shear deformability and torsional effect are generally more suitable for the study of the dynamic behaviour of the GFRP elements and in fact provide results with a good concordance with the experimental results.

In the specific case of a deformed dynamic of the closed-cross section profiles and with low L/h ratio, a strong influence of shear with respect to that of the bending moment is revealed.

As regards the “C” shape, the formulation including shear deformation and torsional stiffness fits quite well to the real performance and accounts for the noticeable effects of open and asymmetrical cross section.

In reference to possible applications of GFRP structural element in engineering field, it is important the comparison with the natural frequencies of traditional material, steel and aluminium. In particular the “I” profile is characterized by a small difference between GFRP

material and the aluminium, while the fundamental frequency of the “H” profile is almost equal to steel element. For the design of bearing structure of a general deck the low dead load of GFRP structural element entail a considerable decrement of fundamental frequency value also with low applied loads. For the same length and for each GFRP profile at the increment of applied load corresponds the decrement of fundamental frequency; this trend is evident above all at the first loads.

On the whole, in terms of 2D and 3D GFRP frameworks, the capacity of acceleration dissipation is similar to GFRP structural elements. With simply supported configuration the damping ratio of profile with maximum moment of inertia changes between 2.25% and 3.5%. The “I” and “C” profiles subjected to axial load are the only one with a high damping ratio, equal to almost 4% in the case of minimum moment of inertia. In detail the interval of damping of two-dimensional framework increased from 1.4% to 1.9%, despite for the three-dimensional structure the capacity of acceleration dissipation changes from 1.66% to 1.96%. Considering the mean values, passing from structural elements to GFRP structures, the damping value undergoes a reduction of about 40%, in fact the mean value of damping determined by experimental tests on 2D and 3D frameworks is equal to 1.7%.

Therefore is particularly interesting the comparison between the dynamic response of structural element with “H” cross section analysed in the configuration both as simply supported (see Figure A.8, Appendix A) and as the beam in the 3D structure (see Figure C.5, Appendix C). This comparison, made possible by the similar dimensions of the beams (same section and length slightly different, 5m for the mono-dimensional structural element and 5.2m for the beam considering a span of 5m between the two external constraints) allows to identify the influence on the dynamic response of the various boundary conditions. As regards the damping ratio are almost similar (3.15% for the beam in the 3D structure and 3.4% as structural element), the damping has a decrease of 7% from the structural element configuration to the beam configuration in the structure.

The results of the study carried out on the damping of the mono-dimensional elements and of the GFRP structures are particularly interesting when compared with the values recorded in the

following table defined by Chopra (1995) and Newmark and Hall (1982) which refers to traditional materials, Table 5.38.

Table 5.38. Damping ξ values

| Structure typologies and boundary conditions | ξ |
|---|-------------|
| <i>Structures with elements below of 50% than elastic limit</i> | |
| RC Structures with first cracks RC Prestressed Structures Welded steel structures | 2-3% |
| RC Structures cracked | 3-5% |
| Bolted or nailed steel structures Bolted or nailed wood structures | 5-7% |
| <i>Structures with elements near to elastic limit</i> | |
| RC Prestressed Structures without pretension loss Welded steel structures | 5-7% |
| RC Prestressed Structures RC Structures | 7-10% |
| Bolted or nailed steel structures Bolted wood structures | 10-15% |
| Nailed wood structures | 15-20% |
| <i>Masonry structures</i> | |
| Normal masonry structures | 3% |
| Reinforced masonry structures | 7% |
| GFRP structures | |
| Bolted GFRP structures | 1.7% |
| Bonded GFRP structures | - |
| Bolted and bonded GFRP structures | - |

The comparison between all the analysed configurations allows to interpret the obtained experimental results of the modal analysis (Table 5.39) in order to identify the solution with the best dynamic performances. With reference to “H” shape profile the geometry of the structure 3D always allows to have similar parameters of the dynamic response with respect to the configuration simply supported without undergoing important decrement of the fundamental frequency, see Table 5.39..

Table 5.39. Comparison between the experimental results of mono-dimensional elements and structures GFRP, first mode of vibration

| Elements, structural system and boundary conditions | Configuration | Hz | Time (s) | ω (rad/sec) | |
|---|---------------|------------|----------|--------------------|-------|
| Mono-dimensional element, supported configuration | “I” | J_{\max} | 24.41 | 0.04 | 157 |
| | “Q” | / | 35.09 | 0.028 | 224.3 |
| | “H” | J_{\max} | 16.47 | 0.06 | 104.6 |
| | “P” | J_{\max} | 11.9 | 0.08 | 78.5 |
| 2D framework | J_{\max} | 7.12 | 0.14 | 44.86 | |
| 3D structure | x | 20.34 | 0.05 | 125.6 | |
| | y | 9.36 | 0.1 | 62.8 | |

References

Abbaker, A., Mottram, J.T., *The influence of shear-flexibility on the elastic critical load for frames of pultruded fiber reinforced plastic section*, in Proc. 2nd Inter. Conf. Advanced Polymer Composites for Structural Applications in Construction -ACIC 2004, Woodhead Publishing Ltd., Cambridge, 2004.

Bachmann, H., Pretlove, A.J., Rainer, H., *Dynamic forces from rhythmical human body motions*. Vibration Problems in Structures: Practical Guidelines, Birkhäuser, Basel, Appendix G, 1995.

Ballio, G., Mazzolani, F.M., *Strutture in acciaio*, Hoepli, Milan, 1987.

Bank, L. C., Kao, C.-H., *Dynamic Response of Thin-Walled Composite Material Timoshenko Beams*. Journal Energy Resources Technology. 112(2), 149-154, 1990.

Bastianini, F., Boscato, G., Russo, S., and Sciarretta, F., *Natural frequencises of pultruded profiles with different cross-sections*, in Proc. 3rd Inter. Conf. Advanced Composites in Construction - ACIC 2007, York Publishing Serives, York, 2007.

Boscato G., Russo S., *Lo smorzamento nel comportamento dinamico degli elementi strutturali in composito fibrorinforzato*, Atti del Workshop Materiali ed Approcci Innovativi per il Progetto in Zona Sismica e la Mitigazione della Vulnerabilità delle Strutture, Università di Salerno, Salerno, Italy, 2007.

British Standards Institution (BSI). (1978). “British Standard Specification for loads; Steel, Concrete and Composite Bridges, Part. 2.” BS 5400, London, 1978.

CEB 209 (1991), *Vibration Problems in Structures*, Practical Guidelines. CEB, Bull. d' Information n. 209, Lausanne, 1991.

Chopra, A.K., *Dynamics of Structures-theory and applications to earthquake engineering*, Prentice-Hall, Englewood Cliffs, New Jersey, 1995.

CNR-DT 205/2007 (2008). *Istruzioni per la Progettazione, l'Esecuzione ed il Controllo di Strutture realizzate con Profili Sottili Pultrusi di Materiale Composito Fibrorinforzato (FRP)*, Roma CNR. CNR-DT 205/2007.

Dallard, P., Fitzpatrick, T., Flint, A., Low, A., Smith, R.R., Willford, M., Roche, M., (2001). "London millennium bridge: Pedestrian-induced lateral vibration." *J. Bridge Eng., ASCE*, 6(6), 412-417, 2001.

Dicuonzo, A., Laudiero, F., Minghini, F., Tullini, N., *Design and construction of a temporary structure composed by FRP pultruded profiles*, Fourth Int. Conference on FRP Composite in Civil Engineering (CICE 2008), 22-24 July, Zurich, Switzerland, 2008.

Eurocodice 3, Part 1.1, CEN (1997), *Joints in Building Frames (Annex J)*, Approved Draft, January, CEN/TC250/SC3-PT9, Comité Européen de Normalisation, 1997.

Eurocodice 8, (2003), *Design of Structures for Earthquake Resistance – part 1: General Rules, Seismic Action and Rules for Buildings*, Draft n°6, January 2003.

Structural Design of Polymer Composites -EUROCOMP Design Code and Handbook, Edited by John L. Clarke, E. & F. N. Spon, London, 1996.

Faella, C., Rizzano, G., Piluso, V. *Structural steel semirigid connections : theory, design and software* / C. Faella, V. Piluso, G. Rizzano. - Boca Raton (Florida) : CRC, c2000).

Gibson, R.F., Plunkett, R., *Dynamic Mechanical Behaviour of Fiber-Reinforced Composites: Measurement and Analysis*, Journal of Composite Materials, Vol.10, October 1976.

Gibson, R.F., *Modal vibration response measurements for characterization of composite materials and structures*, Composites Science and Technology, Elsevier, 2000.

Hashin, Z., Rosen, B. W., *The Elastic Moduli of Fiber-Reinforced Materials*, J. of Applied Mechanics, Vol. 32, 1965.

Holloway, L., *Adhesive and bolted joints, Polymer and Polymer Composites in Construction*, Ed. Holloway, T. Telford, London, 1990.

Huang, T. C., *The Effect of Rotatory Inertia and Shear Deformation on the Frequency and Normal Mode Equations of Uniform Beams With Simple End Conditions*. ASME Journal of Applied Mechanics, Vol. 28, 579-584, 1961

International Standardization Organization (ISO). (2005). "Bases for design of structure Serviceability of building and pedestrian walkways against vibration." ISO/CD 10137, Geneva, 2005.

Lesieutre, G. A., *Modelling Frequency-Dependent Longitudinal Dynamic Behavior of Linear Viscoelastic Long Fiber Composites*, Journal of Composite Materials, Vol. 28, 1994.

Librescu, L., and Song, O., *Thin-Walled Composite Beams Theory and Application*, Published by Springer, Netherlands, 2006.

Mosallam, A.S., Bank, L.C., *Short-term behavior of pultruded fiber reinforced plastic frame*, Journal of Structural Engineering, ASCE, Volume 118, N.7, Luglio, 1992.

Mosallam, A.S., *Design Consideration for Pultruded Composite Beam-to-Column Connections Subjected to Cyclic and Sustained Loading Conditions*, ACMA, Arlington, VA, 1997.

Mottram, J.T. and Zheng, Y., *Further tests on beam-to-column connections for pultruded frames: Web-cleated*, J. Composites for Construction, 3 1, 1999.

Mottram, J.T. and Zheng, Y., *Further tests on beam-to-column connections for pultruded frames: Flange-cleated*, J. Composites for Construction, 3 3, 1999.

Mottram, J. T., *Stability analysis of plane frames of fiber reinforced polymer having semi-rigid joints and shear-flexible members*, in Proc. 3rd Inter. Conf. Advanced Composites in Construction - ACIC 2007, York Publishing Services, York, 2007.

Mottram J.T., *Stability analysis for pitched portal frames of fiber reinforced polymer*, in Proc. 4th Inter. Conf. on FRP Composites in Civil Engineering (CICE2008), Empa, Duebendorf, 2008, Paper 6.D.1. ISBN 978-3-905594-50-8.

Newmark, N.M., Hall, W.J., *Earthquake spectra and design*, Earthquake Engineering Research Institute, Berkeley, California, 1982.

Nori, C.V., McCarty, T.A., Mantena, P.R., *Experimental and Finite Element Analysis of Pultruded Glass-Graphite/Epoxy Hybrids in Axial and Flexural Modes of Vibration*, Journal of Composite Materials, Vol.30, 1996.

Nori, C.V., McCarty, T.A., Mantena, P.R., *Vibration analysis and finite-element modeling for determining shear modulus of pultruded hybrid composites*, Composites Part B-Engineering, Elsevier, 1996.

Nowinski, J. L., *On the Transverse wave Propagation in Orthotropic Timoshenko Bars*. International Journal of Mechanical Science, Vol. 11, 689-693, 1996.

Ordinanza 3274 P.C.M. (2003): Primi elementi in materia di criteri generali per la classificazione sismica del territorio nazionale e di normative tecniche per le costruzioni in zona sismica, 20 marzo 2003.

Oppe, M., Trumpf, H., Feldmann, M. and Sedlacek, G., *Improvement of detachable connections in glass-fiber reinforced polymers*, in Proc. 3rd Inter. Conf. Advanced Composites in Construction - ACIC 2007, York Publishing Services, York, 2007.

Qiao, P., Zou, G., *Analytical and Experimental Study of Vibration Behaviour of FRP Composite I-Beams*, 15th ASCE Engineering Mechanics Conference, Columbia University, New York, June 2-5 2002.

Russo, S., *Strutture in composito – Sperimentazione, teoria e applicazioni*, Ulrico Hoepli Editore S.p.A., Milan, 2007. (In Italian) ISBN 978-88-203-3643-1.

Schultz, A.B., Tsai, S.W., *Dynamic Moduli and Damping Ratios in Fiber-Reinforced Composites*, Journal of Composite Materials, Vol.2, No. 3, July 1968.

Shao, Y., *Characterization of a Pultruded FRP Sheet Pile for Waterfront Retaining Structure*, Journal of Materials in Civil Engineering, Vol.18, No. 5, 2006.

Smith, S.J., Parson, D., Hjelmstad, K.D., *Experimental Comparison of Connections for GFRP Pultruded Frame*, Journal of Composites for Construction, February 1999.

Sun, C. T., Lu, Y. P., *Vibration Damping of Structural Elements*, Prentice Hall PTR, New Jersey, 1995.

Timoshenko, S. P., *On the correction for shear of the differential equation for transverse vibrations of prismatic bars*. Philosophical Magazine, Ser. 6, 41(245), 744-746, 1921.

Timoshenko, S. P., *Théorie des Vibrations*. Paris et Liège, Librairie Polytechnique Ch. Béranger, chapitre IV, Vibrations des corps élastiques, 346-357, 1954.

Turvey, G. J., Cooper, C., *Review of tests on bolted joint between pultruded GRP profiles*, Proceeding of the Institution of Civil Engineers, Structure & Buildings 157, pp. 211-233, June 2004.

Turvey, G.J., Mulcahy, N., Widden, M.B., *Experimental and Computed Natural Frequencies of Square Pultruded GRP Plates: Effects of Anisotropy, Hole Size Ratio and Edge Support Conditions*, Composite Structures, Elsevier, 2000.

Turvey, G.J., Mulcahy, N., *Free Vibration of Clamped Pultruded GRP Circular Plates with Central Circular Cut-Outs*, Fourth International Conference on Thin-Walled Structures, 2004.

Zheng, Y. and Mottram, J.T., *Analysis of pultruded frames with semi-rigid connections*, in Proc. 2nd Inter. Conf. on Advanced Composite Materials in Bridges and Structures (ACMBS/2), The Canadian Society for Civil Engineers (CSCE), 1996.

6. FINAL CONSIDERATIONS

The present research has developed some of the principal themes associated to the structural static and dynamic behaviour of GFRP elements with the aim to define the fields of possible applications with particular reference to the conservation and reinforcement of existing structures.

If, on the one hand, lightness, deformability and strength properties of the composite fiber reinforced qualify the material by defining the possibility of producing specific structural typologies, on the other hand the contained mass in play constitutes a limit for the building of multi-floor frameworks in that it reduces performance induced by the stability ensured by its dead load and therefore the possibility of carrying high overloads.

Nevertheless, the structural interaction of GFRP framework systems with structures built by materials of a high stiffness – as, for example, in the field of historical building conservation – guarantees not only a reduction of buckling phenomena of the GFRP structural elements, but also a global improvement in structural performance of the new system (existing structure-GFRP structure) with respect to static and dynamic action with a low increment of the mass participation. The same approach with equally good results can be adopted for the use of GFRP mono-dimensional elements for deck, pre-existing or built *ex novo*, positioned even at the highest levels in order to increase the flexural and transversal stiffness. This application allows the increment of bearing capacity and to divide the shear action on seismic-resistant vertical structures of the existing buildings.

The connection between the structural elements influences the static and dynamic response of a GFRP framework structure and/or the composed system (existing structure-GFRP structure). The flow of external forces must respect the hierarchy of the bearing elements of the system following the static-structural functions of the single elements, according to which they have been opportunely designed. In reference to dynamic analysis, the simulations carried out on the structural response of the 2D and 3D framework, upon variation of the stiffness of the frame and the rotational stiffness of the restrains, highlight the importance of restrains and of the appropriate values of bearing capacity of light composite structures.

For the more slender frameworks, it is important to build the internal restrains with an high rotational stiffness compared to the actions exercised by the presence of braces; for the stiff frameworks characterised by an high hyper-static state, the dynamic response is influenced above all by the type of external restraint.

Besides the various rigid joint configurations obtainable with irreversible bonding techniques or via pre-moulded joint, it is possible to calibrate the different level of stiffness between the elements via controlled rotational force applied to bolts.

Currently, only the joints built with steel parts seem to guarantee an energy dissipation without brittle failure induced by shear action or by stress orthogonal to the fibres.

The characterising aspects of performances of GFRP structures are:

- the importance of external restraint conditions for frameworks with an high structural stiffness;
- The response of the systems generally more deformable is substantially governed by the rotational capacity of the internal joint and by the action of the braces;
- The design of fixed joints, in order to reduce lateral displacement, must be opportunely supported by adequate dimensioning of the column so that it guarantees an high stiffness. To this end, the joints can be produced in continuity via the creation of geometric joint produced via forming techniques;
- It is opportune to pursue an attentive optimisation of not only of the global geometry of the system but also of the single cross sections of structural elements in play. The GFRP structures – without an evaluation on non-linear behaviour, ductility and failure mode - seem usable in seismic zone and comparable to structural behaviour of wood structures (OPCM 3274);
- The use of pultruded profile in the structural rehabilitation and conservation of the architectural and historical heritage seems a lot desirable;
- In restoration field of architectural heritage are highlight any realizations that can be immediately applicable, as for example:
 - increment of flexural stiffness of wood deck;
 - shear stiffening of masonry wall;

- use with lintel structural function over an opening, such as a door or window ;
- reinforcement of wood deck of historical bridge with a contained increment of dead load;
- execution of reversible applications;
- transitory use of all profiles for complex applications of structural rehabilitation.

The research on the dynamic response is the first step of a much wider study which considers a more complete analysis of a case-study of GFRP systems which vary in the geometry of structures and of the elements, typology-technology of the joints and applied loads.

In conclusion, with respect to previous considerations, the main areas of development for future research regard the micro-mechanics of the material and the macro-mechanics of the all-FRP system. Therefore, the discussion points are (1) the configuration of the element and the structural system, (2) connections and (3) ductility.

For the first discussion point, the principal characteristic of the FRP structural elements, such as reduced dead load, determines the structural configuration and the boundary conditions of the system via the control and design of mass (profiles, frameworks) and form (shell, arch) resistive structures. With regards to the second discussion point, the problem of the connection between GFRP elements must be differently solved by the adopted solutions until now; the bolted joint is at present designed and built with a large over-sizing of the components. The innovative and more adequate bonded connection allows an increment of the joint stiffness, a uniform transfer of the load and the absence of local damage for the execution of the holes; but between the negative aspects it is necessary to specify that, besides the joint irreversibility, the bond connections is sensitive to the eccentric loads, the execution quality cannot be checked and the collapse is brittle. The solution which can actually solve the problems of the connection between the GFRP pultruded elements is the design of a joint in continuity built by the moulded technology.

Finally, the absence of a ductile behaviour of the GFRP material constitutes a limit which can be partially resolved by modifying the composition of the constituent materials or via a superfluous design of the structural configuration and/or sectional of the element which plans a deformation of the joint controlled by successive, calculated collapse mechanisms.

APPENDIX A – Mono-dimensional elements, experimental results

For each GFRP structural element (see chapter 5.2.1) and each boundary condition have been identified the spectra in the frequency domain, modes of vibration, displacement and the damping ratio.

The most significant data of each profile are collected in the Figures from A.1 to A.14; Figures A.1 to A.8 concern the simply supported condition while the Figures A.9 to A.14 refer to the fully clamped configuration.

In each figure, dynamic response corresponding to the excitations (highlighted with B1, B2,... Bn) at L/4 and at L/2 (L=Length of element), is recorded; in each figures are illustrated the first three modes of flexural vibration by excitation at the midpoint and the displacement of fundamental mode. The Table also shows the constraints, geometric characteristics and the position of the accelerometers.

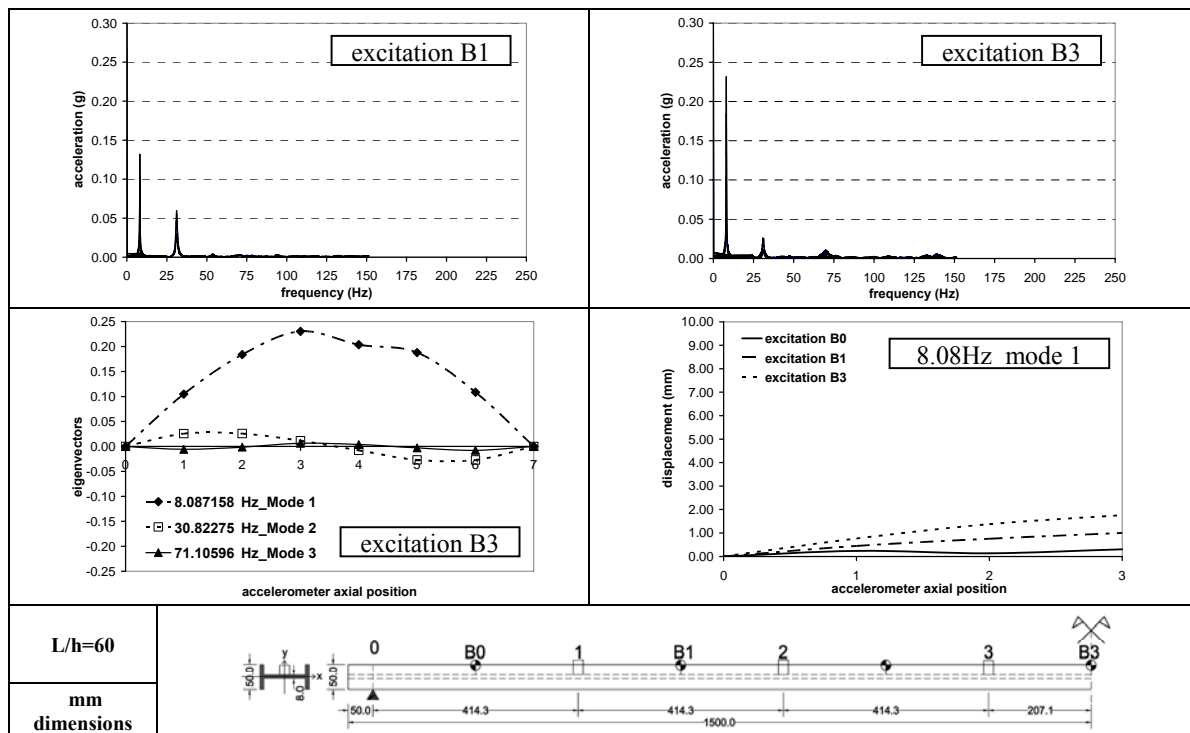


Figure A.1. Spectrum in frequency domain, modal shapes and displacements of “I” profile, J_{min} (simply supported)

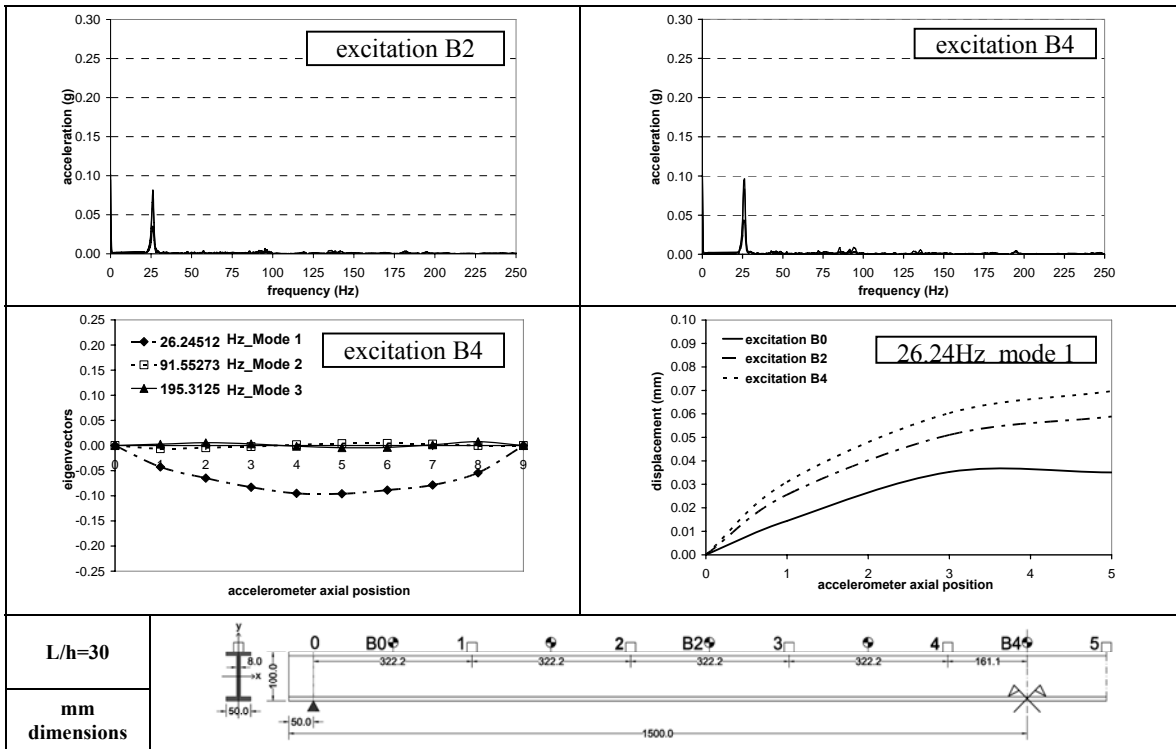


Figure A.2. Spectrum in frequency domain, modal shapes and displacements of "I" profile, J_{max} (simply supported)

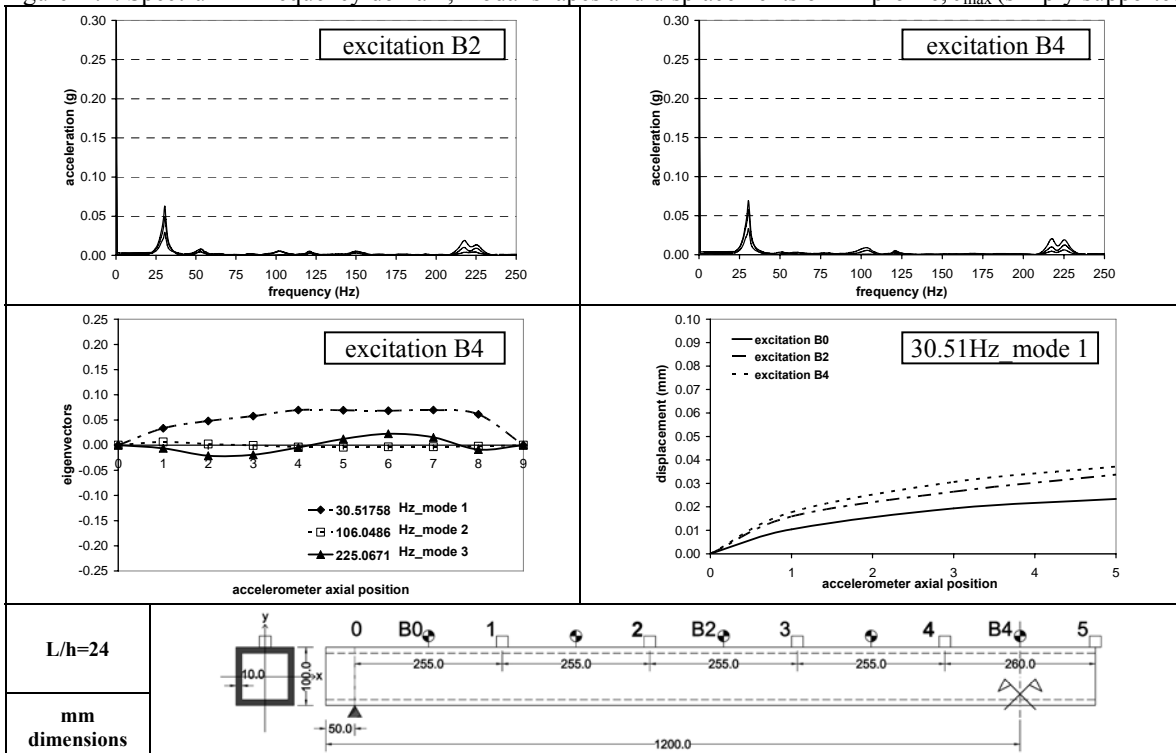


Figure A.3. Spectrum in frequency domain, modal shapes and displacements of "Q" profile, (simply supported)

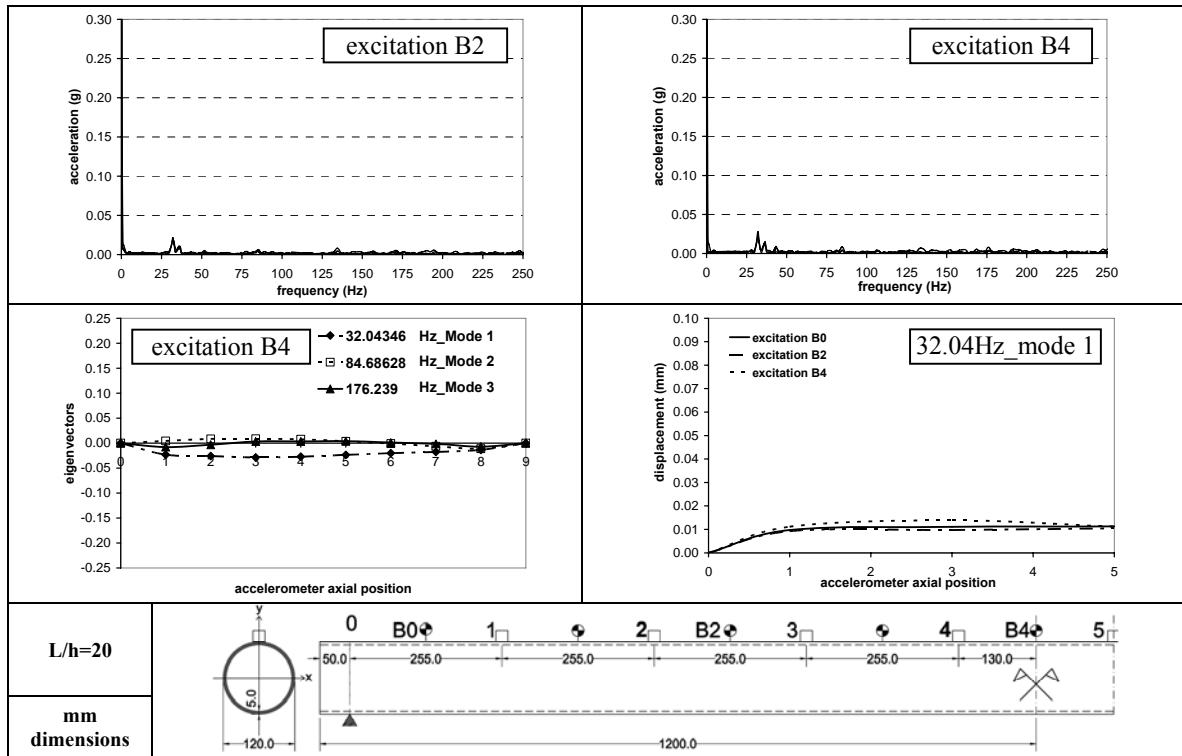


Figure A.4. Spectrum in frequency domain, modal shapes and displacements of “O” profile, (simply supported)

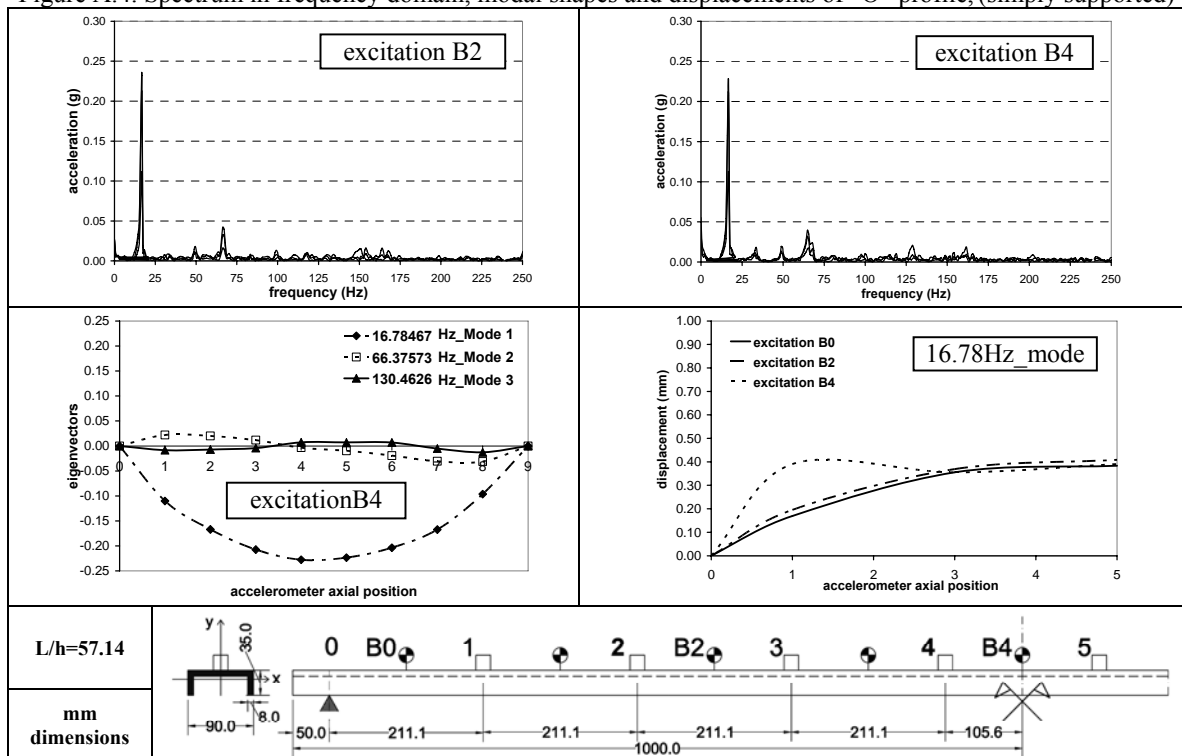


Figure A.5. Spectrum in frequency domain, modal shapes and displacements of “C” profile, J_{min} (simply supported)

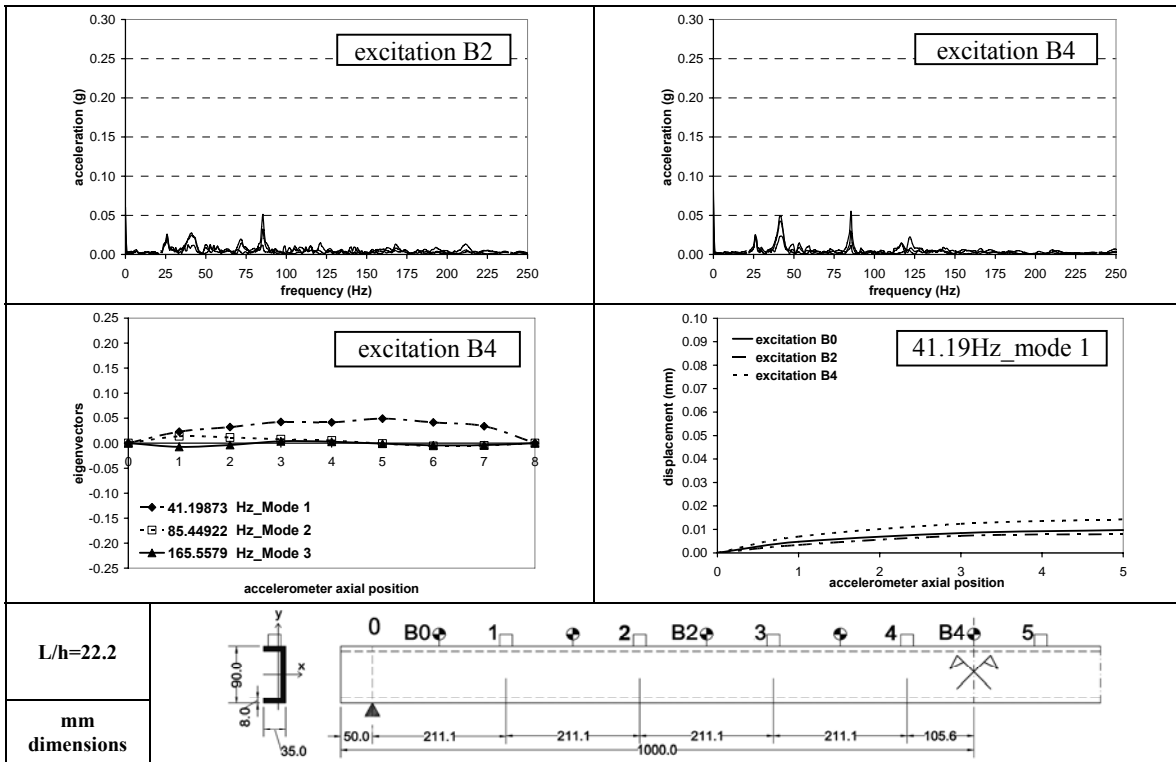


Figure A.6. Spectrum in frequency domain, modal shapes and displacements of “C” profile, J_{max} (simply supported)

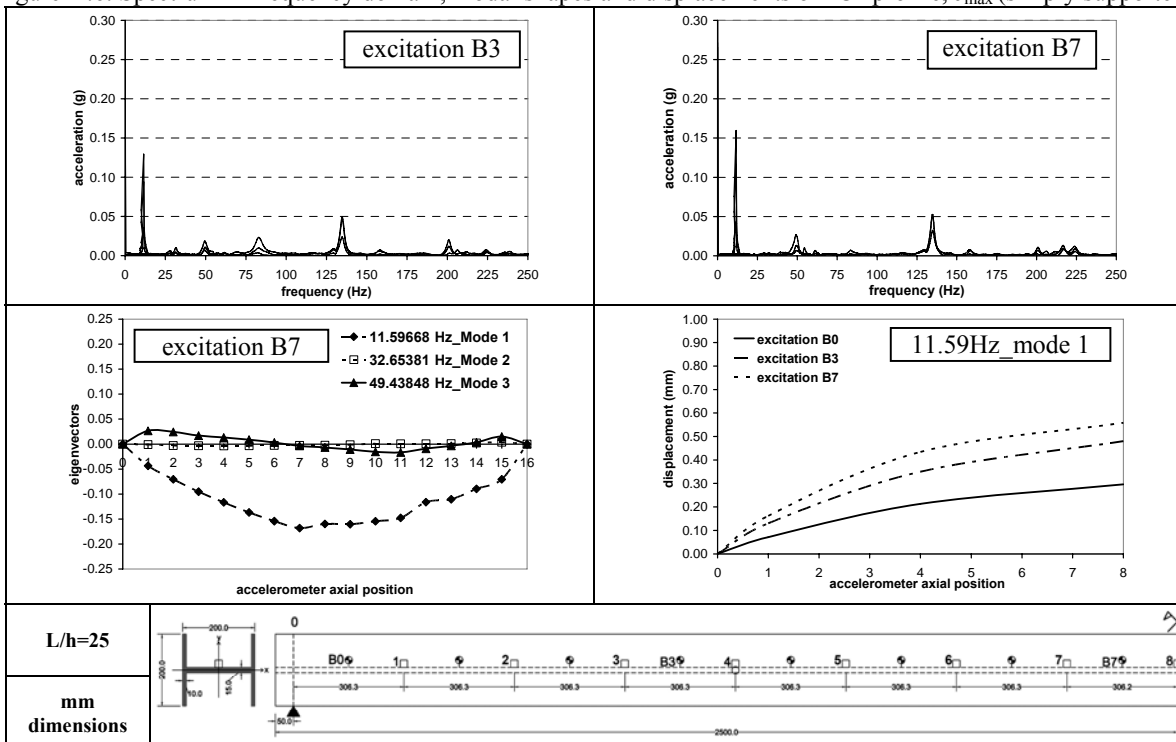


Figure A.7. Spectrum in frequency domain, modal shapes and displacements of “H” profile, J_{min} (simply supported)

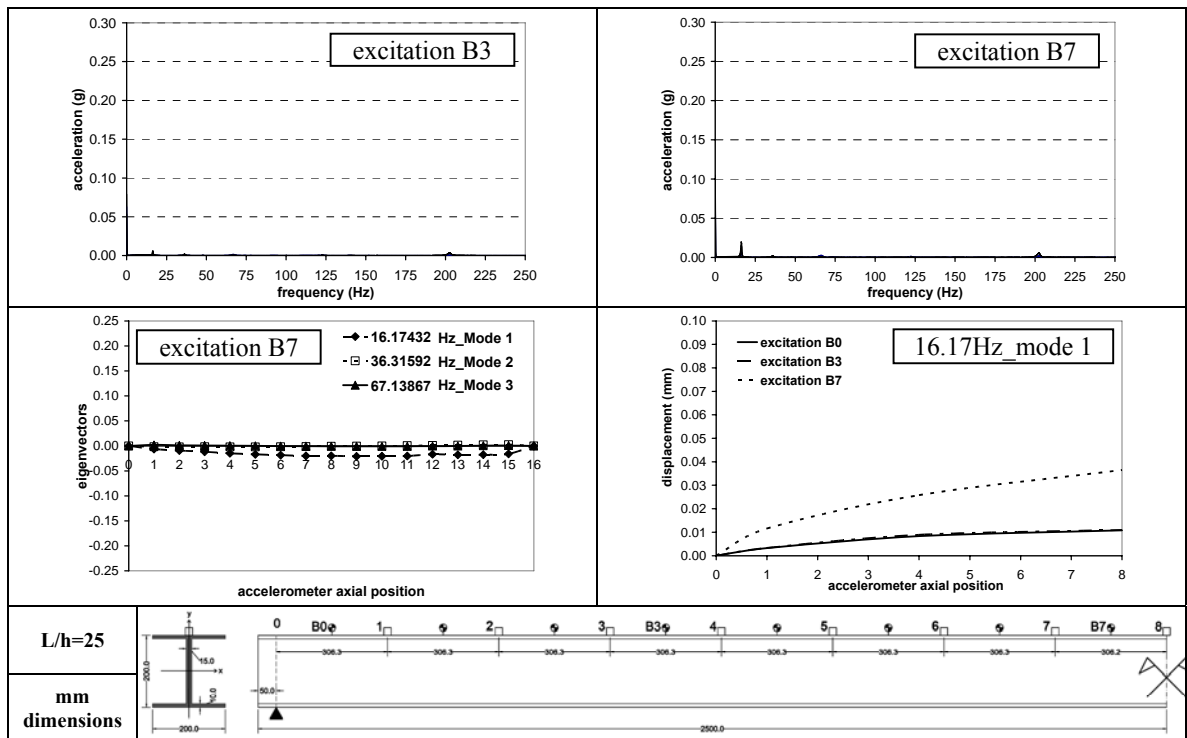


Figure A.8. Spectrum in frequency domain, modal shapes and displacements of “H” profile, J_{max} (simply supported)

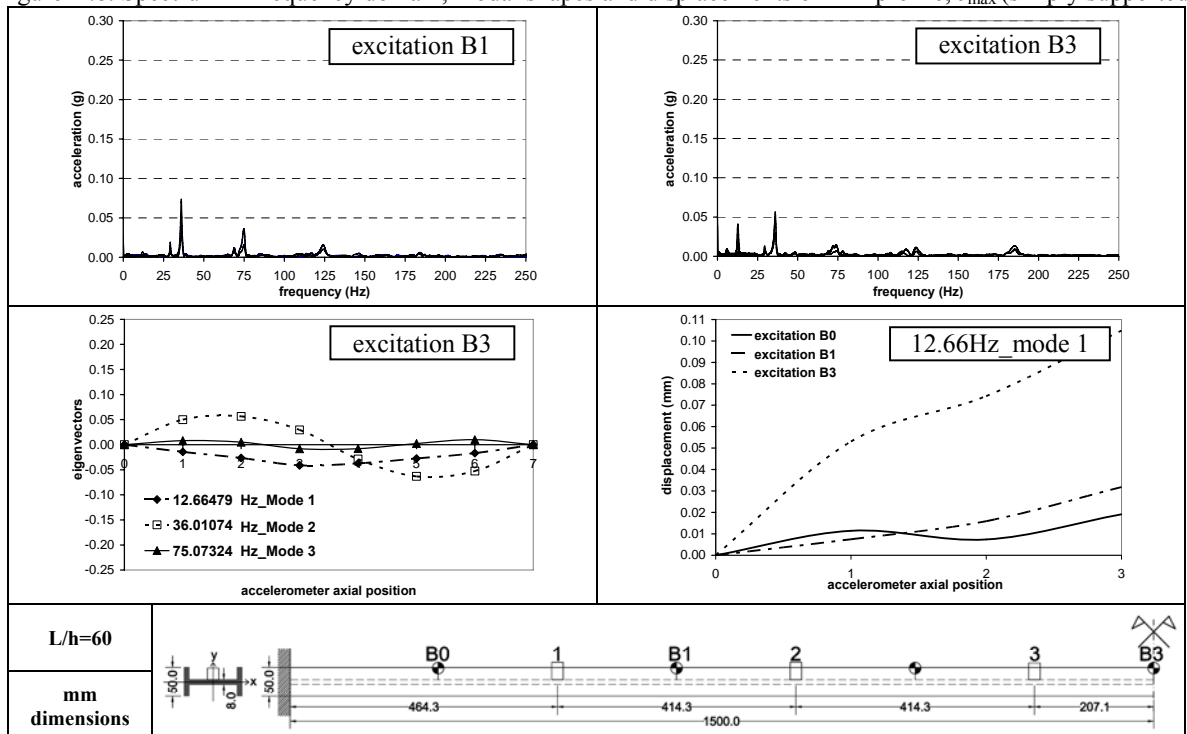


Figure A.9. Spectrum in frequency domain, modal shapes and displacements of “I” profile, J_{min} (clamped)

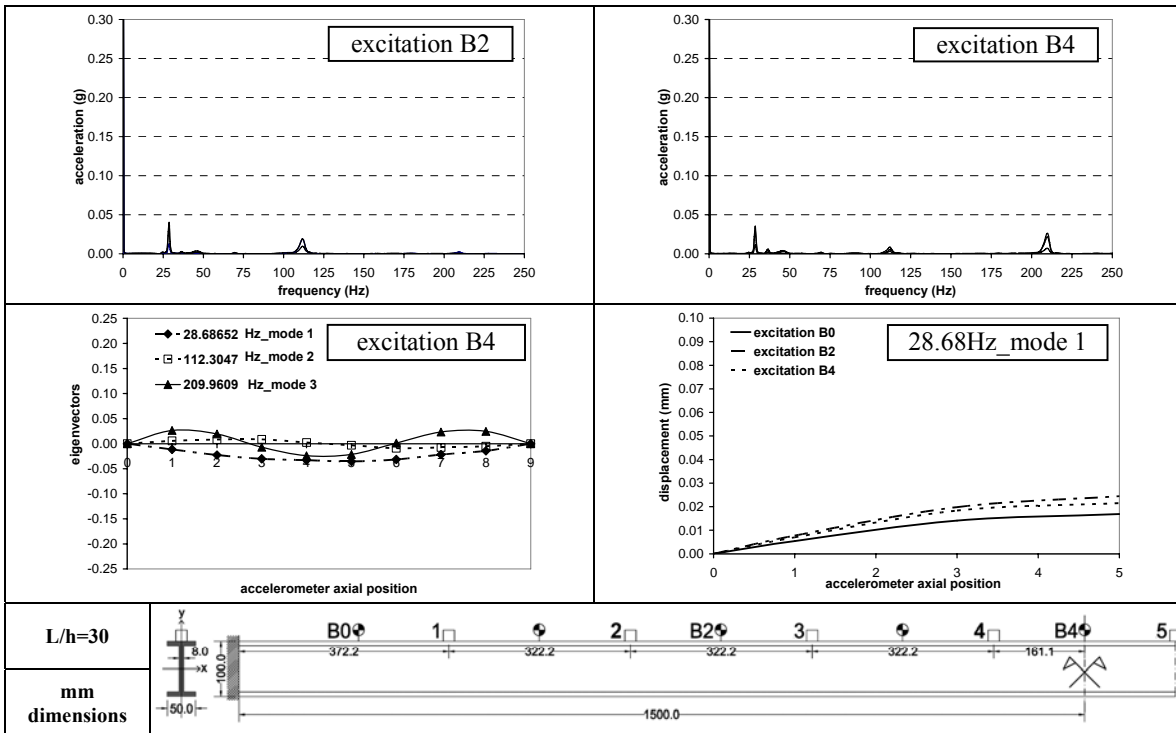


Figure A.10. Spectrum in frequency domain, modal shapes and displacements of "I" profile, J_{max} (clamped)

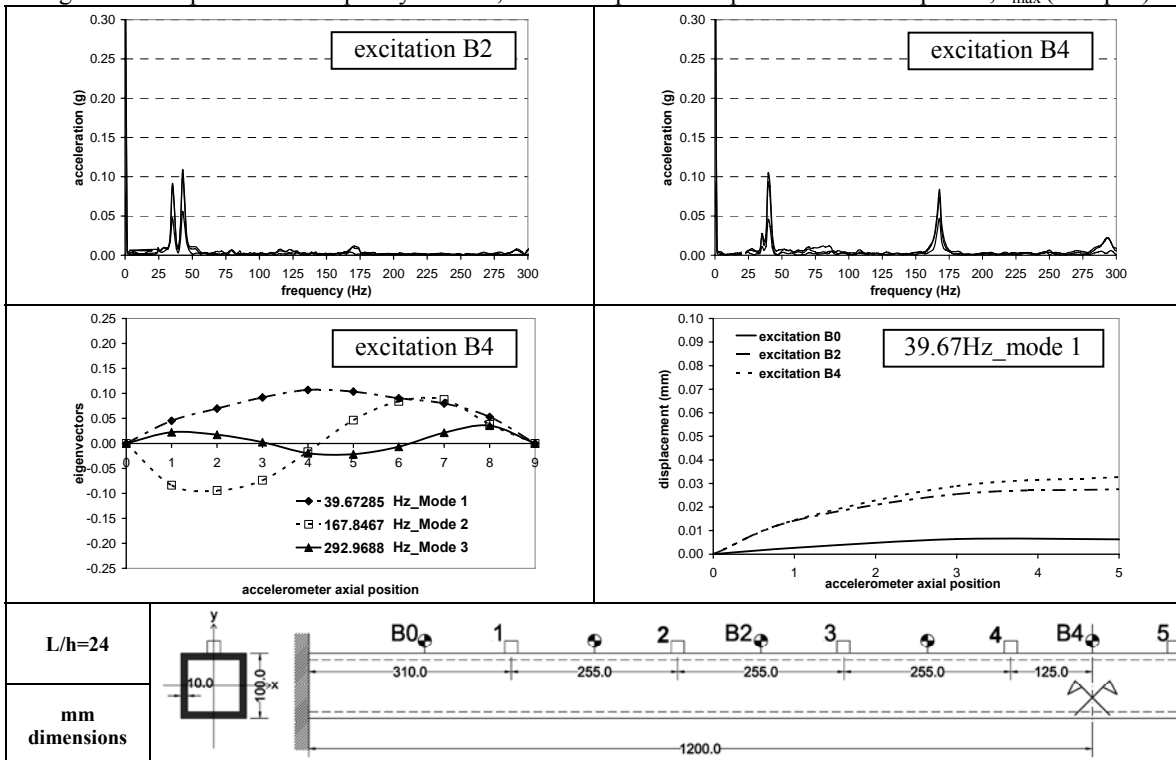


Figure A.11. Spectrum in frequency domain, modal shapes and displacements of "Q" profile, (clamped)

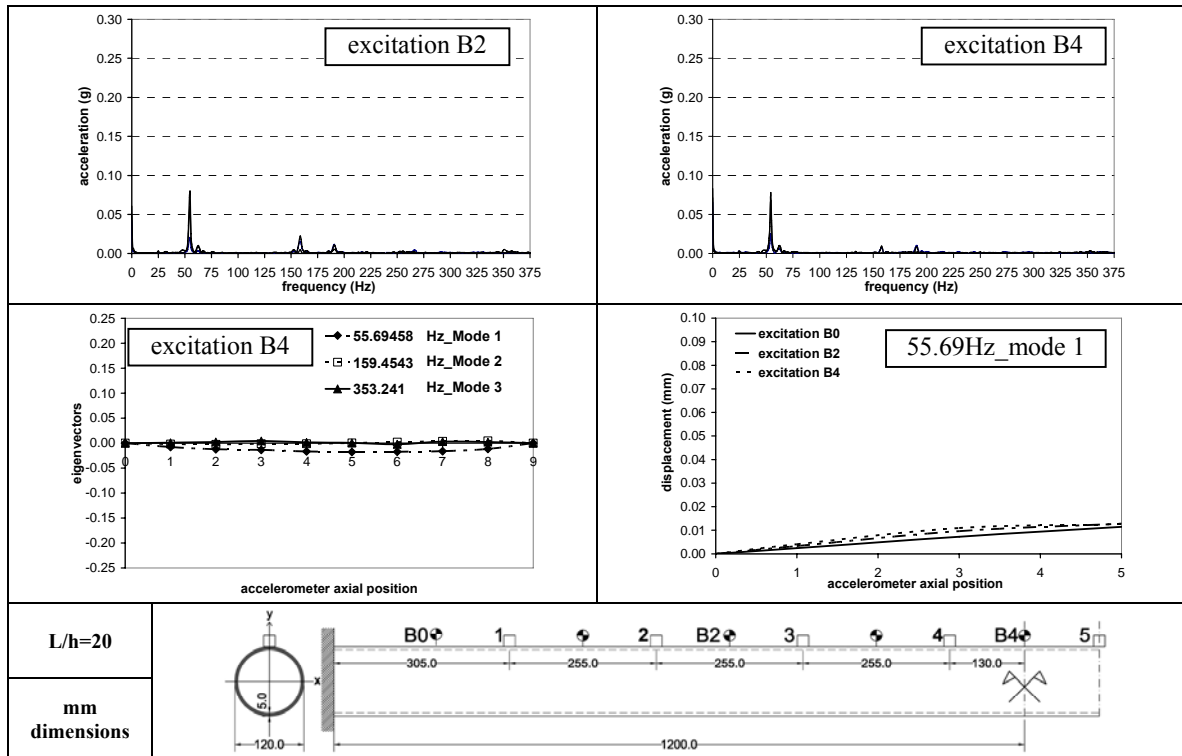


Figure A.12. Spectrum in frequency domain, modal shapes and displacements of "O" profile, (clamped)

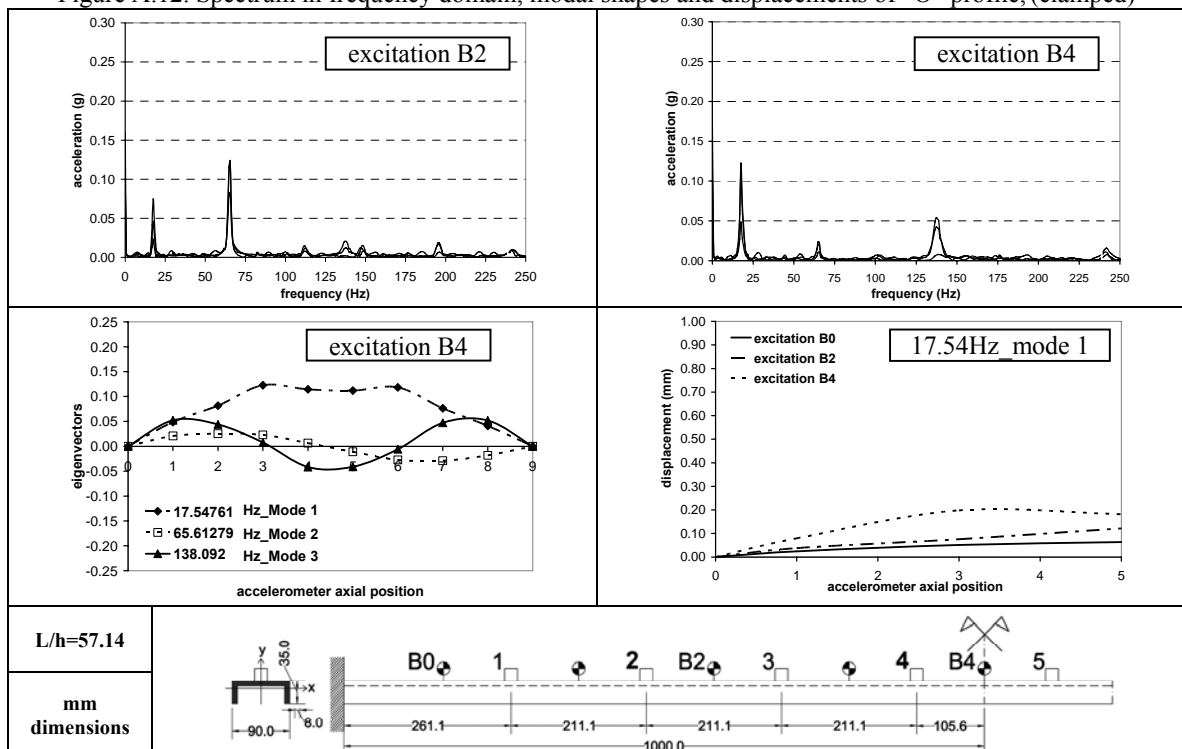


Figure A.13. Spectrum in frequency domain, modal shapes and displacements of "C" profile, J_{min} (clamped)

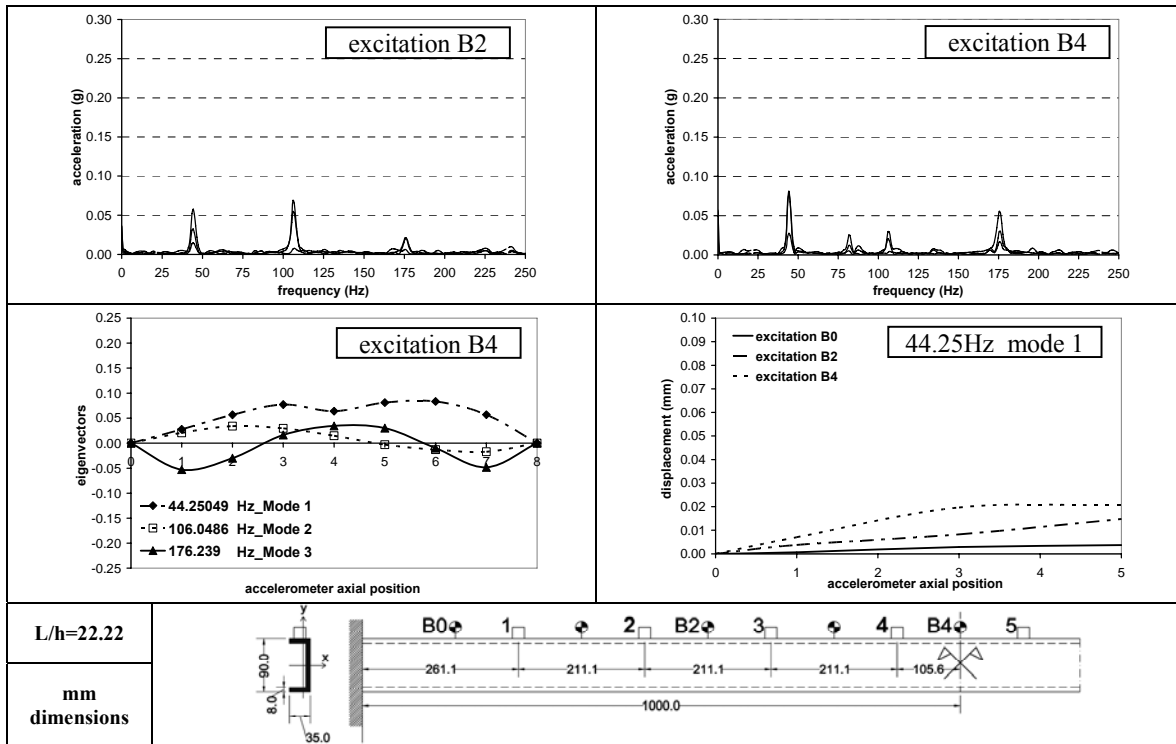
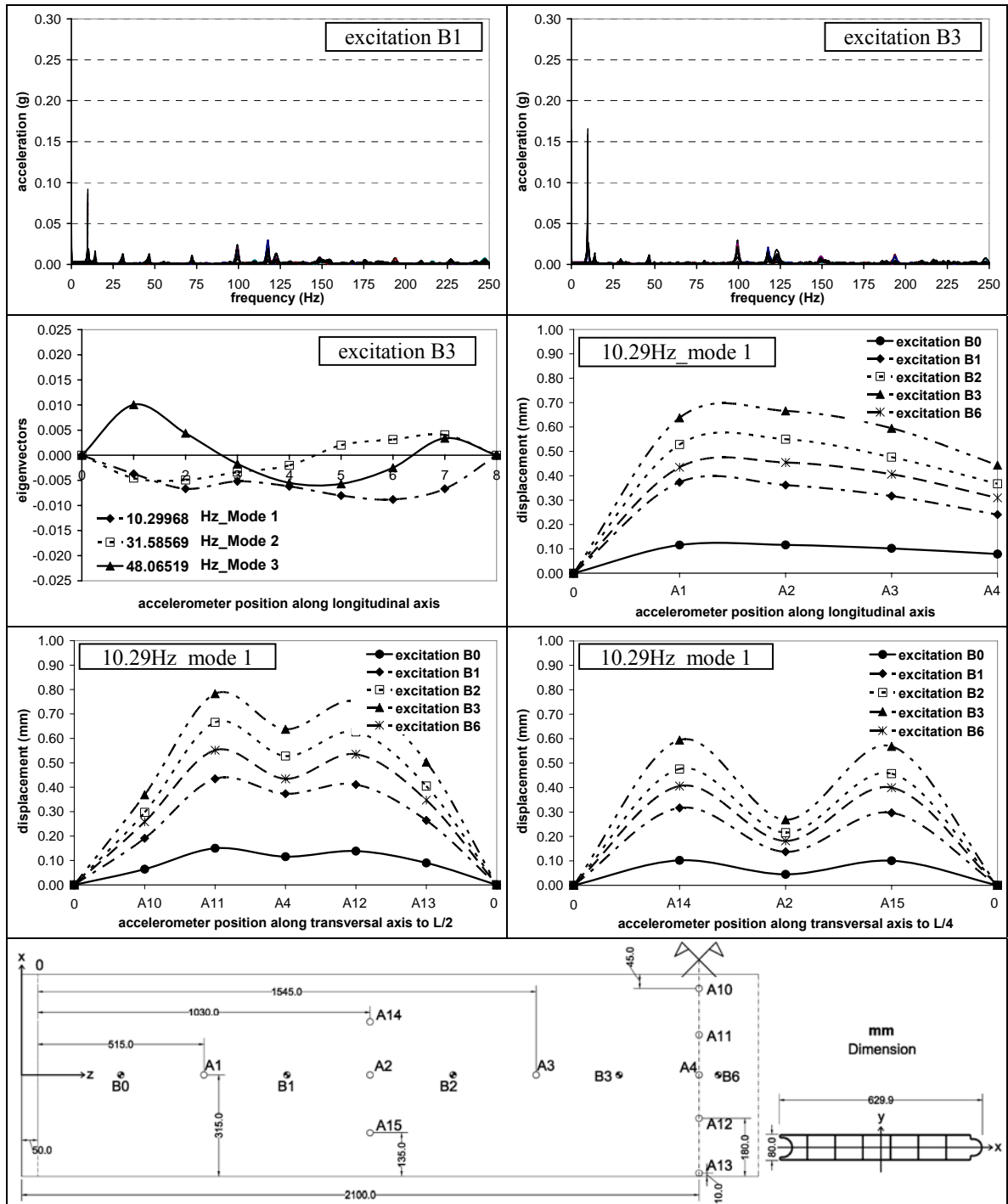


Figure A.14. Spectrum in frequency domain, modal shapes and displacements of “C” profile, J_{max} (clamped)

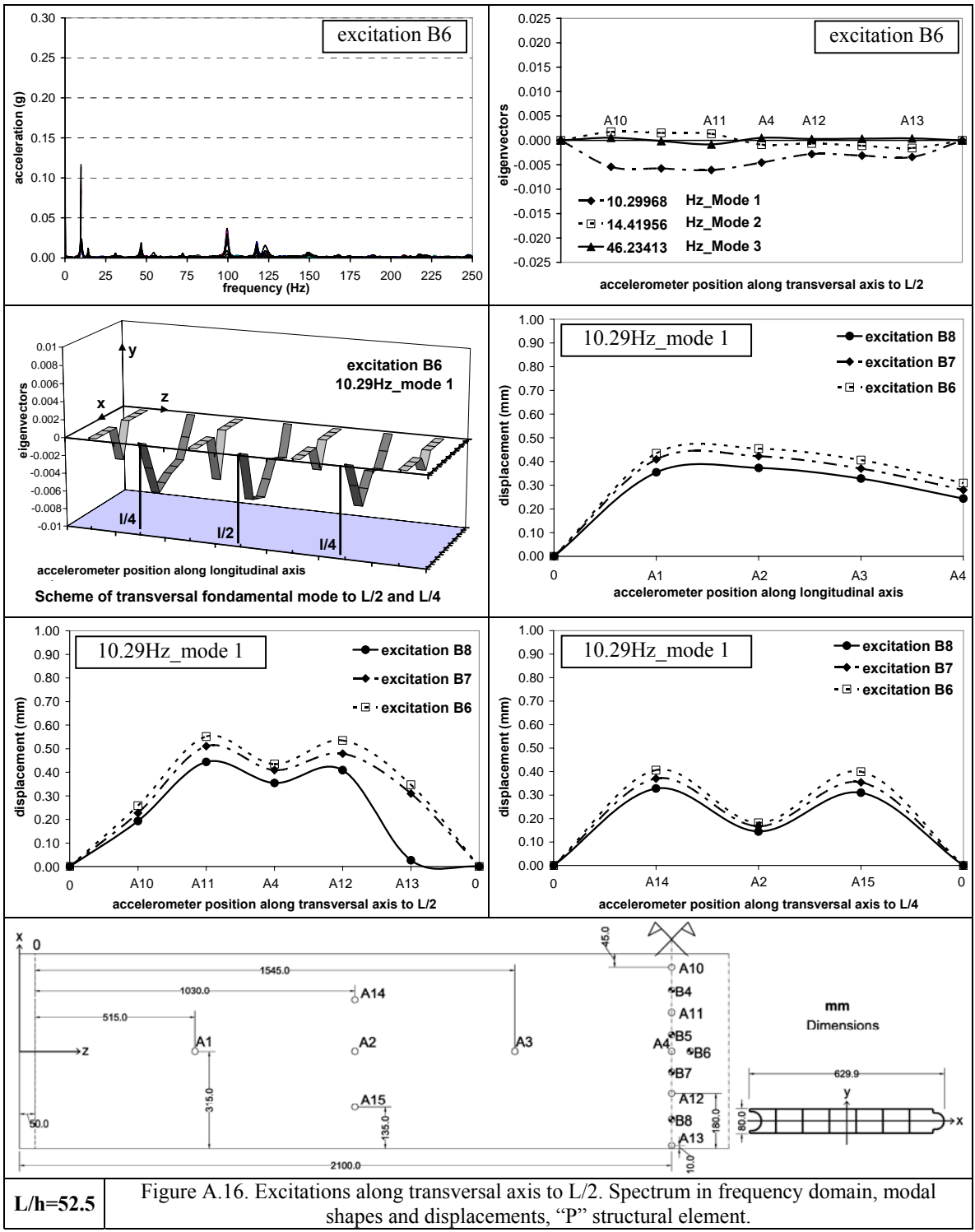
The panel element (Figures from A.15 to A.19) is analysed considering vibration along the vertical plan of the yz axis, thus investigating flexural vibrations, via the spectra of frequency, by the study of eigenvectors and relative displacements.

The twisting displacement induced by asymmetrical excitations have been investigated, along the diagonal of panel (excitations B9, B10, B11 and B12 of Figure A.17) and by the excitations applied simultaneously, at 1/3 and 1/4 of the element’s length, with excitations at B14, B16 (Figure A.18) and B13, B15 (Figure A.19) points. In Figures A.17, A.18 and A.19, the modal shapes are not illustrated as they coincide with the modal shapes of Figures A.15 and A.16.



L/h=52.5

Figure A.15. Excitations along longitudinal axis. Spectrum in frequency domain, modal shapes and displacements, "P" structural element.



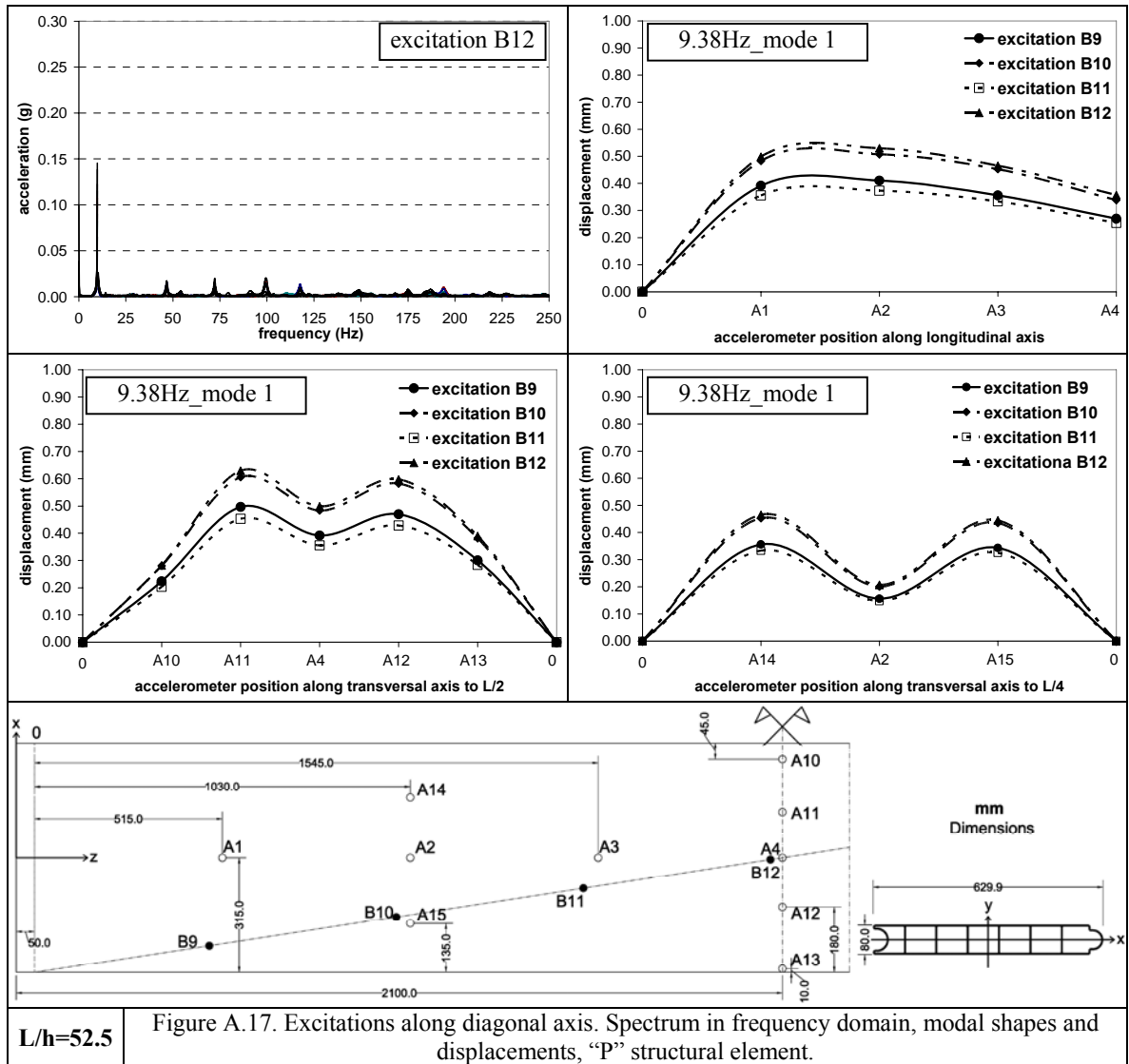


Figure A.17. Excitations along diagonal axis. Spectrum in frequency domain, modal shapes and displacements, "P" structural element.

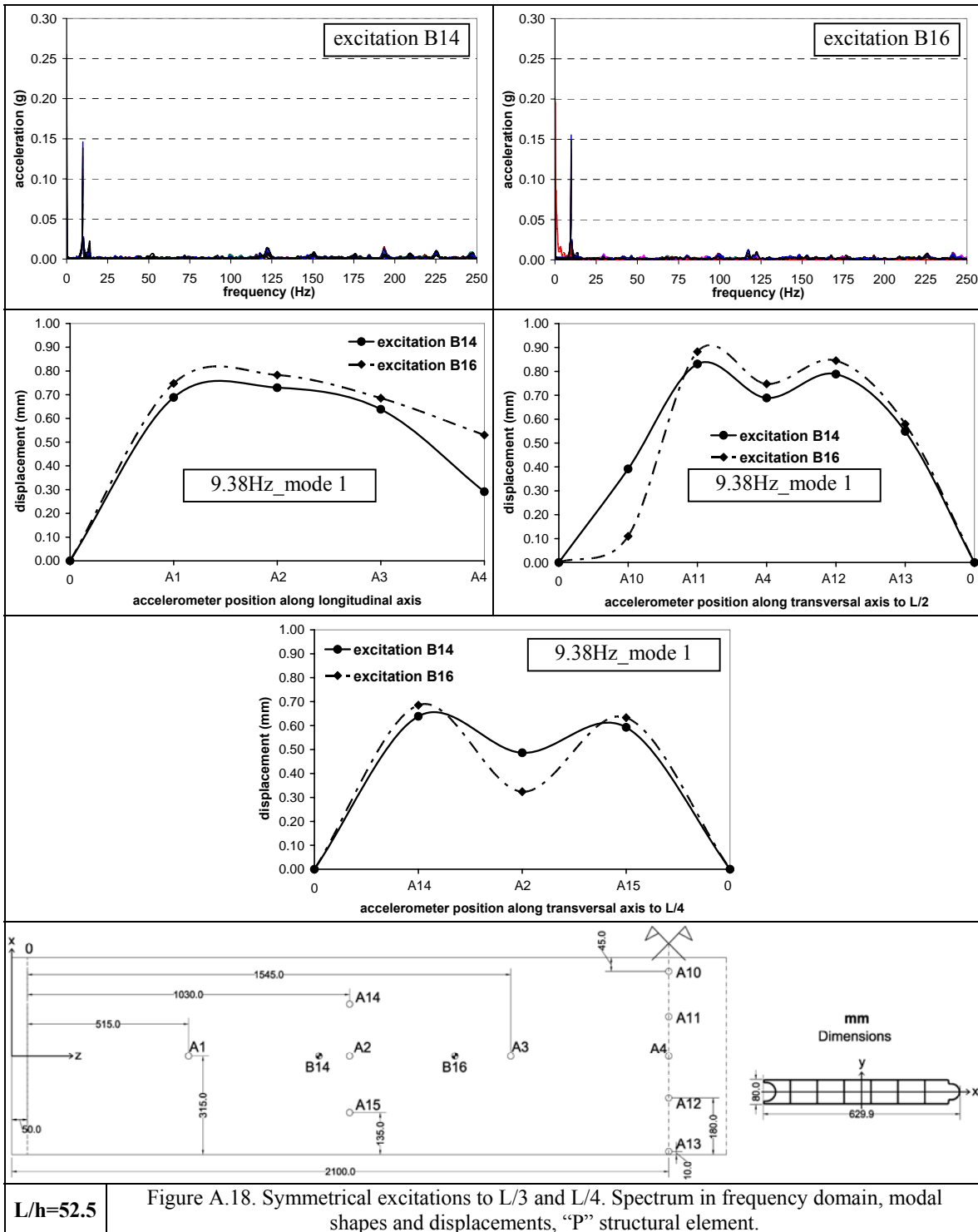


Figure A.18. Symmetrical excitations to L/3 and L/4. Spectrum in frequency domain, modal shapes and displacements, “P” structural element.

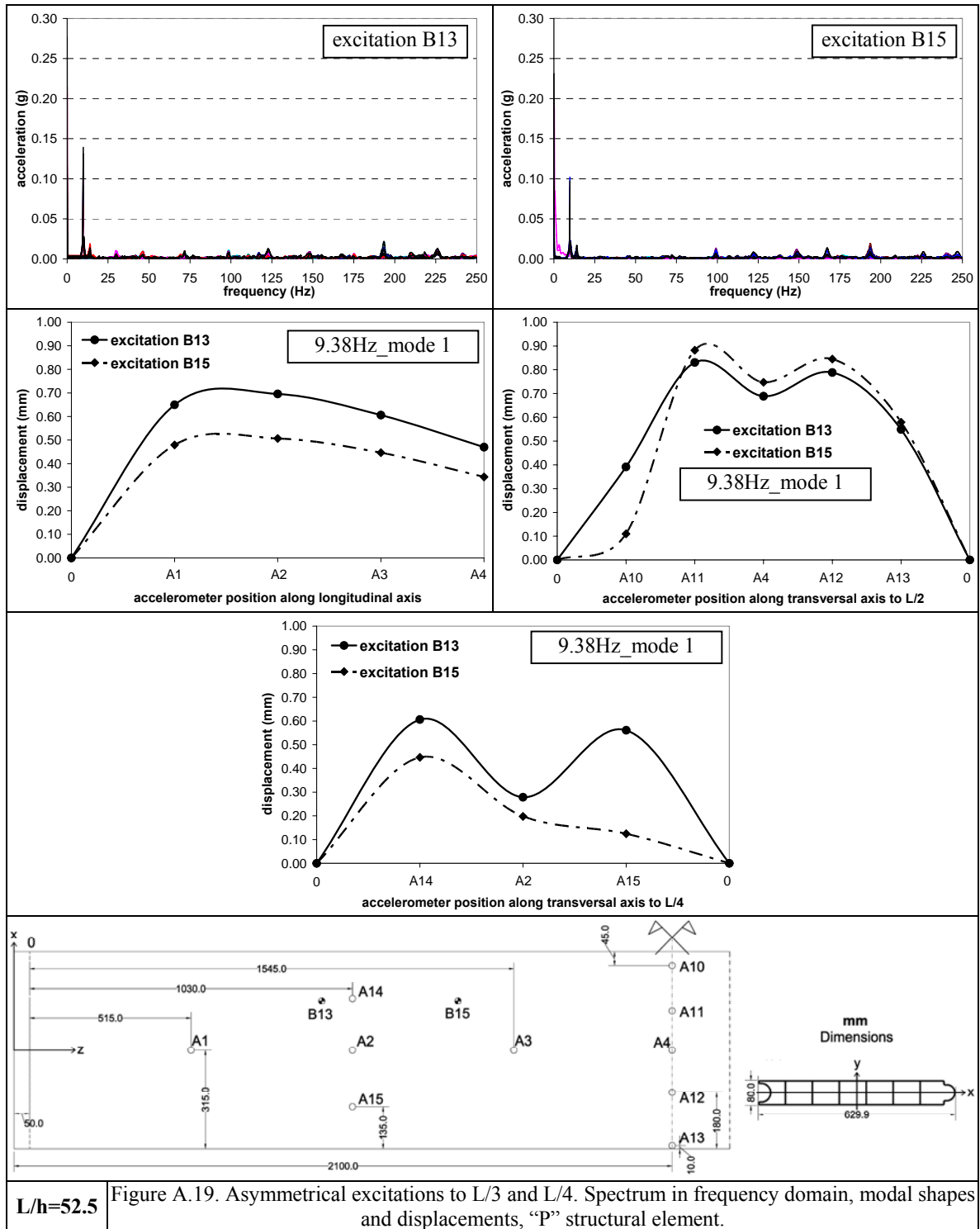


Figure A.19. Asymmetrical excitations to L/3 and L/4. Spectrum in frequency domain, modal shapes and displacements, “P” structural element.

APPENDIX B – Two-dimensional frame, experimental results

Figures from B.1 to B.6 illustrate the dynamic behaviour in free vibrations field of the GFRP two-dimensional framework (see chapter 5.2.2) for every excitation point and accelerometer position. For different configuration, geometry and analysis of elements that constitute the framework have been subdivide the results of vibration in the frequency domain, considering the column (A1, A2, A3 e A4) and beam (A5 e A6). The spectra in time domain have been evaluated separately for every accelerometer. As regards the modal analysis the first three modal shapes of column and the related frequencies have been elaborated.

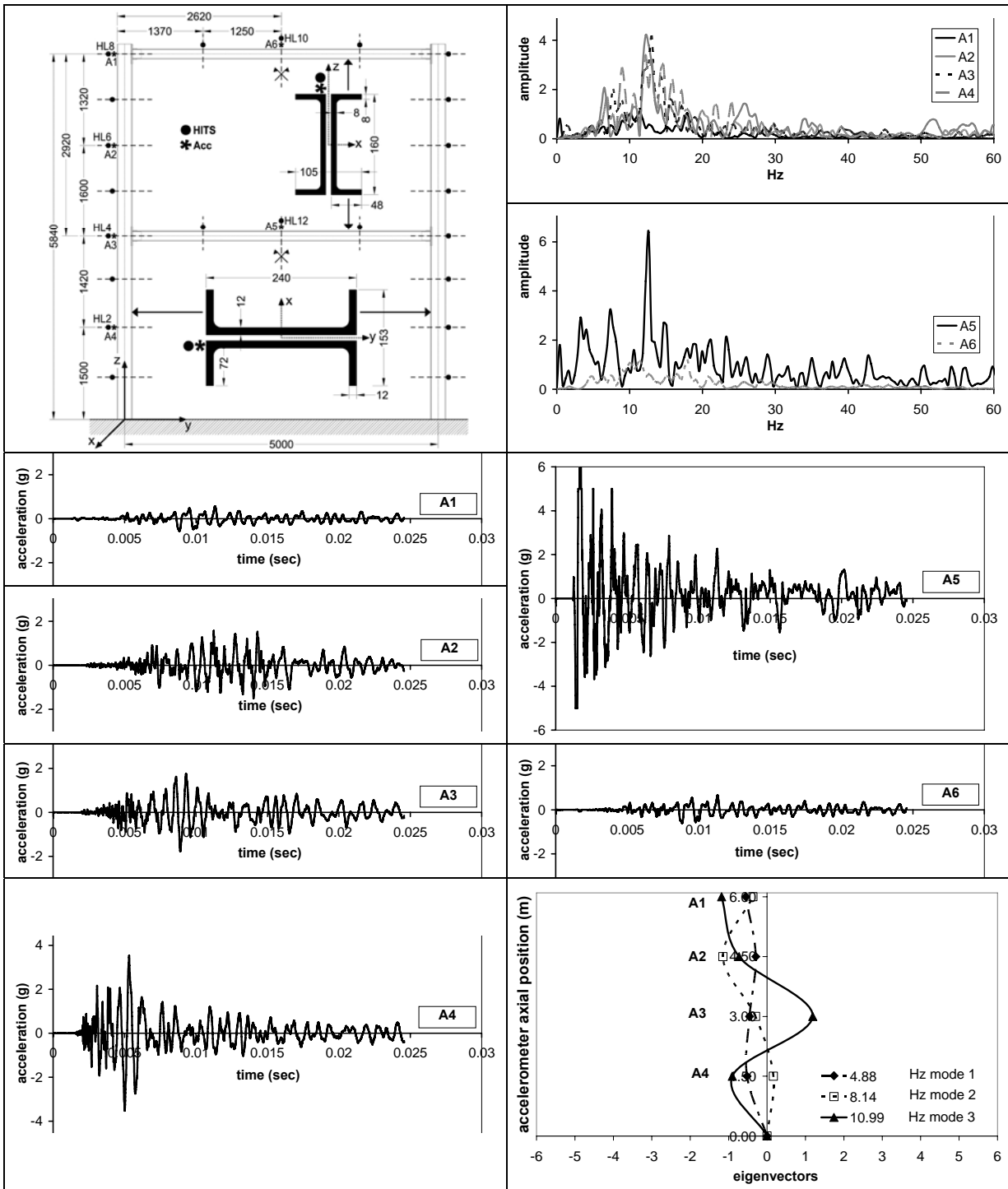


Figure B.1. Free vibration response in frequency and time domain, modal shapes. Excitation HL2

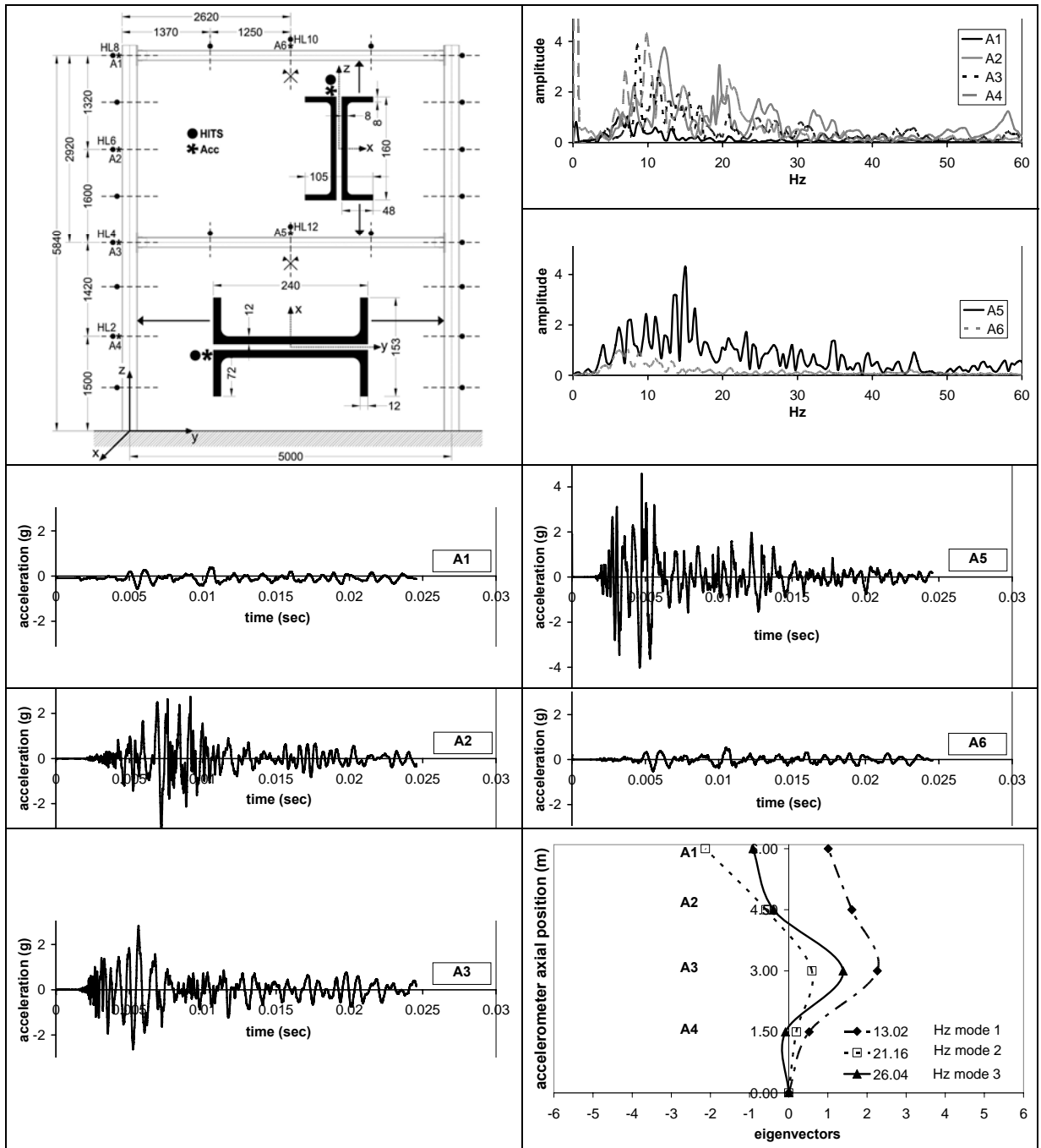


Figure B.2. Free vibration response in frequency and time domain, modal shapes. Excitation HL4

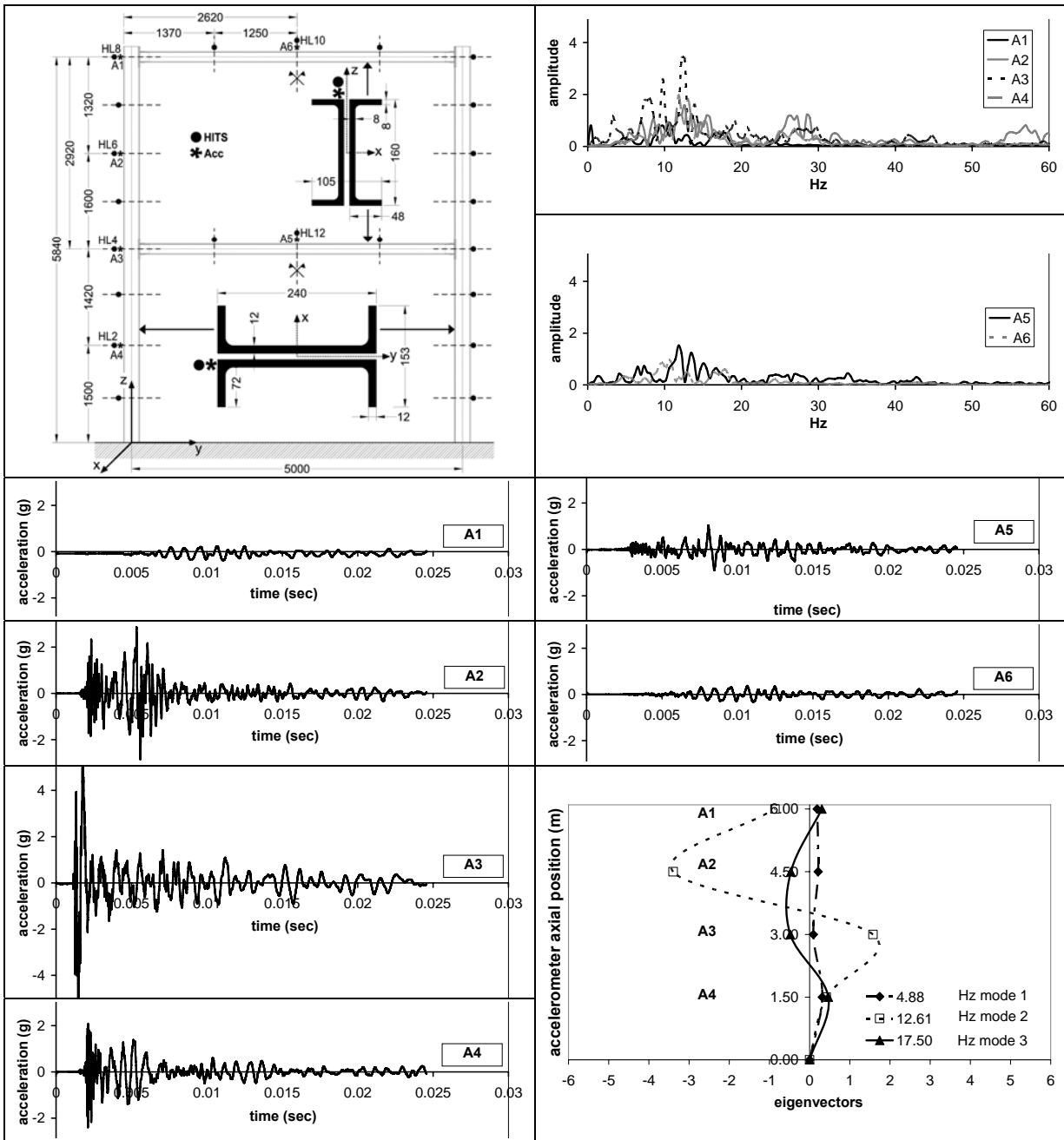


Figure B.3. Free vibration response in frequency and time domain, modal shapes. Excitation HL6

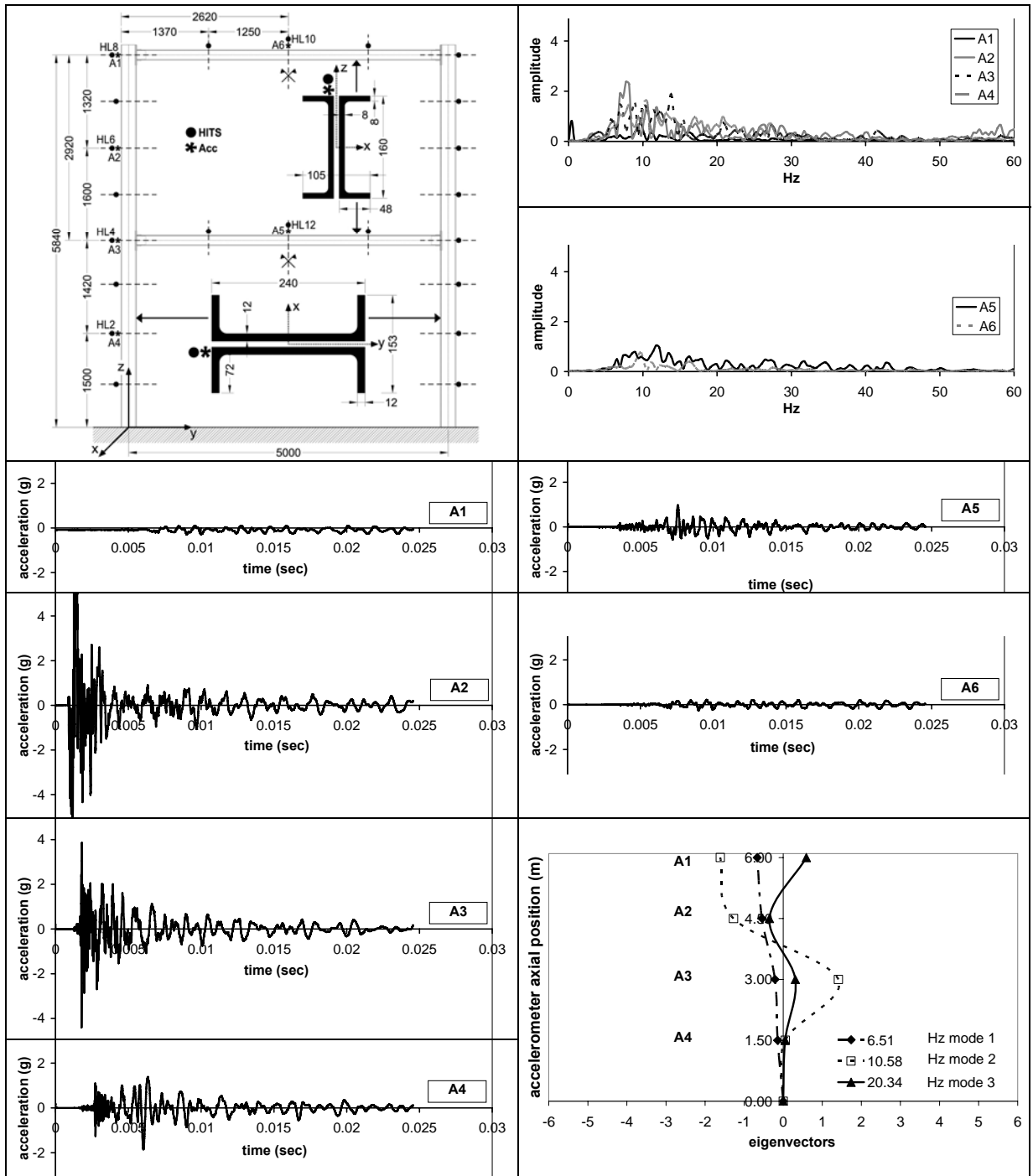


Figure B.4. Free vibration response in frequency and time domain, modal shapes. Excitation HL8

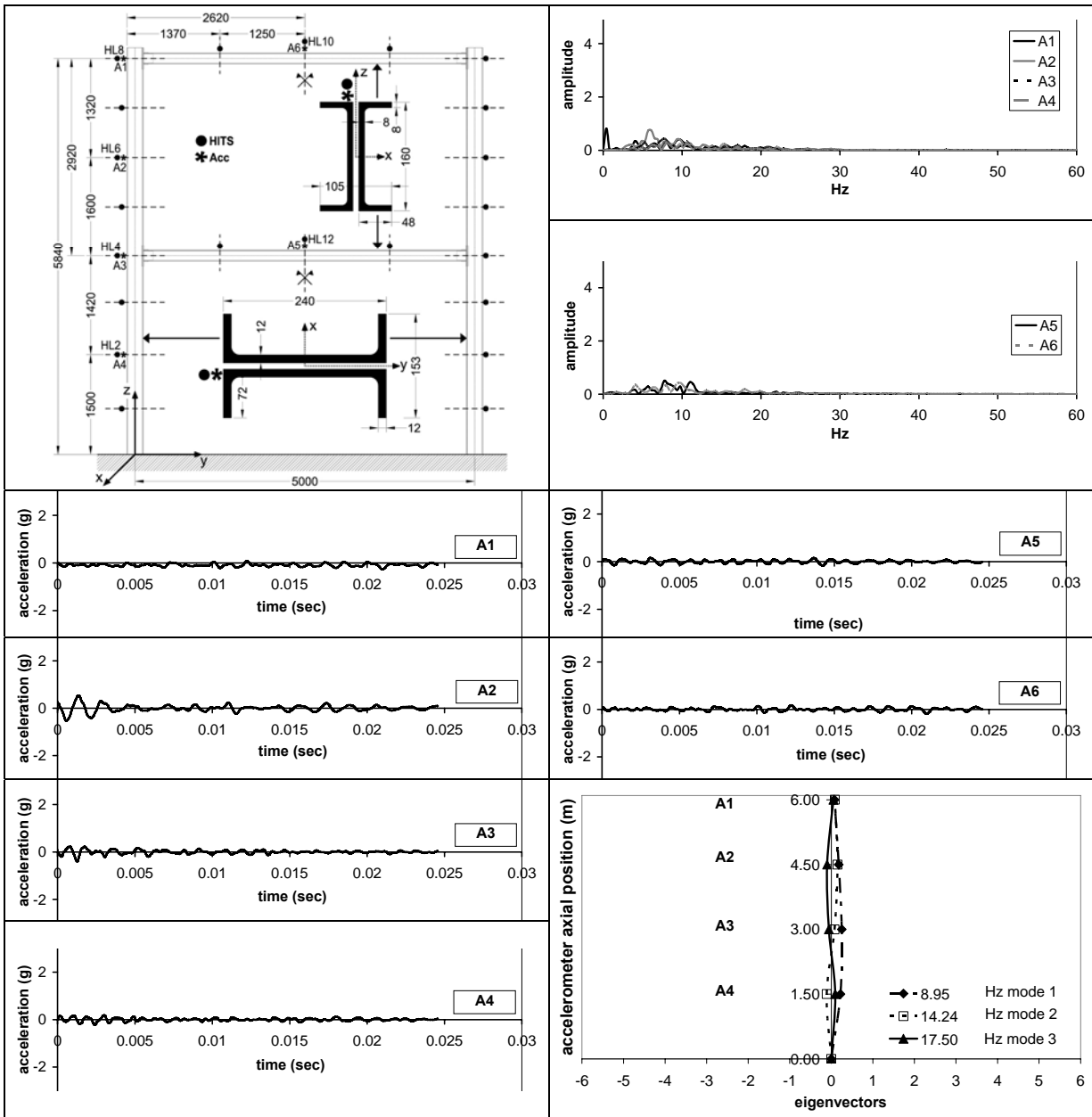


Figure B.5. Free vibration response in frequency and time domain, modal shapes. Excitation HL10

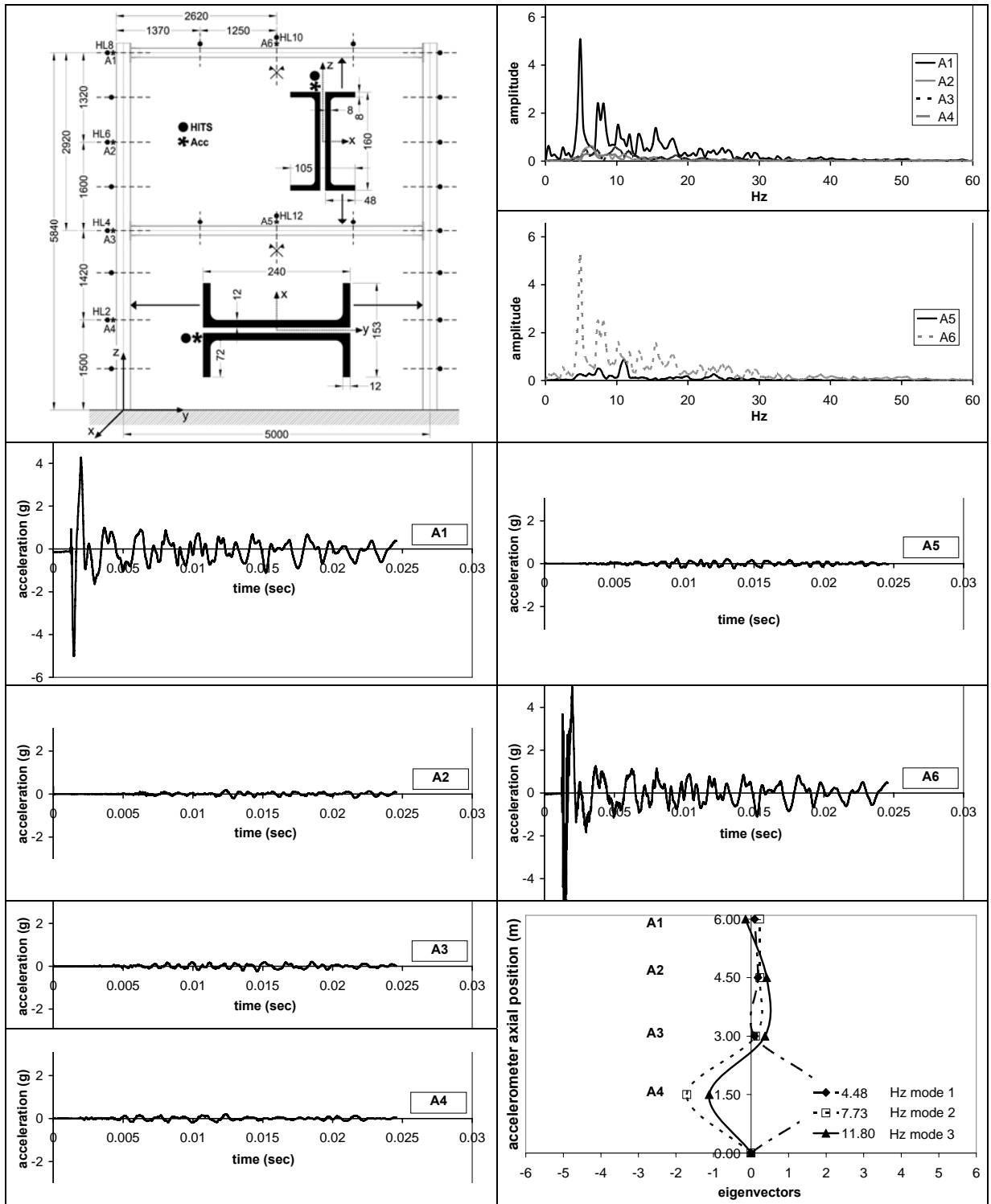


Figure B.6. Free vibration response in frequency and time domain, modal shapes. Excitation HL12

APPENDIX C – Three-dimensional structure, experimental results

Figures from C.1 to C.18 illustrate the dynamic response of the GFRP three-dimensional framework (see chapter 5.2.3.) the spectrum of each signal in time and frequency domain and the modal shapes of the first three modes of vibration. Figures from C.1 to C.12 illustrate the dynamic behaviour of the beams while the response of the columns is reported in the Figures from C.13 to C.18.

In particular the Figures from C.1 to C.6 refer to the beams with the accelerometers and excitations on the plan of maximum moment of inertia of the below flange of profile, while in Figures from C.7 to C.12 the accelerometers and excitations are in the web of the profile itself, as illustrated in detail in the relative layout of each figure.

With regards to the columns, Figures from C.13 to C.18 define the principal parameters of the dynamic response of the GFRP composed columns compared to some of the excitations. The maximum and minimum moment of inertia is referred exclusively to the layout of the structural element with respect to the global configuration of the structure and in relation, therefore, to the direction of the excitations.

The configuration of the accelerometers and the excitation points do not belong to one of the two plans of symmetry of the column, so the dynamic behaviour is partially influenced by the generated twisting effects.

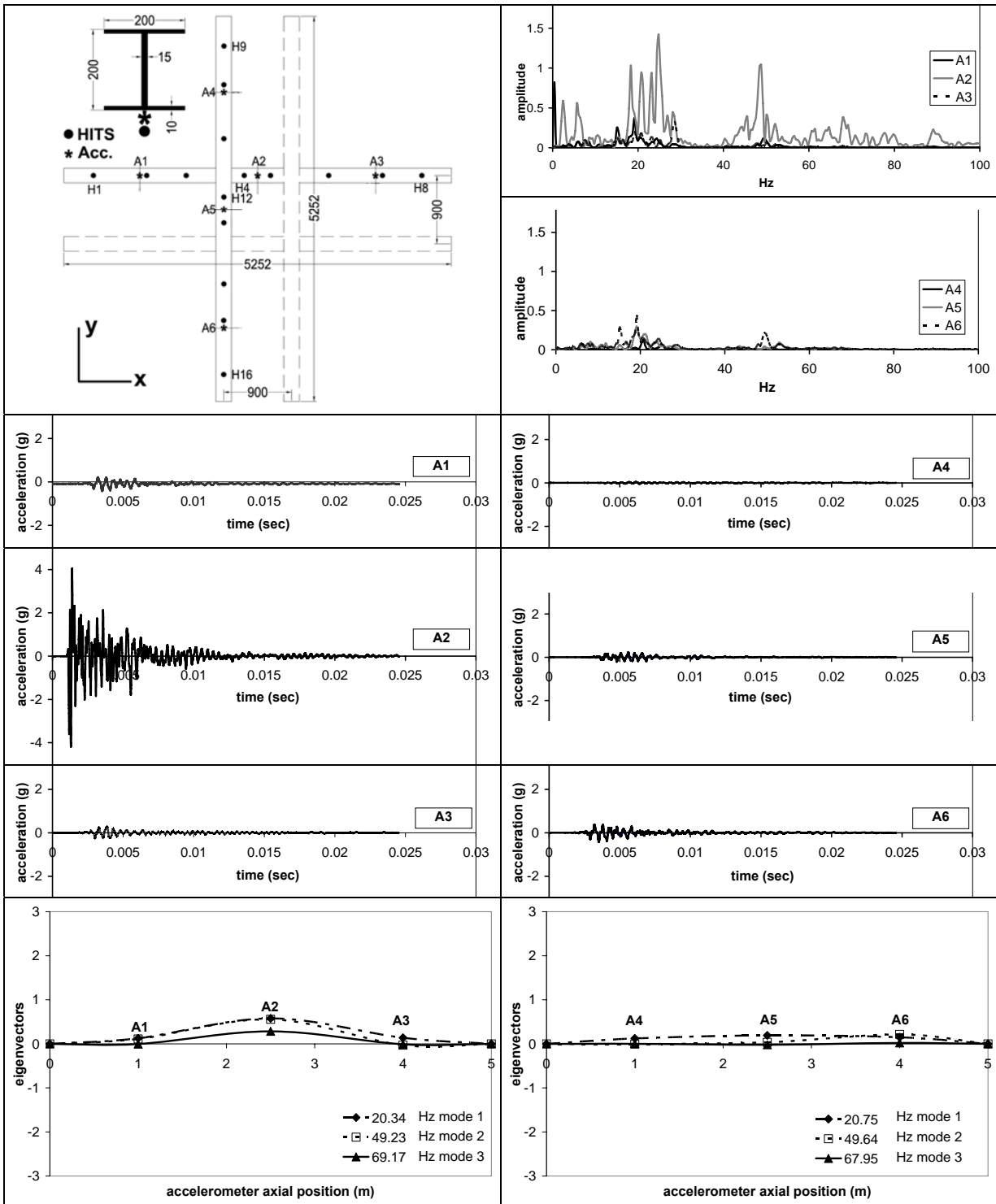


Figure C.1. Free vibration response in frequency and time domain, modal shapes. Excitation $H1_{J_{max}}$

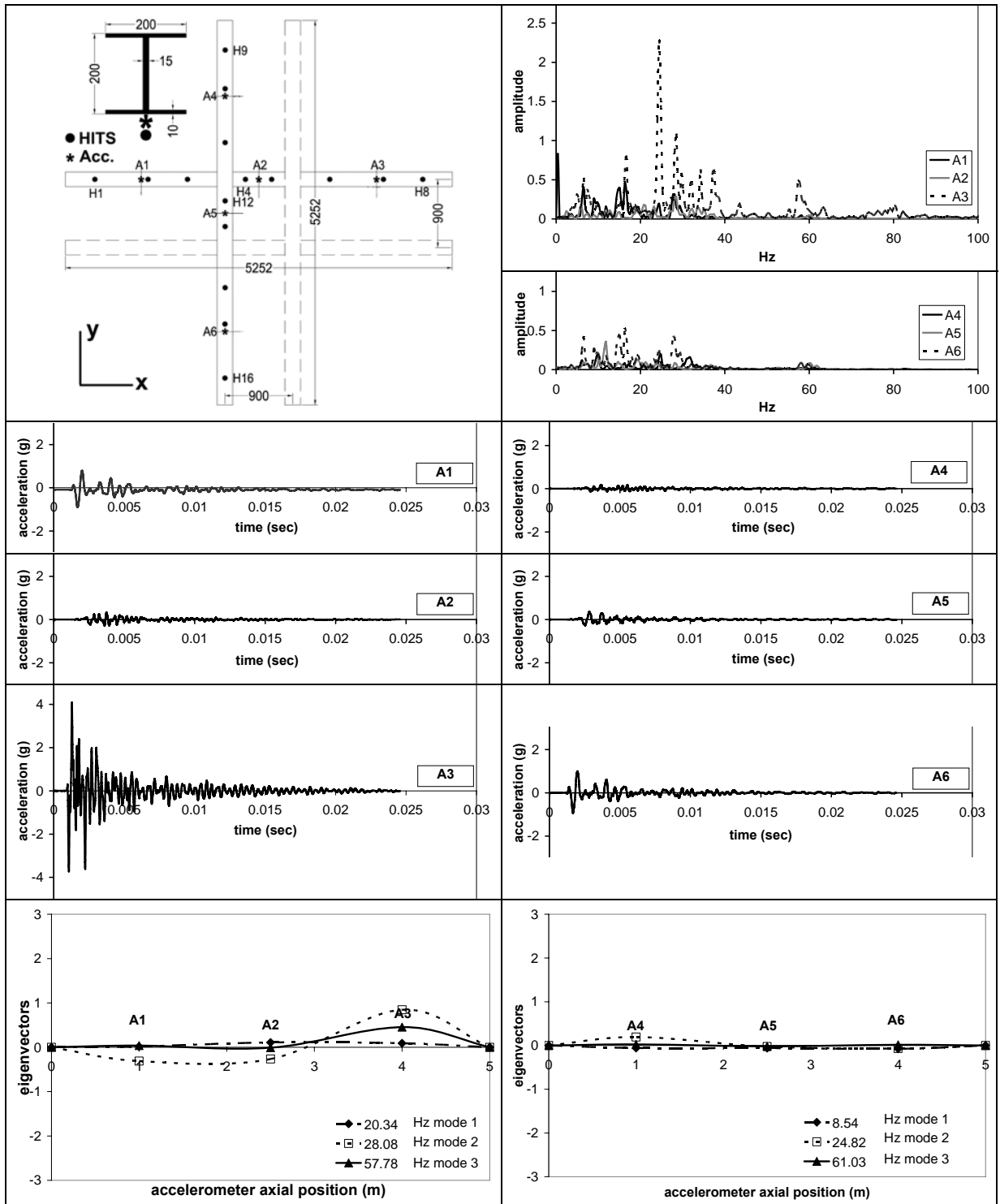


Figure C.2. Free vibration response in frequency and time domain, modal shapes. Excitation $H4_{J_{max}}$

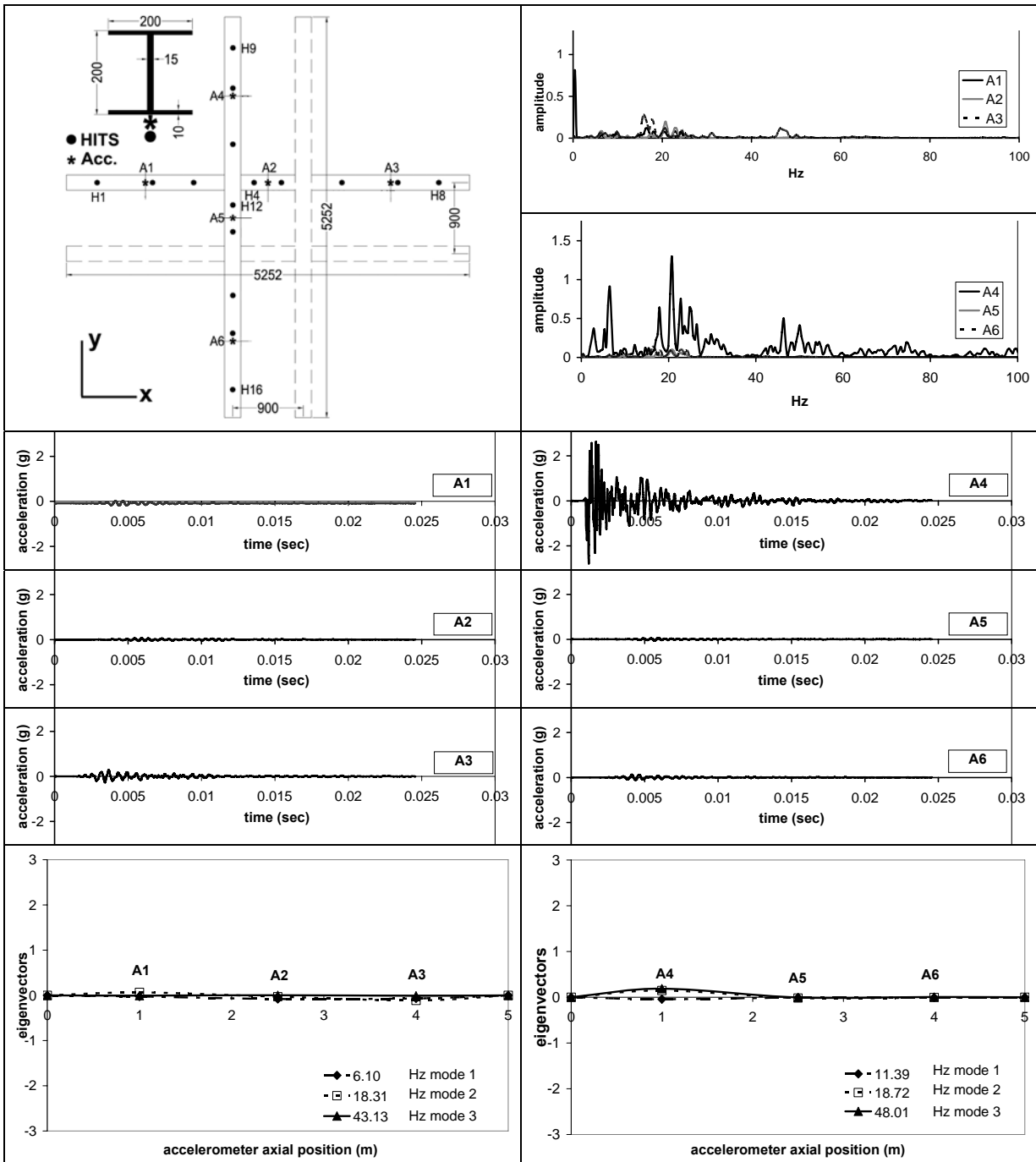


Figure C.3. Free vibration response in frequency and time domain, modal shapes. Excitation $H8_{J_{max}}$

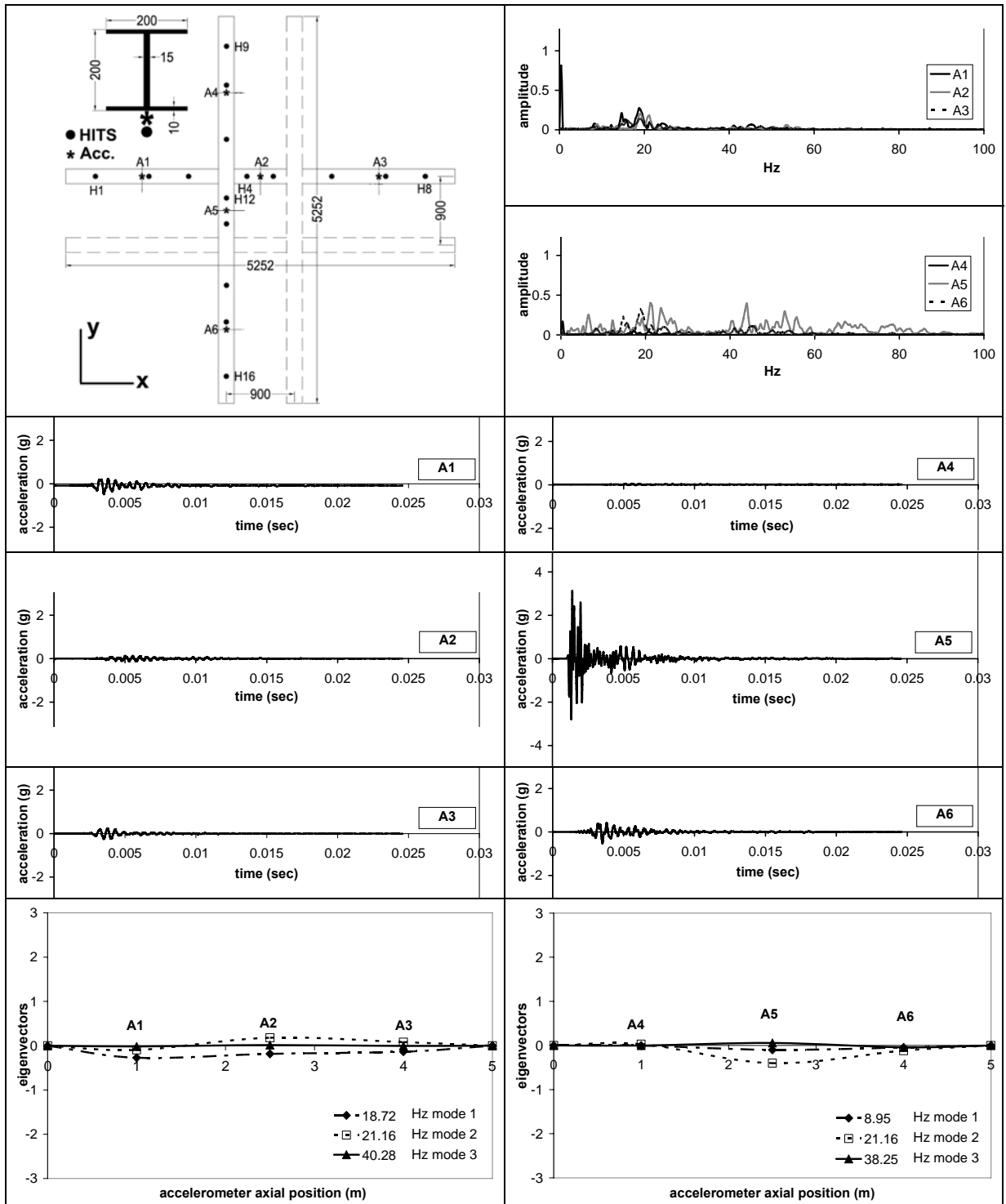


Figure C.4. Free vibration response in frequency and time domain, modal shapes. Excitation $H9_{J_{max}}$

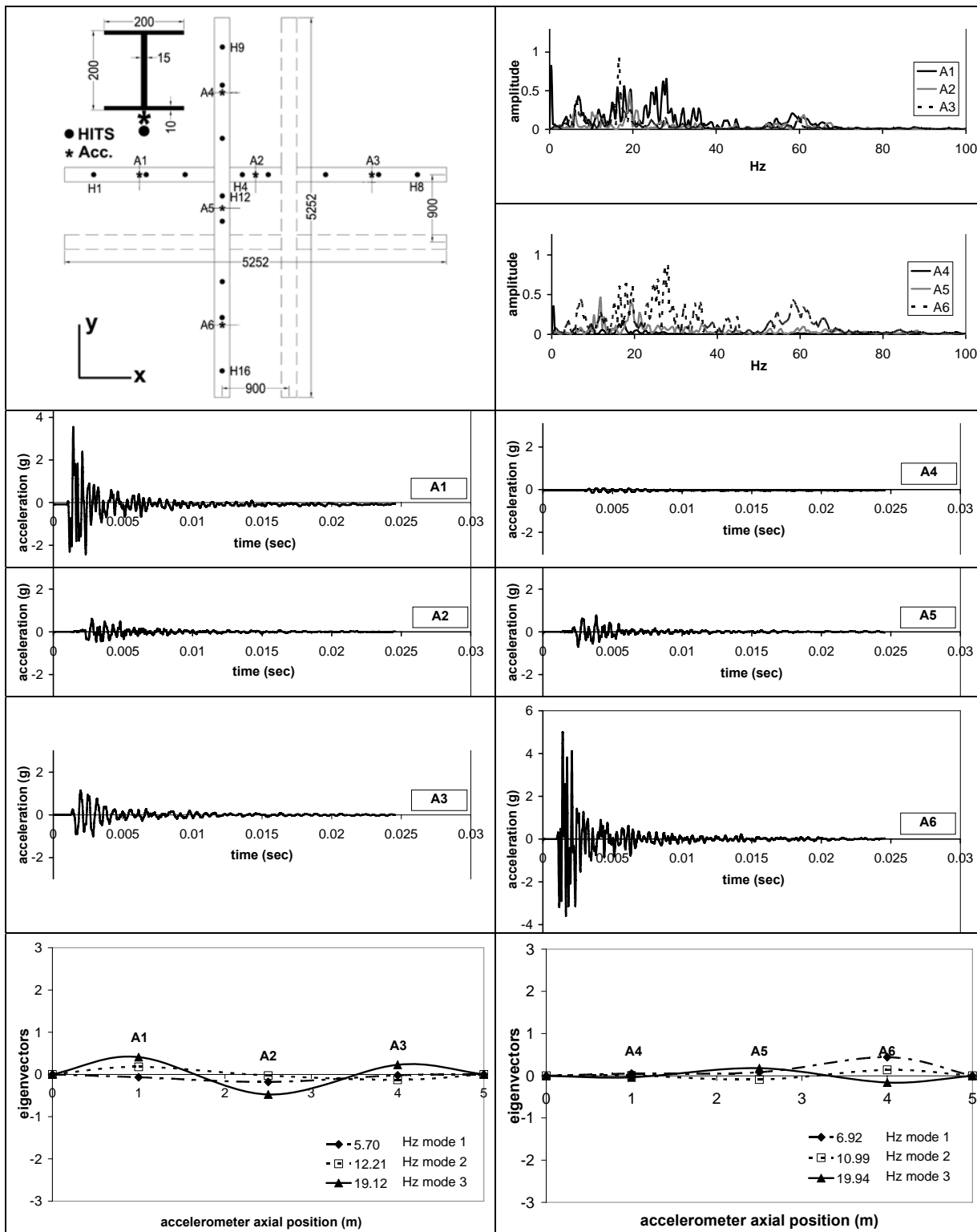


Figure C.5. Free vibration response in frequency and time domain, modal shapes. Excitation H12_ J_{max}

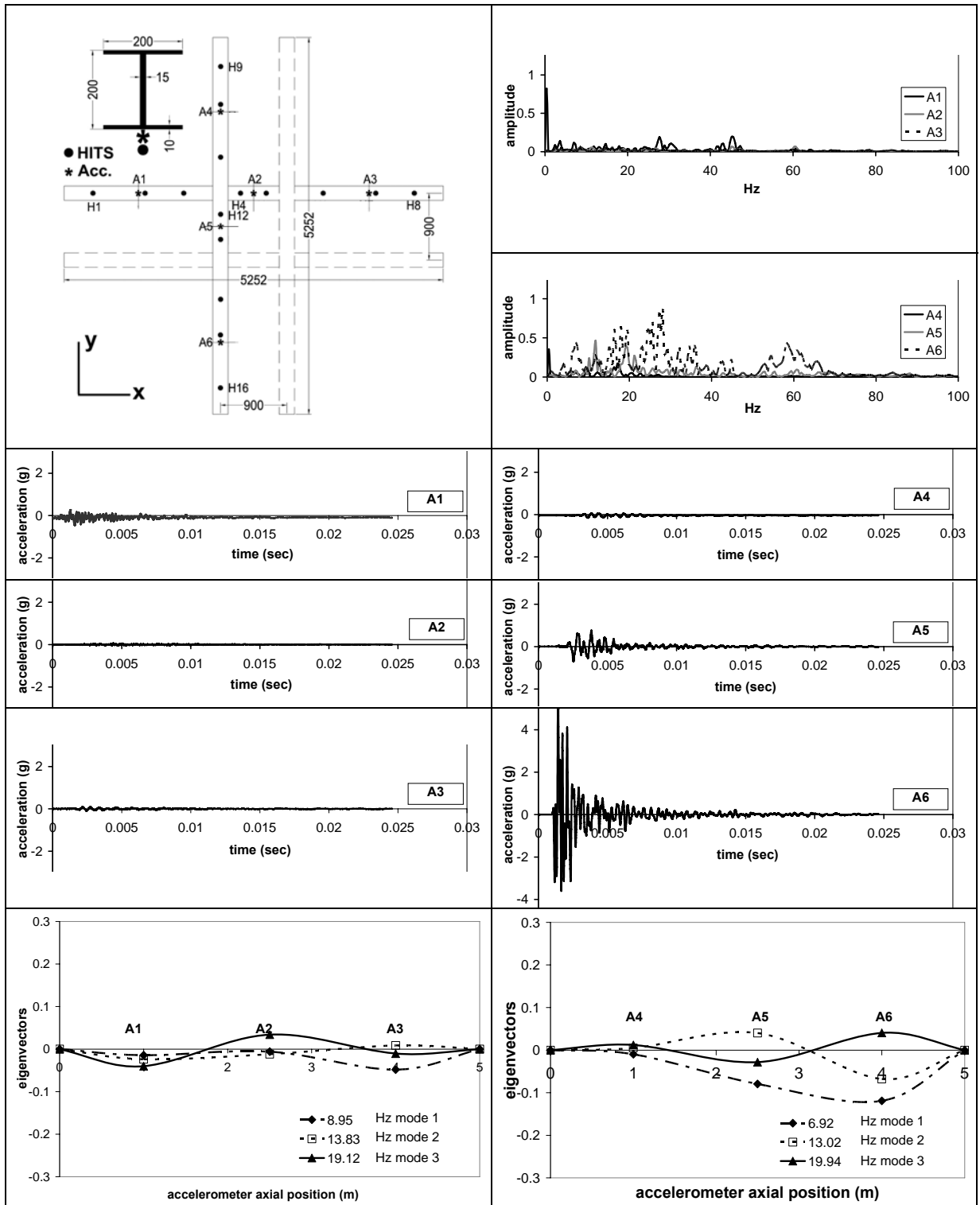


Figure C.6. Free vibration response in frequency and time domain, modal shapes. Excitation $H16_{J_{max}}$

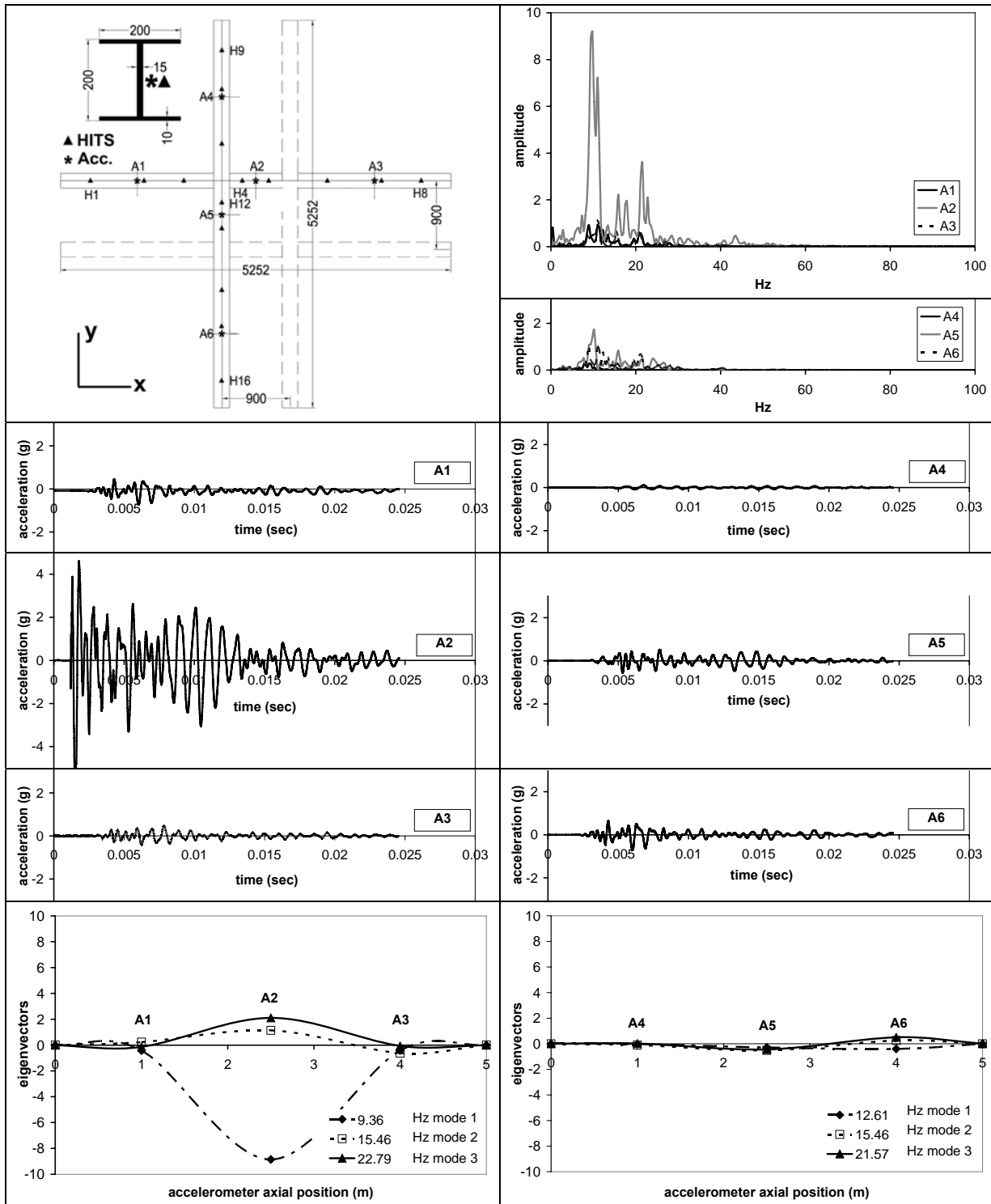


Figure C.7. Free vibration response in frequency and time domain, modal shapes. Excitation H1_ J_{min}

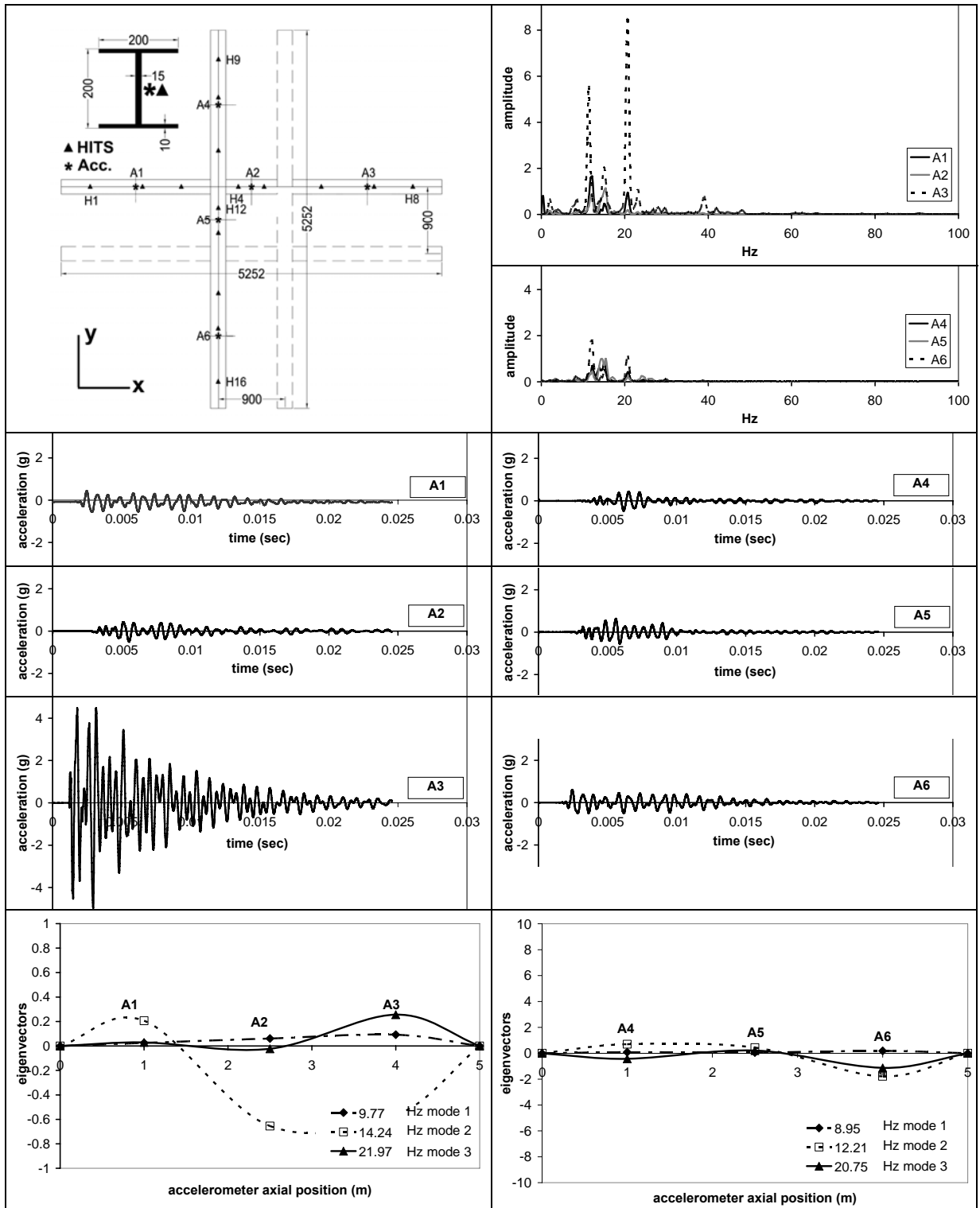


Figure C.8. Free vibration response in frequency and time domain, modal shapes. Excitation $H4_{J_{min}}$

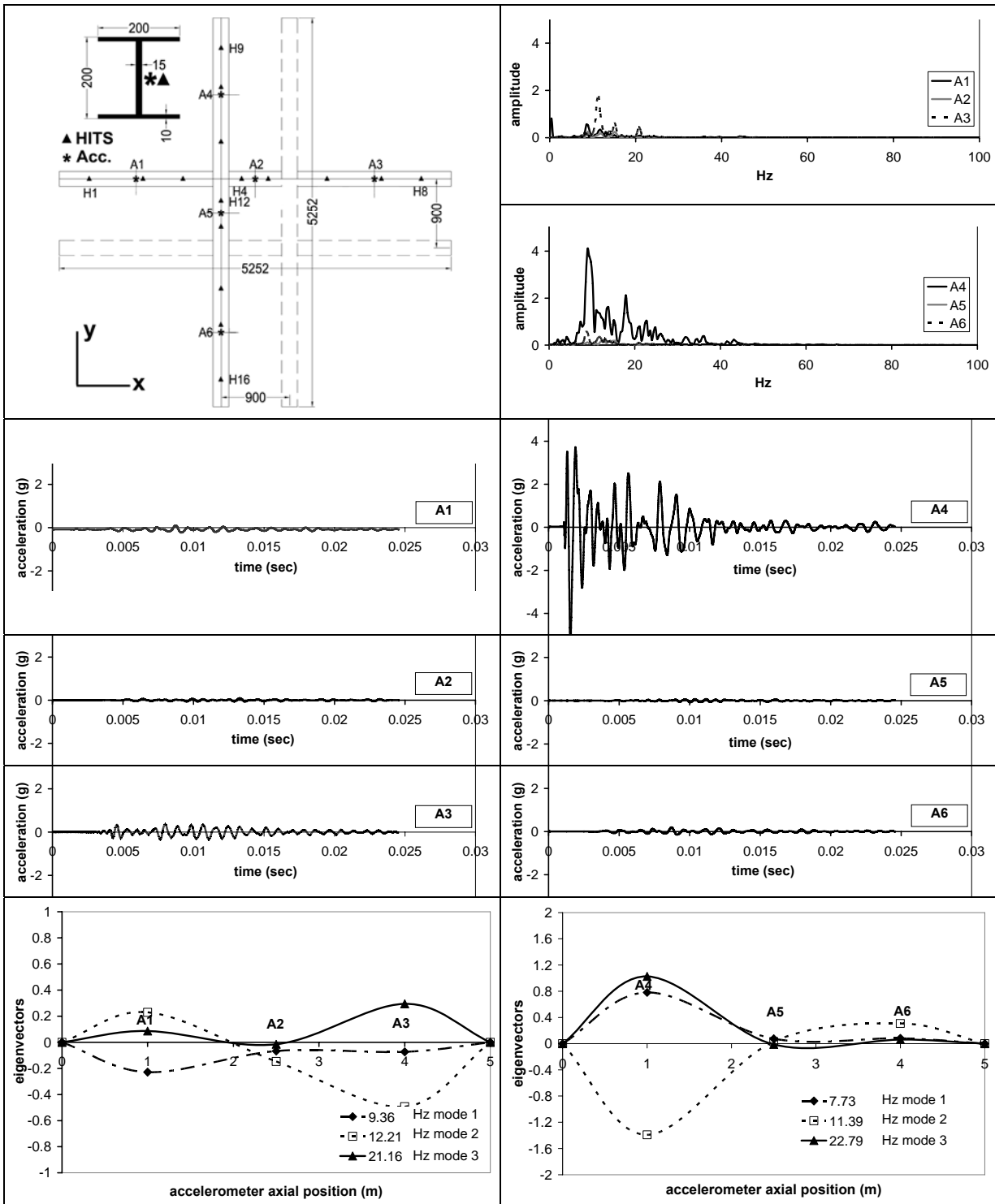


Figure C.9. Free vibration response in frequency and time domain, modal shapes. Excitation H8_J_{min}

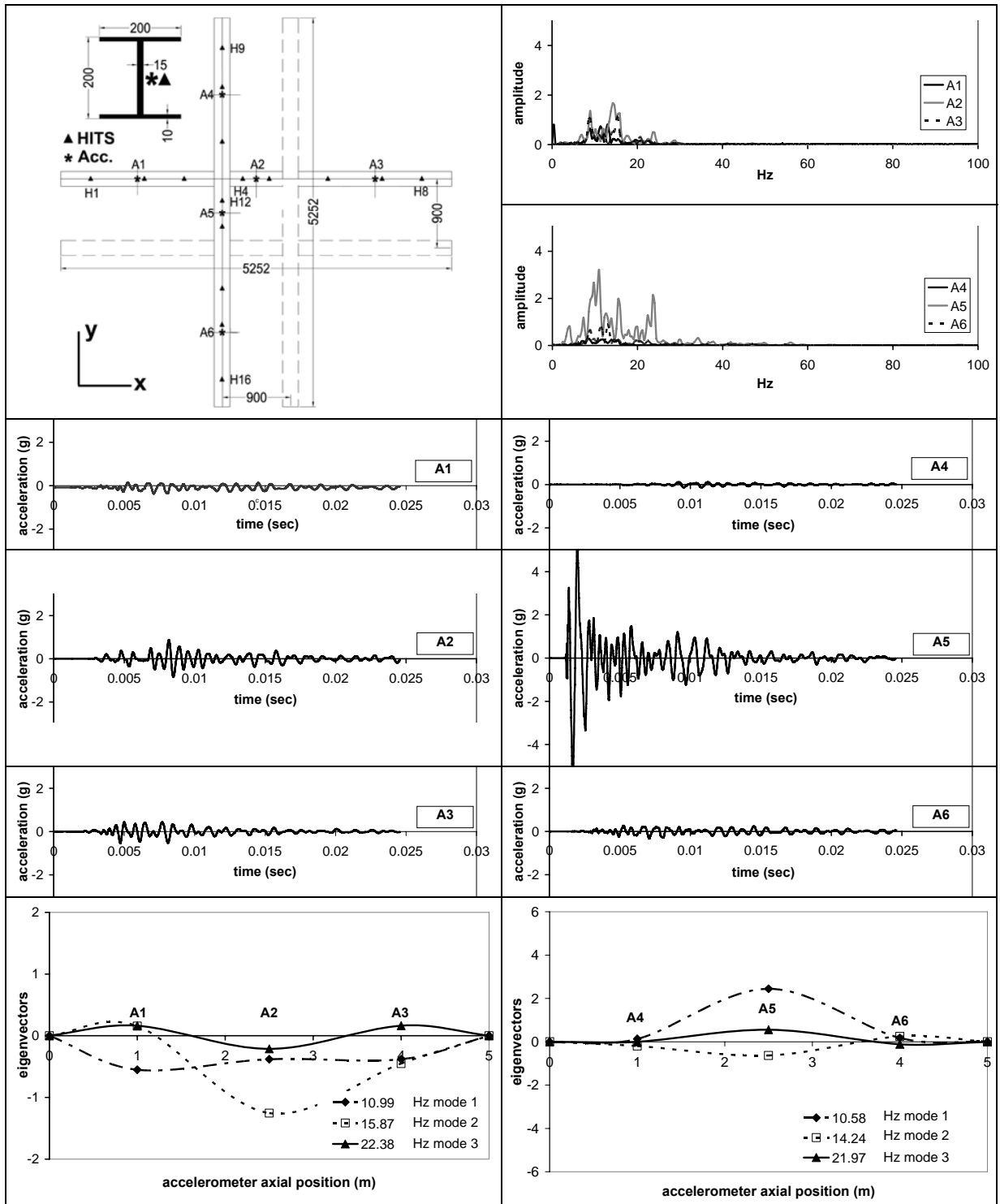


Figure C.10. Free vibration response in frequency and time domain, modal shapes. Excitation H9_J_min

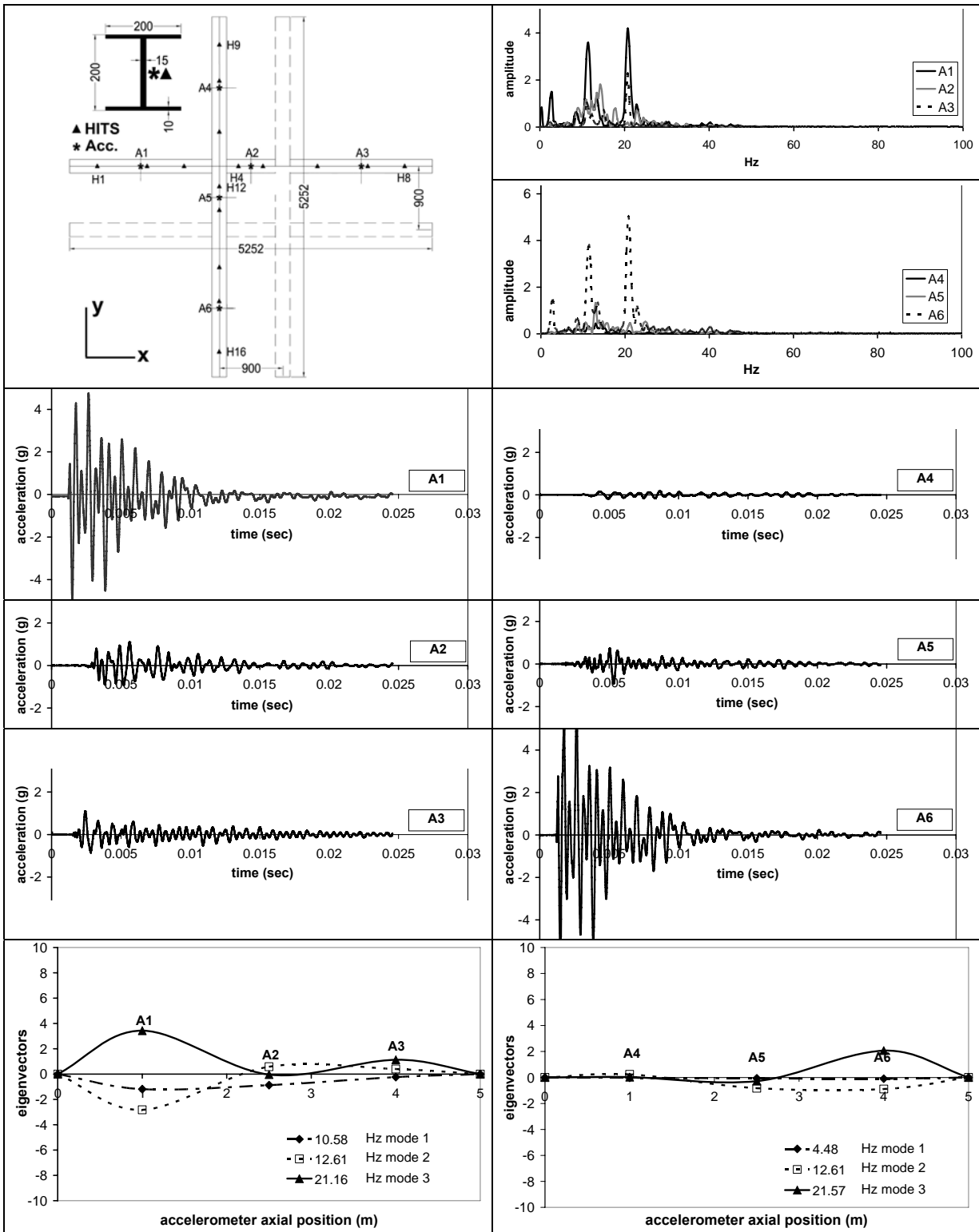


Figure C.11. Free vibration response in frequency and time domain, modal shapes. Excitation H12_{J_{min}}

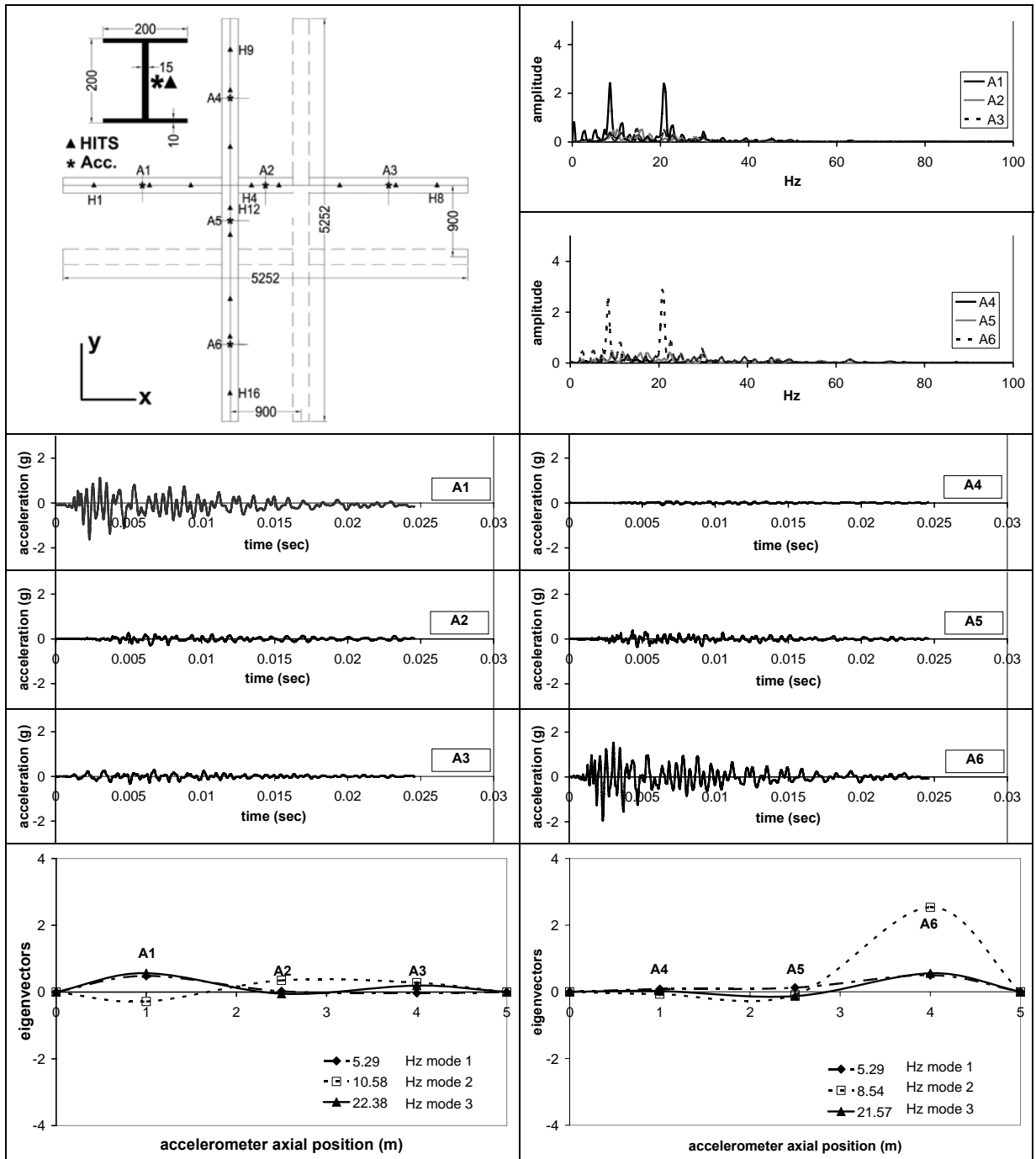


Figure C.12. Free vibration response in frequency and time domain, modal shapes. Excitation H16_J_{min}

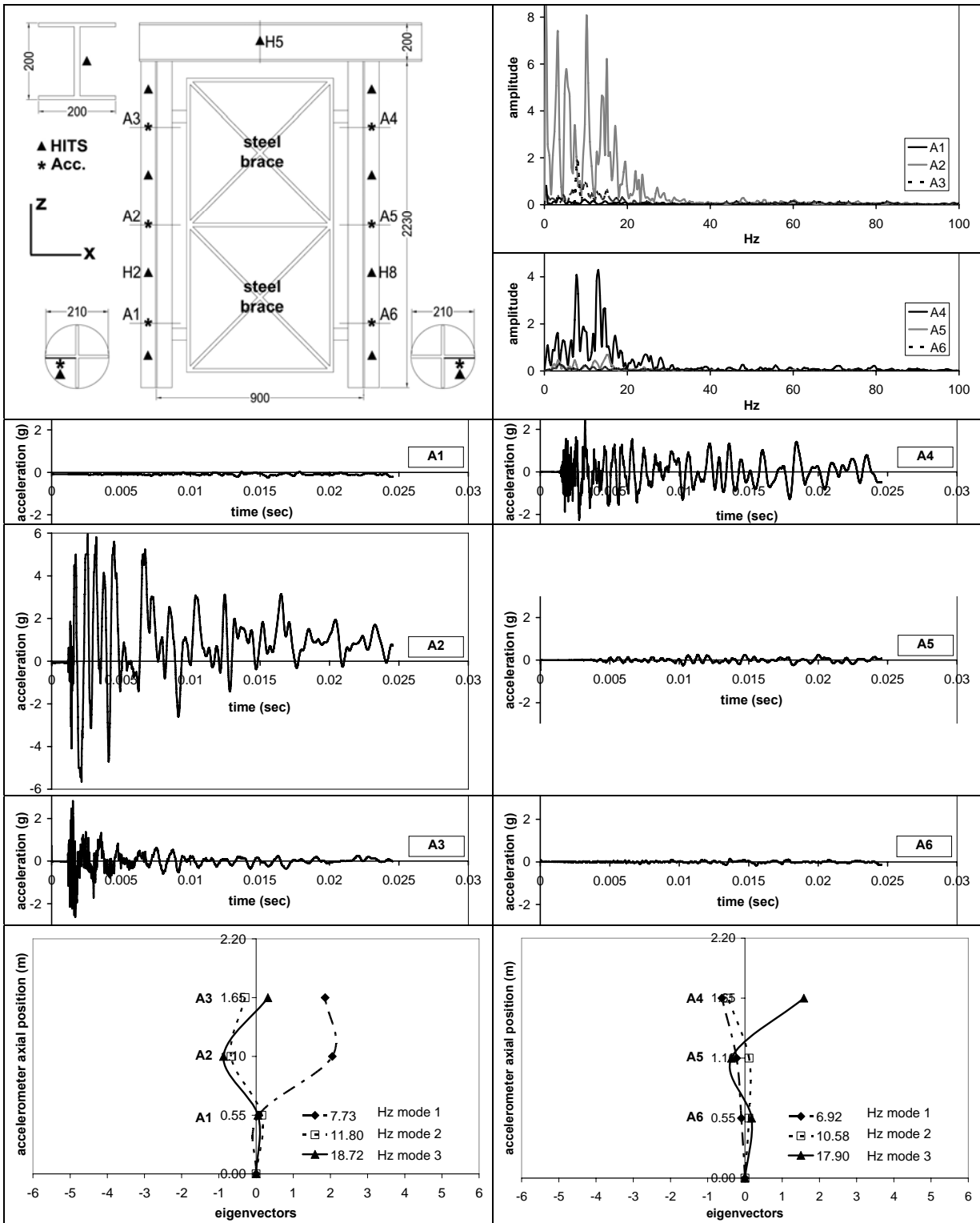


Figure C.13. Free vibration response in frequency and time domain, modal shapes. Excitation $H2_J_{min}$

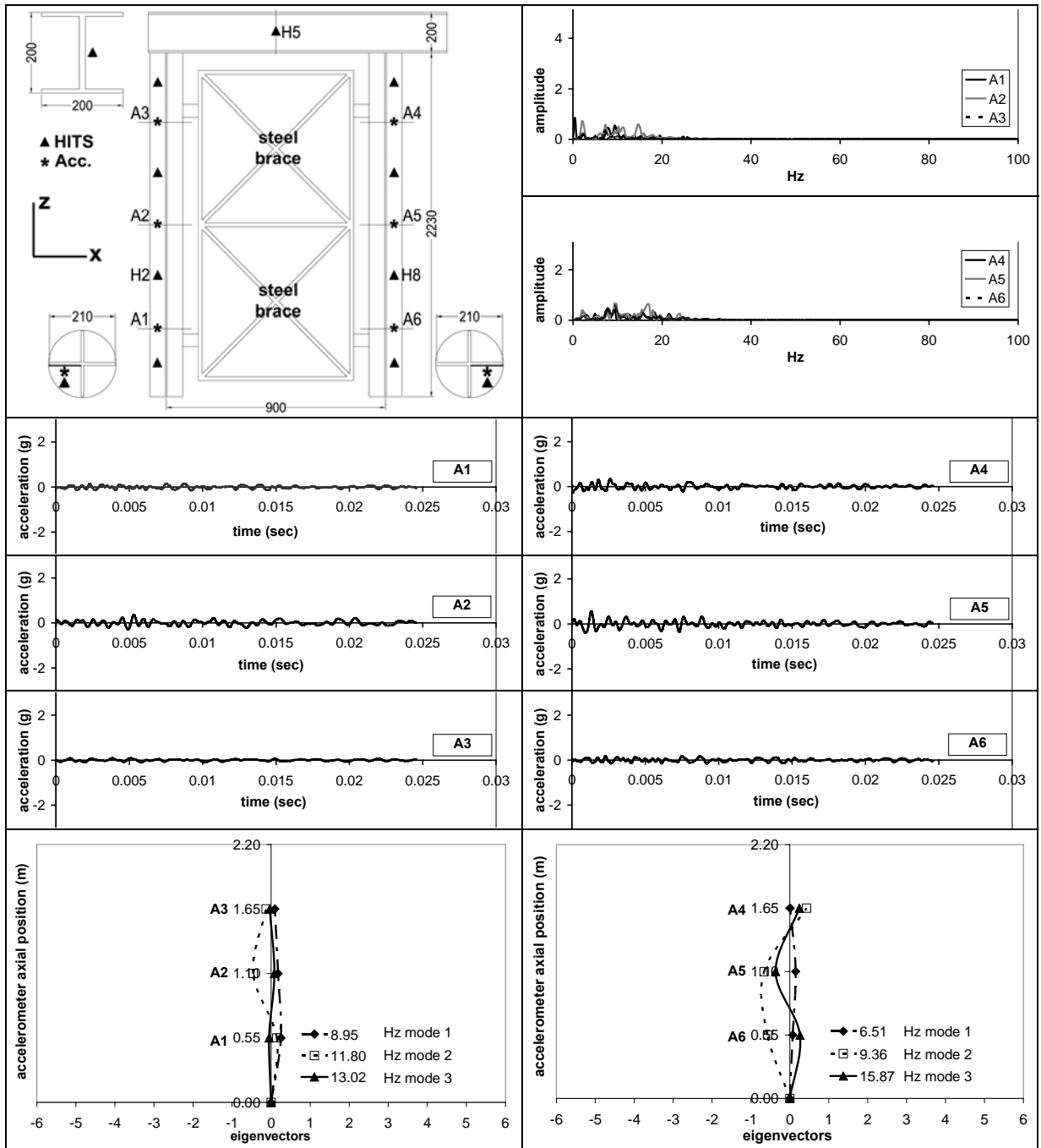


Figure C.14. Free vibration response in frequency and time domain, modal shapes. Excitation H5_J_{min}

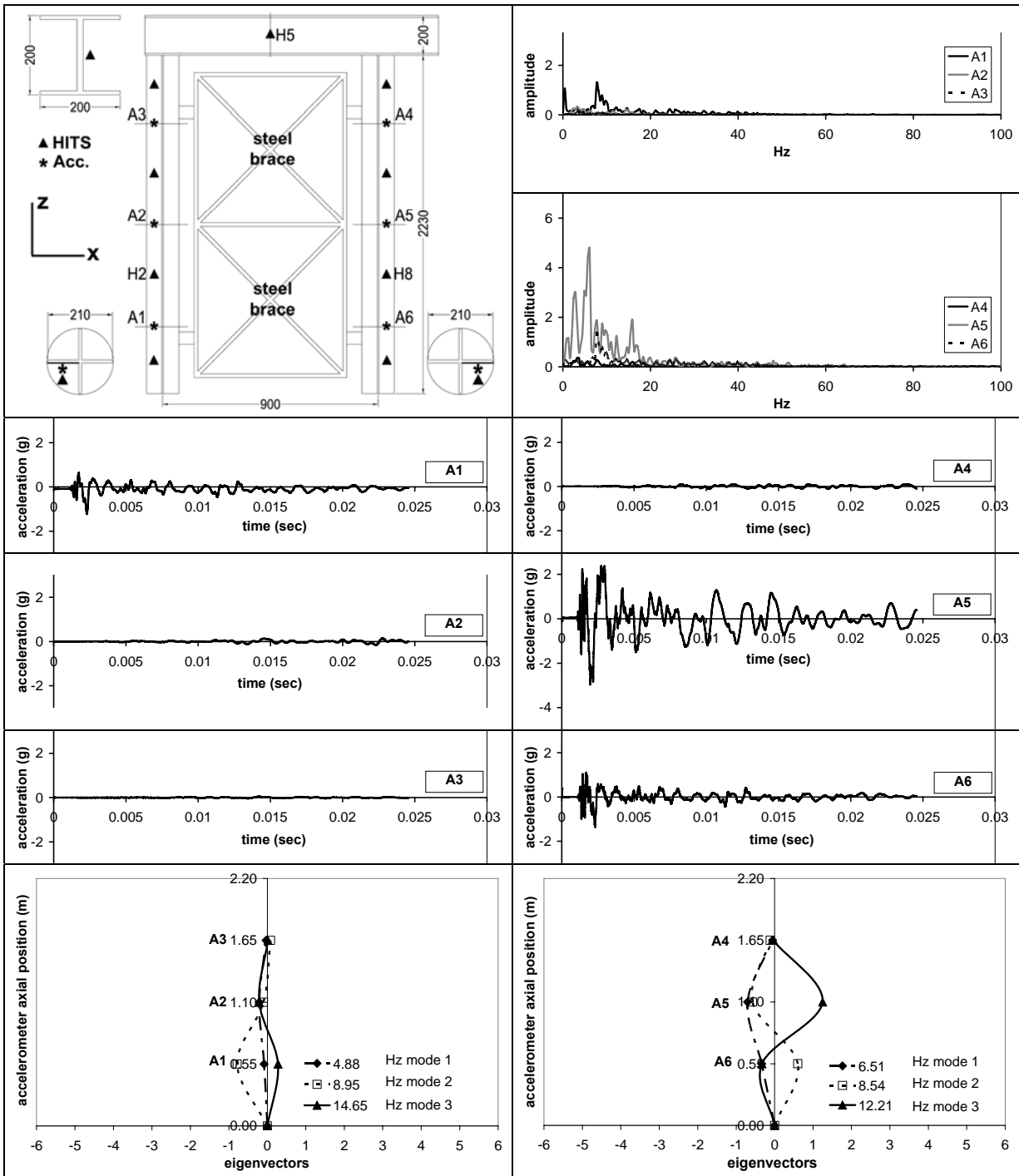


Figure C.15. Free vibration response in frequency and time domain, modal shapes. Excitation $H8_{J_{min}}$

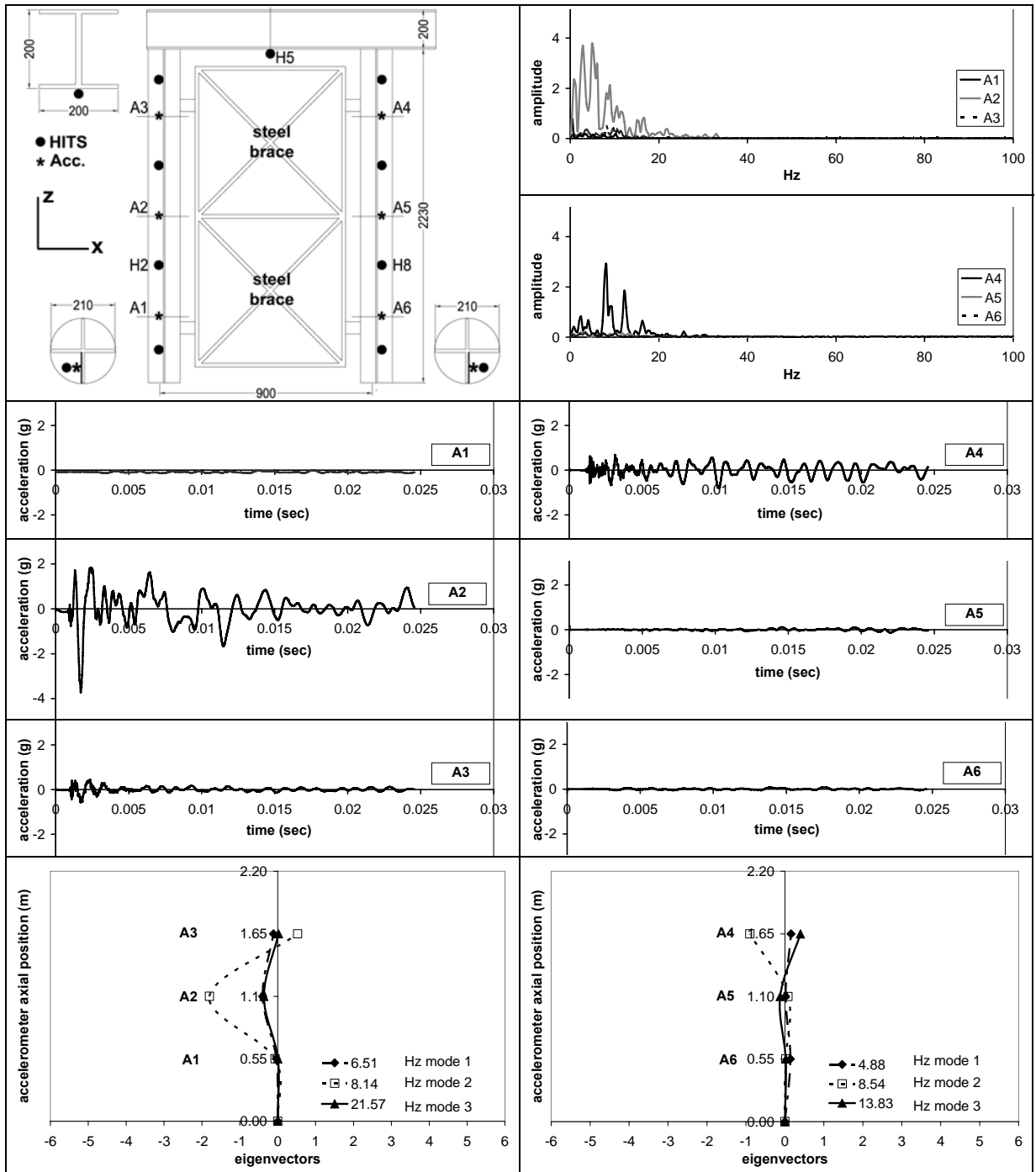


Figure C.16. Free vibration response in frequency and time domain, modal shapes. Excitation H2_ J_{max}

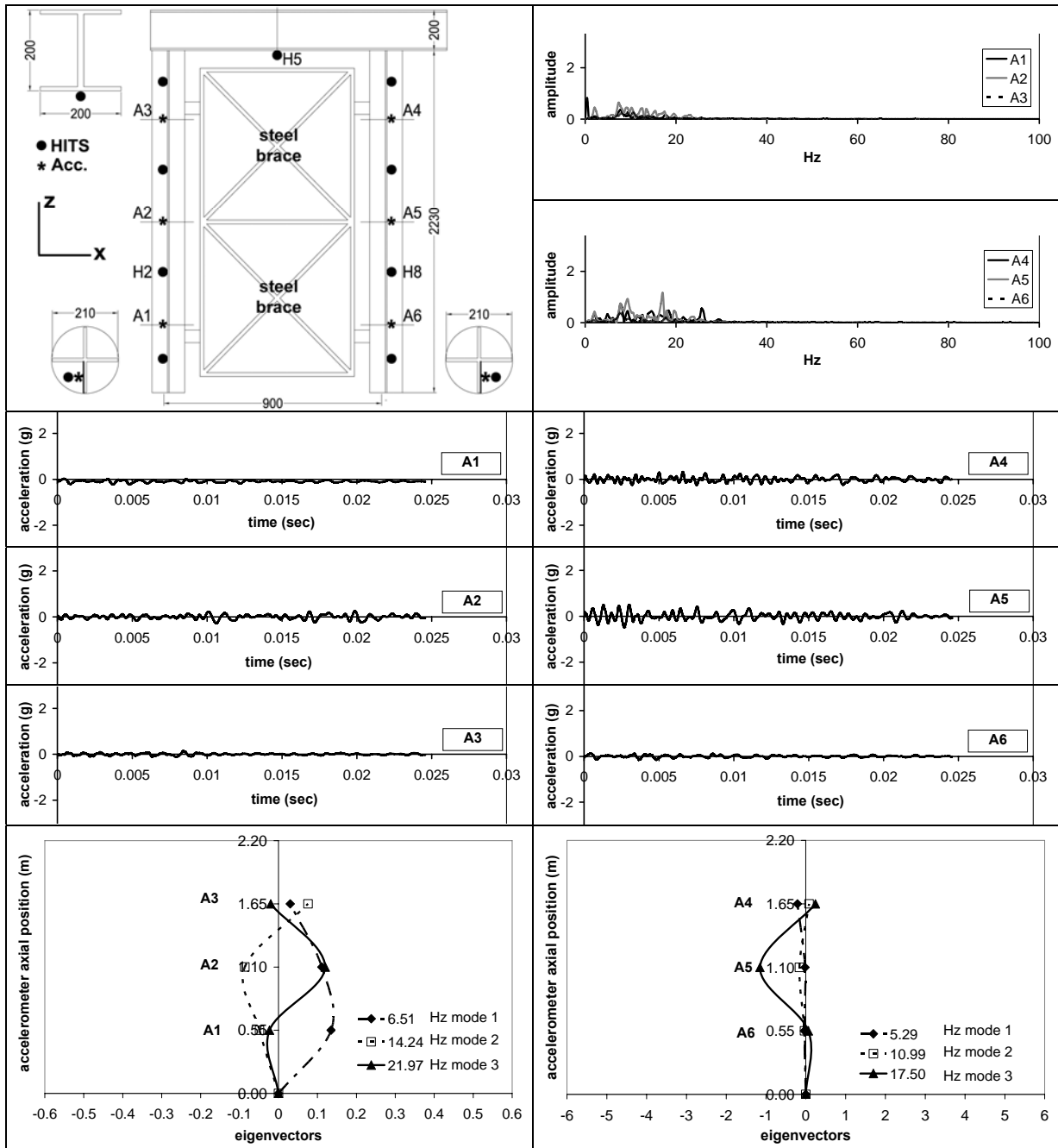


Figure C.17. Free vibration response in frequency and time domain, modal shapes. Excitation H5_ J_{max}

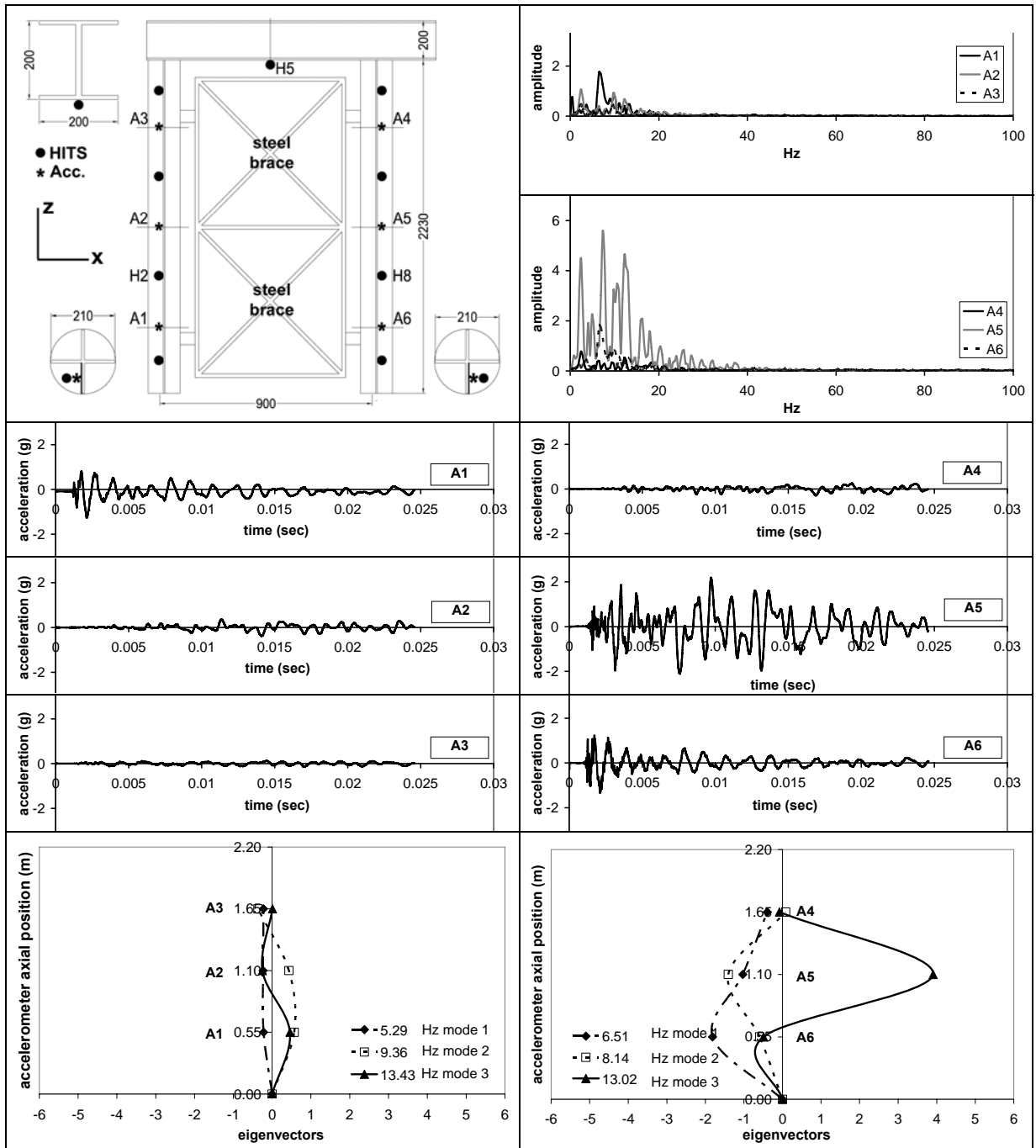


Figure C.18. Free vibration response in frequency and time domain, modal shapes. Excitation H8_ J_{max}